Optically Stimulated Luminescence dating of Palaeolithic cave sites and their environmental context in the western Mediterranean

Proefschrift

ter verkrijging van
de graad van Doctor aan de Universiteit Leiden,
op gezag van Rector Magnificus prof. mr. C.J.J.M. Stolker
volgens besluit van het College voor Promoties
te verdedigen op donderdag 3 mei 2018
klokke 15:00 uur

door

Nina Dörschner
Geboren te Berlijn, Duitsland
In 1986

Promotor: Prof. dr. J.-J. Hublin (Universiteit Leiden, Max Planck Institute for Evolutionary Anthropology, Leipzig)

Co-promotor: Dr. habil. K.E. Fitzsimmons (Max Planck Institute for Chemistry, Mainz)

Promotie commissie:
Prof. dr. W. Roebroeks (Universiteit Leiden)
Prof. dr. M. van Kolfschoten (Universiteit Leiden)
Prof. dr. E.J. Rhodes (University of Sheffield)
Prof. dr. J. Wallinga (Universiteit Wageningen)
Prof. dr. M.A. Soressi (Universiteit Leiden)

This research has been made possible through funding provided by the Max Planck Institute for Evolutionary Anthropology (MPI EVA).

Contents

1. Introduction

1.1. Human interaction with Pleistocene palaeoenvironments

The Quaternary is the most recent epoch in Earth's history and has been characterised by substantial climatic and environmental changes, the evolution of humans in Africa and their subsequent colonisation of most terrestrial landscapes. Successive cycles of global cooling and warmer interglacial phases are the core feature of the Quaternary climate and had major impact on the palaeoenvironments of terrestrial landscapes and thus the habitats of hominin populations occupying these landscapes (Klein, 2009; Lowe and Walker, 2015).

The Pleistocene is a geological period representing the earlier phase of the Quaternary that lasted from about 2.6 millions of years ago (Ma) to the onset of the most recent interglacial, the Holocene (~11.7 thousands of years ago (ka)) (Cohen and Gibbard, 2011). The substantial oscillations of global climate during Pleistocene times were mainly driven by periodic variations in the Earth's main orbital parameters – precession, obliquity and eccentricity – and their interaction with global oceanic and atmospheric circulations (Emiliani and Geiss, 1959; Hays et al., 1976; Milankovitch, 1920; Paillard, 1998). Climatic stages can be detected through variations in the content of oxygen-18 (^{18}O) over oxygen-16 (^{16}O) in marine sediment records with enrichments in ^{18}O representing cold glacial periods - when large amounts of water from the oceans became locked in ice sheets – and ^{18}O depletion reflecting warmer temperatures with decreased ice volumes during interglacial phases (Fig. 1.1.1, odd numbers represent interglacial events) (Shackleton, 1975, 1987).

Expansions and contractions of the Earth's ice sheets and glaciers influenced the rise and fall of global sea-levels (Fig. 1.1.1) and, at a more regional scale, water volume and shape of limnic and fluvial systems. Global cooling during glacial phases was associated with increasing aridification across most terrestrial landscapes with declined precipitation being mostly a consequence of reduced evaporation from the colder oceans (Bigg, 1995).

On the African continent, large rainforest areas became grassland or savanna, while grassland and savannah regions turned into desert (deMenocal, 1995; Sarnthein, 1978). The reduced vegetation cover in turn fostered wind erosion (deflation) and thus the expansion of semi-arid and arid landscapes in these regions (Darkoh, 1998). Around the Miocene/Pliocene boundary, arid conditions coupled with aeolian sand accumulation lead to the formation of the Saharan desert (Micheels et al., 2009; Schuster et al., 2006), which has since then served as a biogeographical barrier between sub-Saharan and North Africa (Lahr, 2010). It was only during the relatively short-termed periods of enhanced humidity in the Pleistocene – the 'green Sahara' events – that subtropical savannah landscapes expanded, enabling human habitation and crossings of the desert (e.g. Larrosaña, 2012; Trauth et al., 2009; Whiting Blome et al., 2012).

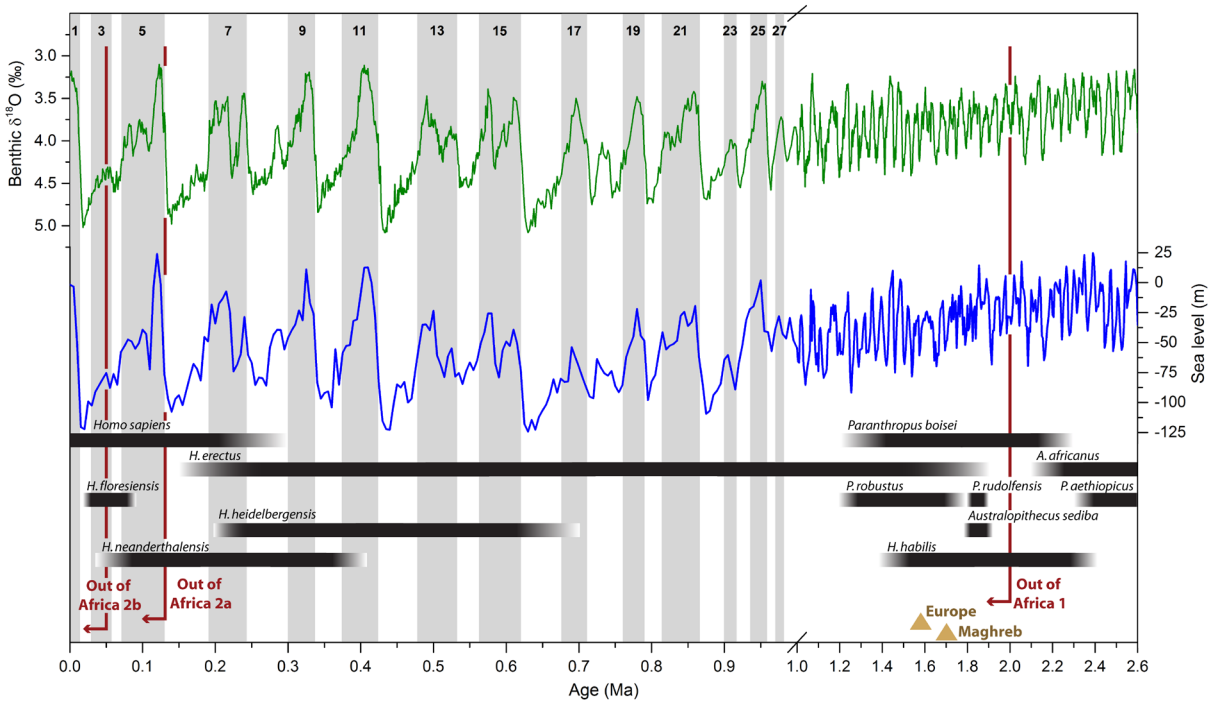

Fig. 1.1.1 Quaternary hominin evolution (after Antón et al., 2014), marine oxygen isotope record after Lisiecki and Raymo (2005) illustrating past glacial cycles and record of global sea-level fluctuations (Miller et al., 2005) with a special emphasis on the last 1 Ma, which are of particular relevance for this thesis. Highlighted are Out of Africa human dispersal events; yellow triangles represent the timing of the first early human settlements in the Maghreb and Europe.

There is a general consensus that the genus *Homo* evolved in Africa sometime between 2.5 and 2 Ma ago (Fig. 1.1.1) and then started to disperse within and out of the continent (Klein, 2009). Most of what is known about the emergence of early *Homo* comes from the East African Rift Valley (e.g. Delagnes and Roche, 2005; Partridge et al., 1995; Quade et al., 2004). Less well understood are, however, the exact timing and the routes human populations took throughout the Pleistocene to extent their range to the far southern and northern margins of Africa (Klein, 1994; Maslin et al., 2014; Raynal et al., 1995) and from the latter further into Eurasia (Klein, 2009).

In recent years, the archaeological and palaeoenvironmental record of the western Mediterranean – comprising north-western Africa and southern Iberia - has gain considerable importance in the study of human evolution (Finlayson et al., 2006; Garcea, 2012; Hublin et al., 2017). The Strait of Gibraltar has been argued by some authors to represent a potential hominin dispersal route from Africa into Europe in the Early Pleistocene at times of when the Mediterranean sea-level was significantly lowered (Alimen, 1975; Gibert et al., 2016; Sharon, 2011). Further interest in the north-western African archaeological sites has arisen in part because of evidence for an early appearance of behavioural modernity which may be linked to the dispersal of anatomically modern humans (AMH) from Africa (d'Errico et al., 2009; Klein, 2008; McBrearty and Brooks, 2000). And the south of the Iberian Peninsula, finally, has been interpreted as an ecological refugium for late Neanderthals before they eventually became extinct in the Late Pleistocene (d'Errico and Sánchez Goñi, 2003; Zilhão, 2006).

The key to understand human dispersal across and their interaction with palaeolandscapes are reliable chronologies of geological and archaeological archives which provide the framework for reconstructing the history of environmental change and human occupation patterns. Caves can safely store complex sedimentary records over millennia by providing permanent protection from sub-aerial weathering and erosion (Sasowsky and Mylroie, 2007). As they concurrently offer natural shelter, caves also often act as focus for Pleistocene human activity traceable in the stratigraphical sequences in form

of artefact concentration, fire features, faunal and human remains. The preservation of disparate sources of chronological, behavioural and environmental evidence in close proximity makes such Palaeolithic cave sequences optimal archives to successfully reconstruct not only environmental and human population responses to climatic change, but also their mutual interactions throughout the Pleistocene (e.g. Barton et al., 2009; Belmaker and Hovers, 2011; Pirson et al., 2012). Quaternary dating methods enable determination of absolute ages for a variety of different materials that can be found at Palaeolithic cave sites such as bones, charcoal, heated artefacts, sediments and speleothems. Optically stimulated luminescence dating is widely applicable in such contexts, as it provides reliable estimates of the time elapsed since sediments were last exposed to sunlight.

In this dissertation, the potential of sand-sized quartz grains as luminescence chronometer to reliably establish the timing of sediment deposition and human occupation at Palaeolithic cave sites in the western Mediterranean is investigated. With this new chronological evidence, this thesis aims to contribute to an improved understanding of the significance of the region in the study of human evolution and dispersal within and out of the African continent that took place under the variable climatic conditions over the course of the Pleistocene.

1.2. The western Mediterranean perspective on human evolution

Humans evolved over Quaternary timescales, but the link between hominin evolution and climatic conditions remains unclear. In the past, the emergence of the genus *Homo* has often been linked global cooling and the subsequent increase of aridity coupled with a progressive expansion of open, grassland habitats on the African continent during the Quaternary (Cerling, 1992; Cerling et al., 2011). This hypothesis was, however, questioned by recent archaeological discoveries - including new hominin fossil evidence (e.g. Berger et al., 2010; Lordkipanidze et al., 2013) – and current synthesis of palaeoenvironmental proxies, i.e. aeolian dust, lake, faunal, stable isotopic and volcanologic records (deMenocal, 2004; Trauth et al., 2009). These evidences suggest that intentional developments of new behavioural patterns and toolkits in early *Homo* could have emerged in response to dynamic environments characterised by fluctuating moisture and aridity, shifting resource regimes and spatial heterogeneity on the African continent between ~2.5 and 1.5 Ma ago (Antón et al., 2014; Bobe and Behrensmeyer, 2004; Potts, 2012).

Irrespective of the reasons or factors eventually leading to the evolutionary success of the human lineage while other coexisting species became extinct, archaeological and palaeoanthropological evidence from the Caucasus show that hominin groups started to settle ‘Out of Africa’ - and reached the edge of south-eastern Europe - by minimally 1.85 Ma ago (Ferring et al., 2011). The opening of a corridor for hominin dispersal from East Africa into Eurasia has often been linked with the end of the humid period at the onset of the Pleistocene (2.6 - 2.0 Ma) (Prat, 2016), during which mean annual temperatures and precipitation rates in the Mediterranean region were substantially higher compared to present-day conditions (Klotz et al., 2006; Leroy et al., 2011). Out of Africa events during the Pleistocene were sporadic and multidirectional (Antón et al., 2014; Garcea, 2016) and according to Prat (2016) “did not occur on a once-off basis, but as many discontinuous occupations, over more or less distant areas and at times with episodes of turning back”. Similar to the persisting debate why people initiated these dispersals from Africa - and the role of climatic and environmental changes or social factors in the process – it remains unclear where on the African continent human groups settled that contributed to the different migration waves, which routes they took and why (e.g. Garcea, 2012; Lahr, 2010), and whether hominin settlements in Europe during the Early Pleistocene were continuous

or discontinuous (e.g. Bermúdez de Castro et al., 2016; Dennell, 2003).

This thesis focusses on the western Mediterranean, a region of potentially high strategic importance for hominin dispersals out of Africa as well as for a late survival of Neanderthal populations on the European continent. With its exceptional archaeological and palaeoenvironmental record, the western Mediterranean is a key region to understand the possible role of north-western African populations in the colonisation of the European continent throughout the Pleistocene and Neanderthal displacement in southern Iberia. Of particular relevance to this work are two migration periods: The first European peopling during the Early Pleistocene (~1.6 - 0.8 Ma) and the dispersal of anatomically modern humans from Africa between 130 ka and 40 ka which lead to the eventual extinction of the indigenous Homo neanderthalensis in Eurasia (Fig. 1.1.1) (e.g. Garcea, 2016; Mellars, 2004; Prat, 2016; Villa and Roebroeks, 2014).

1.2.1. Out of Africa 1 and the early colonisation of Europe

While the earliest stone artefacts are known to occur ~3.3 Ma in Lomekwi 3, Kenya, in eastern Africa (Harmand et al., 2015), evidence for early human settlements in the Maghreb (defined here as Morocco, Algeria, Tunisia and western Libya) are not documented before ~1.7 Ma at Ain Hanech and El-Kherba, Algeria (Figs. 1.1.1 and 1.2.1; Parés et al., 2014; Sahnouni et al., 2002) and coincide with a period of increased aridity on the African continent (deMenocal, 1995, 2004). Although these early Maghrebian dates are not undisputed (Geraads et al., 2004), first hominin migrations into North Africa can be safely placed in a time period between 2.5 Ma and 1.2 Ma (Geraads and Amani, 1998; Raynal et al., 2001). The earliest archaeological sites discovered in the Levant and Europe are 'Ubeidiya, Israel (~1.5 Ma, Martínez-Navarro et al., 2009), Pirro Nord, northern Italy (1.3 - 1.6 Ma, Arzarello et al., 2012) and Orce, Iberia (~1.4 Ma, Toro-Moyano et al., 2013), respectively (Figs. 1.1.1 and 1.2.1).

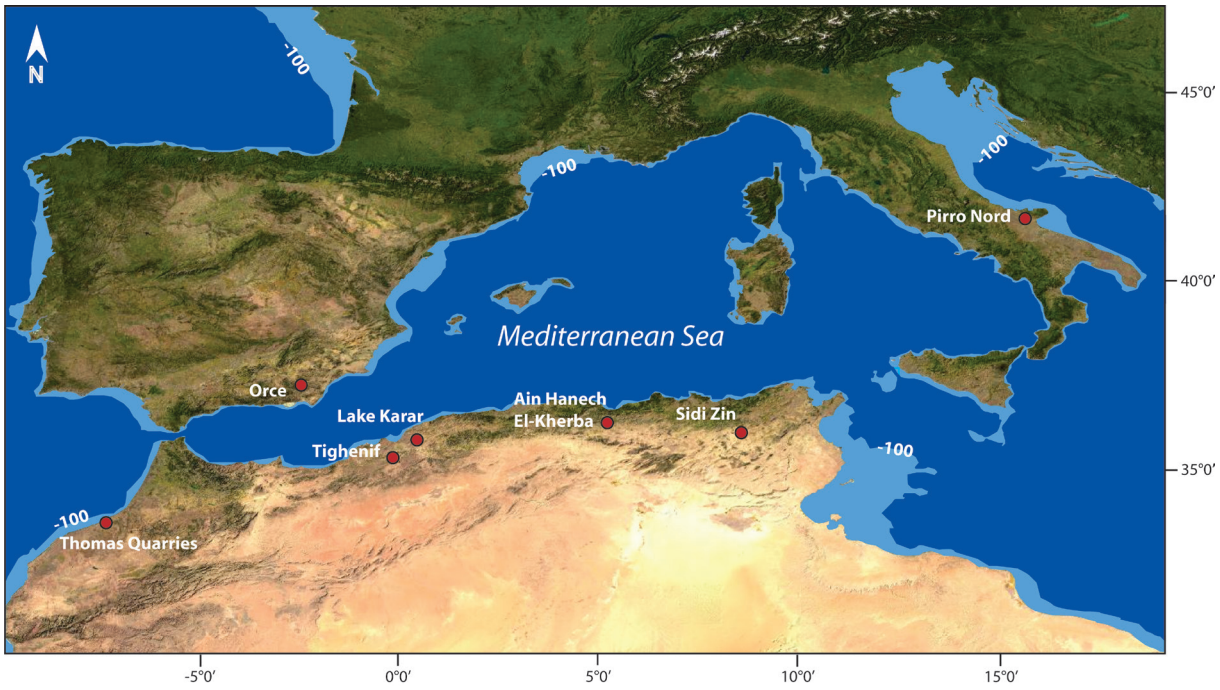

Fig. 1.2.1 Bathymetrical map of the western Mediterranean showing the present-day and the potential palaeo-coastlines during MIS 22, when sea-level was lowered by ~100 m (modified after EMODnet, 2017). Indicated are the locations of Lower Palaeolithic sites from the area mentioned in the text.

Although Early Pleistocene records of human settlements in Europe are sparse and the absolute dating of those sites highly challenging, current scientific evidence (i.e. from Dmanisi, Georgia (Ferring et al., 2011)) suggest a first colonisation of the continent by hominin populations coming from the east (Carbonell et al., 2008; Toro-Moyano et al., 2013). Researchers, however, strongly disagree about the continuity/discontinuity of those early human populations in Europe during the Early-Middle Pleistocene climatic transition (Clark et al., 2006) between 1.2 Ma and 0.7 Ma, when global climatic systems underwent major changes due to the establishment of large ice sheets in the northern hemisphere that covered major parts of the European landmass (Head and Gibbard, 2005; Maslin and Brierley, 2015; Ruddiman et al., 1989). Climate changes are likely to have caused a decrease in human population sizes with repeated episodes of local extinctions and periods of prolonged isolation in climatically favoured refugia, such as the Balkans, the Italian Peninsula and Iberia (e.g. Arribas and Palmqvist, 1999; Bermúdez de Castro et al., 2016; Dennell et al., 2011).

Directly related to this debate, is the similarly controversial question over the emergence of the Acheulian technocomplex in Europe – a distinctive stone tool industry mainly characterised by the production of bifaces (handaxes and cleavers) (Sharon, 2007) - which is placed by chronological evidence to roughly the same period of time, between ~1.0 Ma and 0.7 Ma (Sharon and Barsky, 2016). Central focus of this discussion is whether the European biface assemblages were i) a local European development or whether they originated outside of Europe ii) to the east in Asia or the Levant, or iii) to the south in Africa (e.g. Carbonell et al., 2016; Dennell et al., 2011). As sites yielding pre-Acheulian lithic assemblages in Europe are extremely rare, there is no solid scientific evidence supporting the local development theory (Sharon and Barsky, 2016). While the hypothesis of an eastern origin of the European Acheulian is primarily based on the finds from Caucasian sites (Amirkhanov et al., 2014; Gabunia et al., 2000; Lyubin and Belyaeva, 2006), more recent studies reinforce the potential significance of Northern Africa and suggest that the Acheulian in Europe may have originated through the straits of Gibraltar at times when the Mediterranean sea-level was significantly lowered i.e. during Marine Isotope Stage (MIS) 22 at ~0.9 Ma (Figs. 1.1.1 and 1.2.1; e.g. Alimen, 1975; Santonja et al., 2016; Sharon, 2011).

The strait of Gibraltar is currently ~14.5 km wide and according to Arribas and Palmqvist (1999) a sea-level drop of approximately 300 m would be required to close it, while a decreased sea-level of 100 m – as can be assumed for MIS 22 – would only narrow it (Fig. 1.2.1). Tectonic uplift during Quaternary times as evidenced by a sequence of raised shorelines in Gibraltar (Rodríguez-Vidal et al., 2004) has been used to emphasise that even the lowest Early Pleistocene sea-level lowstand would have had hardly any effect on the extent of the central channel of the Strait of Gibraltar (~5 km wide and 300 m deep) and early human crossings via that passageway are, therefore, considered highly unlikely (Derricourt, 2005; Muttoni et al., 2010; 2014). On the contrary, other authors have argued that a 100 m drop of the Mediterranean sea-level would have exposed several islands (Martinet and Searight, 1994) which together with changes in the salinity of Atlantic waters at that time (MIS 22) and the subsequently reduced intensity of the marine currents in the strait of Gibraltar (Gibert et al., 2003), would have facilitated contact between the Iberian Peninsula and the Maghreb (Lahr, 2010; Santonja and Pérez-González, 2010; Sharon, 2011).

The pre-Acheulian and Acheulian occupation record of the Maghreb is relatively sparse and many of the discovered sites lack chronological control. Acheulian lithic industries are i.e. documented at the sites of Tighenif and Lake Karar in northern Algeria as well as at Thomas Quarries in Morocco and Sidi Zin in northern Tunisia (Fig. 1.2.1; Lahr, 2010 and references therein). For these sites, researchers have made the attempt to produce absolute dates using different chronological methods in the past (e.g. Parés et al., 2014; Rhodes et al., 2006). Their results are, however, often limited by the uncertainties associated with the age estimates, the fact that only few archaeological layers could be dated for

each site or were strongly disputed among the scientific community. In order to understand whether the origin of the European Acheulian lies in North African and was brought to Europe by hominin populations crossing the strait of Gibraltar, further research at archaeological sites of that time period has to be conducted at both sides of the Mediterranean, including reliable absolute dating.

1.2.2. Out of Africa 2 – success and failure of anatomically modern human dispersals from North Africa

Throughout large parts of the Middle Pleistocene, succeeding the Out of Africa 1 migration period, hominin populations evolved separately within and outside of Africa (Hublin, 2009). During MIS 5, descendants of the African clade – early anatomically modern humans – living in North Africa initiated a dispersal into the Levant (often referred to as Out of Africa 2a, ~130 ka – 80 ka (Garcea, 2012)), where the fossil remains of Skhul and Qafzeh (both Israel; Fig. 1.2.2) provide the oldest evidence of AMHs outside of the African continent at between ~135 ka and 100 ka (Fig. 1.1.1; Grün, 2006; Grün et al., 2005). Since this thesis particularly focusses on the western Mediterranean region, the southern AMH dispersal route from Africa – through East Africa into the Arabian peninsula (Armitage et al., 2011; Beyin, 2011; Lahr and Foley, 1994) – is not discussed any further. Of great importance is, however, the northern passageway which included dispersals through north-eastern Africa and the Nile corridor, the Sahara and the Mediterranean coast into the Levant (Garcea, 2016 and references therein).

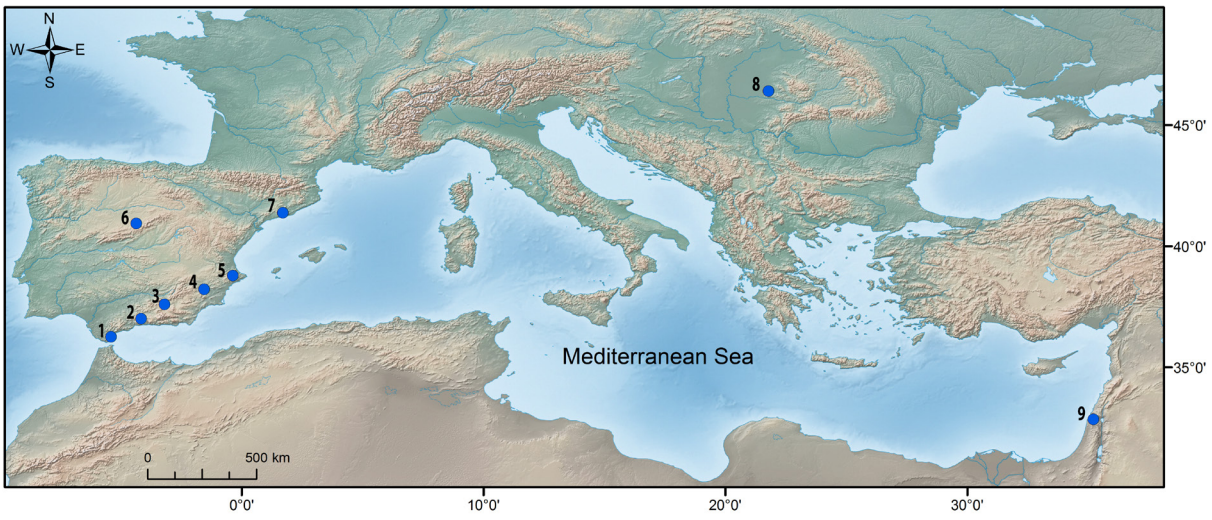

Fig. 1.2.2 Location of the Middle and Upper Palaeolithic sites mentioned in the text. 1 – Gorham's Cave; 2 – Zafarraya; 3 – Carihuela; 4 – Cueva Antón; 5 - El Salt; 6 – Abrigo del Molino; 7 – Cova del Rinoceront; 8 - Peştera cu Oase; 9 – Skhul and Qafzeh.

Climatic conditions became less hospitable - including rapid cooling and increased aridity (Rampino and Self, 1992) - between MIS 5a and MIS 4 (~74 ka) in the south-western Mediterranean basin (Cheddadi and Rossignol-Strick, 1995; Timmermann and Friedrich, 2016; Whiting Blome et al., 2012). This, together with the potential failure in the competition for resources against Neanderthals – the descendants of a western Eurasian clade living in Europe and the Levant – resulted in a massive decline of AMH populations living in the Levant (if not complete depopulation) between about 80 ka and 50 ka (Garcea, 2010a; Shea, 2003, 2010), whereas Neanderthals were still present throughout MIS 4, until about 45 ka (Bailey et al., 2008; Shea, 2008).

Another major dispersal wave was initiated by African AMHs (Out of Africa 2b, Fig. 1.1.1) after 60 ka, which eventually resulted in the displacement of Neanderthals in the Levant and a further expansion of

AMHs into other parts of Europe and Asia (e.g. Mellars, 2006; Shea, 2010; Timmermann and Friedrich, 2016). Various reasons have been proposed to explain the success of Out of Africa 2b compared to the 2a event, i.e. more favourable climatic conditions during MIS 3 (Heterington and Reid, 2010), strong demographic pressure on Neanderthal populations (Powell et al., 2009), AMH adaptation skills (McBrearty and Brooks, 2000), competitive exclusion (Banks et al., 2008) and improved technological equipment, namely projectile armatures (Lombard and Phillipson, 2015; Shea and Sisk, 2010).

While recent genetic evidence has emphasised the role of North Africa for AMH dispersals out of the continent by associating Neanderthal-AMH interbreeding - dated to between 65 ka and 47 ka - with North African populations (Pagani et al., 2015; Sankararaman et al., 2012), little is known about the advent of cultural modernity in AMHs which might be the key factor to understand the evolutionary success of our lineage over Neanderthals (d'Errico et al., 2009; McBrearty and Brooks, 2000; Vanhaeren et al., 2006). The emergence of behavioural modernity – typically associated with instances of symbolic artefacts, pigment use, engravings or formal bone tools at archaeological sites (e.g. d'Errico and Vanhaeren, 2007; Klein, 2008; Kuhn and Stiner, 2007; McBrearty and Brooks, 2000) – in the Maghreb is usually linked to the Middle Stone Age (MSA) lithic technocomplex called the Aterian. This technocomplex is primarily characterised by the appearance of pedunculated tools and bifacial foliates but also known for the presence of blades, bladelets, end-scrapers, small Levallois cores and personal ornaments (Bouzouggar and Barton, 2012). Consequently, many studies have focussed on the technological definition, the timing and the geographical distribution of the Aterian industry to investigate the advent of cultural modernity in AMH populations, and to understand the drivers of population mobilisation out of Northern Africa (e.g. Bouzouggar and Barton, 2012; d'Errico et al., 2009; Garcea, 2010b). Despite the significant progress made in this research field over the last years (see e.g. reviews by Garcea, 2016; Reyes-Centeno, 2016), we still do not fully understand where, when and why technological innovations took place and modern human behaviour emerged on the Africa continent between Out of Africa 2a and 2b and which of the proposed North African migration routes were critical for the eventual AMH dispersal into Eurasia.

1.2.3. Neanderthal habitation of southern Iberia

At the time when AMHs arrived in Europe around 50 ka (Hublin, 2012), they came in contact with indigenous Neanderthal populations living in western Eurasia (Mellars, 2004). Genetic evidence suggest that ancestors of modern humans split from the source population of Neanderthals and Denisovans – a sister group recently identified in the Russian Altai (Meyer et al., 2012) – at the beginning of the Middle Pleistocene, between 765 ka and 550 ka (Meyer et al., 2016). Early Neanderthal artefact assemblages can be classified as Acheulian, while with the onset of the Middle Palaeolithic (~300 ka, MIS 8) archaeological records are characterised by the advent of the Levallois technology (Roebroeks and Soressi, 2016). Levallois is a hierarchical core reduction strategy which entails, according to Adler et al. (2014), the "multistage shaping […] of a mass of stone (core) in preparation to detach a flake of predetermined size and shape from a single preferred surface" (see also Boëda, 1994, 1995). The first AMH fossils in Europe were found in Peştera cu Oase, Romania (Fig. 1.2.2; Trinkhaus et al., 2013). The two main specimens, a mandible (Oase 1) and a skull from a second individual (Oase 2), were directly dated and revealed for the latter a minimum age of 33.5 kcal BP (28.9 +∞/-0.2 ka BP, Trinkhaus et al., 2013), while the former gave an age close to 40 kcal BP (34.3 +1.0/-0.8 and >35.2 ka BP, Trinkaus et al., 2003) which is around the same time when Neanderthals disappeared from most archaeological records on the continent (~40 ka, Villa and Roebroeks, 2014; Zilhão, 2013).

The timing and causes for the demise of the late Neanderthals in Europe is one of the central topics

in palaeoanthropology, and - since it remains unresolved - matter of an ongoing debate. Recent studies have argued that the widely assumed "superiority" of AMHs over Neanderthals – in terms of i.e. weaponry, subsistence strategies and cooperation skills (e.g. Marean, 2015 and references therein) – appear to be less profound than previously thought (Roebroeks and Soressi, 2016; Villa and Roebroeks, 2014). Scientific evidence from the last decade support this view by showing that Neanderthal populations were very similar to their AMH contemporaries in terms of diet, fire use, stone tool technologies and even symbolic behaviour (e.g. Bar-Yosef and Pilbeam, 2000; Finlayson et al., 2012; Henry et al., 2014; Roebroeks and Villa, 2011). Nonetheless, following Roebroeks and Soressi (2016), "there is no doubt that the Neanderthal phenotype ultimately disappeared through (some form of) competition with modern humans" in Eurasia within just a few thousand years, "even though the specifics of that process […] are largely unexplored". Higham et al. (2014) recently quantified the temporal overlap between the two hominin groups on the European continent to 2,600 - 5,400 years, while emphasising that Neanderthal disappearance occurred in different regions at different times.

In the past, the south of the Iberian Peninsula has often been interpreted as an ecological refugium for late Neanderthals with the Ebro River and the Cantabrian Cordillera serving as natural barriers between the areas in the south and the rest of Europe (e.g. d'Errico and Sánchez Goñi, 2003; Zilhão, 2006), a view supported by a number of palaeoenvironmental studies (de Abreu et al., 2003; Moreno et al., 2005; Roucoux et al., 2005; Sánchez Goñi et al., 2000, 2002). Radiocarbon dates from sites like Carihuela, Zafarraya (both Spain) and Gorham's Cave (Gibraltar; Fig. 1.2.2) placed the survival of Neanderthals in southern Iberia to post-42 ka (Fernández et al., 2007; Hublin et al., 1995; Pettitt and Bailey, 2000) and maybe even as late as 28 ka (Finlayson et al., 2006). These dates were, however, strongly disputed by Higham and colleagues, who argue that those early dates suffer from incomplete removal of contamination in the collagen (Higham et al., 2014; Wood et al., 2013). Nevertheless, there still remain reliable evidence for Neanderthal presence in southern Iberia after 40 ka i.e. Cueva Antón, shortly after 38.5 kcal BP (Zilhão et al., 2010a).

While comparatively many studies contribute to the ongoing discussion about the Neanderthal demise in southern Iberia (e.g. Bar-Yosef and Pilbeam, 2000; d'Errico and Sánchez Goñi, 2003; d'Errico et al., 1998; Finlayson et al., 2006; Higham et al., 2014; Zilhão et al., 2010b), relatively little attention has been paid to the time range preceding the last 50 ka. In part this is due to the overwhelming reliance on radiocarbon dating in archaeology which is limited to ~50 ka (Reimer et al., 2016). It is, however, exactly this period of time that has the potential to shed further light into the history of Neanderthal populations and their subsistence strategies in the region, which might eventually help us to better understand the causes of their final extinction in the Iberian Peninsula. Authors have just recently started to fill this gap by providing reliable chronostratigraphies for archaeological cave sites (Fig. 1.2.2) and their palaeoenvironmental context located mostly in the inland – i.e. Cuevá Anton (~80-35 ka, Zilhão et al., 2016), Abrigo del Molino (60-31 ka, Álvarez-Alonso et al., 2016) and El Salt (60-45 ka, Galván et al., 2014) – but also at the Mediterranean coast – Cova del Rinoceront (~210-74 ka, Daura et al., 2015) – of Iberia safely covering MIS 6 to 3.

1.3. Dating Palaeolithic cave sites

Our understanding of the timing of human occupation and palaeoenvironmental changes in a region largely depends on the reliability and suitability of Quaternary dating techniques which enable comparisons between stratigraphical layers on site, regional and global scale (Lowe and Walker, 2015). The most widely applied radiometric methods for dating Palaeolithic cave sites are radiocarbon, luminescence (comprising thermoluminescence (TL) and optically stimulated luminescence (OSL)), U-series and ESR (Electron Spin Resonance) (Fig. 1.3.1). These techniques allow reliable age determination of a variety of different materials, which directly (i.e. bones, charcoal, teeth and heated flint) or indirectly (i.e. sediments and speleothems) store archaeological evidences at those sites and have successfully been used in the past to i.e. date the Middle Pleistocene Neanderthal occupation in Sima de los Huesos ~430 ka (Arsuaga et al., 2014), the use of personal ornaments at MSA sites in Morocco (d'Errico et al., 2009) and Palaeolithic cave art in Iberia (Pike et al., 2012), as well as to reconstruct how wet phases in North Africa affected AMH migration out of and back to the continent (Hoffmann et al., 2016).

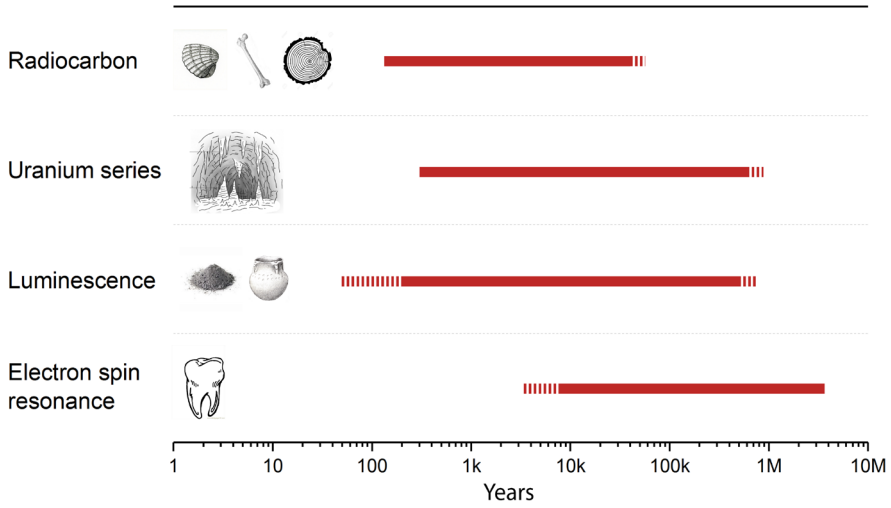

Fig. 1.3.1 The effective dating ranges of the different Quaternary dating techniques mentioned in the text after Walker (2005) and some examples of materials which are typically dated using those methods.

The radiocarbon method (for further methodological details see Jull and Burr, 2015) is undeniably of crucial importance for dating Palaeolithic sites as it provides highly precise ages for organic-bearing archaeological finds (Pollard, 2009; Taylor, 2001). It is, however, restricted by the preservation of collagen in the samples (when dating bones), an upper dating limit of ~50 ka and a calibration to cosmic ray flux through time (Brock et al., 2012; Reimer et al., 2016). While luminescence, ESR and U-series dating, on the other hand, have the advantage of covering much older time periods (usually the whole Middle Palaeolithic, sometimes even parts of the Lower Palaeolithic) by using inorganic materials for dating, determined absolute ages are commonly associated with comparatively larger uncertainties.

Out of all the above-mentioned methods, OSL dating is the least restricted as it determines the time elapsed since sediments were last exposed to sunlight. In principle, it can be used for any given archaeological site, as i) the material desired for age determination - mineral grains such as quartz and feldspar - is ubiquitous in natural sedimentary environments and ii) the only crucial prerequisites are its sufficient contact with sunlight prior to deposition and a consistent dose rate through time (Aitken, 1998). Although the accumulation age of a sediment layer, within which archaeological finds are located, is not per se identical with the age of the human activity reflected by those finds (i.e.

due to redeposition by geologic forces), OSL is a widely applied dating method for Palaeolithic sites (Jacobs and Roberts, 2007) and usually complemented by detailed sedimentological investigations of the stratigraphical context of each sample to ensure the significance of the obtained dates (Feathers, 2015).

It is now almost 20 years since Duller et al. (1999) and Bøtter-Jensen et al. (2000) presented their technical improvements of the standard Risø OSL/TL reader which extended the field of applications for OSL dating to resolve issues of i.e. post-depositional mixing in archaeological sediment layers (Jacobs and Roberts, 2007) by enabling routine measurements of the luminescence signal stored in individual sand-sized quartz grains. Before that only multiple-grain aliquots (containing many grains which are measured simultaneously) could be measured in greater quantities within reasonable times. Further favoured through the development of a new OSL measurement protocol by Murray and Wintle (2000, 2003) at about the same time – the single-aliquot regenerative-dose (SAR) protocol (chapter 1.6.5) - single-grain dating became, over the following years, an increasingly used tool for establishing chronologies of sediment deposits in archaeological contexts all over the world (e.g. Fitzsimmons et al., 2014; Guérin et al., 2012; Jacobs et al., 2011). There are, however, several aspects of single-grain quartz OSL dating – mostly concerning the variability observable in the luminescence behaviour of individual grains within one sample - which up until now remain inexplicable (Jacobs and Roberts, 2007). These include i.e. the occurrence of an extra component of random variation (called overdispersion) in single-grain distributions which restrict the precision of the final age estimates and hamper our ability to distinctly separate different age populations within one sample (Galbraith et al., 1999; Thomsen et al., 2007). Additional complications may arise when sediment samples i) are close to saturation (indicating the upper limit for age determination) or ii) yield large proportions of individual grains which emit luminescence signals unsuitable for OSL dating or no signal at all. While various alternative techniques have been proposed to extend the age range of standard quartz OSL (e.g. Ankjærgaard et al., 2016; Arnold and Demuro, 2015; Singarayer and Bailey, 2003; Wang et al., 2006), conventional multiple-grain and single-grain dating remain the first choice for establishing reliable chronostratigraphies at Palaeolithic cave sites.

1.4. Research questions

The overview of the current knowledge on the history of hominin evolution, dispersal and displacement in the western Mediterranean region shows there are still gaps that hamper our understanding of the contribution of north-western African populations in the colonisation of the European continent and Neanderthal subsistence in southern Iberia prior to the arrival of AMHs in the region. This is despite significant progress made in terms of methodological approaches in the fields of palaeoenvironmental, geochronological and archaeological research in recent years, which have enabled more precise reconstructions of palaeoenvironmental conditions and how hominin groups adapted to those throughout Pleistocene times.

Archaeological caves can safely store records of human activity and climatic fluctuations in their stratigraphical sequences and, therefore, have the potential to provide optimal conditions for studying human-environmental interactions, patterns of human dispersal and the emergence of new lithic technologies or behavioural indicators in a certain region in the past. Fundamental to all those studies are, however, solid geochronological frameworks coupled with archaeological, geological and sedimentological analyses of the Palaeolithic sequences at the investigated sites. Consequently, this thesis addresses the following research questions:

1. *To what extent can reliable chronostratigraphies for archaeological cave sites advance our understanding of Palaeolithic human behaviour and dispersal events in the western Mediterranean?*

2. *To what extent do sedimentary cave records provide evidence of climatic changes throughout the Pleistocene in the region?*

OSL is one of the key methods for establishing absolute chronologies of Pleistocene sedimentological sequences in geological and archaeological contexts all over the world. Of particular relevance for Palaeolithic cave sites is the single-grain dating approach which allows identification of multiple discrete age populations within a single stratigraphic layer. However, the suitability of a certain sediment sample for OSL dating and, consequently, the soundness of its final calculated OSL age, largely depend on the luminescence characteristics of the individual mineral grains desired for age determination. A basic understanding of those characteristics and of potential factors which might have falsely altered the determined burial age of a sediment sample - resulting in substantial over- or underestimations - are crucial for building reliable chronostratigraphies of Palaeolithic cave sites. Therefore:

3. *What are the quartz luminescence characteristics of the investigated Moroccan and southern Iberian sediments? How variable are they at site and regional scale through time?*

4. *What are the challenges to single-grain OSL dating in Palaeolithic cave sites in the western Mediterranean?*

Necessary to answer those research questions are archaeological sites at both sides of the Mediterranean Sea that provide detailed records of Palaeolithic hominin occupation and behaviour, palaeoenvironmental changes, and contain quartz-rich sediments suitable for OSL dating. The case study sites Thomas Quarries and Rhafas in Morocco are known for their Early to Middle Pleistocene and Middle to Late Pleistocene stratigraphical sequences, respectively and, therefore, bear great potential to improve our understanding about the role of northwest African hominin populations in Out of Africa human dispersal events and for the emergence of cultural modernity in AMHs. Vanguard Cave is a Palaeolithic site at the southernmost tip of the Iberian Peninsula providing information about environmental conditions and hominin subsistence strategies during times of Neanderthal dominance in the region since the last interglacial. The next section (chapter 1.5) will briefly introduce the case study sites while in the subsequent chapter 1.6 a methodological overview on OSL dating is given.

1.5. Study sites

This section aims to introduce the Palaeolithic sites studied in this thesis by giving brief overviews of their past research history and summarising their archaeological and geological context. The three main sites discussed in this thesis are located in the western Mediterranean: the cave of Rhafas and the Thomas Quarries are situated in north-eastern and western Morocco, respectively; Vanguard Cave on the other hand faces the Mediterranean Sea at the present-day shoreline of Gibraltar (Fig. 1.5.1). For a methodological study (chapter 4), OSL samples from an archaeological site in Australia, Lake Mungo, are used for comparative reasons; the site is briefly introduced in chapter 1.5.4.

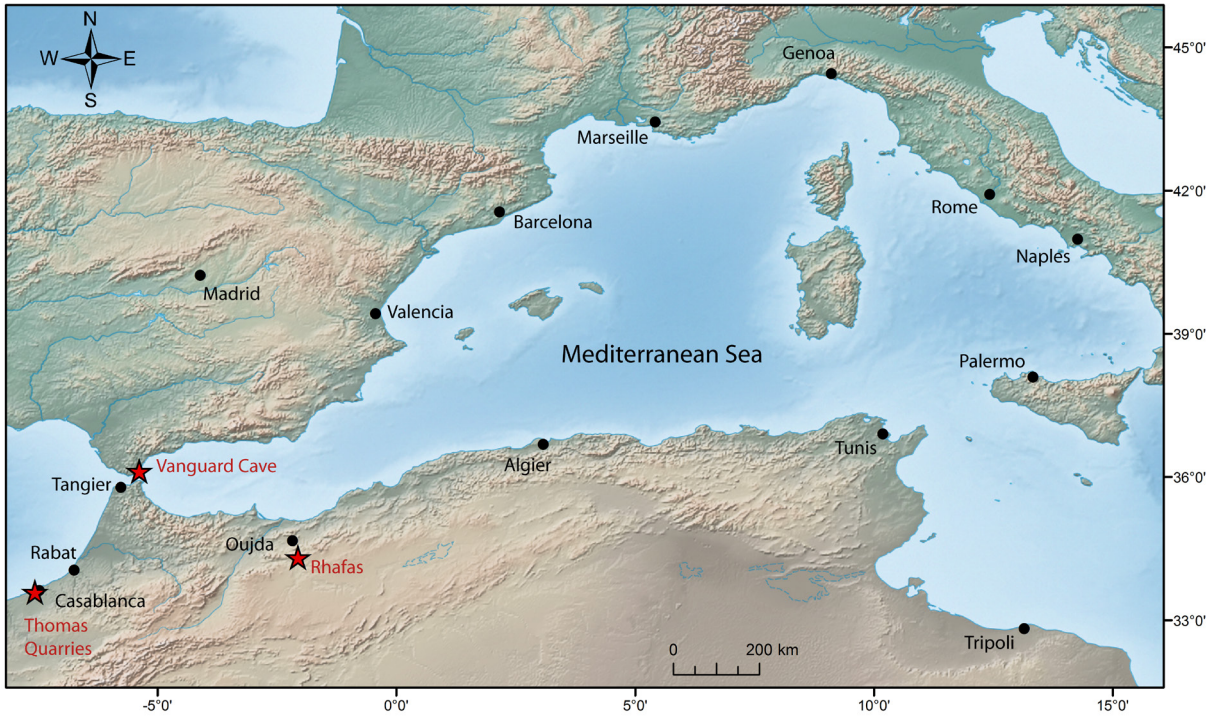

Fig. 1.5.1 Location of the three main study sites of this thesis in the western Mediterranean.

1.5.1. Rhafas Cave, Morocco

Rhafas is an inland archaeological cave site (Fig. 1.5.1) located in the Oujda Mountains in north-eastern Morocco, about 30 km south-eastwards from the city of Oujda and ~900 m above present-day sea-level (Fig. 1.5.2). Since its discovery in 1950, the site experienced several series of systematic excavations first by J.-L. Wengler (e.g. Wengler, 1993; 1997) and, since 2007, by the current excavation team headed by researchers from the Institut National des Sciences de l'Archéologie et du Patrimoine, Rabat, and the Max Planck Institute for Evolutionary Anthropology, Leipzig. With its long stratified archaeological sequence spanning the MSA (including the Aterian) through to the Neolithic, Rhafas contains valuable information about human occupation and dispersal, and cultural changes during the Palaeolithic in north-western Africa. Furthermore, the mostly aeolian sediment deposits at Rhafas – which were partly affected by post-depositional carbonate cementation – provide an important archive of past palaeoenvironmental conditions in the area on a local and regional scale.

The geology in the cave's surrounding is characterised by Palaeozoic substratum unconformably overlain by predominantly Mesozoic carbonates (Fig. 1.5.3, Talbi and Boudchiche, 2012). While the Palaeozoic units are composed of various types of metasediments, volcanic rocks and granitoids of Ordovician to Carboniferous age, the Mesozoic deposits consist mainly of Jurassic dolomite and limestone. The cave itself is situated within a limestone cliff that forms the local hilltop on the north-western slope of a prominent northeast/southwest trending valley (Fig. 1.5.2). The limestone unit unconformably overlies highly deformed meta-sediments and a coarse grained granodiorite that forms the valley floor (Fig. 1.5.3). During the Quaternary, the cave was filled with sand- and silt-rich aeolian sediments.

Since the 1990s, the lithic artefact assemblages of Rhafas, their cultural attribution and the palaeoclimatic conditions during times of human occupation of the cave in the Late Pleistocene and Holocene had been subject of numerous published studies by Wengler and colleagues (Wengler, 1997, 2001; Wengler and Vernet, 1992; Wengler et al., 2002). An absolute chronometric classification of the archaeological layers of Rhafas, however, was not realised until Mercier et al. (2007). For their study,

selected samples were collected from the upper part of the cave fill sequence for thermoluminescence, OSL and radiocarbon dating and revealed ages (twelve TL, one OSL and two ^{14}C) for five archaeological layers of up to 107 ka (Mercier et al., 2007).

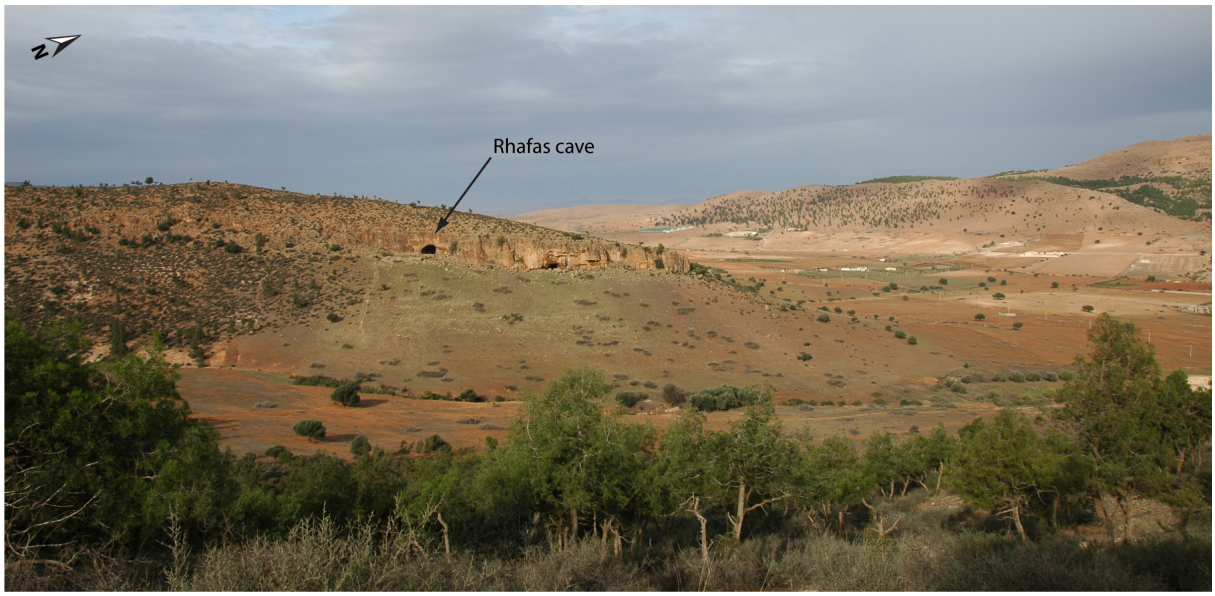

Fig. 1.5.2 Photograph of the Rhafas cave site.

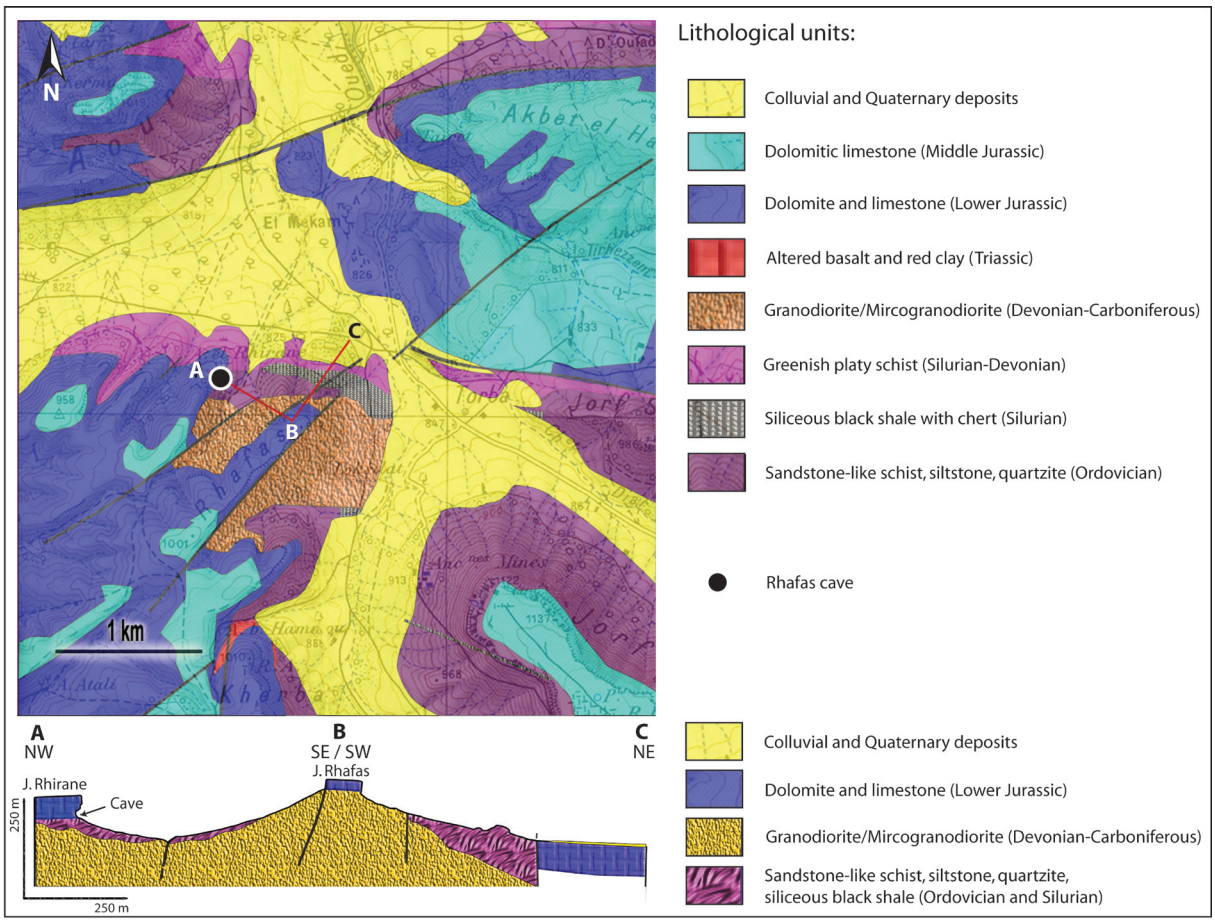

Fig. 1.5.3 Geological map and NW-SE-NE cross section of the Rhafas area (modified after Talbi and Boudchiche, 2012).

The recent field campaign included beside renewed excavations in the cave also the opening of new excavation squares on the relatively flat and terraced area in front of its entrance (Fig. 1.5.4). Geological evidence suggests that this area was formerly part of the cave itself. The large limestone boulders that are widely spread throughout the lower stratigraphical units of the terrace section are likely to represent the collapsed remains of the old cave roof. Some of the stratigraphical layers in this section are attributed to the LSA, a technocomplex which was previously thought to be missing at the site, as it is not preserved in the cave fill sequence.

Fig. 1.5.4 Photographs of the Rhafas cave site with the location of the different excavation sections.

1.5.2. Thomas Quarries, Morocco

The Thomas Quarries are a complex of Palaeolithic quarry sites (Thomas I, Thomas III and Oulad Hamida I) located in the area of Casablanca, western Morocco (Fig. 1.5.1), which is characterised by a series of large Quaternary shoreline barrier systems sub-parallel to the present shoreline of the Atlantic Ocean (Raynal et al., 2001). Since the beginning of a joint Moroccan-French research program in 1978, researchers established an extensive lithostratigraphical, biostratigraphical and archaeological framework for the area (e.g. Daujeard et al., 2016; Geraads et al., 1980; Lefevre et al., 1994; Raynal et al., 2010; Texier et al., 1994). Today the long geomorphological sequence at Casablanca is not only famous for reflecting global Quaternary sea-level fluctuations over the past 5.5 Ma (Lefevre et al., 1994; Texier et al., 1994), but also for the preservation of up to ~1 Ma old Acheulian artefacts (Raynal and Texier, 1989; Rhodes et al., 2006), and for containing rich faunal assemblages (Daujeard et al., 2012; Raynal et al., 1993) as well as Middle Pleistocene human fossils (Ennouchi, 1969; Raynal et al., 2010).

Each of the barrier systems reflect a cyclic deposition comprising underlying marine units covered by aeolian sediments and were affected by intensive post-depositional cementation (Fig. 1.5.5). The Oulad Hamida morpho-stratigraphic unit – within which the Thomas Quarries are situated - represents several major episodes of coastal sedimentation, fossilization and eventual cave development during the final Early and early Middle Pleistocene (Texier et al., 2002). The Hominid Cave (Fig. 1.5.6) at Thomas

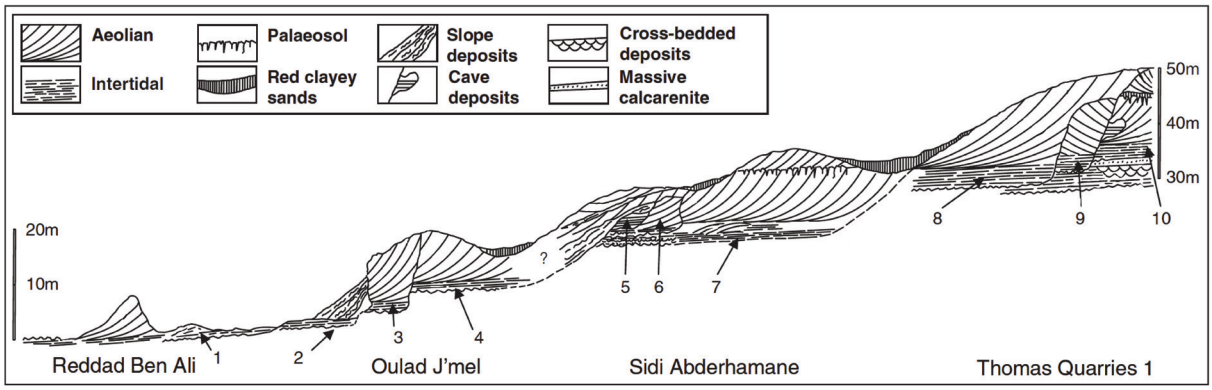

Fig. 1.5.5 Stratigraphic cross section showing the inferred relationships and relative altitudes above present day sea-level of the Quaternary sites Reddad Ben Ali, Oulad J'mel, Sidi Abderhamane and Thomas Quarries I after Texier et al. (2002) (modified after Rhodes et al., 2006). Marine units are numbered in reversed chronological order.

Fig. 1.5.6 Photograph of the Thomas Quarry I site with the location of the Locus I and the Hominid Cave.

Fig. 1.5.7 Photograph of the Rhino Cave site with the location of the upper and lower cave sections.

Quarry I and the Rhino Cave (Fig. 1.5.7) at Oulad Hamida I, are cave sites filled with sediments dated to the Early and Middle Pleistocene based on litho- and biostratigraphy (Geraads, 2002) and absolute dating (between 360 and ~1 Ma using OSL, ESR, U-series and laser ablation ICP-MS) (Raynal et al., 2010; Rhodes et al., 1994; 2006). Despite the large variety of dating methods applied at the Thomas Quarries so far, sample numbers were small (ESR: four rhinoceros teeth, U-series: one speleothem age, laser ablation ICP-MS: one human premolar (Raynal et al., 2010; Rhodes et al., 1994; 2006)), and estimated absolute ages not always consistent with the previously established stratigraphical and lithological interpretation (OSL (Rhodes et al., 2006)).

1.5.3. Vanguard Cave, Gibraltar

The archaeological site of Vanguard Cave is part of a complex of limestone caves which are situated close to the present Mediterranean sea-level at the south-eastern coast of the Gibraltar promontory (Figs. 1.5.1, 1.5.8). Gibraltar is well known for its Neanderthal cave sites which preserve rich archaeological records, including human fossil remains (Busk, 1865; Garrod et al., 1928; Sollas, 1908), and provide evidence for Neanderthal habitation in the south-western extreme of the Iberian Peninsula throughout the Middle Pleistocene (e.g. Barton et al., 2013; Finlayson and Carrión, 2007; Jiménez-Espejo et al., 2013) and maybe even until 28 ka BP (Finlayson et al., 2006).

Fig. 1.5.8 Photographs of the Gorham's and Vanguard Cave sites located at the present shoreline of Gibraltar (modified after www.visitgibraltar.gi).

The Rock of Gibraltar is composed of Early Jurassic limestones and dolomites; the general shape of the promontory, however, was formed mainly as a consequence of the collision between the African and Eurasian tectonic plates in the early Miocene (Rose and Rosenbaum, 1994). In the course of this tectonic activity, the Mediterranean Sea was cut off from the Atlantic Ocean and gradually dried out during the Messinian salinity crisis (~5.6 Ma, Krijgsman et al., 1999). It was only at the beginning of the Pliocene, at 5.33 Ma, that Atlantic waters found a way through the Strait of Gibraltar and refilled the Mediterranean – an event known as the Zanclean flood (Blanc, 2002; Garcia-Castellanos et al., 2009).

Later, neotectonic uplift and eustatic fluctuations combined with surface erosional and depositional processes formed the shape of the Gibraltar promontory as it exists today with e.g. elevated marine terraces, steep cliffs and staircased slopes (Rodríguez-Vidal et al., 2004). During the Pleistocene, the east side of the Rock experienced substantial aeolian accumulation, with windblown sands filling considerable parts of the local caves (e.g. Vanguard, Gorham's and Ibex) which served as large sediment traps.

Marine highstands which are best developed to the south and the east of the Rock represent at least 12 palaeo-shorelines at heights up to 300 m above present-day sea-level (Rose and Rosenbaum, 1994). Raised terraces associated with the last interglacial – an episode which is well represented by several highstands along the southern Iberian littoral (Zazo et al., 2003; Zazo et al., 1999) - are located at 5 m (MIS 5c) and 2 - 1.5 m (MIS 5a) above sea-level at Gibraltar today (Zazo et al., 1994). No younger raised marine terraces are recorded along the Iberian coastline (Rodríguez-Vidal et al., 2004) as the sea-level significantly dropped after the end of MIS 5 until it reached a minimum (~125 m below present level, Fig. 1.1.1) during the last glacial maximum after which it raised again and reached its current height ~6.000 years ago (Miller et al., 2005).

Despite the great scientific interest on the archaeological content of the Gibraltar caves since the discovery of a Neanderthal cranium at Forbes' Quarry in 1848 (Busk, 1865), most studies in the past focussed almost exclusively on Gorham's Cave (Fig. 1.5.8, e.g. Blain et al., 2013; Carrión et al., 2008; Finlayson et al., 2006; Waechter, 1951, 1964) and it was only relatively recently (1995) that first excavations started at Vanguard Cave as part of the Gibraltar Caves Project (Barton et al., 2013; Stringer et al., 2000). Deposited on top of an MIS 5 marine terrace, the cave is filled with >17 m of sand-rich sediments which contain traces for multiple Palaeolithic occupation phases. Chronometric studies by Pettitt and Bailey (2000) and Rhodes (2013) used radiocarbon and OSL dating to provide age estimates for the Vanguard Cave profile. Unfortunately, both studies were limited by relatively small sample sizes and yielded conflicting dating results that placed the age of the uppermost stratigraphical layers to either ~45 ka (Pettitt and Bailey, 2000) or ~74 ka (Rhodes, 2013).

1.5.4. Comparative site: Lake Mungo, Australia

Lake Mungo is a presently dry lake in the Willandra Lakes Region World Heritage Area in the semi-arid zone of south-eastern Australia (Fig. 1.5.9). It preserves a unique archaeological and palaeoenvironmental record and is renowned for some of the earliest archaeological traces of AMHs on the Australian continent, including the world's oldest known cremation and ritual burial (Bowler et al., 2003; Bowler et al., 1970; Bowler and Thorne, 1976). In the past, the Willandra Lakes served as an overflow for the Willandra Creek which had its headwaters in the south-eastern Australian highlands (~1000 km to the east). During the last glacial cycle the lake lunettes experienced episodic sediment deposition, therefore providing important archives reflecting changes in lake palaeohydrologies and human activity for this time period in the area (Bowler, 1998; Stern, 2008).

Over the last decades, the Lake Mungo lunette had been subject to numerous archaeological and palaeoenvironmental studies, including absolute dating (e.g. Adams and Mortlock, 1974; Allen, 1998; Bowler et al., 2012; 2003; 1970; Fitzsimmons, 2017; Fitzsimmons et al., 2014; 2015; Olley et al., 2006). Fitzsimmons et al. (2014; 2015) published chronometric studies on the depositional history of the lunette (ca. 50–3 ka) and its archaeology based on single-grain OSL dating of sediment samples collected from the central portion of the landform. The sediments from the Lake Mungo lunette yield quartz-rich deposits well suited for OSL dating due to relatively high proportions of datable sand-sized grains which exhibit bright, rapidly decaying luminescence signals (Fitzsimmons et al., 2014). The

high sensitisation of the quartz can be attributed to multiple cycles of exposure and burial within the sedimentary system before the eventual deposition at the Lake Mungo lunette (Fitzsimmons, 2011). Feldspar contamination of the quartz is low and although equivalent dose distributions for the younger, Holocene-age samples are comparatively wide - potentially related to dose rate heterogeneities within the sediments as has been reported by Lomax et al. (2007) for dune samples from the Murray-Darling Basin, south-eastern Australia - most of the age distributions are of Gaussian shape, indicating absence of post-depositional mixing in the stratigraphical layers and complete bleaching of the sediments during the last transportation process before burial (Fitzsimmons et al., 2014). The sediments from Lake Mungo, consequently, yield highly sensitised quartz well suited for OSL dating studies which have similarly been reported for various other sites from the Australian continent (e.g. Fitzsimmons et al., 2010; Pietsch et al., 2008; Roberts et al., 1999; Westaway, 2009).

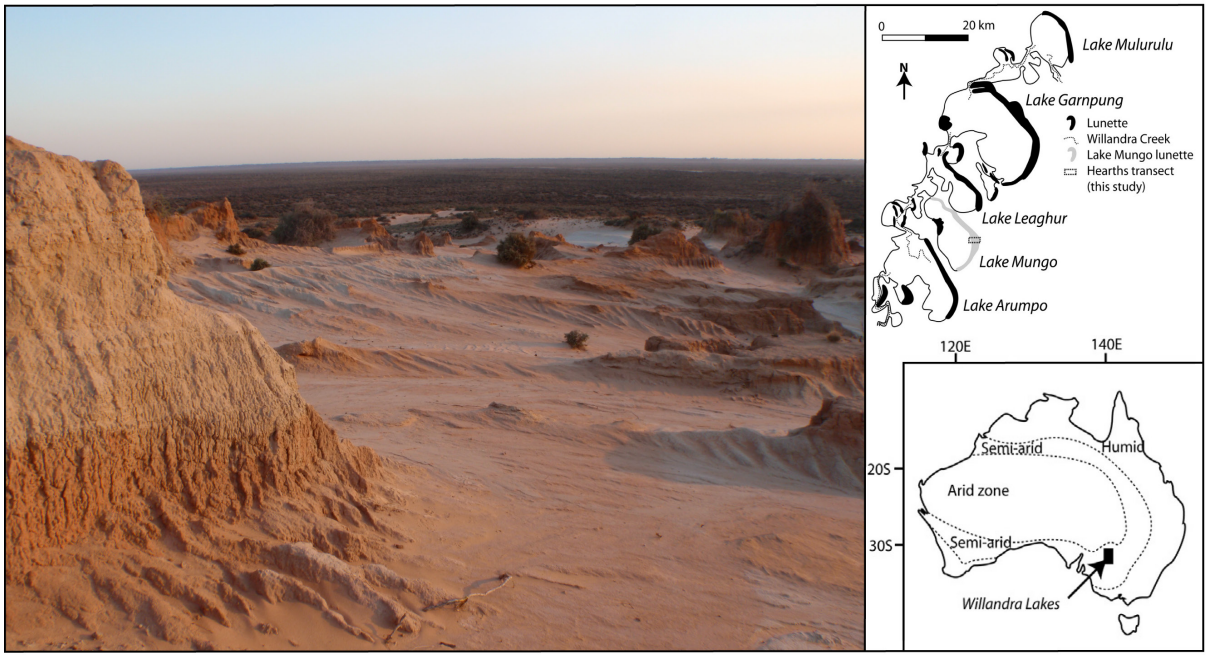

Fig. 1.5.9 Photograph and map of the Lake Mungo lunette within the Willandra Lakes Region in south-eastern Australia (modified after Fitzsimmons et al., 2014).

1.6. Optically Stimulated Luminescence dating

Luminescence is a remarkable, natural phenomenon that was already described as references to fireflies in Chinese literature about 3000 years ago (Harvey, 1957). While bioluminescence manifests in form of e.g. glow worms or luminous bacteria, more relevant to optical dating is the ‘cold light’ luminescence emitted by gems and stones which is known at least since Aristotle times (~2000 years ago) (Harvey, 1957). While the luminescence behaviour of plants, stones and animals was again described by Gesner (1555), first scientific studies on luminescence started not before the mid-seventeenth century when Robert Boyle investigated the encompassing luminescence behaviours of a ‘carbuncle’ – a diamond with the property to emit cold light; he even took the stone with him to bed, warmed it up with his body and described its elicited glimmering light (Boyle, 1664).

Scientific interest in luminescence grew after the advent of photomultiplier - a very sensitive detector of light – near the middle of the twentieth century (Aitken, 1998). In the following decades, increasing numbers of studies were performed eventually leading to the demonstration that the depositional age of sediment can be successfully determined by means of stimulation with visible light (Huntley et al., 1985). Since then, optical dating of quartz and feldspars (Hütt et al., 1988) became a widespread and

powerful tool commonly used in archaeology and Quaternary geology, as it enables the reliable dating of the last sunlight contact of material - ubiquitous in nature – even if this event took place several hundreds of thousands of years ago.

1.6.1. General principles of OSL dating

Luminescence dating techniques are based on the property of naturally occurring minerals – such as quartz and feldspar - to emit measurable light signals (luminescence) when being stimulated by energy in form of either light or heat. While thermoluminescence (TL) dating determines the time since the last heating to 500°C, dating of sediments using optically stimulated luminescence (OSL) measures the time since mineral grains were last exposed to sunlight (Aitken, 1998).

This sunlight exposure – or bleaching event - happens in natural environments during erosion, transport and deposition of sediments. After burial, mineral grains store energy derived from environmental radiation - sourced from the decay of potassium (K), uranium (U) and thorium (Th) isotopes and their daughter products, and cosmic rays - within their crystal lattice (Aitken, 1998). Following the band model after Aitken (1985), electrons move short-term from the valence band to a higher energy level (conduction band) due to ionisation from the environmental radiation (Fig. 1.6.1). While most electrons drop back to the valence band, some become trapped and stored over thousands of years within the crystal lattice. The more prolonged the exposure to environmental radiation the greater the number of trapped electrons. The stability of each trap over time is indicated by its depth under the conduction band (Aitken, 1998). Electrons evict from traps in response to stimulation by heat or light (wavelength is specific depending on mineral and trap), diffuse and then recombine into recombination centres and in turn release energy – some of which is in form of light (Aitken, 1985, 1998).

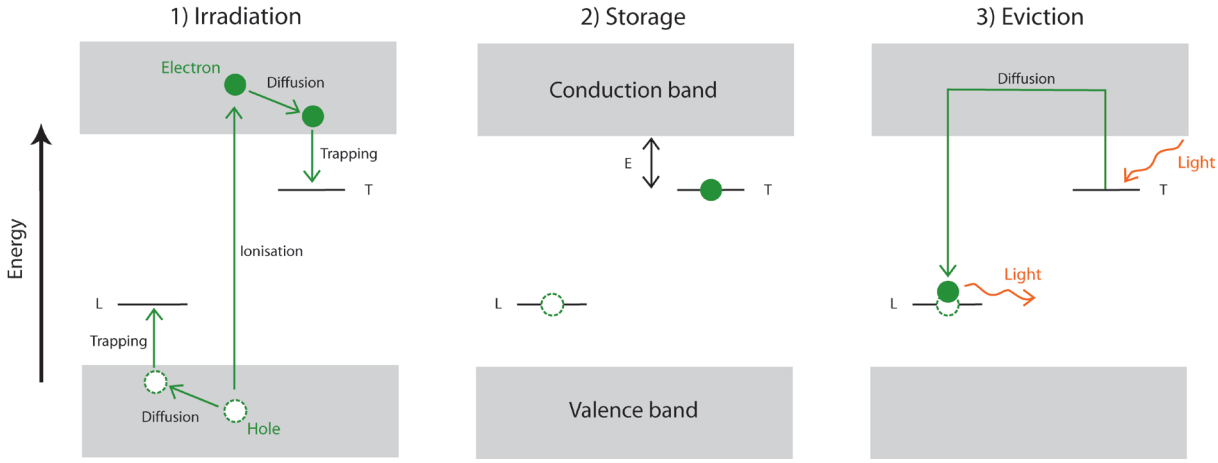

Fig. 1.6.1 OSL band model after Aitken (1985). (1) Ionisation due to exposure of the crystal to environmental radiation, with diffusion and trapping of electrons and holes at traps T and L, respectively; (2) Storage of electrons and holes in stable traps over time, the lifetime of electrons within the traps is determined by the depth E of the trap below the conduction band; (3) Eviction, and recombination of electrons with luminescence centres, L, and emission of luminescence signals in response to light stimulation. Alternatively, electrons may recombine at non-luminescent centres or deeper holes.

The number of electrons trapped in the crystal lattice of a mineral grain is proportional to the flux of environmental radiation (dose rate) it received per year since burial, until the traps approach saturation (a state where all suitable traps have become filled). Exposure to sunlight in a natural environment or intentional stimulation of the crystal by particular wavelengths of light release the stored energy in form of photons (i.e. luminescence) which can be detected by the photomultiplier in the laboratory and which is proportional to the amount of radiation the mineral received since burial. The burial age

of a sediment sample can, therefore, be calculated as:

$$\text{Age (a)} = \frac{\text{Equivalent dose (Gy)}}{\text{Dose rate (Gy a}^{-1})}$$

The equivalent dose (D_e) is defined as the laboratory radiation dose equivalent to that received in the natural environment since the last sunlight exposure, taking into account the conversion between the different energy efficiencies of environmental and laboratory induced radiation (Aitken, 1998). As age determination using OSL is limited by sample saturation, its upper dating limit in turn strongly depends on the intensity of the natural radiation in the sample surrounding.

1.6.2. Luminescence signal characteristics

Luminescence signals released in the laboratory by using intense light sources are often visually displayed as decay curves showing the intensity of the signal over stimulation time (Fig. 1.6.2a). Any luminescence signal, however, derives from multiple signal components (Bulur, 1996) - some of which might not be stable over geological times (Singarayer and Bailey, 2003) - depending on the electron traps in the crystal lattice of the mineral grains. The signal components can be differentiated into ultra-fast, fast, medium and slow (Fig. 1.6.2b) based on their length of time taken to respond to light stimulation (Bailey et al., 1997; Singarayer and Bailey, 2003). Not all components are similarly easy to bleach and each mineral grain must not exhibit every possible component (Bulur, 1996; Bulur et al., 2002). Linearly modulated (or LM) OSL measurements linearly ramp the intensity of the light stimulation source during measurement and, therefore, produce peak-shaped OSL instead of monotonically decaying OSL signals (Bulur, 1996). As the different traps contributing to the OSL signal appear as different peaks in the curve, LM-OSL measurements can be used to identify and illustrate different signal components in a given sample.

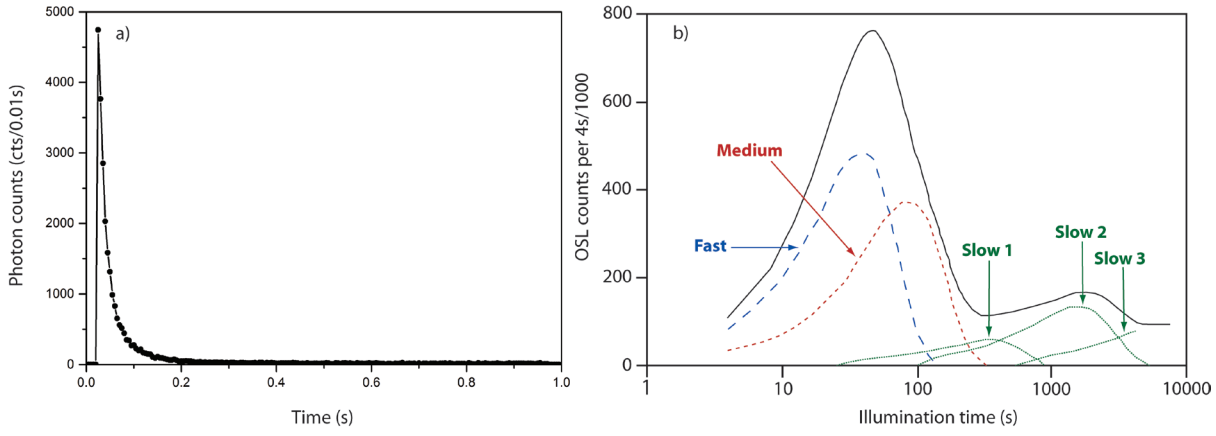

Fig. 1.6.2 (a) Schematic representation of a fast component dominated single-grain quartz luminescence signal decay curve, and (b) OSL signal component characterisation after ramped power (LM OSL) measurement (adapted from Singarayer and Bailey, 2003).

In this thesis, sand-sized quartz grains were used for age determination of the sediment samples. Quartz was chosen over feldspar for dating purposes, as it is i) ubiquitous in the studied areas, ii) more light sensitive and, therefore, readily bleachable under natural sunlight conditions (Wallinga, 2002), iii) known to produce rapidly decaying OSL signals (Aitken, 1998), iv) not suffering from anomalous fading (except volcanic quartz (Westaway, 2009)), a phenomenon which describes the loss of part of the luminescence signal with time, and v) has a less complicated internal dosimetry to account for (Huntley

and Lamothe, 2001). Quartz has, furthermore, been demonstrated in previous studies to be suitable for OSL dating of Pleistocene sediments in both Morocco (e.g. Clark-Balzan et al., 2012; Jacobs et al., 2011; Rhodes et al., 2006) and Gibraltar (Barton et al., 2013).

LM-OSL measurements showed that all quartz samples in this thesis were dominated by the fast luminescence signal component (see i.e. chapter 4), which is known for being relatively easy to bleach. Light stimulations during measurements were kept under constant intensities and signals from the initial seconds of response were used for D_e determination.

1.6.3. Sample collection and preparation

Due to the light-sensitive nature of the luminescence signal stored in sediment grains, it is of critical importance to avoid any sunlight exposure of the samples before OSL measurement in the laboratory (Aitken, 1998). On this account, OSL sampling in the field was conducted – depending on the degree of cementation of the layers - by i) hammering stainless steel tubes horizontally into the freshly cleaned profile walls, or ii) collecting block samples using either hammer and chisel or a drill. Sampling tubes and block samples were quickly capped with light-proof plastic caps and covered in black, light-proof plastic bags, respectively. Sediments from the direct surrounding of the OSL sample holes were collected for subsequent determination of their radioactive element concentration in the laboratory. All samples were carefully sealed to preserve the in situ field moisture content.

In the laboratory, samples were opened and processed (Table 1.6.1) under subdued red light conditions (Fig. 1.6.3). To exclude any sediment grains from the dating process which might have been exposed to sunlight during sampling, material from both ends (1-2 cm) of each sampling tube was removed. Similarly, the outer surfaces (~1 cm) of the block samples were cut off using a circular table saw equipped with a diamond saw blade.

Table 1.6.1 Protocol for coarse-grain quartz processing in the laboratory.

Step	Treatment
1	Sample drying at 50°C
2	Wet and dry sieving to recover sand fraction (90-212 µm or 90-300 µm)
3	HCl (10%) etching to remove carbonates
4	Hydrogen peroxide (30%) wash to remove organic matter
5	Sample drying at 50°C
6	Density separation heavy minerals (Lithium heterotungstate density 2.68 g cm^{-3})
7	Sample drying at 50°C
8	Density separation feldspar (Lithium heterotungstate density 2.62 g cm^{-3})
9	Sample drying at 50°C
10	HF (40%) etching for 60 min and rinsing with HCl and purified water
11	Sample drying at 50°C
12	Dry sieving to recover the 180-212 µm sand fraction

The remaining material was weighted and subsequently dried in an oven at 50°C for calculation of the field moisture content. Coarse-grain sand (usually 90-212 µm; for some samples 90-300 µm, when only little amount of material of the desired sand fraction was available) was extracted from the sediment by a combination of wet and dry sieving. Due to intensive cementation, block samples were treated with hydrochloric acid (HCl, 10%) first to dissolve carbonates before any sieving was possible (Wintle, 1997). The isolated sand-fractions of each sample were then used for further chemical treatments, and eventual for D_e determination.

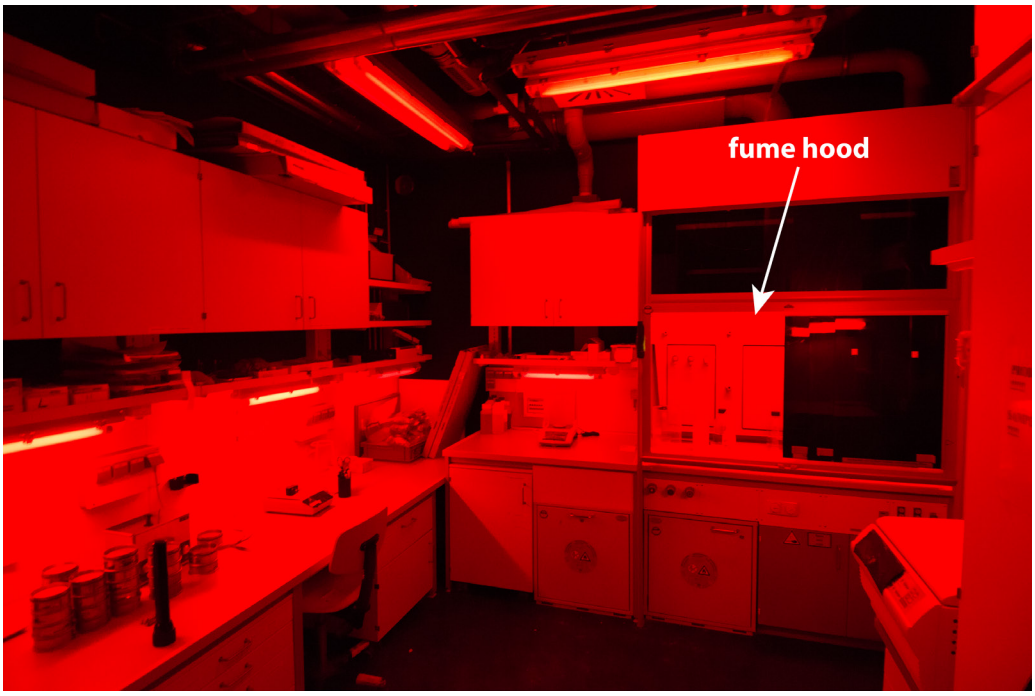

Fig. 1.6.3 The sample preparation room in the luminescence laboratory at the Max Planck Institute for Evolutionary Anthropology, Leipzig, Germany.

The material was washed with dilute HCl (10%) and hydrogen peroxide (H_2O_2, 30%) to remove carbonates and organic matter, respectively (Galbraith et al., 1999). Lithium heterotungstate, prepared to densities of 2.68 g cm^{-3} and 2.62 g cm^{-3} was used to separate quartz grains from heavy minerals and lighter feldspar grains (Aitken, 1998; Wintle, 1997). The extracted quartz was then etched with concentrated hydrofluoric acid (HF, 40%) for 60 min (Wintle, 1997) in order to remove i) the outer surface of the grains (which is affected by α radiation, chapter 1.6.9), and ii) any potentially - after density separation - remaining feldspar minerals (a chemical removal in addition to the density separation step is necessary as feldspar constitutes a solid solution spectrum of minerals with highly variable densities), which store comparatively bright luminescence signals that might otherwise significantly alter quartz OSL measurements. After etching, samples were rinsed first in HCl and subsequently multiple times in purified water to remove fluoride salts and then dried at 50°C. Laboratory processing of the samples was completed by re-sieving of the extracted quartz to recover the grain-size fraction desired for D_e determination (180-212 µm).

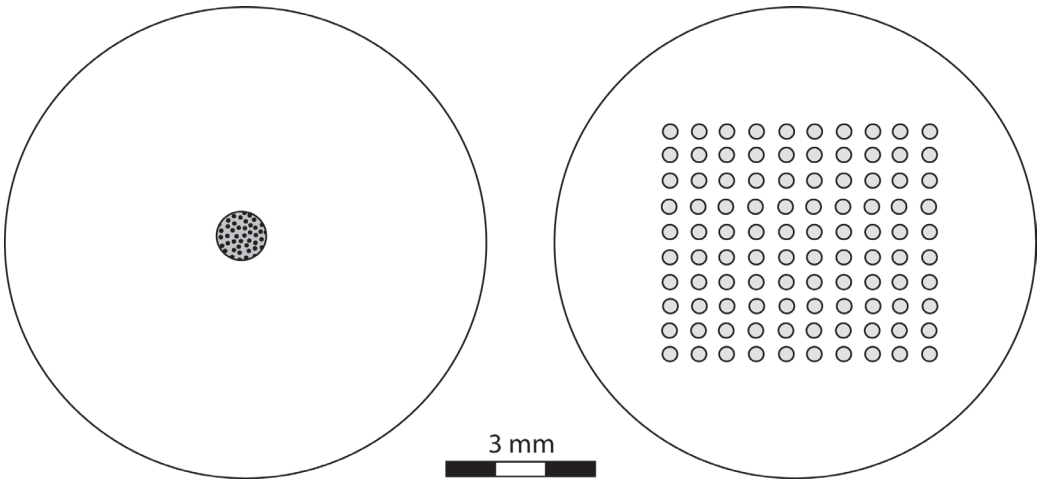

Fig. 1.6.4 Schematic representation of a 1 mm multiple-grain aliquot disc (containing ~30 individual sand grains) and a single-grain disc containing 100 holes (each being 300 µm wide and 300 µm deep).

Multiple-grain and single-grain dating techniques were used for D_e measurement. For preparation of the multiple-grain aliquots, quartz grains were mounted on stainless steel discs using silicon oil and a mask of 1 mm. Single-grain discs were loaded by sweeping individual grains over aluminium discs – containing 100 holes (each 300 µm wide and 300 µm deep) in a 10 by 10 array (Duller et al., 1999) – with a small brush (Fig. 1.6.4).

1.6.4. Multiple-grain vs. single-grain dating

Multiple-grain aliquots contain small subsamples of the desired material to be dated (Duller, 2004; Duller, 2008), and each aliquot provides an independent estimate of D_e. After measurements of many separate aliquots the D_e distribution within a sample can be assessed (Duller, 2008). The fundamental assumption behind this approach is that all sediment grains of a given sample were exposed to sufficient sunlight – as is typical for aeolian sediments - before burial to remove any trapped and stored electron charge. Godfrey-Smith et al. (1988) showed that for quartz an almost complete signal resetting (reduction of the natural unbleached optical signal to 1%) can already be achieved after 10 s of direct sunlight exposure on a clear day and even on an overcast day, samples bleach only 10 times more slowly. Given a complete signal resetting before burial, all grains would have a zero D_e at deposition and - within a homogeneous radiation environment - accumulate the same amount of charge over time. As multiple-grain aliquots usually contain between tens and about a million of individual grains (Duller, 2008) - depending on the grain-size of the measured sediment fraction and the size of the aliquot – the measured D_es represent aggregate, averaged luminescence signals (Rhodes, 2007).

Multiple-grain OSL measurements were performed in this thesis using automated Risø OSL/TL readers (DA-15 and DA-20, Fig. 1.6.5) each equipped with calibrated $^{90}Sr/^{90}Y$ beta sources for radiation dosing (Bøtter-Jensen et al., 2000). Stimulation light was provided by blue light-emitting diodes (470 nm wavelength) and infrared diodes (875 nm). The emitted luminescence signal was filtered by 7.5 mm Hoya U-340 detection filters (Bøtter-Jensen, 1997) before being converted from photons to an electric signal within EMI photomultiplier tubes (Aitken, 1998).

Over the last years, OSL dating of individual sand-sized quartz grains (Bøtter-Jensen et al., 2000; Duller et al., 1999; Roberts et al., 1999) has become a frequently used tool especially in archaeological contexts (e.g. Demuro et al., 2012; Fitzsimmons et al., 2014; Jacobs and Roberts, 2007; Jacobs et al., 2012; Roberts et al., 1998; Tribolo et al., 2010). For this technique Risø readers (Fig. 1.6.5) have to be equipped with a single-grain attachment (Bøtter-Jensen et al., 2003); the D_e of individual grains get measured by light stimulation from a green laser emitting at 532 nm (Bøtter-Jensen et al., 2000). Single-grain luminescence signals are often of low intensity and, therefore, more difficult to measure than multiple-grain aliquots, and as not all grains are necessarily suitable for luminescence dating (some do not exhibit luminescence signals at all (Jacobs et al., 2003, 2006; Porat et al., 2006)) (Fig. 1.6.6), this technique is rather elaborate and time-consuming (Duller, 2008). It, however, enables the identification of multiple age populations within a sediment sample, which is difficult to assess in multiple-grain dating where an averaged luminescence signal from all grains placed on a disc is recorded. Complete bleaching during the last transportation process of the sediment grains cannot always be assumed with sufficient certainty when it comes to e.g. caves (Feathers, 2002; Murray et al., 2012). Furthermore, archaeological sites are often affected by post-depositional mixing of sediments by natural processes and/or human activity (Bateman et al., 2007). In those cases single-grain dating can still provide reliable depositional ages for a sediment layer and, additionally, quantify the amount of older or younger grains in the sample, which might help to understand local site formation processes. Additional problems for OSL dating may arise from the variety of materials in the surrounding of a sediment

sample each providing different dose rates (Olley et al., 1997), which often occurs in archaeological sites (e.g. Steele et al., 2016). Poor sediment sorting and high variability in grain sizes in a sediment layer can, furthermore, result in local radioactive 'hotspots' and 'coldspots' which effect dose rates at an individual grain level. Those inconsistencies in beta dose rates can be identified and visualised using single-grain dating (Jacobs et al., 2011; Jacobs and Roberts, 2007).

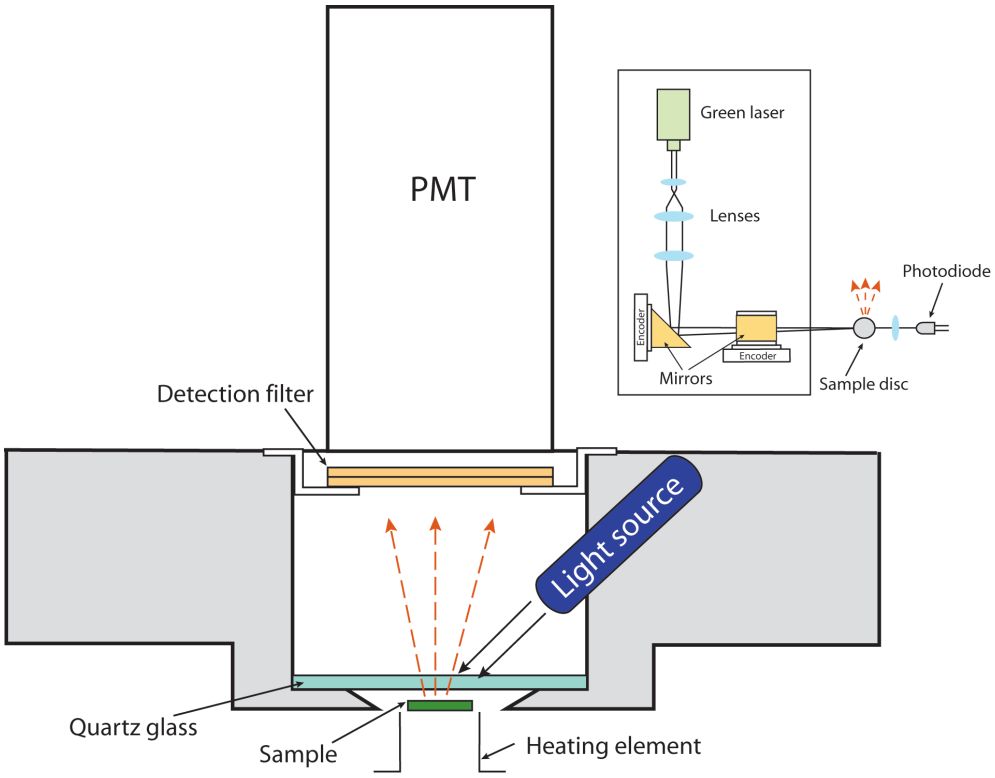

Fig. 1.6.5 Schematic representation of a Risø OSL/TL reader and a single-grain OSL unit adapted from Bøtter-Jensen et al. (2000). Optical stimulation is provided by a light source (blue LEDs, IR diodes or green laser hosted in a separate attachment) directly onto the sample which in turn emits a luminescence signal that passes through detection filters (and a quartz glass when measuring individual grains) into the photomultiplier tube (PMT). The PMT produces an output of photon counts against time (see Fig. 1.6.2a).

Since single-grain dating was first introduced to the scientific community by Galbraith et al. (1999) and Roberts et al. (1999), researchers have performed comparative studies – using both multiple-grain and single-grain dating approaches - to understand the variability observed in luminescence characteristics of sediment samples when being measured with differently sized aliquots and/or single-grains (e.g. Arnold et al., 2012; Duller, 2008; Rhodes, 2007). Rhodes (2007) showed that the brightness of OSL signals might vary considerably between grains within one sample, but also that the proportion of grains yielding detectable signals at all is highly variable between samples. Consequently, the commonly assumed averaging effect in multiple-grain aliquots can be reduced for samples which yield OSL signals dominated by just a few bright grains (Duller, 2008; Rhodes, 2007). And although, single-grain dating is often successfully applied at sites with complicated stratigraphical contexts (e.g. Jacobs et al., 2012; Roberts et al., 2000; Tribolo et al., 2010), researchers have also reported case studies for which single-grain dating was unable to overcome such issues (Guérin et al., 2012; Steele et al., 2016) or when multiple-grain results were scientifically more conclusive than those determined using single-grains (Carr et al., 2007; Guhl et al., 2013).

In this thesis, single-grain dating was used for age determination of sediments from the Moroccan sites (Rhafas and Casablanca), while at Gibraltar (Vanguard Cave) a comparative dual chronology was developed using both methodological approaches (multiple- and single-grain dating).

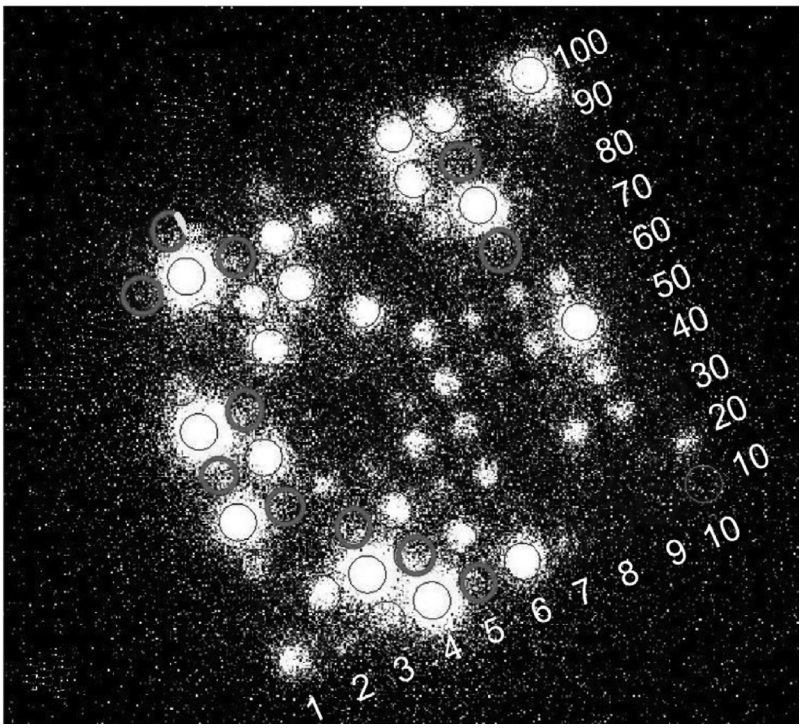

Fig. 1.6.6 EMCCD (electron multiplying charge-coupled device) image for a single-grain disc showing the luminescence signal released by each of the 100 individual grains (modified after Thomsen et al., 2015).

1.6.5. Single-aliquot regenerative-dose protocol for D_e determination

The most frequently applied protocol for optical dating of sediments, today, is the single-aliquot regenerative-dose protocol (SAR) after Murray and Wintle (2000, 2003), which was also used in this thesis for D_e determinations. Laboratory based OSL measurements generally include multiple cycles of light stimulation, heating and radiation dosing, which can cause sensitivity change (unwanted charge transfer to optically sensitive traps) in quartz minerals, resulting in inconsistent responses to light stimulation and radiation dosing and eventually problems for D_e determination. To account for this, the SAR protocol includes correction for sensitivity change by measuring small test doses in between each dose step during the protocol run (Table 1.6.2, Murray and Wintle, 2000; 2003).

Table 1.6.2 Summary of the single-grain SAR protocol used in this thesis.

Run	Treatment	Description
1	Dose (except before first run)	Radiation dose
2	Preheat (PH_1)[a] for 10s	Empties thermally unstable traps
3	Optical stimulation with IR diodes for 100s at 20°C (only for last run)	Quantifies feldspar contamination
4	Optical stimulation with green laser for 1s at 125°C	L_x[b]
5	Test dose	Allows sensitivity change correction
6	Preheat (PH_2)[a] for 10s	Empties thermally unstable traps
7	Optical stimulation with green laser for 1s at 125°C	T_x[c]
8	Start from top	

[a] PH_1/PH_2 was 240°C/200°C or 260°C/220°C; depending on the sample-specific response to preheat plateau and dose recovery preheat plateau tests (section 1.5.6).
[b] L_x is the OSL signal.
[c] T_x is the OSL response to the test dose.

The SAR protocol measures OSL signals (L_X and T_X, Table 1.6.2) derived from natural and laboratory radiation dosing in multiple-grain aliquots and single-grains. After measurement of the natural dose (N) stored in the samples, four regenerative dose cycles (R_1-R_4) with progressively increasing given doses were performed to build up reliable dose response curves (Fig. 1.6.7). The D_e of a sample is then calculated by interpolating N on the laboratory generated dose response curve. Preheats before each optical stimulation were incorporated to remove charge from thermally unstable traps that have been filled during laboratory irradiation and which may otherwise falsify the result by contributing to the recorded OSL signal (Murray and Wintle, 2000, 2003). A zero dose step (also called recuperation, R_0) – which should ideally give zero signal - was measured to assess the effect of charge transfer from deeper traps on the OSL signal caused by preheating, irradiation and optical stimulation during the previous dose cycles (Wintle and Murray, 2006).

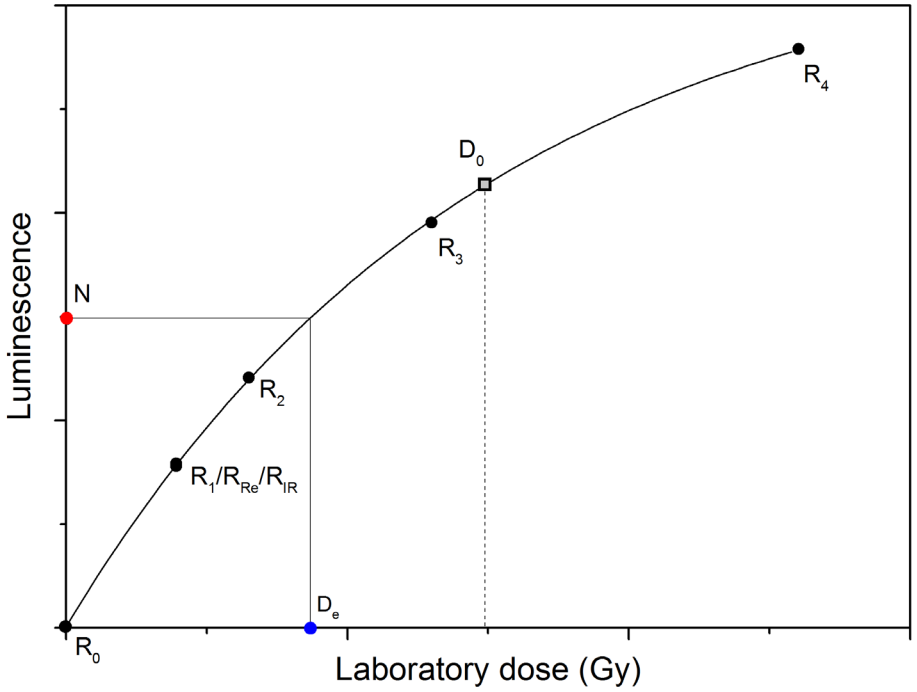

Fig. 1.6.7 Schematic representation of a sensitivity corrected SAR dose-response curve for D_e determination of a single-grain or multiple-grain aliquot with a single saturating exponential curve fit. The dose-response curve is constructed from the regeneration dose points R_1-R_4. R_0 is the OSL response to a zero dose (recuperation), R_{Re} is the recycling point which repeats R_1 at the end of the protocol and R_{IR} represents the IR depletion ratio measurement following Duller (2003). The D_e of a sample is calculated by interpolating the natural dose signal (N) of a sample on the laboratory generated dose response curve. The D_0 value characterises the rate of OSL signal saturation.

Usually sensitivity change progressively increases with each dose step in OSL protocols, which is why one of the already measured dose points is usually repeated towards the end of the protocol to check whether sensitivity change was correctly accounted for (recycling point, R_{Re}) (Murray and Wintle, 2000). The recycling point was chosen to repeat R_1 in this thesis and both values should give the same OSL signal assuming that the SAR protocol is successfully correcting for any sensitivity change in the samples. The recycling ratio is calculated according to Murray and Wintle (2000) as R_{Re} divided by R_1.

The purity of a quartz sample after chemical treatment and its potential contamination by feldspar can be examined by measuring the IR-depletion ratio after Duller (2003) in the end of the SAR protocol, which allows efficient distinction between quartz and feldspar based solely on their luminescence behaviour. The IR-depletion point (R_{IR}) is measured similarly to the recycling point, by repeating the first regenerative dose cycle. Prior to optical stimulation, however, the sample is additionally exposed

to infrared light stimulation (Table 1.6.2). As quartz OSL traps are not sensitive to IR light stimulation, while feldspar traps are, the calculated IR-depletion ratio enables quantification of quartz OSL signal depletion caused by IR stimulation, or, in other words, quantification of contamination of the quartz sample by feldspar (Duller, 2003).

Age determination in OSL dating is limited by the sample-dependent signal saturation level ($2D_0$), a status which is approached when the majority of existing electron traps in the crystal lattice of a mineral are filled. OSL growth curves will reach a stable plateau when given radiation doses exceed sample saturation level.

The reliability of each measured D_e value can be assessed by testing its response to the previously outlined quality criteria (test dose, recuperation, recycling, IR-depletion, signal saturation), but also by the ability of its natural signal to be interpolated on the dose response curve and the size of the D_e error. As luminescence characteristics of quartz samples can be highly variable, quality criteria were defined individually for each site in this thesis and are discussed in greater detail in the corresponding chapters 2-5.

1.6.6. SAR performance tests

Thermal treatments (preheats) are essential to any SAR protocol (Table 1.6.2) as they empty light-sensitive shallow traps, particularly those filled by laboratory irradiations, prior to optical stimulation and measurement of the stored luminescence signal (Murray and Wintle, 2000, 2003). Preheats, however, may also cause sensitivity change resulting in erroneously high luminescence signals and, subsequently, miscounted D_es (Wintle and Murray, 2006). A thorough testing of the most appropriate thermal treatment in a SAR protocol is, therefore, required for each sample prior to D_e determination.

In this thesis, standard preheat plateau and combined dose recovery preheat plateau tests were performed on each sample. For both tests seven different temperatures - varying between 160°C and 280°C in 20°C steps – for the 10 s preheat ahead of the main OSL measurement (L_X) were tested with a fixed low temperature test dose cutheat at 160°C (Wallinga, 2002; Wintle and Murray, 2006).

For the preheat plateau test, natural D_es are measured and the ability of the test dose signal (T_X) to monitor sensitivity change should be shown as an absence of D_e dependence on the preheat temperature (Wintle and Murray, 2006). In other words, if determined D_es reach a stable plateau value independent of the applied preheat temperature then sensitivity change is correctly accounted for in the respective SAR protocols, as shown for preheat temperatures between 180°C and 260°C in the hypothetical example of a preheat plateau test in Fig. 1.6.8a. The chosen preheat temperature for the final D_e measurements should, consequently, be selected from the plateau region of the preheat plateau test (Wintle and Murray, 2006).

As the most distinct sensitivity change during SAR measurements usually occur when a sample is first heated, dose recovery tests on unheated sample material can be carried out to check whether the first sensitivity measurement (T_N) is appropriate to the preceding natural signal (L_N) (Murray and Wintle, 2003; Roberts et al., 1999). For this test, the unheated, laboratory bleached or modern analogous (with zero D_e) sample is given a known radiation dose (close to the expected natural D_e of the sample) and the SAR protocol is then run. Since a known dose is given, the ability of the protocol to accurately measure this dose can be directly tested and is mathematically expressed as ratio of measured over given dose (Fig. 1.6.8b).

Ideally, dose recovery experiments should mimic the processes of bleaching and radiation dosing in nature. This is, however, an impossible task as i) artificial bleaching sources are different to natural

sunlight i.e. with respect to wavelength and light intensity, and ii) irradiation in the laboratory is administered by strong beta or gamma sources within seconds, while radiation dosing occurs slowly over millennia due to the decay of radioactive elements in natural sedimentary deposits. Researchers have performed intensive experiments in the past years using beta and gamma radiation and different kinds of bleaching sources (natural sunlight, solar simulator, blue LEDs, green laser) to test the reliability of dose recovery test results under varying experimental settings (e.g. Choi et al., 2009; Thomsen et al., 2012; 2016; Wang et al., 2011) and chapter 4 of this thesis contributes to this discussion by examining single-grain dose recovery characteristics of Moroccan and Australian samples.

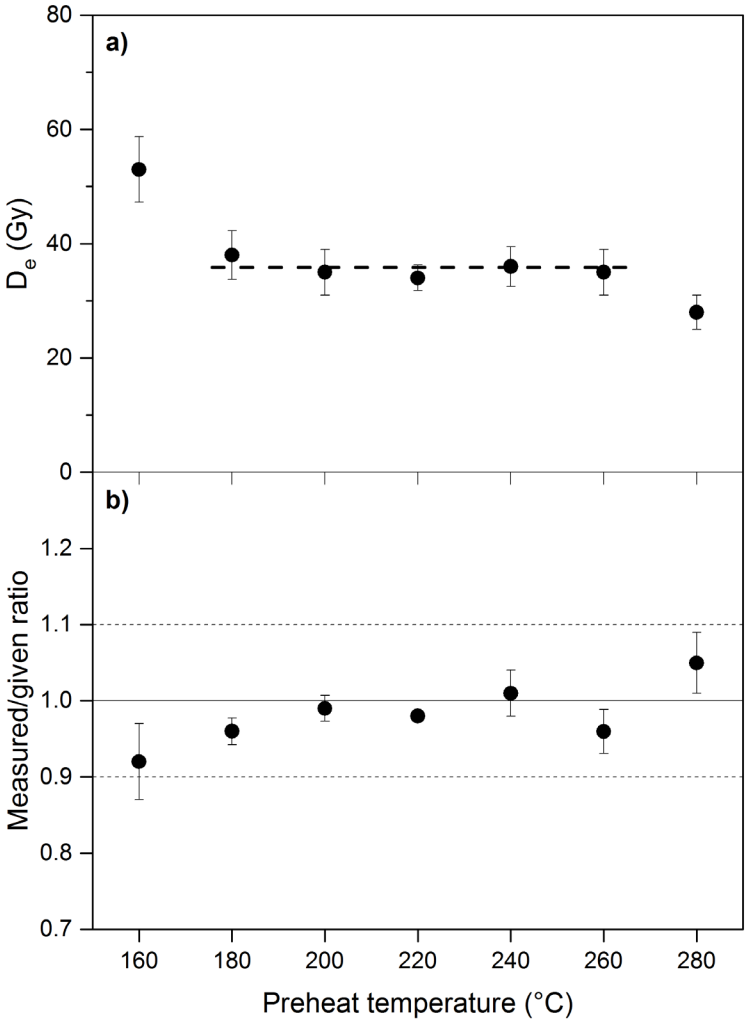

Fig. 1.6.8 Hypothetical example of a (a) preheat plateau test, and (b) dose recovery preheat plateau test as a function of preheat temperature. (a) Determined D_e are independent of the preheat temperature (preheat plateau) at 180-260°C. (b) Calculated measured/given dose ratios describe the ability of a sample to recover a laboratory given dose within acceptable ranges (2-sigma of unity).

For this thesis, standard dose recovery test are combined with a preheat plateau test to assess the ability of the respective SAR protocol to reproduce a known laboratory dose depending on a chosen preheat temperature (Fig. 1.6.8). Based on the results of the preheat plateau tests and dose recovery preheat plateau tests of each individual sample, preheat temperatures were selected for final D_e measurements.

1.6.7. Presentation of data

Radial plots – which were initially proposed by Galbraith (1988, 1990) for data presentation in fission track dating - are often used in OSL dating studies to graphically display D_e distributions of single-grains and multiple-grain aliquots (Fig. 1.6.9). Luminescence intensities of single-grains and consequently also

the precision of their calculated D_es may vary greatly, which is why e.g. histograms are likely to be uninformative or even misleading for the interpretation of D_e distributions (Galbraith et al., 1999). Each data point in a radial plot represents a single grain/multiple-grain aliquot and its measured D_e can be read by tracing a line from the y-axis origin through the point until the line intersects the radial plot axis (log scale). The standard error (in %) and the precision (reciprocal standard error) of each D_e value can be read by extending a line vertically to intersect the x-axis (Olley et al., 2004). D_e values with the highest precision (and the smallest relative standard error) fall furthest to the right, whereas those measured with least precision lie furthest to the left. The y-axis extends only from -2 to +2 thereby effectively displaying the length of a 2-sigma error bar applicable to any point (Galbraith et al., 1999). The shaded region of the plot indicates those D_e values that are consistent (at 1-sigma) with the weighted mean of a discrete age population.

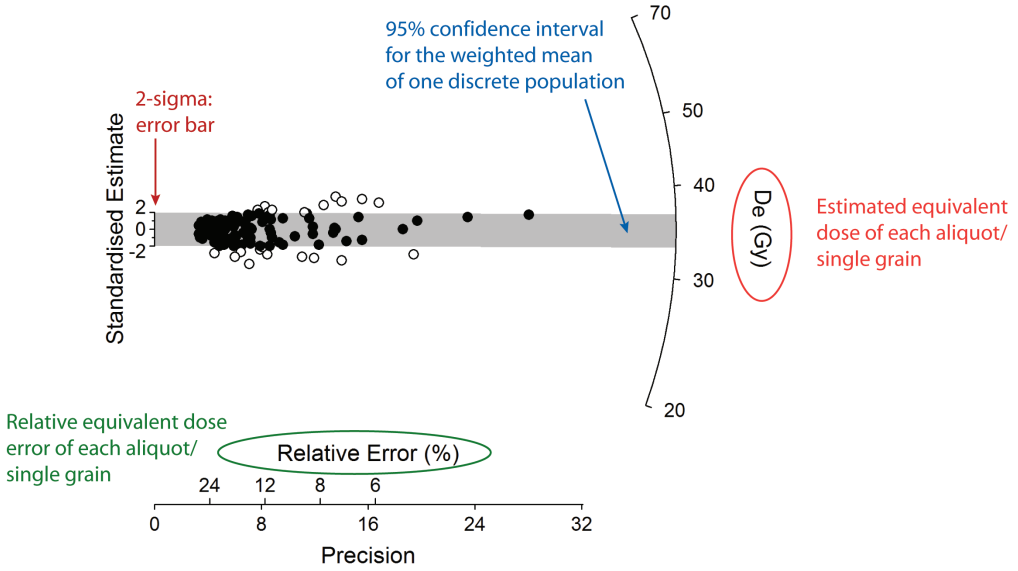

Fig. 1.6.9 Illustration of a radial plot with a hypothetical D_e distribution. The graphical display allows visual assignment of the measured D_e and relative standard error for each single-grain or multiple-grain aliquot, while at the same time visualises potential discrete D_e populations.

1.6.8. Analysis of data: age models for D_e determination

D_e distributions of sediment samples may i) contain multiple age populations (due to i.e. post-depositional mixing, roof spall in caves or incomplete bleaching), ii) show extremely wide scattering (due to heterogeneous dose rates), or iii) simply display an ideal image of a single age population. In the first two cases, single-grain dating should be favoured over multiple-grain dating approaches as it allows not only to identify and quantify those multiple age populations in a sample, but also to calculate ages separately for each of these populations.

The most commonly used statistical model to calculate the age of a single homogeneous D_e distribution (Fig. 1.6.10a) in the past years, was the Central Age Model (CAM) of Galbraith et al. (1999), which calculates a weighted geometric mean of individual D_es and gives an estimate for the overdispersion of the D_e distribution. The overdispersion is defined as the scatter beyond measurement uncertainties and allows quantification of the variability in D_e distributions (Galbraith et al., 1999). It comprises both extrinsic and intrinsic factors; the former of which can be caused by dose rate heterogeneity, incomplete bleaching and/or post-depositional mixing, while the latter arises from thermal transfer, instrument reproducibility, counting statistics or other sample-specific OSL characteristics (Thomsen et al., 2007). While researchers have recently started discussing the application of alternative mean age

models such as the Bayesian central-dose model or the calculation of unweighted arithmetic means (e.g. Combès et al., 2015; Guérin et al., 2016; Thomsen et al., 2016), in this thesis, the CAM was used when D_e distributions were characterised by a single homogeneous dose population.

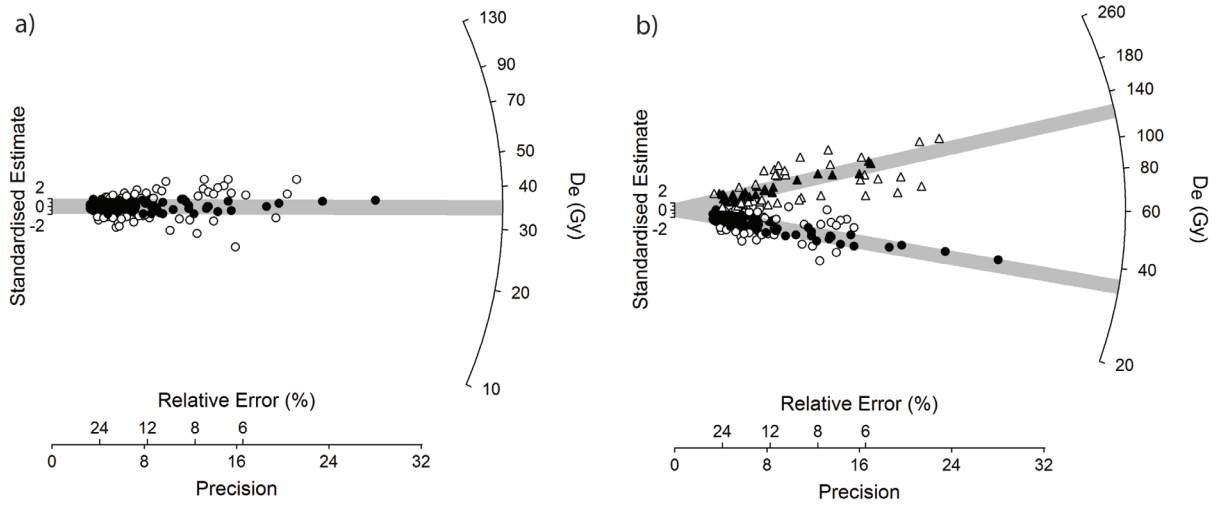

Fig. 1.6.10 Radial plots showing hypothetical examples of D_e distributions comprising (a) one discrete, and (b) two discrete age populations. For the purposes of a simplified illustration, D_es of individual grains in (b) are displayed as dots or triangles depending on the age population they are assigned to.

For samples in this thesi characterised by mixed single-grain D_e distributions (Fig. 1.6.10b), the number of discrete D_e populations (components), their relative proportion and their respective weighted mean age was determined using the Finite Mixture Model (FMM) after Galbraith et al. (1999) and Roberts et al. (2000). In the FMM, it is assumed that the log equivalent doses for single grains represent a mixture of discrete, normally distributed populations, each of which has the same relative overdispersion. The model can be run by inserting values for the number of fitted components and the overdispersion; it then uses maximum likelihood to estimate the mean D_es, their standard errors and the proportion of grains for each component (Roberts and Jacobs, 2015).

1.6.9. Dose rate determination

Equally important to the D_e determination in OSL dating is the correct assessment of the dose rate received by the sediment grains per year, as the rate at which trapped electrons are accumulated is proportional to the energy absorbed by the mineral grains from the surrounding radiation flux since its last sunlight exposure (Aitken, 1998). The annual ionising radiation arising from i) the radioactive decay of K, Th and U in the sediments, and ii) cosmic rays contribute to the total dose rate (Fig. 1.6.11) which can only be measured under present day conditions. The fundamental assumption underlying OSL dating studies, therefore, is that the total dose rate for each sediment sample remained constant with time or in other words that the present-day dose rate is the same as that in the past. Large uncertainties are incorporated into dose rate calculations to account for potential small variations in the radiation flux over time (Aitken, 1998).

Naturally occurring radiation in sedimentary bodies is mostly a result of the radioactive decay of ^{40}K - emitting β particles and γ rays - and uranium (^{238}U and ^{235}U) and ^{232}Th which both produce α and β particles as well as γ rays (Fig. 1.6.11). There is also a minor contribution from the decay of rubidium which is usually considered negligible due to its strongly absorbable, low energy β particles (Aitken, 1985, 1998).

α particle are characterised by relatively limited travel ranges within sediment samples (~20 µm, Guérin, 2015), penetrating only the outer rinds of sand-sized quartz grains (Fig. 1.6.11c). HF etching applied during chemical treatment of the samples in the laboratory removes these outer rinds of the quartz grains (section 1.6.3) and, therefore, α contribution to the total dose rate is rendered negligible. In contrast, travel ranges of β and γ particles in sedimentary bodies are 2-3 mm and up to 40-50 cm, respectively (Aitken, 1998; Guérin, 2015).

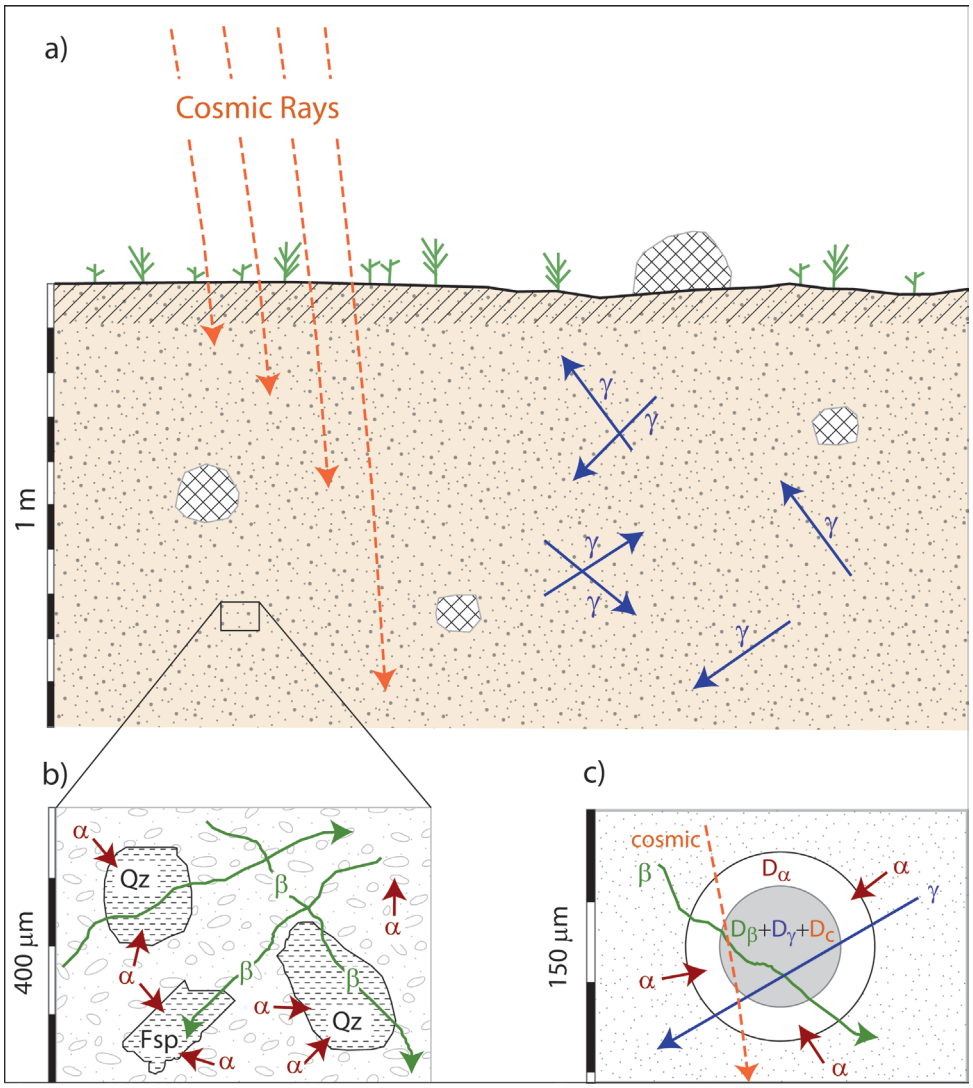

Fig. 1.6.11 Schematic representation of the sources of environmental radiation affecting individual sediment grains on different resolution levels (from low (a) to high (c)) adapted from S. Stokes in Aitken (1998) and Fleming (1970). Grains are irradiated by cosmic rays from outer space as well as alpha particles, beta particles and gamma rays originating from the radioactive decay of naturally occurring K, Th and U in the sediment. Alpha particles travel only short distances (<20 µm) compared to beta particles (2-3 mm), gamma rays (up to 40-50 cm) and cosmic rays, which is why they only penetrate the outer rind of sand-sized grains (b,c).

Sources of uncertainty in sediment dose rate determination may arise from attenuation of β particles by moisture and/or secular disequilibrium in the uranium- or thorium-series decay chain (Olley et al., 1996). Water present in the pore spaces of sediments absorbs part of the radiation that would otherwise reach individual grains (Mejdahl, 1979). Consequently, the dose rate of moist sediment is lower compared to in the same, dry material (Aitken, 1998). In this thesis, in situ and full-saturation moisture contents were taken into account to allow estimation of reliable average burial-time moisture contents for each individual OSL sample.

In radioactive decay chains, a secular equilibrium represents the condition in which activities of daughter isotopes are equal to those of the parent. Disequilibrium, hence, indicates an imbalance between daughter and parent isotope, either due to introduction of new material from an allochthonous source, or by escape or removal of the daughter isotope (e.g. gaseous escape, leaching in groundwater, absorption) (Aitken, 1985, 1998; Krbetschek et al., 1994). While the thorium decay chain is generally assumed to be in secular equilibrium due to low solubility of ^{232}Th and the short-lived nature of its unstable daughter isotopes (Fig. 1.6.12), disequilibrium in the uranium decay chain occurs more frequently – as ^{238}U produces e.g. water soluble daughter isotopes ^{226}Ra and ^{222}Rn (Fig. 1.6.12) – and can introduce substantial changes (up to ~30%) to the OSL age estimate (Olley et al., 1996; 1997). Therefore, in depositional environments where water naturally percolates through the sediment body (i.e. fluvial deposits or caves), disequilibrium is more likely to occur and should, consequently, be thoroughly assessed.

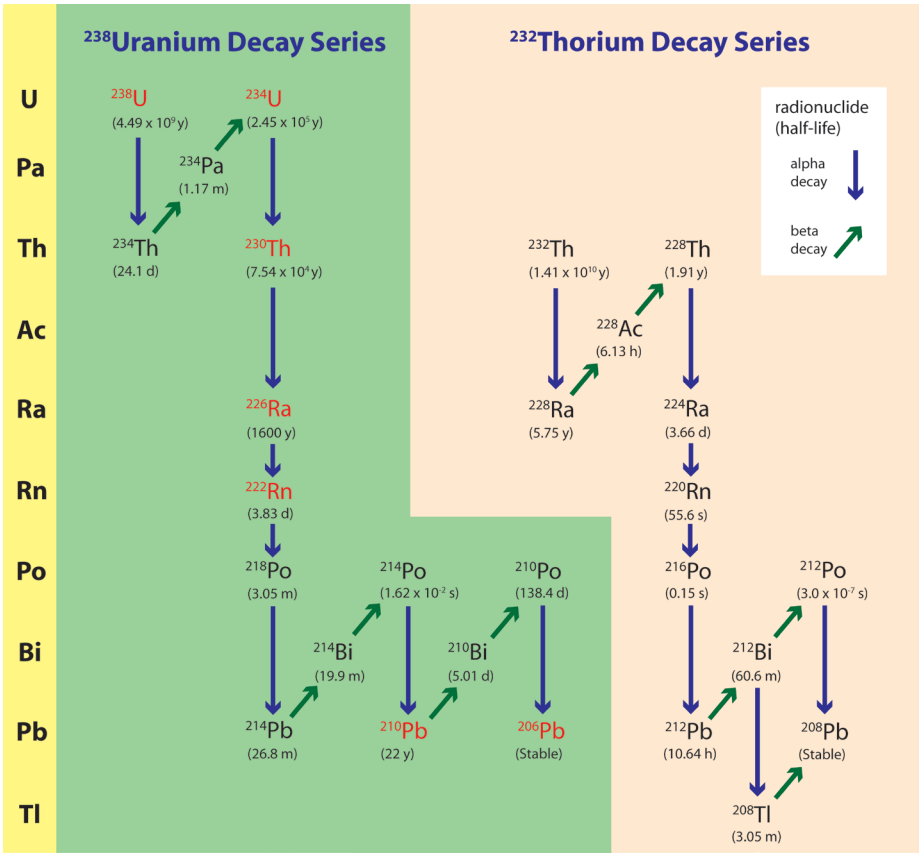

Fig. 1.6.12 Summary of the ^{238}U and ^{232}Th decay chains, including half-lives of their daughter isotopes; data from Lorenz (1983). Daughter isotopes of the ^{238}U decay chain with long half-lives for which disequilibrium might be an issue in sediments are highlighted in red.

β and γ dose rates for sediment samples can be determined by various techniques. In this thesis, dose rates were measured using primarily beta counting and in situ gamma spectrometry. Beta counting was performed on a Risø low-level multicounter system (GM-25-5) which allows β dose rate determination on small sample sizes (<10 g) (Bøtter-Jensen and Mejdahl, 1985; 1988). The system measures the total counts of β emission derived from radioactive sources in the sediment for a defined time span (usually 24h), it, however, does not give information on the concentration of the specific elements the radiation originates from. In situ gamma spectrometry (Fig. 1.6.13) allows the measurement of the natural γ radiation in a 30 cm radius sphere surrounding each OSL sampling hole in the field with a crystal detector (NaI or $LaBr_3$). This technique is particularly useful for samples from sedimentary

contexts which are likely to be affected by high spatial heterogeneity in the γ radiation field, such as archaeological sites.

To allow assessment of the reliability of the calculated β and γ dose rates and to detect and quantify potential disequilibria in the Th and U decay chains (Fig. 1.6.12), the specific activities of the radioelements ^{238}U, ^{232}Th, ^{40}K and their daughter products were determined on sediment samples from the direct surrounding of each OSL sample in the laboratory using high-resolution gamma spectrometry (HRGS). The conversion factors for radioactivity of Guérin et al. (2011) were applied to calculate the corresponding β and γ dose rates, which were then compared with those derived from beta counting and in situ gamma spectrometry.

Fig. 1.6.13 In situ gamma spectrometry measurement using a $LaBr_3$ detector at an OSL sample hole at Vanguard Cave, Gibraltar.

The contribution from cosmic radiation (Fig. 1.6.11) to the total dose rate in this thesis was calculated according to Prescott and Hutton (1988, 1994) as a function of i) the site's longitude, geomagnetic latitude and altitude, and ii) the burial depth and density of the overburden for each of the dated samples. Cosmic radiation is classically grouped into a soft and a hard component, the former is absorbed within ~80 centimetres of sediment, whereas the latter is capable of penetrating much further into the ground (Aitken, 1985). While in most studies, cosmic radiation contributes only a low percentage (<10%) to the total dose rate compared to the dose rate derived from the decay of radioactive elements (Guérin, 2015), it can be 25% or more in quartz-rich sediments (e.g. Fitzsimmons et al., 2014).

1.7. Outline of thesis chapters

The following four chapters aim to investigate the luminescence characteristics of individual quartz grains of Pleistocene archaeological cave sites in the western Mediterranean and to build reliable chronological frameworks for those sites using single-grain OSL dating to improve our understanding of the timing of hominin occupation phases and their palaeoenvironmental context at local and regional scales:

Chapter 2 (Paper 1) – Rhafas, NE Morocco – linking a long stratified Palaeolithic sequence to records of palaeoenvironmental variability and modern human dispersal across the Maghreb

Much attention has been devoted to the study of modern human origins and dispersal within and out of Africa; more recently, growing interest has been placed on the archaeological record of the Maghreb and especially the Aterian technocomplex which is often associated with personal ornaments interpreted to represent cultural modernity. Building reliable chronologies for archaeological sites containing multiple Palaeolithic stone tool industries is of critical importance to understand both timing and geographical dispersal of the emergence of modern human behaviour in Africa. The cave of Rhafas is one of the few sites in the Maghreb known to contain an exceptional Palaeolithic record spanning the MSA through to the Neolithic.

Chapter 2 focusses on the development of an absolute chronostratigraphy for the site using single-grain OSL dating. Geological and sedimentological investigations are conducted to gain insights into local site formation processes as well as Middle to Late Pleistocene palaeoenvironmental conditions in the area. The results of this multi-proxy approach allows not only to obtain reliable age estimates for large parts of the stratigraphic sequence but also to identify local processes (sediment mixing, carbonate cementation, ground water flux) which substantially affected the sediments well after deposition. This chapter provides valuable support for future OSL studies dealing with highly complicated cave settings and discusses the new ages for Rhafas in the broader chronological context of the Palaeolithic sites in the Maghreb.

Chapter 3 (unpublished study) – Casablanca, Atlantic Morocco – attempt to construct reliable chronologies for Acheulian sites close to the upper limit of quartz OSL dating

In chapter 3 the regional focus is shifted towards Atlantic Morocco where the Casablanca sites provide rich archaeological records for the study of Early and Middle Pleistocene Acheulian assemblages and their palaeoclimatic context. Eight collected OSL samples from two cave sites - which were subject to chronological investigations in the past - are used to test the potential of single-grain quartz for age determination of sediments close to the upper dating limit of this method, with the overall aim to build refined chronostratigraphies for both sites.

The OSL signal characteristics of the samples are investigated using laboratory-based experiments. It is demonstrated that while stored luminescence signals are usually bright and fast component dominated, samples are very close to saturation level and tend to fail standard OSL performance tests. The obtained test results between differently sized aliquots are often conflicting, which hampers the drawing of solid conclusions and creates more questions than initially intended to solve.

Subsequently, single-grain OSL ages are determined and critically discussed. The validity of the age estimates is highly questionable for both sites, as they are neither chronostratigraphically consistent nor in agreement with independent age controls. It is argued that while standard single-grain quartz luminescence appears to be unsuitable for the dating of these archaeological sediments, this does not necessarily applies for all quartz OSL approaches.

Chapter 4 (Paper 2) - investigating single-grain dose recovery characteristics of archaeological sediments from Moroccan and Australian sites

The question whether a specific quartz sample is suitable for OSL dating given predetermined measurement protocol parameters and whether its calculated natural D_e is, consequently, considered reliable, is commonly checked by a dose recovery test. These laboratory based experiments can, however, only mimic the processes of sunlight bleaching and radiation dosing that occur in natural environments and as yet it is unclear which effects artificial bleaching sources or differently sized recovery doses might have on the obtained test results of a sample.

Chapter 4 addresses these issues by systematically examining single-grain quartz OSL dose recovery characteristics of archaeological samples from Morocco (Rhafas and Casablanca) in comparison to those from an Australian site. This study demonstrates that dose recovery test results primarily depend on the size of the administered dose. It is furthermore shown that sample-specific responses to the chosen test parameters can significantly alter experimental results, especially in samples which underwent relatively few numbers of sensitisation cycles. As this is the case for considerable numbers of sedimentary sequences in archaeological sites – including Rhafas and Casablanca – special caution is advised for conducting dose recovery experiments on such sediments in general and more specifically for the interpretation of the obtained results.

Chapter 5 (Paper 3) – Vanguard Cave, Gibraltar – testing two OSL approaches on a high resolution sedimentary cave sequence in the context of Neanderthal occupation and Mediterranean sea-level fluctuations

Substantial amount of work on the Palaeolithic of southern Iberia has focused on the timing of Neanderthal persistence in the area as well as their potential interaction and eventual replacement by AMH. Less attention has been given to reconstruct past ecological and climatic conditions during times of Neanderthal dominance that pre-date the arrival modern human populations in the region.

In chapter 5, a chronostratigraphy for the upper part of the >17 m sedimentary sequence of Vanguard Cave is developed, a site located on top of a MIS 5 marine terrace at the present-day shoreline of Gibraltar. Sediment accumulation rates are high at Vanguard Cave, which allows a critical testing of the soundness of OSL ages derived from differently sized aliquots by means of the high resolution stratigraphical cave sequence. A dual chronology – comprising quartz single-grain and multiple-grain ages – is thus created demonstrating a high level of consistency between the two OSL dating approaches and, consequently, a great suitability of the method for age determination of the Vanguard Cave sediments. It is argued in this chapter that the stratigraphy of the cave deposits generally supports a scenario of relatively stable palaeoenvironmental conditions between MIS 5 and MIS 3 in the region. The site, thus, offers great potential for detailed studies of human-environmental interactions in southern Iberia at that time building on a robust chronostratigraphical framework.

Chapter 6 - Conclusion

The last chapter provides a synthesis of the accomplishments and conclusions of this thesis and integrates the research questions posed in the introduction.

References

Adams, G., Mortlock, A.J., 1974. Thermoluminescence dating of baked sand from fire hearths at Lake Mungo, New South Wales. Archaeology and Physical Anthropology in Oceania 9, 236-237.

Adler, D.S., Wilkinson, K.N., Blockley, S., Mark, D.F., Pinhasi, R., Schmidt-Magee, B.A., Nahapetyan, S., Mallol, C., Berna, F., Glauberman, P.J., Raczynski-Henk, Y., Wales, N., Frahm, E., Jöris, O., MacLeod, A., Smith, V.C., Cullen, V.L., Gasparian, B., 2014. Early Levallois technology and the Lower to Middle Paleolithic transition in the Southern Caucasus. Science 345, 1609.

Aitken, M.J., 1985. Thermoluminescence dating. Academic, London.

Aitken, M.J., 1998. An Introduction to Optical Dating. Oxford University Press, Oxford

Alimen, M.H., 1975. Les "Isthmes" hispano-marocain et Siculo-Tunisien au temps Acheuléens. L'Anthropologie 79, 399-436.

Allen, H., 1998. Reinterpreting the 1969-1972 Willandra Lakes archaeological surveys. Archaeology in Oceania 33, 207-220.

Álvarez-Alonso, D., de Andrés-Herrero, M., Díez-Herrero, A., Medialdea, A., Rojo-Hernández, J., 2016. Neanderthal settlement in central Iberia: Geo-archaeological research in the Abrigo del Molino site, MIS 3 (Segovia, Iberian Peninsula). Quaternary International.

Amirkhanov, H.A., Ozherel'ev, D.V., Gribchenko, Y.N., Sablin, M.V., Semenov, V.V., Trubikhin, V., 2014. Early Humans at the eastern gate of Europe: The discovery and investigation of Oldowan sites in northern Caucasus. Comptes Rendus Palevol 13, 717-725.

Ankjærgaard, C., Guralnik, B., Buylaert, J.P., Reimann, T., Yi, S.W., Wallinga, J., 2016. Violet stimulated luminescence dating of quartz from Luochuan (Chinese loess plateau): Agreement with independent chronology up to ~600 ka. Quaternary Geochronology 34, 33-46.

Antón, S.C., Potts, R., Aiello, L.C., 2014. Evolution of early Homo: An integrated biological perspective. Science 345.

Armitage, S.J., Jasim, S.A., Marks, A.E., Parker, A.G., Usik, V.I., Uerpmann, H.-P., 2011. The Southern Route "Out of Africa": Evidence for an Early Expansion of Modern Humans into Arabia. Science 331, 453.

Arnold, L.J., Demuro, M., 2015. Insights into TT-OSL signal stability from single-grain analyses of known-age deposits at Atapuerca, Spain. Quaternary Geochronology.

Arnold, L.J., Demuro, M., Ruiz, M.N., 2012. Empirical insights into multi-grain averaging effects from 'pseudo' single-grain OSL measurements. Radiation Measurements 47, 652-658.

Arribas, A., Palmqvist, P., 1999. On the Ecological Connection Between Sabre-tooths and Hominids: Faunal Dispersal Events in the Lower Pleistocene and a Review of the Evidence for the First Human Arrival in Europe. Journal of Archaeological Science 26, 571-585.

Arsuaga, J.L., Martínez, I., Arnold, L.J., Aranburu, A., Gracia-Téllez, A., Sharp, W.D., Quam, R.M., Falguères, C., Pantoja-Pérez, A., Bischoff, J., Poza-Rey, E., Parés, J.M., Carretero, J.M., Demuro, M., Lorenzo, C., Sala, N., Martinón-Torres, M., García, N., Alcázar de Velasco, A., Cuenca-Bescós, G., Gómez-Olivencia, A., Moreno, D., Pablos, A., Shen, C.C., Rodríguez, L., Ortega, A.I., García, R., Bonmatí, A., Bermúdez de Castro, J.M., Carbonell, E., 2014. Neandertal roots: Cranial and chronological evidence from Sima de los Huesos. Science 344, 1358.

Arzarello, M., Pavia, G., Peretto, C., Petronio, C., Sardella, R., 2012. Evidence of an Early Pleistocene hominin presence at Pirro Nord (Apricena, Foggia, southern Italy): P13 site. Quaternary International 267, 56-61.

Bailey, G., Carrión, J.S., Fa, D.A., Finlayson, C., Finlayson, G., Rodríguez-Vidal, J., 2008. The coastal shelf of the Mediterranean and beyond: Corridor and refugium for human populations in the Pleistocene. Quaternary Science Reviews 27, 2095-2099.

Bailey, R.M., Smith, B.W., Rhodes, E.J., 1997. Partial bleaching and the decay form characteristics of quartz OSL. Radiation Measurements 27, 123-136.

Banks, W.E., d'Errico, F., Peterson, A.T., Kageyama, M., Sima, A., Sánchez-Goñi, M.-F., 2008. Neanderthal Extinction by Competitive Exclusion. PLOS ONE 3, e3972.

Bar-Yosef, O., Pilbeam, D., 2000. The Geography of Neanderthals and Modern Humans in Europe and the Greater Mediterranean. Peabody Museum of Archaeology and Ethnology, Harvard University, Cambridge, Massachusetts, p. 197.

Barton, R.N.E., Bouzouggar, A., Collcutt, S.N., Schwenninger, J.-L., Clark-Balzan, L., 2009. OSL dating of the Aterian levels at Dar es-Soltan I (Rabat, Morocco) and implications for the dispersal of modern Homo sapiens. Quaternary Science Reviews 28, 1914-1931.

Barton, R.N.E., Stringer, C.B., Finlayson, J.C., 2013. Neanderthals in Context. A report of the 1995-1998 excavations at Gorham's and Vanguard Caves, Gibraltar. Oxford University School of Archaeology, Oxford, p. 328.

Bateman, M.D., Boulter, C.H., Carr, A.S., Frederick, C.D., Peter, D., Wilder, M., 2007. Preserving the palaeoenvironmental record in Drylands: Bioturbation and its significance for luminescence-derived chronologies. Sedimentary Geology 195, 5-19.

Belmaker, M., Hovers, E., 2011. Ecological change and the extinction of the Levantine Neanderthals: implications from a diachronic study of micromammals from Amud Cave, Israel. Quaternary Science Reviews 30, 3196-3209.

Berger, L.R., de Ruiter, D.J., Churchill, S.E., Schmid, P., Carlson, K.J., Dirks, P.H.G.M., Kibii, J.M., 2010. Australopithecus sediba: A New Species of Homo-Like Australopith from South Africa. Science 328, 195.

Bermúdez de Castro, J.M., Martinón-Torres, M., Rosell, J., Blasco, R., Arsuaga, J.L., Carbonell, E., 2016. Continuity versus discontinuity of the human settlement of Europe between the late Early Pleistocene and the early Middle Pleistocene. The mandibular evidence. Quaternary Science Reviews 153, 51-62.

Beyin, A., 2011. Upper Pleistocene Human Dispersals out of Africa: A Review of the Current State of the Debate. International Journal of Evolutionary Biology 2011, 17.

Bigg, G.R., 1995. Aridity of the Mediterranean Sea at the Last Glacial Maximum: A reinterpretation of the δ18O record. Paleoceanography 10, 283-290.

Blain, H.-A., Gleed-Owen, C.P., López-García, J.M., Carrión, J.S., Jennings, R., Finlayson, G., Finlayson, C., Giles-Pacheco, F., 2013. Climatic conditions for the last Neanderthals: Herpetofaunal record of Gorham's Cave, Gibraltar. Journal of Human Evolution 64, 289-299.

Blanc, P.-L., 2002. The opening of the Plio-Quaternary Gibraltar Strait: assessing the size of a cataclysm. Geodinamica Acta 15, 303-317.

Bobe, R., Behrensmeyer, A.K., 2004. The expansion of grassland ecosystems in Africa in relation to mammalian evolution and the origin of the genus Homo. Palaeogeography, Palaeoclimatology, Palaeoecology 207, 399-420.

Boëda, É., 1994. Le Concept Levallois: Variabilité des Méthodes, Paris.

Boëda, É., 1995. Levallois: A Volumetric Construction, Method, A Technique, in: Dibble, H.L., Bar-Yosef, O. (Eds.), The Definition and Interpretation of Levallois Technology. Prehistory Press, Madison, WI, pp. 42-68.

Bøtter-Jensen, L., 1997. Luminescence techniques: instrumentation and methods. Radiation Measurements 27, 749-768.

Bøtter-Jensen, L., Andersen, C.E., Duller, G.A.T., Murray, A.S., 2003. Developments in radiation, stimulation and observation facilities in luminescence measurements. Radiation Measurements 37, 535-541.

Bøtter-Jensen, L., Bulur, E., Duller, G.A.T., Murray, A.S., 2000. Advances in luminescence instrument systems. Radiation Measurements 32, 523-528.

Bøtter-Jensen, L., Mejdahl, V., 1985. Determination of potassium in feldspars by beta counting using a GM multicounter system. Nuclear Tracks and Radiation Measurements (1982) 10, 663-666.

Bøtter-Jensen, L., Mejdahl, V., 1988. Assessment of beta dose-rate using a GM Multicounter system. Radiation Measurements 14, 187-191.

Bouzouggar, A., Barton, N., 2012. The identity and the timing of the Aterian in Morocco, in: Hublin, J.-J., McPherron, S.P. (Eds.), Modern Origins: A North African Perspective Springer, New York, pp. 93-105.

Bowler, J.M., 1998. Willandra Lakes revisited: environmental framework for human occupation. Archaeology in Oceania 33, 120-155.

Bowler, J.M., Gillespie, R., Johnston, H., Boljkovac, K., 2012. Wind v water: glacial maximum records from the Willandra Lakes. , in: Haberle, S., David, B. (Eds.), Peopled Landscapes: Archaeological and Biogeographic Approaches to Landscapes. The Australian National University, Canberra, pp. 271-296.

Bowler, J.M., Johnston, H., Olley, J.M., Prescott, J.R., Roberts, R.G., Shawcross, W., Spooner, N.A., 2003. New ages for human occupation and climatic change at Lake Mungo, Australia. Nature 421, 837-840.

Bowler, J.M., Jones, R., Allen, H., Thorne, A.G., 1970. Pleistocene human remains from Australia: A living site and human cremation from Lake Mungo, western New South Wales. World Archaeology 2, 39-60.

Bowler, J.M., Thorne, A.G., 1976. Human remains from Lake Mungo: discovery and excavation of Lake Mungo III, in: Kirk, R., Thorne, A.G. (Eds.), The Origin of the Australians Australian Institute of Aboriginal Studies, Canberra, pp. 127-138.

Boyle, R., 1664. Observations made this 27th of October, 1663, about Mr. Clayton's diamond, Experiments and considerations touching colours. Henry Herringham, London.

Brock, F., Wood, R., Higham, T.F.G., Ditchfield, P., Bayliss, A., Ramsey, C.B., 2012. Reliability of Nitrogen Content (%N) and Carbon:Nitrogen Atomic Ratios (C:N) as Indicators of Collagen Preservation Suitable for Radiocarbon Dating. Radiocarbon 54, 879-886.

Bulur, E., 1996. An alternative technique for optically stimulated luminescence (OSL) experiment. Radiation Measurements 26, 701-709.

Bulur, E., Duller, G.A.T., Solongo, S., Bøtter-Jensen, L., Murray, A.S., 2002. LM-OSL from single grains of quartz: a preliminary study. Radiation Measurements 35, 79-85.

Busk, G., 1865. On a very ancient human cranium from Gibraltar, Report of the 34th meeting of the British Association for the Advancement of Science, Bath 1864, pp. 91-92.

Carbonell, E., Barsky, D., Sala, R., Celiberti, V., 2016. Structural continuity and technological change in Lower Pleistocene toolkits. Quaternary International 393, 6-18.

Carbonell, E., Bermudez de Castro, J.M., Pares, J.M., Perez-Gonzalez, A., Cuenca-Bescos, G., Olle, A., Mosquera, M., Huguet, R., van der Made, J., Rosas, A., Sala, R., Vallverdu, J., Garcia, N., Granger, D.E., Martinon-Torres, M., Rodriguez, X.P., Stock, G.M., Verges, J.M., Allue, E., Burjachs, F., Caceres, I., Canals, A., Benito, A., Diez, C., Lozano, M., Mateos, A., Navazo, M., Rodriguez, J., Rosell, J., Arsuaga, J.L., 2008. The first hominin of Europe. Nature 452, 465-469.

Carr, A.S., Bateman, M.D., Holmes, P.J., 2007. Developing a 150 ka luminescence chronology for the barrier dunes of the southern Cape, South Africa. Quaternary Geochronology 2, 110-116.

Carrión, J.S., Finlayson, C., Fernández, S., Finlayson, G., Allué, E., López-Sáez, J.A., López-García, P., Gil-Romera, G., Bailey, G., González-Sampériz, P., 2008. A coastal reservoir of biodiversity for Upper Pleistocene human populations: palaeoecological investigations in Gorham's Cave (Gibraltar) in the context of the Iberian Peninsula. Quaternary Science Reviews 27, 2118-2135.

Cerling, T.E., 1992. Development of grasslands and savannas in East Africa during the Neogene. Palaeogeography, Palaeoclimatology, Palaeoecology 97, 241-247.

Cerling, T.E., Wynn, J.G., Andanje, S.A., Bird, M.I., Korir, D.K., Levin, N.E., Mace, W., Macharia, A.N., Quade, J., Remien, C.H., 2011. Woody cover and hominin environments in the past 6 million years. Nature 476, 51-56.

Cheddadi, R., Rossignol-Strick, M., 1995. Eastern Mediterranean Quaternary paleoclimates from pollen and isotope records of marine cores in the Nile Cone Area. Paleoceanography 10, 291-300.

Choi, J.H., Murray, A.S., Cheong, C.S., Hong, S.C., 2009. The dependence of dose recovery experiments on the bleaching of natural quartz OSL using different light sources. Radiation Measurements 44, 600-605.

Clark-Balzan, L.A., Candy, I., Schwenninger, J.-L., Bouzouggar, A., Blockley, S., Nathan, R., Barton, R.N.E., 2012. Coupled U-series and OSL dating of a Late Pleistocene cave sediment sequence, Morocco, North Africa: Significance for constructing Palaeolithic chronologies. Quaternary Geochronology 12, 53-64.

Clark, P.U., Archer, D., Pollard, D., Blum, J.D., Rial, J.A., Brovkin, V., Mix, A.C., Pisias, N.G., Roy, M., 2006. The middle Pleistocene transition: characteristics, mechanisms, and implications for long-term changes in atmospheric pCO2. Quaternary Science Reviews 25, 3150-3184.

Cohen, K.M., Gibbard, P., 2011. Global chronostratigraphical correlation table for the last 2.7 million years. Subcommission on Quaternary Stratigraphy (International Commission on Stratigraphy), Cambridge.

Combès, B., Philippe, A., Lanos, P., Mercier, N., Tribolo, C., Guerin, G., Guibert, P., Lahaye, C., 2015. A Bayesian central equivalent dose model for optically stimulated luminescence dating. Quaternary Geochronology 28, 62-70.

d'Errico, F., Vanhaeren, M., Barton, N., Bouzouggar, A., Mienis, H., Richter, D., Hublin, J.-J., McPherron, S.P., Lozouet, P., 2009. Additional evidence on the use of personal ornaments in the Middle Paleolithic of North Africa. Proceedings of the National Academy of Sciences 106, 16051-16056.

d'Errico, F., Sánchez Goñi, M.a.F., 2003. Neandertal extinction and the millennial scale climatic variability of OIS 3. Quaternary Science Reviews 22, 769-788.

d'Errico, F., Vanhaeren, M., 2007. Evolution or Revolution? New Evidence for the Origin of Symbolic Behavious In and Out of Africa, in: Mellars, P., Boyle, K., Bar-Yosef, O., Stringer, C.B. (Eds.), Rethinking the Human Revolution: New Behavioral and Biological Perspectives on the Origin and Dispersal of Modern Humans. McDonald Institute Monographs, Cambridge, pp. 275-286.

d'Errico, F., Zilhão, J., Julien, M., Baffier, D., Pelegrin, J., 1998. Neanderthal acculturation in western Europe? Current Anthropology 39, S1-S44.

Darkoh, M.B.K., 1998. The nature, causes and consequences of desertification in the drylands of Africa. Land Degradation & Development 9, 1-20.

Daujeard, C., Geraads, D., Gallotti, R., Lefèvre, D., Mohib, A., Raynal, J.-P., Hublin, J.-J., 2016. Pleistocene Hominins as a Resource for Carnivores: A c. 500,000-Year-Old Human Femur Bearing Tooth-Marks in North Africa (Thomas Quarry I, Morocco). PLOS ONE 11, e0152284.

Daujeard, C., Geraads, D., Gallotti, R., Mohib, A., Raynal, J.-P., 2012. Carcass acquisition and consumption by carnivores and hominins in Middle Pleistocene sites of Casablanca (Morocco). Journal of Taphonomy 10, 349-372.

Daura, J., Sanz, M., Julià, R., García-Fernández, D., Fornós, J.J., Vaquero, M., Allué, E., López-García, J.M., Blain, H.A., Ortiz, J.E., Torres, T., Albert, R.M., Rodríguez-Cintas, À., Sánchez-Marco, A., Cerdeño, E., Skinner, A.R., Asmeron, Y., Polyak, V.J., Garcés, M., Arnold, L.J., Demuro, M., Pike, A.W.G., Euba, I., Rodríguez, R.F., Yagüe, A.S., Villaescusa, L., Gómez, S., Rubio, A., Pedro, M., Fullola, J.M., Zilhão, J., 2015. Cova del Rinoceront (Castelldefels, Barcelona): a terrestrial record for the Last Interglacial period (MIS 5) in the Mediterranean coast of the Iberian Peninsula. Quaternary Science Reviews 114, 203-227.

de Abreu, L., Shackleton, N.J., Schönfeld, J., Hall, M., Chapman, M., 2003. Millennial-scale oceanic climate variability off the Western Iberian margin during the last two glacial periods. Marine Geology 196, 1-20.

Delagnes, A., Roche, H., 2005. Late Pliocene hominid knapping skills: The case of Lokalalei 2C, West Turkana, Kenya. Journal of Human Evolution 48, 435-472.

deMenocal, P.B., 1995. Plio-Pleistocene African Climate. Science 270, 53.

deMenocal, P.B., 2004. African climate change and faunal evolution during the Pliocene–Pleistocene. Earth and Planetary Science Letters 220, 3-24.

Demuro, M., Froese, D.G., Arnold, L.J., Roberts, R.G., 2012. Single-grain OSL dating of glaciofluvial quartz constrains Reid glaciation in NW Canada to MIS 6. Quaternary Research 77, 305-316.

Dennell, R., 2003. Dispersal and colonisation, long and short chronologies: how continuous is the Early Pleistocene record for hominids outside East Africa? Journal of Human Evolution 45, 421-440.

Dennell, R.W., Martinón-Torres, M., Bermúdez de Castro, J.M., 2011. Hominin variability, climatic instability and population demography in Middle Pleistocene Europe. Quaternary Science Reviews 30, 1511-1524.

Derricourt, R., 2005. Getting "Out of Africa": Sea Crossings, Land Crossings and Culture in the Hominin Migrations. Journal of World Prehistory 19, 119-132.

Duller, G.A.T., 2003. Distinguishing quartz and feldspar in single grain luminescence measurements. Radiation Measurements 37, 161-165.

Duller, G.A.T., 2004. Luminescence dating of quaternary sediments: recent advances. Journal of Quaternary Science 19, 183-192.

Duller, G.A.T., 2008. Single-grain optical dating of Quaternary sediments: why aliquot size matters in luminescence dating. Boreas 37, 589-612.

Duller, G.A.T., Bøtter-Jensen, L., Murray, A.S., Truscott, A.J., 1999. Single grain laser luminescence (SGLL) measurements using a novel automated reader. Nuclear Instruments and Methods in Physics Research BNuclear Instruments and Methods in Physics Research B 155, 506-514.

Emiliani, C., Geiss, J., 1959. On glaciations and their causes. Geologische Rundschau 46, 576-601.

EMODnet, 2017. Seabed Habitats project. Funded by the European Commission's Directorate-General for Maritime Affairs and Fisheries (DG MARE), www.emodnet-seabedhabitats.eu.

Ennouchi, E., 1969. Découvertes d'un Pithécanthropien au Maroc. Comptes Rendus de l'Académie des Sciences de Paris 269, 763-765.

Feathers, J., 2015. Luminescence Dating of Archaeological Sediments, in: Jack Rink, W., Thompson, J.W. (Eds.), Encyclopedia of Scientific Dating Methods. Springer Netherlands, Dordrecht, pp. 404-409.

Feathers, J.K., 2002. Luminescence Dating in Less Than Ideal Conditions: Case Studies from Klasies River Main Site and Duinefontein, South Africa. Journal of Archaeological Science 29, 177-194.

Fernández, S., Fuentes, N., Carrión, J.S., González-Sampériz, P., Montoya, E., Gil, G., Vega-Toscano, G., Riquelme, J.A., 2007. The Holocene and Upper Pleistocene pollen sequence of Carihuela Cave, southern Spain. Geobios 40, 75-90.

Ferring, R., Oms, O., Agustí, J., Berna, F., Nioradze, M., Shelia, T., Tappen, M., Vekua, A., Zhvania, D., Lordkipanidze, D., 2011. Earliest human occupations at Dmanisi (Georgian Caucasus) dated to 1.85–1.78 Ma. Proceedings of the National Academy of Sciences 108, 10432-10436.

Finlayson, C., Brown, K., Blasco, R., Rosell, J., Negro, J.J., Bortolotti, G.R., Finlayson, G., Sánchez Marco, A., Giles Pacheco, F., Rodríguez Vidal, J., Carrión, J.S., Fa, D.A., Rodríguez Llanes, J.M., 2012. Birds of a Feather: Neanderthal Exploitation of Raptors and Corvids. PLoS ONE 7, e45927.

Finlayson, C., Carrión, J.S., 2007. Rapid ecological turnover and its impact on Neanderthal and other human populations. Trends in Ecology & Evolution 22, 213-222.

Finlayson, C., Giles Pacheco, F., Rodriguez-Vidal, J., Fa, D.A., Maria Gutierrez Lopez, J., Santiago Perez, A., Finlayson, G., Allue, E., Baena Preysler, J., Caceres, I., Carrion, J.S., Fernandez Jalvo, Y., Gleed-Owen, C.P., Jimenez Espejo, F.J., Lopez, P., Antonio Lopez Saez, J., Antonio Riquelme Cantal, J., Sanchez Marco, A., Giles Guzman, F., Brown, K., Fuentes, N., Valarino, C.A., Villalpando, A., Stringer, C.B., Martinez Ruiz, F., Sakamoto, T., 2006. Late survival of Neanderthals at the southernmost extreme of Europe. Nature 443, 850-853.

Fitzsimmons, K.E., 2011. An assessment of the luminescence sensitivity of Australian quartz with respect to sediment history. Geochron 38, 199-208.

Fitzsimmons, K.E., 2017. Reconstructing palaeoenvironments on desert margins: New perspectives from Eurasian loess and Australian dry lake shorelines. Quaternary Science Reviews 171, 1-19.

Fitzsimmons, K.E., Rhodes, E.J., Barrows, T.T., 2010. OSL dating of southeast Australian quartz: A preliminary assessment of luminescence characteristics and behaviour. Quaternary Geochronology 5, 91-95.

Fitzsimmons, K.E., Stern, N., Murray-Wallace, C.V., 2014. Depositional history and archaeology of the central Lake Mungo lunette, Willandra Lakes, southeast Australia. Journal of Archaeological Science 41, 349-364.

Fitzsimmons, K.E., Stern, N., Murray-Wallace, C.V., Truscott, W., Pop, C., 2015. The Mungo Mega-Lake Event, Semi-Arid Australia: Non-Linear Descent into the Last Ice Age, Implications for Human Behaviour. PLOS ONE 10, e0127008.

Fleming, S.J., 1970. Thermoluminescent dating: refinement of the quartz inclusion method. Archaeometry 12, 133-143.

Gabunia, L., Vekua, A., Lordkipanidze, D., Swisher, C.C., Ferring, R., Justus, A., Nioradze, M., Tvalchrelidze, M., Antón, S.C., Bosinski, G., Jöris, O., Lumley, M.-A.d., Majsuradze, G., Mouskhelishvili, A., 2000. Earliest Pleistocene Hominid Cranial Remains from Dmanisi, Republic of Georgia: Taxonomy, Geological Setting, and Age. Science 288, 1019.

Galbraith, R.F., 1988. Graphical display of estimates having differing standard errors. Technometrics 30, 271-281.

Galbraith, R.F., 1990. The radial plot: Graphical assessment of spread in ages. International Journal of Radiation Applications and Instrumentation. Part D. Nuclear Tracks and Radiation Measurements 17, 207-214.

Galbraith, R.F., Roberts, R.G., Laslett, G.M., Yoshida, H., Olley, J.M., 1999. Optical dating of single and multiple grains of quartz from Jinmium rock shelter, northern Australia: Part I, experimental design and statistical models. Archaeometry 41, 339-364.

Galván, B., Hernández, C.M., Mallol, C., Mercier, N., Sistiaga, A., Soler, V., 2014. New evidence of early Neanderthal disappearance in the Iberian Peninsula. Journal of Human Evolution 75, 16-27.

Garcea, E.A.A., 2010a. Bridging the gap between in and out of Africa, in: Garcea, E.A.A. (Ed.), South-Eastern Mediterranean Peoples between 130,000 and 10,000 Years Ago. Oxbow Books, Oxford, pp. 174-181.

Garcea, E.A.A., 2010b. The Spread of Aterian Peoples in North Africa, in: Garcea, E.A.A. (Ed.), South-Eastern Mediterranean Peoples Between 130,000 and 10,000 Years Ago. Oxbow Books, Oxford, pp. 37-53.

Garcea, E.A.A., 2012. Successes and failures of human dispersals from North Africa. Quaternary International 270, 119-128.

Garcea, E.A.A., 2016. Dispersals Out of Africa and Back to Africa: Modern origins in North Africa. Quaternary International 408, Part B, 79-89.

Garcia-Castellanos, D., Estrada, F., Jiménez-Munt, I., Gorini, C., Fernàndez, M., Vergés, J., De Vicente, R., 2009. Catastrophic flood of the Mediterranean after the Messinian salinity crisis. Nature 462, 778-781.

Garrod, D.A.E., Buxton, L.H.D., Elliot Smith, G., Bate, D.M.A., Spiller, R.C., Hinton, M.A.C., Fischer, P., 1928. Excavation of a Mousterian Rock-Shelter at Devil's Tower, Gibraltar. The Journal of the Royal Anthropological Institute of Great Britain and Ireland 58, 33-113.

Geraads, D., 2002. Plio-Pleistocene mammalian biostratigraphy of Atlantic Morocco / Biostratigraphie des mammifères Plio-Pléistocènes du Maroc atlantique. Quaternaire, 43-53.

Geraads, D., Amani, F., 1998. Bovidae (Mammalia) du Pliocène final d'Ahl al Oughlam, Casablanca, Maroc. Paläontologische Zeitschrift 72, 191.

Geraads, D., Beriro, P., Roche, H., 1980. La faune et l'industrie des sites a Homo erectus des carrieres Thomas (Maroc). Comptes Rendus de l'Académie des Sciences de Paris série D 291, 195-198.

Geraads, D., Raynal, J.-P., Eisenmann, V., 2004. The earliest human occupation of North Africa: a reply to Sahnouni et al. (2002). Journal of Human Evolution 46, 751-761.

Gesner, C., 1555. De raris et admirandis herbis, quæ sive quod noctu luceant, sive alias ob causas, Lunariæ nominantur, Commentariolus et obiter de alijs etiam rebus quæ in tenebris lucent (A short commentary on rare and marvellous plants that are called lunar either because they shine at night or for other reasons; and also on other things that shine in darkness). Tiguri, Zurich.

Gibert, J., Gibert, L., Iglesias, A., 2003. The Gibraltar Strait: A Pleistocene door of Europe? Human Evolution 18, 147-160.

Gibert, L., Scott, G.R., Scholz, D., Budsky, A., Ferràndez, C., Ribot, F., Martin, R.A., Lería, M., 2016. Chronology for the Cueva Victoria fossil site (SE Spain): Evidence for Early Pleistocene Afro-Iberian dispersals. Journal of Human Evolution 90, 183-197.

Godfrey-Smith, D.I., Huntley, D.J., Chen, W.H., 1988. Optical dating studies of quartz and feldspar sediment extracts. Quaternary Science Reviews 7, 373-380.

Grün, R., 2006. Direct dating of human fossils. American Journal of Physical Anthropology 131, 2-48.

Grün, R., Stringer, C., McDermott, F., Nathan, R., Porat, N., Robertson, S., Taylor, L., Mortimer, G., Eggins, S., McCulloch, M., 2005. U-series and ESR analyses of bones and teeth relating to the human burials from Skhul. Journal of Human Evolution 49, 316-334.

Guérin, G., 2015. Luminescence Dating, Dose Rates, in: Jack Rink, W., Thompson, J.W. (Eds.), Encyclopedia of Scientific Dating Methods. Springer Netherlands, Dordrecht, pp. 414-417.

Guérin, G., Discamps, E., Lahaye, C., Mercier, N., Guibert, P., Turq, A., Dibble, H.L., McPherron, S.P., Sandgathe, D., Goldberg, P., Jain, M., Thomsen, K., Patou-Mathis, M., Castel, J.-C., Soulier, M.-C., 2012. Multi-method (TL and OSL), multi-material (quartz and flint) dating of the Mousterian site of Roc de Marsal (Dordogne, France): correlating Neanderthal occupations with the climatic variability of MIS 5–3. Journal of Archaeological Science 39, 3071-3084.

Guérin, G., Frouin, M., Tuquoi, J., Thomsen, K.J., Goldberg, P., Aldeias, V., Lahaye, C., Mercier, N., Guibert, P., Jain, M., Sandgathe, D., McPherron, S.J.P., Turq, A., Dibble, H.L., 2016. The complementarity of luminescence dating methods illustrated on the Mousterian sequence of the Roc de Marsal: A series of reindeer-dominated, Quina Mousterian layers dated to MIS 3. Quaternary International.

Guérin, G., Mercier, N., Adamiec, G., 2011. Dose-rate conversion factors: update. Ancient TL 29, 5-8.

Guhl, A., Bertran, P., Zielhofer, C., Fitzsimmons, K.E., 2013. Optically Stimulated Luminescence (OSL) dating of sand-filled wedge structures and their fine-grained host sediment from Jonzac, SW France. Boreas 42, 317-332.

Harmand, S., Lewis, J.E., Feibel, C.S., Lepre, C.J., Prat, S., Lenoble, A., Boes, X., Quinn, R.L., Brenet, M., Arroyo, A., Taylor, N., Clement, S., Daver, G., Brugal, J.-P., Leakey, L., Mortlock, R.A., Wright, J.D., Lokorodi, S., Kirwa, C., Kent, D.V., Roche, H., 2015. 3.3-million-year-old stone tools from Lomekwi 3, West Turkana, Kenya. Nature 521, 310-315.

Harvey, E.N., 1957. A history of luminescence. Memoirs of the American Philosophical society 44, 1-351.

Hays, J.D., Imbrie, J., Shackleton, N.J., 1976. Variations in the Earth's Orbit: Pacemaker of the Ice Ages. Science 194, 1121.

Head, M.J., Gibbard, P.L., 2005. Early-Middle Pleistocene transitions: an overview and recommendation for the defining boundary. Geological Society, London, Special Publications 247, 1.

Henry, A.G., Brooks, A.S., Piperno, D.R., 2014. Plant foods and the dietary ecology of Neanderthals and early modern humans. Journal of Human Evolution 69, 44-54.

Heterington, R., Reid, R.G.B., 2010. The Climate Connection: Climate Change and Modern Human Evolution. Cambridge University Press, Cambridge.

Higham, T., Douka, K., Wood, R., Ramsey, C.B., Brock, F., Basell, L., Camps, M., Arrizabalaga, A., Baena, J., Barroso-Ruiz, C., Bergman, C., Boitard, C., Boscato, P., Caparros, M., Conard, N.J., Draily, C., Froment, A., Galvan, B., Gambassini, P., Garcia-Moreno, A., Grimaldi, S., Haesaerts, P., Holt, B., Iriarte-Chiapusso, M.-J., Jelinek, A., Jorda Pardo, J.F., Maillo-Fernandez, J.-M., Marom, A., Maroto, J., Menendez, M., Metz, L., Morin, E., Moroni, A., Negrino, F., Panagopoulou, E., Peresani, M., Pirson, S., de la Rasilla, M., Riel-Salvatore, J., Ronchitelli, A., Santamaria, D., Semal, P., Slimak, L., Soler, J., Soler, N., Villaluenga, A., Pinhasi, R., Jacobi, R., 2014. The timing and spatiotemporal patterning of Neanderthal disappearance. Nature 512, 306-309.

Hoffmann, D.L., Rogerson, M., Spötl, C., Luetscher, M., Vance, D., Osborne, A.H., Fello, N.M., Moseley, G.E., 2016. Timing and causes of North African wet phases during the last glacial period and implications for modern human migration. Scientific Reports 6, 36367.

Hublin, J.-J., 2012. The earliest modern human colonization of Europe. Proceedings of the National Academy of Sciences 109, 13471-13472.

Hublin, J.-J., Ben-Ncer, A., Bailey, S.E., Freidline, S.E., Neubauer, S., Skinner, M.M., Bergmann, I., Le Cabec, A., Benazzi, S., Harvati, K., Gunz, P., 2017. New fossils from Jebel Irhoud, Morocco and the pan-African origin of Homo sapiens. Nature 546, 289-292.

Hublin, J.J., 2009. The origin of Neandertals. Proceedings of the National Academy of Sciences 106, 16022-16027.

Hublin, J.J., Barroso-Ruíz, C., Lara, P.M., Fontugne, M., Reyss, J.L., 1995. The Mousterian site of Zafarraya (Andalucia, Spain): dating and implications on the Palaeolithic peopling processes of Western Europe. Comptes Rendus de l'Académie des Sciences de Paris, série IIa 32, 931-937.

Huntley, D.J., Godfrey-Smith, D.I., Thewalt, M.L.W., 1985. Optical dating of sediments. Nature 313, 105-107.

Huntley, D.J., Lamothe, M., 2001. Ubiquity of anomalous fading in K-feldspars and the measurement and correction for it in optical dating. Canadian Journal of Earth Sciences 38, 1093-1106.

Hütt, G., Jaek, I., Tchonka, J., 1988. Optical dating: K-feldspars optical response stimulation spectra. Quaternary Science Reviews 7, 381-385.

Jacobs, Z., Duller, G.A.T., Wintle, A.G., 2003. Optical dating of dune sand from Blombos Cave, South Africa: II—single grain data. Journal of Human Evolution 44, 613-625.

Jacobs, Z., Duller, G.A.T., Wintle, A.G., 2006. Interpretation of single grainDe distributions and calculation of De. Radiation Measurements 41, 264-277.

Jacobs, Z., Meyer, M.C., Roberts, R.G., Aldeias, V., Dibble, H., El Hajraoui, M.A., 2011. Single-grain OSL dating at La Grotte des Contrebandiers ('Smugglers' Cave'), Morocco: improved age constraints for the Middle Paleolithic levels. Journal of Archaeological Science 38, 3631-3643.

Jacobs, Z., Roberts, R.G., 2007. Advances in Optically Stimulated Luminescence Dating of Individual Grains of Quartz from Archeological Deposits. Evolutionary Anthropology 16, 210-223.

Jacobs, Z., Roberts, R.G., Nespoulet, R., El Hajraoui, M.A., Debénath, A., 2012. Single-grain OSL chronologies for Middle Palaeolithic deposits at El Mnasra and El Harhoura 2, Morocco: Implications for Late Pleistocene humaneenvironment interactions along the Atlantic coast of northwest Africa. Journal of Human Evolution 62, 377-394.

Jiménez-Espejo, F.J., Rodríguez-Vidal, J., Finlayson, C., Martínez-Ruiz, F., Carrión, J.S., García-Alix, A., Paytan, A., Giles Pacheco, F., Fa, D.A., Finlayson, G., Cortés-Sánchez, M., Rodrigo Gámiz, M., González-Donoso, J.M., Linares, M.D., Cáceres, L.M., Fernández, S., Iijima, K., Martínez Aguirre, A., 2013. Environmental conditions and geomorphologic changes during the Middle–Upper Paleolithic in the southern Iberian Peninsula. Geomorphology 180–181, 205-216.

Jull, A.J.T., Burr, G.S., 2015. Radiocarbon Dating, in: Jack Rink, W., Thompson, J.W. (Eds.), Encyclopedia of Scientific Dating Methods. Springer Netherlands, Dordrecht, pp. 669-676.

Klein, R.G., 1994. Southern Africa before the Iron Age, in: Corruccini, R.S., Ciochon, R.L. (Eds.), Integrative paths to the past: Paleoanthropological advances in honor of F. Clark Howell. Prentice Hall, Englewood Cliffs, pp. 471-519.

Klein, R.G., 2008. Out of Africa and the evolution of human behavior. Evolutionary Anthropology: Issues, News, and Reviews 17, 267-281.

Klein, R.G., 2009. The human career : human biological and cultural origins. The University of Chicago Press, Chicago.

Klotz, S., Fauquette, S., Combourieu-Nebout, N., Uhl, D., Suc, J.-P., Mosbrugger, V., 2006. Seasonality intensification and long-term winter cooling as a part of the Late Pliocene climate development. Earth and Planetary Science Letters 241, 174-187.

Krbetschek, M.R., Rieser, U., Zöller, L., Heinicke, J., 1994. Radioactive disequilibria in palaeodosimetric dating of sediments. Radiation Measurements 23, 485-489.

Krijgsman, W., Hilgen, F.J., Raffi, I., Sierro, F.J., Wilson, D.S., 1999. Chronology, causes and progression of the Messinian salinity crisis. Nature 400, 652-655.

Kuhn, S.L., Stiner, M.C., 2007. Body Ornamentation as Information Technology: Towards an Understanding of the Significance of Early Beads, in: Mellars, P., Boyle, K., Bar-Yosef, O., Stringer, C.B. (Eds.), Rethinking the Human Revolution: New Behavioral and Biological Perspectives on the Origin and Dispersal of Modern Humans. McDonald Institute Monographs, Cambridge, pp. 45-54.

Lahr, M.M., 2010. Saharan Corridors and Their Role in the Evolutionary Geography of 'Out of Africa I', in: Fleagle, J.G., Shea, J.J., Grine, F.E., Baden, A.L., Leakey, R.E. (Eds.), Out of Africa I: The First Hominin Colonization of Eurasia. Springer Netherlands, Dordrecht, pp. 27-46.

Lahr, M.M., Foley, R., 1994. Multiple dispersals and modern human origins. Evolutionary Anthropology: Issues, News, and Reviews 3, 48-60.

Larrosaña, J.C., 2012. Saharan Climate and Modern Human Origins, in: Hublin, J.-J., McPherron, S.P. (Eds.), Modern Origins. Springer, New York, pp. 19-34.

Lefevre, D., Texier, J.-P., Raynal, J.-P., Occhietti, S., Evin, J., 1994. Enregistrements-réponses des variations climatiques du Pléistocène supérieur et de l'Holocène sur le littoral de Casablanca (Maroc) / Upper Pleistocene and Holocene records on the Casablanca coast (Morocco). Quaternaire, 173-180.

Leroy, S.A.G., Arpe, K., Mikolajewicz, U., 2011. Vegetation context and climatic limits of the Early Pleistocene hominin dispersal in Europe. Quaternary Science Reviews 30, 1448-1463.

Lisiecki, L.E., Raymo, M.E., 2005. A Pliocene-Pleistocene stack of 57 globally distributed benthic δ18O records. Paleoceanography 20.

Lomax, J., Hilgers, A., Twidale, C.R., Bourne, J.A., Radtke, U., 2007. Treatment of broad palaeodose distributions in OSL dating of dune sands from the western Murray Basin, South Australia. Quaternary Geochronology 2, 51-56.

Lombard, M., Phillipson, L., 2015. Indications of bow and stone-tipped arrow use 64 000 years ago in KwaZulu-Natal, South Africa. Antiquity 84, 635-648.

Lordkipanidze, D., Ponce de León, M.S., Margvelashvili, A., Rak, Y., Rightmire, G.P., Vekua, A., Zollikofer, C.P.E., 2013. A Complete Skull from Dmanisi, Georgia, and the Evolutionary Biology of Early Homo. Science 342, 326.

Lorenz, A., 1983. Proposed Recommended List of Heavy Element Radionuclide Decay Data. International Nuclear Data Committee, Vienna.

Lowe, J.J., Walker, M.J., 2015. Reconstructing Quaternary Environments, 3. ed. Routledge, London.

Lyubin, V.P., Belyaeva, E.V., 2006. Cleavers and handaxes with transverse cutting edge in the Acheulian of the Caucasus, in: Goren-Inbar, N., Sharon, G. (Eds.), Axe Age: Acheulian Tool-making from Quarry to Discard. Equinox, London, pp. 347-364.

Marean, C.W., 2015. An Evolutionary Anthropological Perspective on Modern Human Origins. Annual Review of Anthropology 44, 553-556.

Martinet, G., Searight, S., 1994. Le Maghreb préhistrorique et la navigation Bulletin de la Société d'Etudes et de Recherches Préhistorique des Eyzies 43, 85-111.

Martínez-Navarro, B., Belmaker, M., Bar-Yosef, O., 2009. The large carnivores from 'Ubeidiya (early Pleistocene, Israel): biochronological and biogeographical implications. Journal of Human Evolution 56, 514-524.

Maslin, M.A., Brierley, C.M., 2015. The role of orbital forcing in the Early Middle Pleistocene Transition. Quaternary International 389, 47-55.

Maslin, M.A., Brierley, C.M., Milner, A.M., Shultz, S., Trauth, M.H., Wilson, K.E., 2014. East African climate pulses and early human evolution. Quaternary Science Reviews 101, 1-17.

McBrearty, S., Brooks, A.S., 2000. The revolution that wasn't: a new interpretation of the origin of modern human behavior. Journal of Human Evolution 39, 453-563.

Mejdahl, V., 1979. Thermoluminescence dating: beta-dose attenuation in quartz grains. Archaeometry 21, 61-72.

Mellars, P., 2004. Neanderthals and the modern human colonization of Europe. Nature 432, 461-465.

Mellars, P., 2006. A new radiocarbon revolution and the dispersal of modern humans in Eurasia. Nature 439, 931-935.

Mercier, N., Wengler, L., Valladas, H., Joron, J.-L., Froget, L., Reyss, J.L., 2007. The Rhafas Cave (Morocco): Chronology of the mousterian and aterian archaeological occupations and their implications for Quaternary geochronology based on luminescence (TL/OSL) age determinations. Quaternary Geochronology 2, 309-313.

Meyer, M., Arsuaga, J.-L., de Filippo, C., Nagel, S., Aximu-Petri, A., Nickel, B., Martínez, I., Gracia, A., de Castro, J.M.B., Carbonell, E., Viola, B., Kelso, J., Prüfer, K., Pääbo, S., 2016. Nuclear DNA sequences from the Middle Pleistocene Sima de los Huesos hominins. Nature 531, 504-507.

Meyer, M., Kircher, M., Gansauge, M.-T., Li, H., Racimo, F., Mallick, S., Schraiber, J.G., Jay, F., Prüfer, K., de Filippo, C., Sudmant, P.H., Alkan, C., Fu, Q., Do, R., Rohland, N., Tandon, A., Siebauer, M., Green, R.E., Bryc, K., Briggs, A.W., Stenzel, U., Dabney, J., Shendure, J., Kitzman, J., Hammer, M.F., Shunkov, M.V., Derevianko, A.P., Patterson, N., Andrés, A.M., Eichler, E.E., Slatkin, M., Reich, D., Kelso, J., Pääbo, S., 2012. A High-Coverage Genome Sequence from an Archaic Denisovan Individual. Science.

Micheels, A., Eronen, J., Mosbrugger, V., 2009. The Late Miocene climate response to a modern Sahara desert. Global and Planetary Change 67, 193-204.

Milankovitch, M., 1920. Théorie Mathématique des Phénomènes Thermiques Produits par la Radiation Solaire. Gauthier-Villars, Paris.

Miller, K.G., Kominz, M.A., Browning, J.V., Wright, J.D., Mountain, G.S., Katz, M.E., Sugarman, P.J., Cramer, B.S., Christie-Blick, N., Pekar, S.F., 2005. The Phanerozoic Record of Global Sea-Level Change. Science 310, 1293.

Moreno, A., Cacho, I., Canals, M., Grimalt, J.O., Sánchez-Goñi, M.F., Shackleton, N., Sierro, F.J., 2005. Links between marine and atmospheric processes oscillating on a millennial time-scale. A multi-proxy study of the last 50,000yr from the Alboran Sea (Western Mediterranean Sea). Quaternary Science Reviews 24, 1623-1636.

Murray, A.S., Thomsen, K.J., Masuda, N., Buylaert, J.P., Jain, M., 2012. Identifying well-bleached quartz using the different bleaching rates of quartz and feldspar luminescence signals. Radiation Measurements 47, 688-695.

Murray, A.S., Wintle, A.G., 2000. Luminescence dating of quartz using an improved single-aliquot regenerative-dose protocol. Radiation Measurements 32, 57-73.

Murray, A.S., Wintle, A.G., 2003. The single aliquot regenerative dose protocol: potential for improvements in reliability. Radiation Measurements 37, 377-381.

Muttoni, G., Kent, D.V., Scardia, G., Monesi, E., 2014. Migration of hominins with megaherbivores into Europe via the Danube-Po gateway in the Late Matuyama climate revolution. Rivista Italiana di Paleontologia e Stratgrafia 120, 351-365.

Muttoni, G., Scardia, G., Kent, D.V., 2010. Human migration into Europe during the late Early Pleistocene climate transition. Palaeogeography, Palaeoclimatology, Palaeoecology 296, 79-93.

Olley, J.M., Murray, A., Roberts, R.G., 1996. The effects of disequilibria in the uranium and thorium decay chains on burial dose rates in fluvial sediments. Quaternary Science Reviews 15, 751-760.

Olley, J.M., Pietsch, T., Roberts, R.G., 2004. Optical dating of Holocene sediments from a variety of geomorphic settings using single grains of quartz. Geomorphology 60, 337-358.

Olley, J.M., Roberts, R.G., Murray, A.S., 1997. Disequilibria in the uranium decay series in sedimentary deposits at Allen's cave, nullarbor plain, Australia: Implications for dose rate determinations. Radiation Measurements 27, 433-443.

Olley, J.M., Roberts, R.G., Yoshida, H., Bowler, J.M., 2006. Single-grain optical dating of grave-infill associated with human burials at Lake Mungo, Australia. Quaternary Science Reviews 25, 2469-2474.

Pagani, L., Schiffels, S., Gurdasani, D., Danecek, P., Scally, A., Chen, Y., Xue, Y., Haber, M., Ekong, R., Oljira, T., Mekonnen, E., Luiselli, D., Bradman, N., Bekele, E., Zalloua, P., Durbin, R., Kivisild, T., Tyler-Smith, C., 2015. Tracing the Route of Modern Humans out of Africa by Using 225 Human Genome Sequences from Ethiopians and Egyptians. The American Journal of Human Genetics 96, 986-991.

Paillard, D., 1998. The timing of Pleistocene glaciations from a simple multiple-state climate model. Nature 391, 378-381.

Parés, J.M., Sahnouni, M., Van der Made, J., Pérez-González, A., Harichane, Z., Derradji, A., Medig, M., 2014. Early human settlements in Northern Africa: paleomagnetic evidence from the Ain Hanech Formation (northeastern Algeria). Quaternary Science Reviews 99, 203-209.

Partridge, T.C., Wood, B.A., deMenocal, P.B., 1995. The influence of global climatic change and regional uplift on large-mammal evolution in East and southern Africa, in: Vrba, E.S., Denton, G.H., Partridge, T.C., Burckle, L.H. (Eds.), Paleoclimate and Evolution, with Emphasis on Human Origins. Yale University Press, New Haven, pp. 331-355.

Pettitt, P.B., Bailey, R.M., 2000. AMS Radiocarbon and Luminescence Dating of Gorham's and Vanguard Caves, Gibraltar, and Implications for the Middle to Upper Palaeolithic Transition in Iberia, in: Stringer, C.B., Barton, R.N.E., Finlayson, J.C. (Eds.), Neanderthals on the Edge. Oxbow Books, Oxford, pp. 155-162.

Pietsch, T.J., Olley, J.M., Nanson, G.C., 2008. Fluvial transport as a natural luminescence sensitiser of quartz. Quaternary Geochronology 3, 365-376.

Pike, A.W.G., Hoffmann, D.L., García-Diez, M., Pettitt, P.B., Alcolea, J., De Balbín, R., González-Sainz, C., de las Heras, C., Lasheras, J.A., Montes, R., Zilhão, J., 2012. U-Series Dating of Paleolithic Art in 11 Caves in Spain. Science 336, 1409.

Pirson, S., Flas, D., Abrams, G., Bonjean, D., Court-Picon, M., Di Modica, K., Draily, C., Damblon, F., Haesaerts, P., Miller, R., Rougier, H., Toussaint, M., Semal, P., 2012. Chronostratigraphic context of the Middle to Upper Palaeolithic transition: Recent data from Belgium. Quaternary International 259, 78-94.

Pollard, A.M., 2009. Measuring the Passage of Time: Achievements and Challenges in Archaeological Dating, in: Cunliffe, B., Gosden, C., Joyce, R.A. (Eds.), The Oxford handbook of archaeology. Oxford University Press, Oxford.

Porat, N., Rosen, S.A., Boaretto, E., Avni, Y., 2006. Dating the Ramat Saharonim Late Neolithic desert cult site. Journal of Archaeological Science 33, 1341-1355.

Potts, R., 2012. Environmental and Behavioral Evidence Pertaining to the Evolution of Early Homo. Current Anthropology 53, 299-317.

Powell, A., Shennan, S., Thomas, M.G., 2009. Late Pleistocene Demography and the Appearance of Modern Human Behavior. Science 324, 1298.

Prat, S., 2016. First hominin settlements out of Africa. Tempo and dispersal mode: Review and perspectives. Comptes Rendus Palevol.

Prescott, J.R., Hutton, J.T., 1988. Cosmic ray and gamma ray dosimetry for TL and ESR. International Journal of Radiation Applications and Instrumentation. Part D. Nuclear Tracks and Radiation Measurements 14, 223-227.

Prescott, J.R., Hutton, J.T., 1994. Cosmic ray contributions to dose rates for luminescence and ESR dating: Large depths and long-term time variations. Radiation Measurements 23, 497-500.

Quade, J., Levin, N., Semaw, S., Stout, D., Renne, P., Rogers, M., Simpson, S., 2004. Paleoenvironments of the earliest stone toolmakers, Gona, Ethiopia. GSA Bulletin 116, 1529-1544.

Rampino, M.R., Self, S., 1992. Volcanic winter and accelerated glaciation following the Toba super-eruption. Nature 359, 50-52.

Raynal, J.-P., Magoga, L., Sbihi-Alaoui, F.Z., Geraads, D., 1993. La grotte des Rhinocéros (Carrière Oulad Hamida I, anciennnment Thomas III, Casablanca), nouveau site acheuléen du Maroc atlantique. Comptes Rendus de l'Académie des Sciences de Paris série II 316, 1477-1483.

Raynal, J.-P., Magoga, L., Sbihi-Alaoui, F.Z., Geraads, D., 1995. The earliest occupation of Atlantic Morocco: the Casablanca evidence, in: Roebroeks, W., Van Kolfschoten, T. (Eds.), The earliest occupation of Europe. University of Leiden, Leiden, pp. 255-262.

Raynal, J.-P., Sbihi-Alaoui, F.-Z., Geraads, D., Magoga, L., Mohi, A., 2001. The earliest occupation of North-Africa: the Moroccan perspective. Quaternary International 75, 65-75.

Raynal, J.-P., Sbihi-Alaoui, F.-Z., Mohib, A., El Graoui, M., Lefèvre, D., Texier, J.-P., Geraads, D., Hublin, J.-J., Smith, T., Tafforeau, P., Zouak, M., Grün, R., Rhodes, E.J., Eggins, S., Daujeard, C., Fernandes, P., Gallotti, R., Hossini, S., Queffelec, A., 2010. Hominid Cave at Thomas Quarry I (Casablanca, Morocco): Recent findings and their context. Quaternary International 223-224, 369-382.

Raynal, J.-P., Texier, J.P., 1989. Découverte d'Acheuléen ancien dans la carrière Thomas I à Casablanca et problème de l'ancienneté de la présence humaine au Maroc. Comptes Rendus de l'Académie des Sciences de Paris série II 308, 1743-1749.

Reimer, P.J., Bard, E., Bayliss, A., Beck, J.W., Blackwell, P.G., Ramsey, C.B., Buck, C.E., Cheng, H., Edwards, R.L., Friedrich, M., Grootes, P.M., Guilderson, T.P., Haflidason, H., Hajdas, I., Hatté, C., Heaton, T.J., Hoffmann, D.L., Hogg, A.G., Hughen, K.A., Kaiser, K.F., Kromer, B., Manning, S.W., Niu, M., Reimer, R.W., Richards, D.A., Scott, E.M., Southon, J.R., Staff, R.A., Turney, C.S.M., van der Plicht, J., 2016. IntCal13 and Marine13 Radiocarbon Age Calibration Curves 0–50,000 Years cal BP. Radiocarbon 55, 1869-1887.

Reyes-Centeno, H., 2016. Out of Africa and into Asia: Fossil and genetic evidence on modern human origins and dispersals. Quaternary International 416, 249-262.

Rhodes, E.J., 2007. Quartz single grain OSL sensitivity distributions: implications for multiple grain single aliquot dating Geochron 26, 19-29.

Rhodes, E.J., 2013. OSL age estimates from Vanguard Cave, in: Barton, R.N.E., Stringer, C.B., Finlayson, J.C. (Eds.), Neanderthals in Context. A report of the 1995-1998 excavations at Gorham's and Vanguard Caves, Gibraltar. Oxford University School of Archaeology, Oxford, pp. 211-217.

Rhodes, E.J., Raynal, J.-P., Geraads, D., Sbihi-Alaoui, F.Z., 1994. Prenières dates RPE pour l'Acheuléen du Maroc atlantique (Grotte des Rhinocéros, Casablanca). Comptes Rendus de l'Académie des Sciences de Paris série II 319, 1109-1115.

Rhodes, E.J., Singarayer, J.S., Raynal, J.-P., Westaway, K.E., Sbihi-Alaoui, F.Z., 2006. New age estimates for the Palaeolithic assemblages and Pleistocene succession of Casablanca, Morocco. Quaternary Science Reviews 25, 2569-2585.

Roberts, R., Bird, M., Olley, J., Galbraith, R., Lawson, E., Laslett, G., Yoshida, H., Jones, R., Fullagar, R., Jacobsen, G., Hua, Q., 1998. Optical and radiocarbon dating at Jinmium rock shelter in northern Australia. Nature 393, 358-362.

Roberts, R.G., Galbraith, R.F., Olley, J.M., Yoshida, H., Laslett, G.M., 1999. Optical dating of single and multiple grains of quartz from Jinmium rock shelter, northern Australia: part II, results and implications. Archaeometry 41, 365-395.

Roberts, R.G., Galbraith, R.F., Yoshida, H., Laslett, G.M., Olley, J.M., 2000. Distinguishing dose populations in sediment mixtures: a test of single-grain optical dating procedures using mixtures of laboratory-dosed quartz. Radiation Measurements 32, 459-465.

Roberts, R.G., Jacobs, Z., 2015. Luminescence Dating, Single-Grain Dose Distribution, in: Jack Rink, W., Thompson, J.W. (Eds.), Encyclopedia of Scientific Dating Methods. Springer Netherlands, Dordrecht, pp. 435-440.

Rodríguez-Vidal, J., Cáceres, L.M., Finlayson, J.C., Gracia, F.J., Martínez-Aguirre, A., 2004. Neotectonics and shoreline history of the Rock of Gibraltar, southern Iberia. Quaternary Science Reviews 23, 2017-2029.

Roebroeks, W., Soressi, M., 2016. Neandertals revised. Proceedings of the National Academy of Sciences 113, 6372-6379.

Roebroeks, W., Villa, P., 2011. On the earliest evidence for habitual use of fire in Europe. Proceedings of the National Academy of Sciences 108, 5209-5214.

Rose, E.P.F., Rosenbaum, M.S., 1994. The rock of Gibraltar and its Neogene tectonics. Paleontologia i evolució 24-25, 411-421.

Roucoux, K.H., de Abreu, L., Shackleton, N.J., Tzedakis, P.C., 2005. The response of NW Iberian vegetation to North Atlantic climate oscillations during the last 65 kyr. Quaternary Science Reviews 24, 1637-1653.

Ruddiman, W.F., Prell, W.L., Raymo, M.E., 1989. Late Cenozoic uplift in southern Asia and the American West: Rationale for general circulation modeling experiments. Journal of Geophysical Research: Atmospheres 94, 18379-18391.

Sahnouni, M., Hadjouis, D., van der Made, J., Derradji, A.-E.-K., Canals, A., Medig, M., Belahrech, H., Harichane, Z., Rabhi, M., 2002. Further research at the Oldowan site of Ain Hanech, North-eastern Algeria. Journal of Human Evolution 43, 925-937.

Sánchez Goñi, M., Cacho, I., Turon, J., Guiot, J., Sierro, F., Peypouquet, J., Grimalt, J., Shackleton, N., 2002. Synchroneity between marine and terrestrial responses to millennial scale climatic variability during the last glacial period in the Mediterranean region. Climate Dynamics 19, 95-105.

Sánchez Goñi, M.a.F., Turon, J.-L., Eynaud, F., Gendreau, S., 2000. European Climatic Response to Millennial-Scale Changes in the Atmosphere–Ocean System during the Last Glacial Period. Quaternary Research 54, 394-403.

Sankararaman, S., Patterson, N., Li, H., Pääbo, S., Reich, D., 2012. The date of interbreeding between Neandertals and modern humans arXiv 1208.2238v1.

Santonja, M., Pérez-González, A., 2010. Mid-Pleistocene Acheulean industrial complex in the Iberian Peninsula. Quaternary International 223–224, 154-161.

Santonja, M., Pérez-González, A., Panera, J., Rubio-Jara, S., Méndez-Quintas, E., 2016. The coexistence of Acheulean and Ancient Middle Palaeolithic techno-complexes in the Middle Pleistocene of the Iberian Peninsula. Quaternary International 411, Part B, 367-377.

Sarnthein, M., 1978. Sand deserts during glacial maximum and climatic optimum. Nature 272, 43-46.

Sasowsky, I.D., Mylroie, J., 2007. Studies of Cave Sediments. Physical and Chemical Records of Paleoclimate. Springer, Dordrecht.

Schuster, M., Duringer, P., Ghienne, J.-F., Vignaud, P., Mackaye, H.T., Likius, A., Brunet, M., 2006. The Age of the Sahara Desert. Science 311, 821.

Shackleton, N.J., 1975. The stratigraphic record of deep-sea cores and its implications for the assessment of glacials, interglacials, stadials and interstadials in the Mid-Pleistocene, in: Butzer, K.W., Isaac, G.L. (Eds.), After the australopithecines. Mouton Publishers, Paris, pp. 1-24.

Shackleton, N.J., 1987. Oxygen isotopes, ice volume and sea level. Quaternary Science Reviews 6, 183-190.

Sharon, G., 2007. Acheulian large flake industries: technology, chronology, and significance. BAR International Series, Oxford.

Sharon, G., 2011. Flakes Crossing the Straits? Entame Flakes and Northern Africa–Iberia Contact During the Acheulean. African Archaeological Review 28, 125-140.

Sharon, G., Barsky, D., 2016. The emergence of the Acheulian in Europe – A look from the east. Quaternary International 411, Part B, 25-33.

Shea, J.J., 2003. Neandertals, competition, and the origin of modern human behavior in the Levant. Evolutionary Anthropology: Issues, News, and Reviews 12, 173-187.

Shea, J.J., 2008. Transitions or turnovers? Climatically-forced extinctions of Homo sapiens and Neanderthals in the east Mediterranean Levant. Quaternary Science Reviews 27, 2253-2270.

Shea, J.J., 2010. Neanderthals and early Homo sapiens in the Levant, in: Garcea, E.A.A. (Ed.), South-Eastern Mediterranean Peoples Between 130,000 and 10,000 Years Ago. Oxbow Books, Oxford, pp. 126-143.

Shea, J.J., Sisk, M.L., 2010. Complex Projectile Technology and Homo sapiens Dispersal into Western Eurasia. Paleoanthropologie 2010, 100-122.

Singarayer, J.S., Bailey, R.M., 2003. Further investigations of the quartz optically stimulated luminescence components using linear modulation. Radiation Measurements 37, 451-458.

Sollas, W.J., 1908. On the Cranial and Facial Characters of the Neandertal Race. Proceedings of the Royal Society of London. Series B, Containing Papers of a Biological Character 80, 28.

Steele, T.E., Mackay, A., Fitzsimmons, K.E., Igreja, M., Marwick, B., Orton, J., Schwortz, S., Stahlschmidt, M.C., 2016. Varsche Rivier 003: A Middle and Later Stone Age Site with Still Bay and Howieson's Poort Assemblages in Southern Namaqualand, South Africa. PalaeoAnthropologie, 100-163.

Stern, N., 2008. Stratigraphy, depositional environments and palaeolandscape reconstruction in landscape archaeology, in: David, B., Thomas, J. (Eds.), Handbook of Landscape Archaeology. Left Coast Press, Walnut Creek, California, pp. 365-378.

Stringer, C.B., Barton, R.N.E., Finlayson, J.C., 2000. Neanderthals on the Edge. Oxbow, Oxford, p. 267.

Talbi, E.H., Boudchiche, L., 2012. Report about the geology of the Rhafas zone. Université Mohammed Premier, Oujda, Oujda, p. 8.

Taylor, R.E., 2001. Radiocarbon dating in archaeology, in: Brothwell, R., Pollard, A.M. (Eds.), Handbook of archaeological sciences. John Wiley & Sons, London, pp. 23-34.

Texier, J.-P., Lefèvre, D., Raynal, J.-P., El Graoui, M., 2002. Lithostratigraphy of the littoral deposits of the last one million years in the Casablanca region (Morocco). Quaternaire 13, 23-41.

Texier, J.P., Lefevre, D., Raynal, J.-P., 1994. Contribution pour un nouveau cadre stratigraphique des formations littorales quaternaires de la région de Casablanca. Comptes Rendus de l'Académie des Sciences de Paris série II 318, 1247-1253.

Thomsen, K.J., Kook, M., Murray, A.S., Jain, M., Lapp, T., 2015. Single-grain results from an EMCCD-based imaging system. Radiation Measurements 81, 185-191.

Thomsen, K.J., Murray, A., Jain, M., 2012. The dose dependency of the over-dispersion of quartz OSL single grain dose distributions. Radiation Measurements 47, 732-739.

Thomsen, K.J., Murray, A.S., Bøtter-Jensen, L., Kinahan, J., 2007. Determination of burial dose in incompletely bleached fluvial samples using single grains of quartz. Radiation Measurements 42, 370-379.

Thomsen, K.J., Murray, A.S., Buylaert, J.P., Jain, M., Hansen, J.H., Aubry, T., 2016. Testing single-grain quartz OSL methods using sediment samples with independent age control from the Bordes-Fitte rockshelter (Roches d'Abilly site, Central France). Quaternary Geochronology 31, 77-96.

Timmermann, A., Friedrich, T., 2016. Late Pleistocene climate drivers of early human migration. Nature 538, 92-95.

Toro-Moyano, I., Martínez-Navarro, B., Agustí, J., Souday, C., Bermúdez de Castro, J.M., Martinón-Torres, M., Fajardo, B., Duval, M., Falguères, C., Oms, O., Parés, J.M., Anadón, P., Julià, R., García-Aguilar, J.M., Moigne, A.-M., Espigares, M.P., Ros-Montoya, S., Palmqvist, P., 2013. The oldest human fossil in Europe, from Orce (Spain). Journal of Human Evolution 65, 1-9.

Trauth, M.H., Larrasoaña, J.C., Mudelsee, M., 2009. Trends, rhythms and events in Plio-Pleistocene African climate. Quaternary Science Reviews 28, 399-411.

Tribolo, C., Mercier, N., Rasse, M., Soriano, S., Huysecom, E., 2010. Kobo 1 and L'Abri aux Vaches (Mali, West Africa): Two case studies for the optical dating of bioturbated sediments. Quaternary Geochronology 5, 317-323.

Trinkaus, E., Moldovan, O., Milota, ş., Bîlgăr, A., Sarcina, L., Athreya, S., Bailey, S.E., Rodrigo, R., Mircea, G., Higham, T., Ramsey, C.B., van der Plicht, J., 2003. An early modern human from the Peştera cu Oase, Romania. Proceedings of the National Academy of Sciences 100, 11231-11236.

Trinkhaus, E., Constantin, S., Zilhão, J., 2013. Life and Death at the Peştera cu Oase. A Setting for Modern Human Emergence in Europe. Oxford University Press, New York.

Vanhaeren, M., d'Errico, F., Stringer, C., James, S.L., Todd, J.A., Mienis, H.K., 2006. Middle Paleolithic Shell Beads in Israel and Algeria. Science 312, 1785-1788.

Villa, P., Roebroeks, W., 2014. Neandertal Demise: An Archaeological Analysis of the Modern Human Superiority Complex. PLOS ONE 9, e96424.

Waechter, J.d.A., 1951. The excavations at Gorham's Cave, Gibraltar, preliminary report for the seasons 1948 and 1950. Proceedings of the Prehistoric Society 17, 83-92.

Waechter, J.d.A., 1964. The excavations at Gorham's Cave, Gibraltar, 1951-1954. Bulletin of the Institute of Archaeology of London 4, 189-221.

Walker, M.J.C., 2005. Quaternary Dating Methods. John Wiley & Sons, Chichester.

Wallinga, J., 2002. Optically stimulated luminescence dating of fluvial deposits: a review. Boreas 31, 303-322.

Wang, X.L., Wintle, A.G., Du, J.H., Kang, S.G., Lu, Y.C., 2011. Recovering laboratory doses using fine-grained quartz from Chinese loess. Radiation Measurements 46, 1073-1081.

Wang, X.L., Wintle, A.G., Lu, Y.C., 2006. Thermally transferred luminescence in fine-grained quartz from Chinese loess: Basic observations. Radiation Measurements 41, 649-658.

Wengler, L., 1993. Cultures préhistoriques et formations quaternaires au Maroc oriental. Relations entre comportements et paléoenvironments au Paléolithique moyen, Thèse de Doctorat d'Etat ès Sciences. Université de Bordeaux I, p. 1433.

Wengler, L., 1997. La transition du Moustérien à l'Atérien. L'Anthropologie 101, 448-481.

Wengler, L., 2001. Settlements during the Middle Paleolithic of the Maghreb, in: Conard, N. (Ed.), Settlement dynamics of the Middle Paleolithic and Middle Stone Age. Kerns Verlag, Tübingen, Germany, pp. 65-89.

Wengler, L., Vernet, J.-L., 1992. Vegetation, sedimentary deposits and climates during the Late Pleistocene and Holocene in eastern Morocco. Palaeogeography. Palaeoclimatology, Palaeoecology 94, 141-167.

Wengler, L., Weisrock, A., Borchier, J.-E., Brugal, J.-P., Fontugne, M., Magnin, F., 2002. Enregistrement fluviatile et paleoenvironnements au Pleistocene superieur sur la bordure atlantique de l'Anti-Atlas (Oued Assaka, S-O marocain). Quaternaire 13, 179-192.

Westaway, K.E., 2009. The red, white and blue of quartz luminescence: A comparison of De values derived for sediments from Australia and Indonesia using thermoluminescence and optically stimulated luminescence emissions. Radiation Measurements 44, 462-466.

Whiting Blome, M., S. Cohen, A., Tryon, C.A., Brooks, A.S., Russell, J., 2012. The environmental context for the origins of modern human diversity: A synthesis of regional variability in African climate 150,000 - 30,000 years ago. Journal of Human Evolution 62, 563-592.

Wintle, A.G., 1997. Luminescence dating: laboratory procedures and protocols. Radiation Measurements 27, 769-817.

Wintle, A.G., Murray, A.S., 2006. A review of quartz optically stimulated luminescence characteristics and their relevance in single-aliquot regeneration dating protocols. Radiation Measurements 41, 369-391.

Wood, R.E., Barroso-Ruíz, C., Caparrós, M., Jordá Pardo, J.F., Galván Santos, B., Higham, T.F.G., 2013. Radiocarbon dating casts doubt on the late chronology of the Middle to Upper Palaeolithic transition in southern Iberia. Proceedings of the National Academy of Sciences 110, 2781-2786.

Zazo, C., Goy, J.L., Dabrio, C.J., Bardají, T., Hillaire-Marcel, C., Ghaleb, B., González-Delgado, J.-Á., Soler, V., 2003. Pleistocene raised marine terraces of the Spanish Mediterranean and Atlantic coasts: records of coastal uplift, sea-level highstands and climate changes. Marine Geology 194, 103-133.

Zazo, C., Goy, J.L., Hillaire-Marcel, C., Dabrio, C.J., Hoyos, M., Lario, J., Bardají, T., Somoza, L., Silva, P.G., 1994. Variaciones del nivel del mar: Estadios isotópicos 7, 5 y 1 en las costas peninsulares (S y SE) e insulares españolas, in: Rodríguez Vidal, J., Díaz del Olmo, F., Finlayson, C., Giles, F. (Eds.), Gibraltar during the Quaternary, AEQUA Monografías, Sevilla, pp. 26-35.

Zazo, C., Silva, P.G., Goy, J.L., Hillaire-Marcel, C., Ghaleb, B., Lario, J., Bardají, T., González, A., 1999. Coastal uplift in continental collision plate boundaries: data from the Last Interglacial marine terraces of the Gibraltar Strait area (south Spain). Tectonophysics 301, 95-109.

Zilhão, J., 2006. Chronostratigraphy of the Middle-to-Upper Palaeolithic transition in the Iberian Peninsula. Pyrenae 37, 7-84.

Zilhão, J., 2013. Neandertal-Modern Human Contact in Western Eurasia: Issues of Dating, Taxonomy, and Cultural Associations, in: Akazawa, T., Nishiaki, Y., Aoki, K. (Eds.), Dynamics of Learning in Neanderthals and Modern Humans Volume 1: Cultural Perspectives. Springer Japan, Tokyo, pp. 21-57.

Zilhão, J., Ajas, A., Badal, E., Burow, C., Kehl, M., López-Sáez, J.A., Pimenta, C., Preece, R.C., Sanchis, A., Sanz, M., Weniger, G.-C., White, D., Wood, R., Angelucci, D.E., Villaverde, V., Zapata, J., 2016. Cueva Antón: A multi-proxy MIS 3 to MIS 5a paleoenvironmental record for SE Iberia. Quaternary Science Reviews 146, 251-273.

Zilhão, J., Angelucci, D.E., Badal-García, E., d'Errico, F., Daniel, F., Dayet, L., Douka, K., Higham, T.F.G., Martínez-Sánchez, M.J., Montes-Bernárdez, R., Murcia-Mascarós, S., Pérez-Sirvent, C., Roldán-García, C., Vanhaeren, M., Villaverde, V., Wood, R., Zapata, J., 2010a. Symbolic use of marine shells and mineral pigments by Iberian Neandertals. Proceedings of the National Academy of Sciences 107, 1023-1028.

Zilhão, J., Davis, S.J.M., Duarte, C., Soares, A.M.M., Steier, P., Wild, E., 2010b. Pego do Diabo (Loures, Portugal): Dating the Emergence of Anatomical Modernity in Westernmost Eurasia. PLOS ONE 5, e8880.

2. A new chronology for Rhafas, NE Morocco, spanning the MSA through to the Neolithic

A case study of single-grain OSL dating for the Palaeolithic site of Rhafas and its palaeoenvironmental context.

Doerschner, N., Fitzsimmons, K.E., Ditchfield, P., McLaren, S.J., Steele, T.E., Zielhofer, C., McPherron, S.P., Bouzouggar, A., Hublin, J.-J.

Published in PLoS ONE (2016, Volume 11)

PLOS | ONE

RESEARCH ARTICLE

A New Chronology for Rhafas, Northeast Morocco, Spanning the North African Middle Stone Age through to the Neolithic

Nina Doerschner[1]*, Kathryn E. Fitzsimmons[1], Peter Ditchfield[2], Sue J. McLaren[3], Teresa E. Steele[1,4], Christoph Zielhofer[5], Shannon P. McPherron[1], Abdeljalil Bouzouggar[1,6,7], Jean-Jacques Hublin[1]

1 Department of Human Evolution, Max Planck Institute for Evolutionary Anthropology, Leipzig, Germany, **2** Research Laboratory for Archaeology and the History of Art, University of Oxford, Oxford, United Kingdom, **3** Department of Geography, University of Leicester, Leicester, United Kingdom, **4** Department of Anthropology, University of California Davis, Davis, California, United States of America, **5** Institute of Geography, University of Leipzig, Leipzig, Germany, **6** Institut National des Sciences de l'Archéologie et du Patrimoine, Rabat, Morocco, **7** Institute of Advanced Study, Aix-Marseille University, Marseille, France

* nina_doerschner@eva.mpg.de

Citation: Doerschner N, Fitzsimmons KE, Ditchfield P, McLaren SJ, Steele TE, Zielhofer C, et al. (2016) A New Chronology for Rhafas, Northeast Morocco, Spanning the North African Middle Stone Age through to the Neolithic. PLoS ONE 11(9): e0162280. doi:10.1371/journal.pone.0162280

Editor: Nuno Bicho, Universidade do Algarve, PORTUGAL

Received: February 4, 2016

Accepted: August 19, 2016

Published: September 21, 2016

Data Availability Statement: All relevant data are within the paper and its Supporting Information files.

Funding: This study was funded by the Max Planck Society. A. Bouzouggar's work was also supported by Aix-Marseille University, IMéRA, with the support of LabexMed, of Labex RFIEA and ANR - Investissements d'Avenir. The funders had no role in study design, data collection and analysis, decision to publish, or preparation of the manuscript.

Competing Interests: The authors have declared that no competing interests exist.

Abstract

Archaeological sites in northern Africa provide a rich record of increasing importance for the origins of modern human behaviour and for understanding human dispersal out of Africa. However, the timing and nature of Palaeolithic human behaviour and dispersal across north-western Africa (the Maghreb), and their relationship to local environmental conditions, remain poorly understood. The cave of Rhafas (northeast Morocco) provides valuable chronological information about cultural changes in the Maghreb during the Palaeolithic due to its long stratified archaeological sequence comprising Middle Stone Age (MSA), Later Stone Age (LSA) and Neolithic occupation layers. In this study, we apply optically stimulated luminescence (OSL) dating on sand-sized quartz grains to the cave deposits of Rhafas, as well as to a recently excavated section on the terrace in front of the cave entrance. We hereby provide a revised chronostratigraphy for the archaeological sequence at the site. We combine these results with geological and sedimentological multi-proxy investigations to gain insights into site formation processes and the palaeoenvironmental record of the region. The older sedimentological units at Rhafas were deposited between 135 ka and 57 ka (MIS 6 –MIS 3) and are associated with the MSA technocomplex. Tanged pieces start to occur in the archaeological layers around 123 ka, which is consistent with previously published chronological data from the Maghreb. A well indurated duricrust indicates favourable climatic conditions for the pedogenic cementation by carbonates of sediment layers at the site after 57 ka. Overlying deposits attributed to the LSA technocomplex yield ages of ~21 ka and ~15 ka, corresponding to the last glacial period, and fall well within the previously established occupation phase in the Maghreb. The last occupation phase at Rhafas took place during the Neolithic and is dated to ~7.8 ka.

Introduction

In recent years, data from cave sites in the Maghreb (comprising Morocco, Algeria, Tunisia and western Libya) have gain considerable importance in the study of modern human origins and dispersals within and out of Africa [1]. Not only are these sites relatively plentiful and their locations highly strategic, rich faunal and archaeological records are often well preserved within stratified sedimentological sequences (e.g. [2, 3]). This situation provides optimal conditions for the successful combination of classical archaeological methods with chronometric dating and palaeoenvironmental reconstruction. Despite this, there are few sites in this region that span multiple Palaeolithic technocomplexes.

Interest in the chronology of North African archaeological sites has arisen in part because of evidence for the early appearance of symbolic artefacts and other behavioural indicators–present in the Maghreb—interpreted to represent cultural modernity and which may be linked to the dispersal of anatomically modern humans from Africa [4–7]. The timing and geographic distribution of the emergence of these behaviours is of critical importance for modelling the drivers of population mobilisation and the eventual replacement of other human species [1].

In North Africa, particular interest is placed on an MSA technocomplex known as the Aterian (S1 File). Although the Aterian is primarily known for its pedunculated tools and bifacial foliates, that Aterian assemblages can additionally be characterised by the presence of blades, bladelets, end-scrapers, small Levallois cores [8] and the appearance of shell beads and other personal ornaments [5]. However, while the definition and concept of the Aterian is better defined today, there are still issues that remain, especially in northwest Africa [8, 9]. While current definitions recognize that there is more to the Aterian than tanged pieces, there remains the difficulty of reliably distinguishing the Aterian from the North African MSA when these characteristic finds are absent (e.g. [1, 10]). When the chronological position of the Aterian was thought to fall within an age range of 40–20 thousands of years ago (ka) [11], meaning clearly post non-Aterian MSA, its status as a distinct entity seemed clearer. However, more recent dating studies have extended the beginning of the Aterian to >100 ka [10, 12–17] and perhaps as early as 145±9 ka [10], which juxtaposes with the timing of the MSA in north Africa. Thus debate continues as to whether once the Aterian first occurs all subsequent assemblages are Aterian (meaning that the Aterian represents a phase within the MSA) or whether there is still a continuation of a non-Aterian MSA (meaning that the Aterian is a separate entity in North Africa) [9, 18].

The origins of the LSA are also of importance in North Africa; they are connected to a major change in human subsistence behaviour, as well as the emergence of elaborate funerary activities between ~40–20 ka [19, 20]. The LSA is characterised by the occurrence of microlithic bladelet industries, including large bladelets in the earliest phase labelled as Iberomaurusian in the Maghreb and "*Eastern Oranian*" in Libyan Cyrenaica [19, 21]. The LSA in the Maghreb starts ~22 kcal BP if not earlier [2], while it already appears >42 kcal BP in some sites [22, 23] elsewhere on the continent, but is–especially in South Africa—also a matter of ongoing debate (see e.g. [24]). Despite the substantial progress made in the last years [10, 16, 17, 25], there is clearly a need for additional data on the timing of the earliest LSA in the Maghreb.

The cave of Rhafas, located in north-eastern Morocco (Fig 1), is one of the few sites known to contain evidence of human occupation spanning the MSA, including the Aterian, through to the Neolithic. The first chronology for the upper layers of the cave fill sequence was produced by Mercier et al. [26] using both radiocarbon and luminescence dating techniques. ^{14}C-dating gave ages of 5,963±150 cal BP (5,190±100 a BP, Gif-6185) for the uppermost Layer 1 (Neolithic) and 17,319±258 cal BP (14,060±150 a BP, Gif-6489) for Layer 2, although the latter date was considered incompatible with the archaeological context (Aterian).

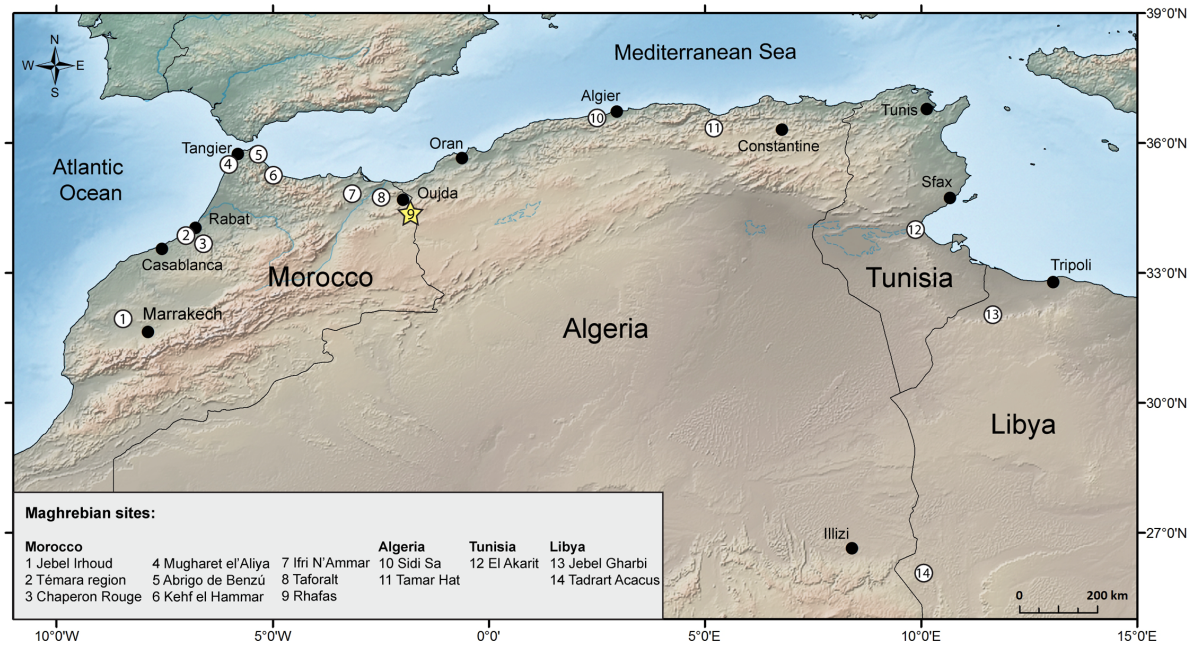

Fig 1. Map of archaeological sites cited in the text. The Témara region (2) includes the neighboring sites of El Mnasra, El Harhoura 1 & 2, Dar es-Soltan 1 & 2 and La Grotte de Contrebandiers; Jebel Gharbi (13) includes the sites of Ain Zargha, Jado, Shakshuk, Wadi Basina, Wadi Ghan and Wadi Sel; Tadrart Acacus (14) includes the sites of Uan Tabu and Uan Afuda.

doi:10.1371/journal.pone.0162280.g001

Thermoluminescence (TL) age estimates were obtained on burnt lithics from the sublevels of the MSA Layer 3 (92–60 ka). Additionally, one sediment sample from Layer 6d (also MSA) was dated by optically stimulated luminescence (OSL) on multiple grain aliquots using the 40–50 μm silt fraction (107±12 ka).

In this study, as part of renewed excavations, we build on the work by Mercier et al. [26] by applying single-grain OSL dating of quartz, providing a higher resolution, more complete chronostratigraphy for Rhafas. The application of ^{14}C, while more precise than luminescence dating, is limited to dating the last 50 ka and cannot assist with constraining the timing of the older sediment deposits associated with the early emergence of MSA assemblages. OSL dating provides a reliable estimate of the time elapsed since mineral grains, such as quartz, were last exposed to sunlight [27], and therefore can be used to calculate the depositional age of sediments [15]. Although the first OSL ages for a Moroccan site (Chaperon Rouge I) were published by Texier in 1988 [28], the reliability of these ages is limited by the methods available at the time, such as aliquot size and lack of sensitivity change correction in the dating protocols. Major technical improvements in recent years [29, 30] have made optical dating of quartz the optimal tool for determining the age of sedimentological sequences in archaeological sites across Morocco [5, 6, 13–17, 26, 31–34]. Single grain dating has the advantage of enabling the identification of incomplete signal resetting, beta dose rate inconsistencies or post-depositional mixing of sediments, all of which are common in cave deposits (e.g. [16, 35, 36–39]). Each of these factors may result in significant over- or underestimation of the real depositional age of the sediment layer when using multi-grain OSL dating. Consequently, we have applied single grain dating to the Rhafas sequences to provide a more reliable chronology by identifying and

mitigating potential problems in the luminescence signal which otherwise may not have been identified.

Thus here we present a chronology for the long, stratified, archaeological sequence at Rhafas based on OSL dating of individual quartz grains to better understand the temporal dimension of changes in human behaviour documented in the cave. We combine our chronological framework with geological and sedimentological analyses of the site's' sediments, a pedogenic carbonate crust and local bedrock samples to examine the depositional history of the sediment layers in further detail and to discuss the implications of the results in the context of Quaternary palaeoenvironmental change in the region.

Regional setting

Rhafas is a cave site ~900 m above present day sea level in the north-eastern Oujda Mountains, ~50 km inland from the Mediterranean coast and ~7 km west of the Algerian border (34° 33'28"N, 1°52'26"W) (Fig 1). Situated on the north-western slope of a prominent northeast/southwest trending valley, the cave is a simple dome-shaped dissolution feature within the local dolomitic limestone, opening to the southeast. It has a maximum distance from the back wall to the current drip line of ~15 m, a width at the entrance of ~16 m, and a height of ~10 m (Fig 2).

Geological setting and cave formation. The local geology of the area is dominated by three main lithological units: a coarse-grained granodiorite intrusion forms the valley floor; a series of highly deformed low grade meta-sediments outcrop along the north-western slope of the valley; and an overlying dolomitic limestone sequence caps the local hilltops [40]. The meta-sediments are absent from the south-eastern side of the valley where the carbonate units rest directly on a weathered granodiorite surface. This may be related to the presence of a fault, with downthrow to the northwest running along the valley axis. The horizontally bedded dolomitic limestones at the north-western slope unconformably overlie the steeply dipping and strongly deformed meta-sediments and form a line of cliffs along both valley margins within which the cave is located. At the base of the cliff the unconformable contact is clearly exposed, and the outcrop of the unconformity can be traced below the cave entrance and further along the outcrop to the southwest.

The unconformity between the limestones and meta-sediments has acted as a locus for mineralisation within the area and is characterised by fractures infilled by carbonates, with abundant hematite mineralisation and localised lead sulphide precipitation. The unconformity is estimated to sit within 1–2 metres below the present excavated level of the cave floor. This has important implications for groundwater flow and dissolution of radiogenic isotopes from the granodiorite and metasediments into the lower parts of the cave fill which might have changed the radiation environment of these sediments subsequent to deposition. Consequently, it also has implications for environmental radiation dose rate determination for the lower cave sediments and, therefore, for the accuracy of the OSL ages.

The cave exhibits a simple morphology with no other entrance for sediments other than the current cave mouth and with only minor amounts of water reaching the cave from wall or roof seepage. However, on the eastern side of the cave mouth is a zone of fractured dolomitic limestone with closely spaced joints. This forms a prominent fabric (space cleavage) parallel with the main valley axis fault and possibly relating to late reactivation of this fault. This zone of fractured rock can be visually traced in front of the cave mouth where a largely buried boulder field forms the present hillslope. It is possible that this area of increased fracture porosity was the initial locus of dissolution and karstification with the present cave representing a lateral extension of this. If this was the case, then the dolomitic limestone boulders may represent the

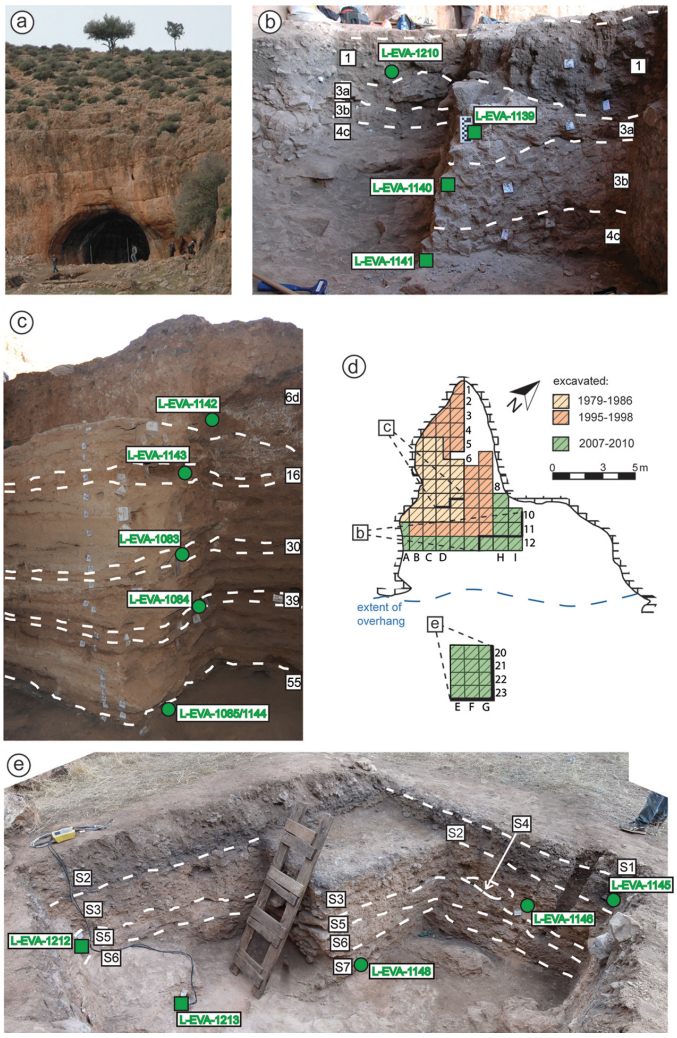

Fig 2. Overview of the Rhafas site and excavated sections. Photograph of the cave (a), plan view map with the excavation sectors (d) and photographs showing section walls of the cave mouth (b), the lower cave (c) and the terrace section (e). Indicated are layer boundaries and positions of the OSL samples.

doi:10.1371/journal.pone.0162280.g002

collapsed remains of an extension of the cave roof to the southeast. The timing of any such collapse remains unknown, but is likely to predate the deposition of sediments in the terrace area which appear to have vertically infilled the spaces between existing boulders.

History of archaeological research at Rhafas. The cave was first discovered in 1950 by J. Marion, and the stone tool assemblage was described by J. Roche [41] as similar to the "*Eastern Oranian*" or even earlier. The first series of systematic excavations were conducted from 1979 to 1986 by J.-L. Wengler [42, 43] over a large portion of the interior of the cave and to a depth of 4.5 m. Three additional seasons followed in the 1990s. In 2007, a new series of excavations

forming the current campaign started in the cave as well as on the relatively flat and partially terraced area in front of the cave (Fig 2D and 2E) that separates the cave from the main valley slope.

The stratigraphy of the cave sediments was described by Wengler [42] on the basis of a reference section running from excavation square C4 to C10 (Fig 2D). 71 distinct sedimentary layers were identified, of which 39 are associated with archaeological finds. These were combined into four main units, numbered from top (I) to bottom (IV). Except for Unit I, all stratigraphic units end with important phases of carbonate formation (Layer 3, 6 and 69) and are separated by significant erosional breaks. The combined sequence within the cave contains artefact assemblages that can be attributed to the Neolithic (Layer 1) and the MSA, which was originally separated into Aterian (2, 3a) and Mousterian (3b to 71) Layers [42].

Although Wengler's original section line no longer exists due to erosion and later excavation, his stratigraphic framework and numbering system have been retained. During the most recent excavations two additional reference profiles were developed to describe the cave mouth area and lower cave infill, respectively (Fig 2B and 2C). The current base of the cave does not reach Wengler's Unit IV and ends at Layer 55 (Fig 2C). Additional units were opened and excavated on the level, approximately 25 m wide, terrace in front of the cave (terrace section, Fig 2E).

Materials and Methods

Permission to undertake fieldwork and to collect bedrock and sediment samples at Rhafas was granted by the Institut National des Sciences de l'Archéologie et du Patrimoine, Rabat, Morocco.

Luminescence dating. *OSL sampling and preparation*

Fifteen OSL samples were collected from three different sections at Rhafas, and span the entire archaeological sequence from MSA to Neolithic (Fig 2). Samples were either collected in stainless steel tubes (4 cm diameter, 10 cm long) or as blocks using hammer and chisel, depending on the degree of cementation of the layers. The samples were carefully sealed to preserve the field moisture content.

Gamma dose rate measurements were performed in situ with two portable sodium iodide gamma spectrometers and material surrounding the samples was collected for subsequent laboratory analysis. Gamma ray spectra were measured (except sample L-EVA-1139 from Layer 3a) using a three-inch crystal detector counting for 1800 s. Due to intensive cementation of the sediment layer, which made enlargement of the sampling hole difficult, a smaller, one-inch NaI detector was used for Layer 3a with a 5040 s counting interval.

Sample preparation and measurements were conducted in the luminescence laboratory of the Max Planck Institute for Evolutionary Anthropology under subdued red light conditions. The outer surfaces (~1 cm) of the block samples and 1.5 cm from both ends of the sampling tubes were removed because of potential light exposure during sampling. The remaining material was prepared to isolate pure sand-sized quartz grains for equivalent dose (D_e) determination. After drying the block, samples were treated with hydrochloric acid (HCl, 10%) to dissolve carbonates. All samples were sieved to isolate the 90–212 μm in diameter sand fraction, which was used for further chemical treatments (removal of carbonates and organic matter with HCl (15%) and hydrogen peroxide (30%), respectively). Density separation was performed using a lithium heterotungstate solution (at 2.62 g cm^{-3} and 2.68 g cm^{-3} densities) in order to separate quartz from lighter feldspars and heavy minerals. The quartz was then treated with hydrofluoric acid (40%) for 60 min to etch the outer surface of the grains and to remove

Table 1. Results of dose rate determination.

Sample	Depth	Moisture	Specific activities (Bq kg^{-1})					Dose rate (Gy/ka)			
	(cm)	content (%)	^{238}U	^{226}Ra	^{210}Pb	^{232}Th	^{40}K	Beta[a]	Gamma[a]	Cosmic[a]	Total
Cave mouth section											
L-EVA-1210	40	10±5	15.7±1.9	14.5±0.7	13.5±1.6	10.5±0.5	207±11	0.90±0.02	0.34±0.02	0.05±0.01	1.29±0.07
L-EVA-1139	55	5±3	12.4±1.5	11.0±0.8	9.6±1.7	11.1±0.6	220±14	0.73±0.01	0.23±0.01	0.05±0.01	1.01±0.04
L-EVA-1140	70	5±3	9.6±1.4	8.7±0.8	8.8±2.9	6.4±0.4	105±9	0.69±0.03	0.22±0.01	0.05±0.01	0.96±0.04
L-EVA-1141	110	5±3	10.3±1.1	8.8±0.6	7.1±1.1	8.9±0.4	160±10	0.68±0.01	0.26±0.01	0.05±0.01	0.99±0.04
Lower cave section											
L-EVA-1142	185	5±3	15.4±3.2	15.7±1.1	12.9±2.7	18.8±1.0	931±53	1.49±0.02	0.61±0.03	0.05±0.01	2.14±0.07
L-EVA-1143	210	10±5	20.8±3.3	21.1±1.5	15.5±2.6	26.3±1.2	600±35	1.74±0.05	0.66±0.04	0.04±0.01	2.44±0.17
L-EVA-1083	260	10±5	22.3±3.1	20.6±1.0	14.0±3.8	25.7±1.2	707±17	2.32±0.05	0.75±0.04	0.04±0.01	3.11±0.18
L-EVA-1084	300	10±5	28.9±3.1	21.9±1.0	15.2±4.2	25.2±1.2	554±14	1.87±0.03	0.74±0.04	0.04±0.01	2.65±0.15
L-EVA-1085	375	10±5	22.1±3.1	18.9±0.9	18.3±4.1	24.7±1.1	495±12	1.81±0.03	0.49±0.03	0.04±0.01	2.34±0.13
L-EVA-1144	375	10±5	26.2±4.7	24.8±2.1	21.4±6.2	25.4±1.5	508±38	1.72±0.04	0.49±0.03	0.04±0.01	2.25±0.15
Terrace section											
L-EVA-1145	45	10±5	15.0±2.5	14.9±1.0	9.6±1.8	15.6±0.8	284±18	0.76±0.02	0.33±0.02	0.22±0.03	1.31±0.09
L-EVA-1146	70	5±3	14.9±3.9	15.5±1.2	14.6±2.2	13.7±0.8	197±15	0.79±0.01	0.36±0.02	0.21±0.02	1.36±0.08
L-EVA-1212	100	5±3	9.5±1.5	9.6±0.5	10.0±1.8	8.9±0.5	136±6	0.62±0.01	0.22±0.01	0.21±0.02	1.05±0.04
L-EVA-1213	115	5±3	11.5±1.8	9.4±0.5	15.4±1.6	10.0±0.5	130±7	0.93±0.02	0.27±0.01	0.20±0.02	1.40±0.05
L-EVA-1148	150	5±3	14.2±2.6	15.1±1.0	12.2±1.8	15.3±0.8	242±15	0.81±0.02	0.27±0.01	0.20±0.02	1.27±0.07

[a]Attenuated with respect to the moisture content of each individual sample.

doi:10.1371/journal.pone.0162280.t001

the remaining feldspar minerals. Finally, the samples were rinsed with HCl, dried and re-sieved to recover grains in size fractions of 90–125 μm, 125–180 μm and 180–212 μm in diameter.

Dose rate measurements. For the calculation of the external dose rate, high resolution germanium gamma spectrometry (HRGS), in situ gamma spectrometry and beta counting measurements were performed. The specific activities of radioactive elements ^{238}U, ^{232}Th, ^{40}K and their daughter products (Table 1) were measured at the low-background underground laboratory Felsenkeller (VKTA, Dresden/Germany) using HRGS. Since this method measures the activities of multiple daughter isotopes within the uranium- and thorium-series decay chains, potential disequilibrium resulting from dissolution and transport of soluble daughter products–which causes time-dependent changes in the dose rate [44, 45]–can be identified. Comparisons of the ^{238}U, ^{226}Ra and ^{210}Pb activities (S1 Fig) revealed no significant discrepancies indicating equilibrium for the uranium decay chain. It is, therefore, assumed that the dose rate of the sediments dated in this study remained constant through time. The conversion factors of Guérin et al. [46] were used to calculate the beta and gamma dose rates (S1 Table).

Gamma dose rates based on field gamma-ray spectra, reflecting the in situ radiation geometry of each sample point, and on HRGS show varying degrees of agreement with one another. Given the heterogeneous gamma radiation environments of the majority of samples at Rhafas results from in situ measurements were preferred.

Beta dose rates were calculated using a Risø low-level beta multicounter system GM-25-5 [47, 48]. Dried material from the ends of the OSL-sampling tubes or the outer surface of the block samples was milled to fine powder. About 1.5 g of homogenised sample was placed in each plastic sample holder, covered with cling film (to avoid contamination) and a plastic ring was pressed around the sample holder to hold the assemblage in place. For each OSL sample, four sub-samples and one standard were counted simultaneously for 24 h.

Comparisons between beta dose rates calculated using low level beta counting and HRGS show discrepancies in some samples while for others the results are consistent between methods (S1 Table). In the lower cave section, below Layer 6d, where sediments are comparatively homogeneous, beta dose rates for both techniques are in agreement with one another. In the sedimentologically more complex layers of the cave and in the terrace section, beta dose rate comparisons are more likely to show deviations. As beta particles are only able to travel <1 cm in sediments, we consider the beta dose rates from low-level beta counting on material from the same sampling tube (or block) used for D_e determination to be more reliable than HRGS results measured on bulk material of 0.5–1.5 kg of sediment surrounding the OSL sample.

The average moisture content was estimated with respect to both in situ and saturation moisture content. The field moisture values were determined by weighing raw and oven-dried samples. Full-saturation moisture content was estimated as the ratio of weight of absorbed water to dry sample weight. Based on the results, dose rates were calculated assuming average burial-time moisture contents of 5±3% for the cemented and 10±5% for the uncemented layers to account for attenuation [49].

The cosmic dose rate was calculated according to Prescott and Hutton [50] from the altitude and geomagnetic latitude of the site, the burial depth, and the density of the overburden. The results of the dose rate determination are summarised in Table 1.

Equivalent dose determination. Luminescence measurements were performed on three Risø OSL/TL readers (DA-15 and DA-20 with single grain attachments), each equipped with calibrated $^{90}Sr/^{90}Y$ beta sources [51] and fitted with 7.5 mm Hoya U-340 detection filters [52]. The machines were equipped with infrared diodes (875 nm) and blue light-emitting diodes (470 nm). Green lasers (90% power) emitting at 532 nm were used for light stimulation of single grains [51]. Because only small amounts of material were available after the chemical treatment, standard performance tests on small aliquots (1 mm) were performed using the 125–180 μm in diameter sand fraction. Single grain dating of sand-sized quartz grains (180–212 μm) was used for D_e determination. Single grain discs were loaded by sweeping individual quartz grains over aluminium discs each containing 100 holes with a small brush. The single-aliquot regenerative-dose (SAR) protocol based on Murray and Wintle [29, 53] was applied for initial tests and D_e determination (Table 2). In addition to the recycling ratio and the recuperation test, which are normally incorporated within a SAR protocol, the OSL IR depletion ratio [54] was applied to detect feldspar contamination.

Preheat temperatures were determined individually for each sample by performing standard preheat plateau tests as well as combined dose recovery preheat plateau tests at seven different preheat steps (160–280°C, three small aliquots were measured per preheat temperature) [53, 55]. S2 Fig shows that a preheat plateau for all temperatures can be observed for sample L-EVA-1146, whereas sample L-EVA-1139 shows more variable results that stabilise at higher

Table 2. Single aliquot regeneration (SAR) protocol for single grains used in this study.

Run	Treatment
1	Dose (except before first run)
2	Preheat (240°C or 260°C for 10s)
3	Optical stimulation with IR diodes for 100s at 20°C (only for last run)
4	Optical stimulation with green laser for 1s at 125°C
5	Test dose
6	Cutheat (200°C or 220°C for 10s)
7	Optical stimulation with green laser for 1s at 125°C
8	Start from top

doi:10.1371/journal.pone.0162280.t002

temperatures (S2A Fig). Dose recovery ratios are close to unity and are independent of the preheat temperature (S2B Fig). Based on these results, preheat temperatures for D_e measurements were set to 260°C or 240°C and cutheat temperatures to 220°C or 200°C, respectively (S1 Table). To gather more information about the luminescence characteristics and the signal reproducibility of each sample, dose recovery tests were performed on a single grain basis.

Early background subtraction was used for D_e determination of single grains to minimize the proportions of interfering OSL signal components [56, 57]; initial and subsequent 0.035 s of the decay curve were taken for signal and background integration, respectively. Since not all individual grains yield useful luminescence signals for OSL dating [39, 58], only those passing a set of strict selection criteria–single saturating exponential curve fitting, intersection with the dose response curve, signal >3x background counts, test dose signal error <20%, recycling ratio <20%, recuperation <5%, IR depletion ratio <5%, and D_e error <30%—were chosen for analyses. Between 900 and 4100 single grains were measured until at least 50 D_e values for each OSL sample passed the rejection criteria [59].

Sediment and bedrock analyses

Fresh bedrock samples were collected from the three main lithological units (granodiorite, meta-sediments and dolomitic limestone) in the Rhafas area for X-ray fluorescence (XRF) analyses. Material from the dried ends of the OSL sampling tubes and the outer surfaces of the block samples were used for XRF and grain size analyses. All analyses were carried out at the Institute of Geography, University of Leipzig. A subsample from the prominent duricrust at the top of Layer S5 in the terrace section was analysed at the Department of Geography, University of Leicester, for stable-isotope composition of the carbonates and thin section microscopy. Further details on the methods used for sediment and bedrock analyses can be found in S2 File.

Results

Cave stratigraphy

The sediments of the lower cave section contain assemblages attributed to the MSA and correspond to Wengler's Unit III [42]. The section is characterised by alternating unconsolidated brown or red sands and silts with interbedded thin calcareous horizons (layers 7–55). Grain size analyses indicate approximately equal proportions for clay, silt and sand in the non-calcareous layers (S5 Table, S5 Fig), and relatively consistent calcium carbonate ($CaCO_3$) concentrations (19–33%). Concentrations of Cl and S, which serve as indicators for evaporate enrichment and consequently more arid climatic conditions, vary within the sediments of the lower cave section, while the Na/Cl mol ratio remains homogeneous and close to zero (Fig 3). Layer 6 forms a thick cemented cap on the top of this section and contains limestone clasts in a brown sandy matrix. Both sand and $CaCO_3$ content in Layer 6 markedly increase relative to the underlying units to 60% and 61%, respectively (Fig 3). Its cementation further increases in intensity and thickness towards a prominent tufa/flowstone mound on the southwestern wall of the cave, which may represent deposits formed during a period of increased water availability within the cave. The contact between Layer 6 and underlying layers 7–55 is also clearly recognizable from the element concentrations of siliciclastic origin in the XRF data, especially in the K/Al and Rb/K ratios (Fig 3).

The deposits of the cave mouth section are dominated by stratigraphic Units I and II in Wengler's (1993) framework [42]. The stratigraphic Unit II consists of MSA Layers 2 to 5, while Unit I contains a single layer which shows significant human impact (reworking, ash deposits and archaeological remains) of Neolithic age. The current excavation in the cave

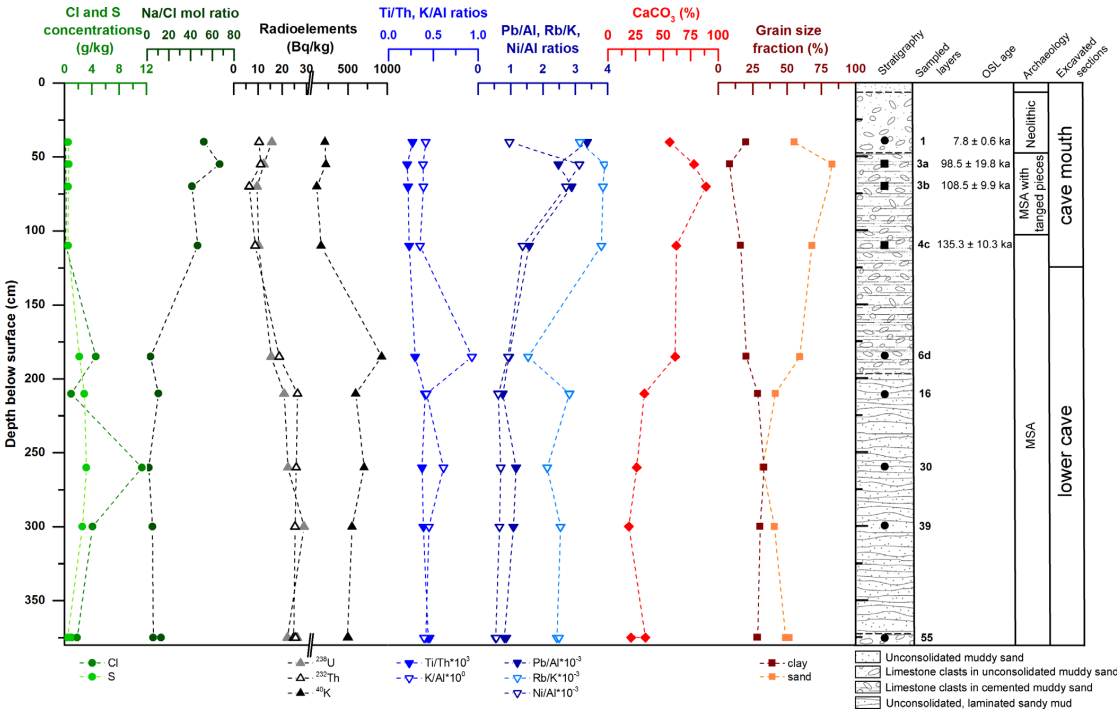

Fig 3. Sedimentological characteristics and stratigraphy of the Rhafas cave deposits. Results of XRF analyses, high resolution gamma spectrometry, calcium carbonate and grain size determination are displayed for each sampled layer from the cave mouth and the lower cave section at Rhafas, together with the determined OSL ages and the corresponding archaeological information.

doi:10.1371/journal.pone.0162280.g003

mouth did not excavate Layer 2 at all—which appears to have had laterally a rather limited extend—and ends at Layer 4d which forms a prominent floor within the cave (Fig 2B). The layers of the cave mouth section differ substantially from the underlying lower cave section sediments with respect to geochemistry. The siliciclastic ratios of Pb/Al, RB/K and Ni/Al, and carbonate concentrations are higher in the cave mouth sediments than in the underlying units. Likewise, proportions of sand and clay are higher and lower, respectively, in these upper units (S5 and S6 Tables, Fig 3). The sand fraction clearly dominates (up to 83% in Layer 3a) in all layers of the cave mouth section (S5 Fig); $CaCO_3$ concentration is also high (up to 90%, also 3a); and there is minimal variability in Cl and S concentrations (<0.6 g/kg). The Na/Cl mol ratio substantially increases (up to 67) in the cave mouth sediments relative to the lower cave section (Fig 3). Layer 3a to 4c show minimal lateral variation and are dominated by angular limestone clasts in a cemented sandy or silty brown matrix. In our excavation area, Layer 1 unconformably overlies Layer 3a and consists of unconsolidated dark grey sediments. The change in sedimentology at the contact between Layers 3a and 1 is reflected by the non-soluble element concentrations with decreasing Pb/Al and increasing Rb/K and Ni/Al ratios (Fig 3).Variations in the Ni/Al and Pb/Al ratios reflect again sedimentologic changes between Layers 3a and 3b (showing a decrease and increase, respectively), as well as 3b and 4c (both ratios decreasing).

The new excavations of the terrace section (Fig 2E) revealed a stratigraphically complex sequence at least ~1.5 m thick. Seven layers were identified (S1 top to S7 base), and these are

comprised predominantly of silts and sands alternating with carbonate crusts, the latter most likely the result of post-depositional cementation (S5 and S6 Tables). By the end of the last excavation season in 2010, the base of Layer S7 had not yet been reached.

The sediments of the two lowermost Layers (S6 and S7) were deposited around a field of large limestone boulders, which may be related to an earlier extension of the cave roof, as described in the geological description of the site. These layers contain assemblages attributed to the MSA and are characterised by diagenetic cementation and varying proportions of limestone clasts. Layer S5 is strongly cemented and also contains MSA finds. On top of it, a prominent, finely laminated and several centimetres thick carbonate crust was formed that distinctively marks the contact between S3 and S5. Layer S3 is cemented and comprises reddish grey sediments with abundant limestone clasts. Layer S2 is composed of dark grey ashy sediments with lower carbonate content. Both S2 and S3 yielded lithic assemblages attributed to the LSA, but they are separated by an unconformable contact. S4 displays a cemented conglomeratic facies variation of S3, but it is limited in extent and is most likely associated with cementation of a narrow channel feature.

Though the terrace and the cave sequence are not yet connected physically through excavation, given the lithological and archaeological similarities, it seems likely that terrace Layer S1, consisting of poorly consolidated grey ashy sediments with abundant Neolithic remains and limestone pebbles, correlates with Layer 1 of the cave fill sequence [60]. Layers S2 and S3 contain LSA which is not represented in the cave sequence. Layers S4 through S7 contain MSA with tanged pieces and, therefore, perhaps correlate with Levels 2-3a in the cave sequence. Though the material culture and sedimentological observations provides some general indications in the absence of physically connected stratigraphies, one important additional element for linking the two sections is the robust chronological control described in this paper.

Grain size and geochemical analyses of the terrace section layers show no major variations (S6 Fig), except for the distinctly decreasing Pb/Al ratio between Layer S2 and S3, which is most likely caused by post-depositional, anthropogenic overprint. The values for all sedimentological proxies of the layers from the terrace section are comparable with those obtained for the cave mouth sediments (S5 and S6 Tables). The sand fraction clearly dominates in all layers (54–62%, S5 Fig), while $CaCO_3$ content reaches up to 79%. Concentrations of both radioelements and major elements are comparable with the sediments from the cave mouth section.

The bedrock sample from the limestone unit at Rhafas–within which the cave is situated—yields a Ca/Mg ratio of 1.2 and can, therefore, be clearly classified as dolomitic limestone. However, there is no evidence for weathered dolomitic bedrock in the sediments, as Ca and Mg show no significant correlation in the samples (S7A Fig). This suggests that the sediments at Rhafas originate from an allochthonous source.

XRF results of the sediments show negative correlations between Ca and Al and between Ca and Fe (S7B and S7C Fig). The high Ca contents reflect a carbonate-rich sedimentological context at Rhafas, while at the same time the siliciclastic fractions, represented by Al and Fe, are reduced. The Ca correlates positively with the coarse sand (gS) fraction but is relatively insignificant in the silt and fine sand fractions (S7D Fig). This indicates local, secondary carbonate enrichment processes at the site through precipitation of percolating carbonate-rich waters and contradicts an exclusively aeolian origin for the carbonates in the sediments. The highest contents of Ca and gS can be found in the cave mouth and the terrace section, where most layers are presently cemented by carbonates. S7B and S7C Fig illustrate the aforementioned sedimentological similarities between these two sections. Layer 6d, however, shares the same characteristics, which again underlines its exceptional position in the lower cave section.

Archaeological context. Four main technological groups were identified in the new excavations. The Neolithic (Layer 1 and S1) is rich in pottery with rare types of cardial ware (A. El

Idrissi, pers. comm.) and bone tools (mainly points and some *lissoirs*). The lithic artefacts from Layer S2 and especially S3 in the terrace section show a significant use of microlithis/bladelets, which is characteristic of the LSA [20]. Single platform and opposed platform bladelet cores are common, and the retouched tools are backed bladelets. The MSA (Layers 2 to 55 and S4 to S7) can be separated into two distinct groups defined by the regular occurrence or absence of tanged pieces. Layers 2 to 3b and S4 to S7 contain considerable quantities of tanged pieces and are also characterised by retouched tools such as side scrapers, notches and some end scrapers. A significant Levallois component is present mainly in Layers 2, 3a and S6. In the underlying Layers 3b to 55 tanged pieces do not occur on a regular basis. Large Levallois flakes, laminar flakes, side scrapers and bifacial foliates are common in Layers 4 to 6, whereas only a few such artefacts were recovered from Layers 7 to 51 and Layers 52 to 55 display a variety of side scrapers on Levallois blanks.

Faunal remains are preserved throughout the sequence (S2 Table), although the specimen numbers are small and decrease with depth. Michel [61] provided a list of identified species by layer for the early Wengler excavations, and the assemblages from the recent excavations are being analysed from a zooarchaeological and taphonomic perspective in addition to basic taxonomic identifications. The Neolithic layers include remains of Caprinae (sheep/goat) and Suidae (pigs), which likely derive from domesticated stock, and some Bovinae (cattle/aurochs) remains also likely represent domesticates (continuing work with the faunal aims to investigate this in detail). In addition, the Neolithic assemblages contain a variety of wild taxa, particularly Alcelaphinae (hartebeest/wildebeest), Equidae (horse/zebra), and a few gazelles (*Gazella* sp.). Although overall species diversity is lower in the LSA immediately below, the dominate taxa remain the same, alcelaphines and equids are still most common with a few gazelles and one Barbary sheep (*Ammotragus lervia*) specimen. Sample sizes are too small to provide reliable relative abundances for the older layers, but equids are still most common, and isolated warthog (*Phacochoerus africanus*), Rhinocerotidae (rhinoceros), and Bovinae (aurochs) specimens are present. The persistence of equids through the sequences indicates the consistent exploitation of open, grassy landscapes by the site's occupants.

Duricrust characteristics. Thin section microscopy identified the carbonates immediately overlying Layer S5 (S6 Fig) as a diagenetically complex and well indurated duricrust, ranging in composition from calcrete to intergrade duricrusts through to silcrete (Fig 4A–4D). Duricrusts are geochemical sediments that form a zone of accumulation of soluble chemical precipitates within or replace underlying deposits through the movement of mineral-bearing waters [62]. Further detailed descriptions on the various components of the duricrust can be found in S3 File.

Analyses of isotopic compositions were undertaken on subsamples from a well indurated calcrete *sensu stricto* (Fig 4A), as well as from organic layers and a laminar crust (S7 Table), both preserved within the calcrete. Mean values for $\delta^{13}C$ are -6.14, -2.03 and -9.12 and for $\delta^{18}O$ -6.39, -8.82 and -5.33 for the calcrete, the organic layer and the laminar crust, respectively (S3 File).

OSL dating

Luminescence signal and equivalent dose characteristics. Individual grains from Rhafas exhibit rapidly decaying luminescence signals typical for fast component dominated quartz (Fig 5, S11 Fig), but only 1.3–7.9% of all measured single sand-sized quartz grains proved suitable for OSL dating using the SAR procedure (S3 Table). Dose recovery tests on individual grains demonstrate the ability of the samples to consistently recover a known laboratory dose within two 2-sigma of unity (S4 Table).

In most instances, the samples from the terrace section yield normal D_e distributions (S3A–S3D Fig), characteristic for well bleached and unmixed samples. Overdispersions are below

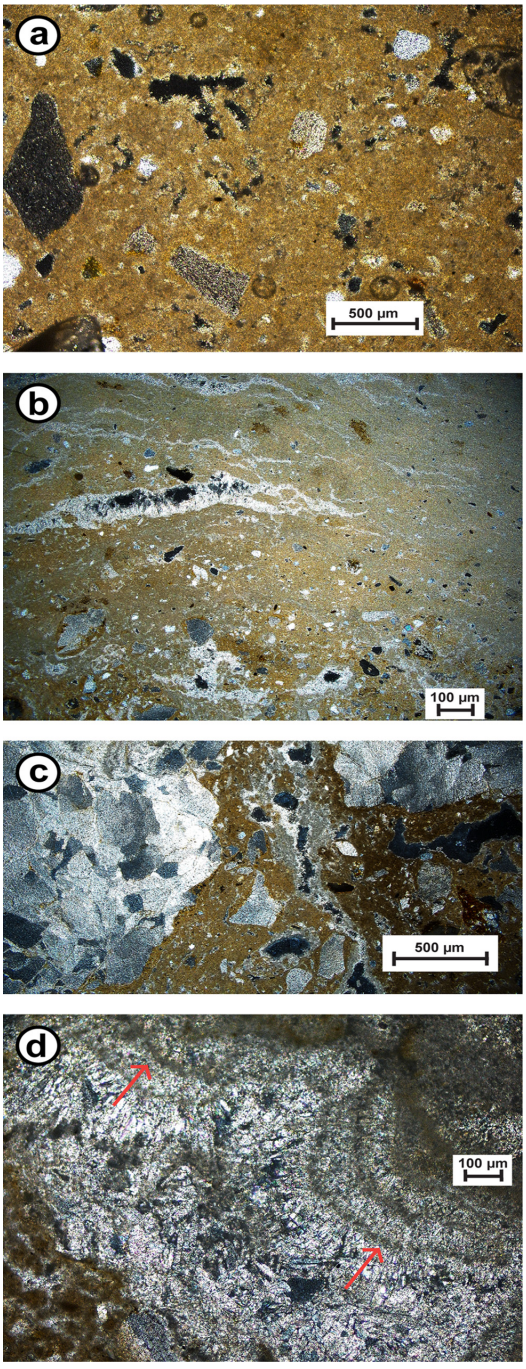
a
500 µm
b
100 µm
c
500 µm
d
100 µm

Fig 4. Thin section photographs. (a) Micritic calcrete with displaced semi-rounded lithoclasts and secondary porosity; (b) silcrete-calcrete intergrade duricrusts with silica crystals developed within stringers in the calcrete; (c) calcrete-silcrete intergrade duricrust with clear domination of silica cement over calcrete; (d) silcrete cements: amorphous brown opal followed by fibrous crystals of lussatite, also note the mammillary structured quartz crystals (arrows). All photographs were taken under cross-polarised light.

doi:10.1371/journal.pone.0162280.g004

30% (Table 3), with the exception of sample L-EVA-1212 (Fig 5B), which yields a higher value of 44%. The radial plot of sample L-EVA-1212 shows a one-grain-population (D_e ~5 Gy) that clearly separates from all other accepted grains and does not belong to the population of grains representing the depositional age of the sample (Fig 5B). It remains ambiguous whether this single grain was introduced into the layer by post-depositional mixing, which seems unlikely, or was shielded by carbonates during burial time or simply exhibits insufficient luminescence characteristics. This individual grain was considered an outlier and excluded from further analyses even though it was not identified as such by the Grubbs test [63]. As a consequence, the overdispersion for L-EVA-1212 was reduced to 30%. The Central Age Model (CAM) [64], which assumes a single homogeneous age population, was used for age calculation of the terrace section samples.

The samples from the cave mouth section yield generally more widespread single grain distributions with overdispersions ranging from 23 to 44% (Figs 5A and 6; S4 Fig; Table 3). As there is no indication of incomplete bleaching or proportionally high dose rate heterogeneity attributed to the samples, the most likely explanation for the observed spread is the post-depositional introduction of younger grains.

To correctly account for the possibility of multiple depositional and/or mixing phases, in addition to the CAM, the Finite Mixture Model (FMM) [65] was systematically applied to all samples from the cave mouth section (Table 3). We ran the FMM for 2–3 discrete dose components using overdispersion values between 15 and 30% and compared the obtained estimates of the Bayes Information Criterion (BIC) and the values of maximum log likelihood (llik) to correctly assess the minimum number of statistically supported D_e components for each sample [65, 66]. The smallest BIC values were obtained when running the FMM with two discrete components and overdispersions of 15% (L-EVA-1139), 20% (L-EVA-1140) and 25% (L-EVA-1210 and L-EVA-1141). A substantial increase of llik (by at least 2) when running the model with three components was not observed [65, 66]. Further details on the determined D_e values for all samples, their associated D_e errors and the relative proportion of individual grains in each identified component are listed in S8 Table.

The FMM statistically supports two discrete components for each sample of the cave mouth section with the minor components containing, with the exception of sample L-EVA-1139, 5–23% of the total amount of accepted grains, which seems reasonable for post-depositional mixing events. Final ages were calculated based on the FMM results, and for sample L-EVA-1139, which yielded a comparatively low overdispersion value (22%), on both the CAM and FMM results, respectively (Table 3).

Dosimetry. The total dose rates of the samples in this study vary substantially, ranging from 0.96±0.04 Gy/ka to 3.11±0.18 Gy/ka (Table 1). Lower dose rates were observed for the sediment layers of the cave mouth section and the terrace section (between ~1 Gy/ka and ~1.4 Gy/ka). Units with large proportions of calcium carbonates at Rhafas (L-EVA-1139, 1140, 1141, 1212) also yielded comparatively low total dose rates.

In the cemented and uncemented layers of the lower cave section, dose rates increase significantly for both the beta and the gamma component (Table 1). Concentrations of the radioactive minerals within the sediment layers of the cave mouth section and the lower cave section reflect this growth (Fig 7).

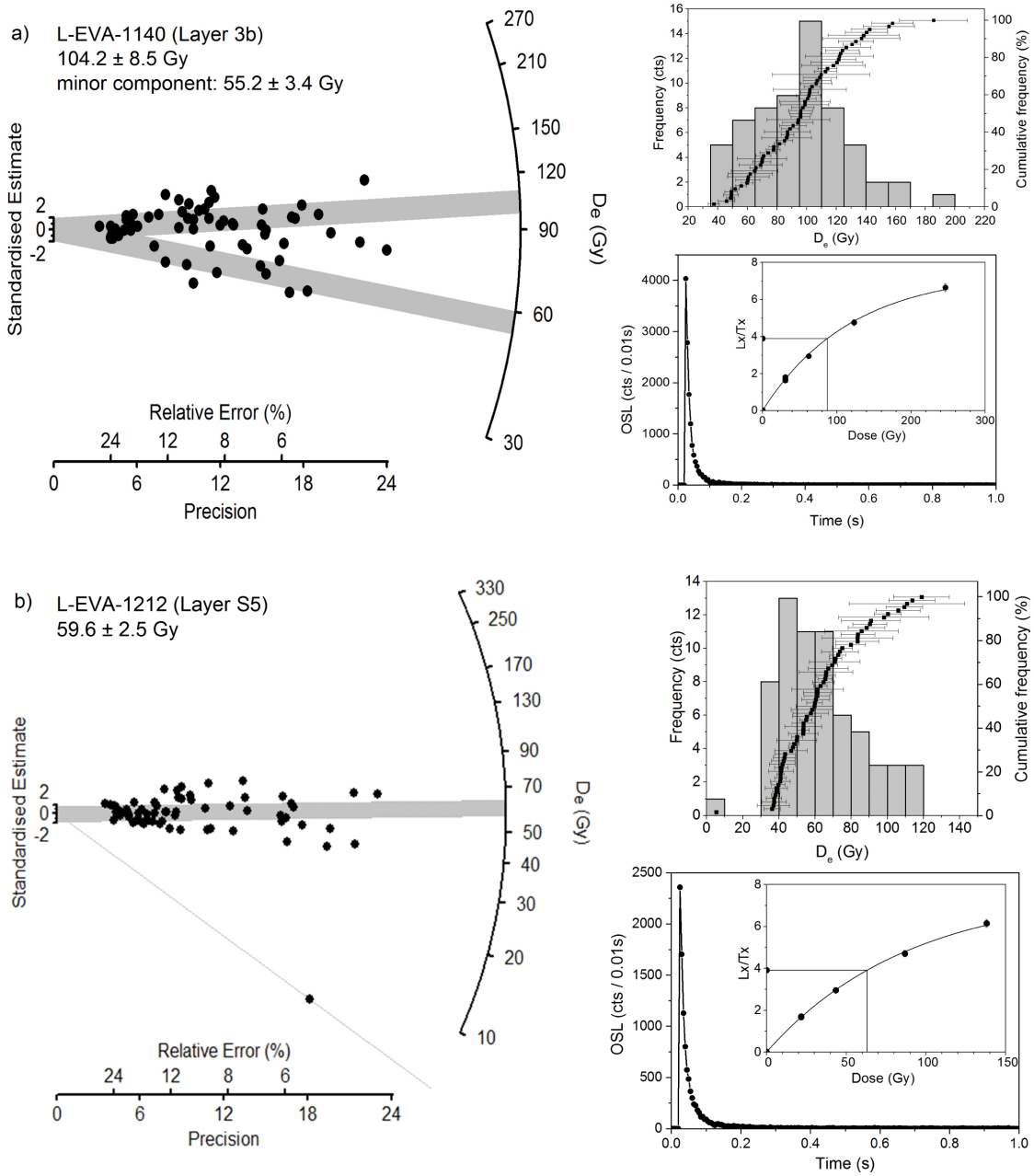

Fig 5. Representative OSL characteristics for two sediment samples from Rhafas. Radial plots and frequency histograms show the dose distributions of single grains, and a natural OSL decay curve with dose response curve (as inset) for samples (a) L-EVA-1140 and (b) L-EVA-1212, respectively. The shaded bands in the radial plots correspond to the standard error deviation from the calculated D_e.

doi:10.1371/journal.pone.0162280.g005

Table 3. Results of OSL dating.

Sample	Unit	CAM[a]	Overdispersion	FMM[b] D_e values (Gy) and proportions (%)				Total dose	Age[c]	Age of minor
		D_e		Component 1		Component 2		rate		component
		(Gy)	(%)	D_e	proportion	D_e	proportion	(Gy/ka)	(ka)	(ka)
Cave mouth section										
L-EVA-1210	1	10.0±0.6	37±4	2.7±0.1	4.8	**10.7±0.5**	95.2	1.29±0.07	7.8±0.6	2.1±0.1
L-EVA-1139	3a	**86.2±2.7**	23±2	71.3±14.1	42.2	**99.4±19.7**	57.6	1.01±0.04	85.4±4.5/98.5±19.8	70.7±14.2
L-EVA-1140	3b	90.5±4.0	33±3	56.7±4.6	23.1	**104.2±8.5**	76.9	0.96±0.04	108.5±9.9	59.0±5.4
L-EVA-1141	4c	116.7±6.6	44±4	55.2±3.4	16.4	**134.0±8.3**	83.6	0.99±0.04	135.3±10.3	55.7±4.2
Terrace section										
L-EVA-1145	S2	**20.2±0.6**	20±2	-	-	-	-	1.31±0.09	15.4±1.2	-
L-EVA-1146	S3	**29.2±1.1**	29±3	-	-	-	-	1.36±0.08	21.4±1.5	-
L-EVA-1212	S5	**59.6±2.5**	30±3	-	-	-	-	1.05±0.05	56.9±3.5	-
L-EVA-1213	S6	**121.4±5.0**	29±3	-	-	-	-	1.40±0.05	86.4±4.9	-
L-EVA-1148	S7	**155.5±6.4**	30±3	-	-	-	-	1.27±0.07	122.5±8.8	-

[a]Central Age Model [64].

[b]Finite Mixture Model.

[c]Calculated using the D_e highlighted in bold.

doi:10.1371/journal.pone.0162280.t003

Chronology

The ages were calculated based on the model-derived D_e values outlined in the preceding section and on the dose rate determined for each individual sample. A summary of the obtained values is given in Table 3; the D_e values highlighted in bold were used for final age calculations.

The MSA deposits in the terrace section accumulated between 123–57 ka. The two basal samples collected from Layers S6 and S7 (L-EVA-1213 and -1148) give ages of 86±5 ka and 123±9 ka respectively, indicating deposition during the last interglacial (Marine Isotope Stage (MIS) 5). Layer S5 (L-EVA-1212) dates to 57±4 ka and represents an occupation and sediment accumulation phase at the site during MIS 3. The two overlying Layers S3 and S2 (L-EVA-1145 and -1146) give ages of 21±2 ka and 15±1 ka, respectively, and are associated with LSA techno-complexes. The sediment deposition took place during MIS 2, more specifically, during the middle and late stages of the last glacial maximum (LGM).

There is a major erosional break in the cave mouth section separating the Neolithic Layer 1 (L-EVA-1210) deposited ~7.8 ka from the underlying sediments associated with the MSA (Layer 3a to 4c) and deposited >85 ka. The FMM-derived ages suggest deposition of Layer 4c and 3b (L-EVA-1141 and -1140) at 135±10 ka (MIS 6) and 109±10 ka (MIS 5), respectively, and a phase of post-depositional introduction of younger grains between 56±4 and 59±5 ka (MIS 3). For sample L-EVA-1139 (Layer 3a) ages were calculated for both CAM- and FMM-derived D_e values. With the CAM, Layer 3a gives an age of 85±5 ka (Fig 6A). The FMM gives ages for the major component (58%) and the minor component (42%) of 99±20 ka and 71±14 ka, respectively (Fig 6B). Both calculated depositional ages for Layer 3a (85±5 ka and 99±20 ka) are consistent with the archaeological finds and date to MIS 5.

Discussion

Remarks on dating the lower cave section

Within this study, a substantial dose rate inconsistency was detected between the cave mouth and the lower cave section at Rhafas. Radioactive elements increase substantially from Layer 4c

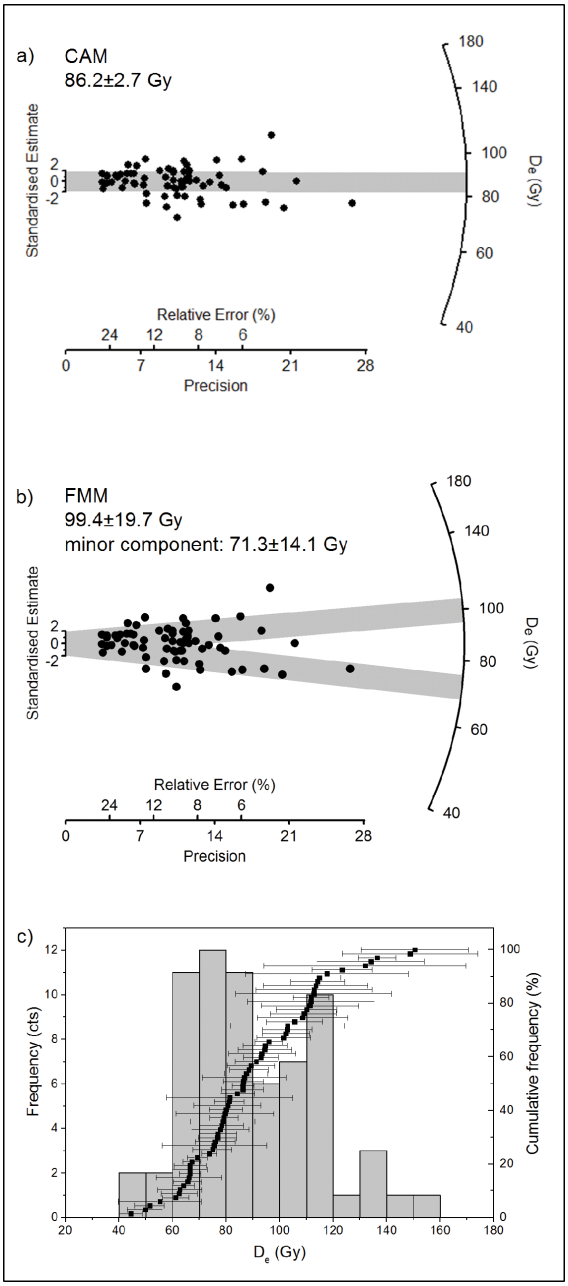

Fig 6. Dose distributions of single grain values obtained for sample L-EVA-1139. The shaded bands in the radial plots correspond to the standard error deviation from the D_e calculated using the (a) Central Age Model or (b) Finite Mixture Model. (c) Frequency histogram of single grain D_e values.

doi:10.1371/journal.pone.0162280.g006

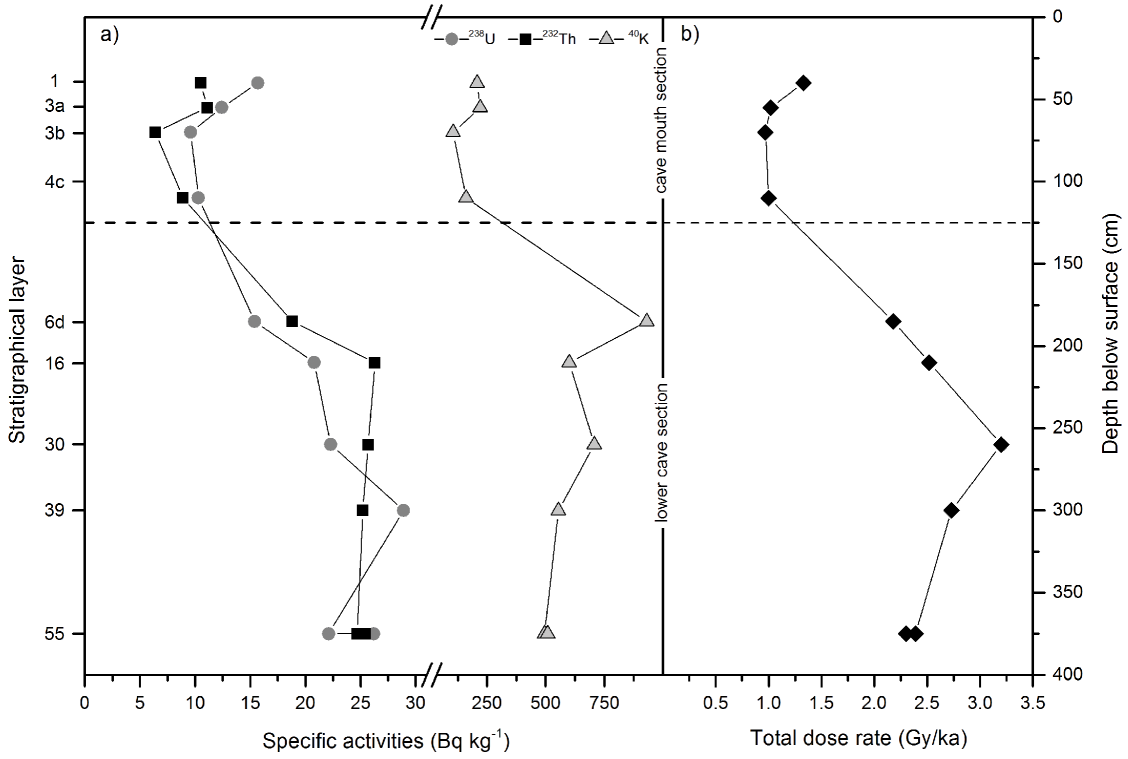

Fig 7. Determined dose rate changes throughout the cave sections at Rhafas. Distribution of (a) radioactive elements ^{238}U, ^{232}Th, ^{40}K and (b) total dose rate for the sampled layers within the cave of Rhafas.

doi:10.1371/journal.pone.0162280.g007

to 6d leading to a rise of the total dose rate by more than a factor of 2 (Table 1; Fig 7). Mercier et al. [26] determined the radioisotopic content for the only OSL sample in their study with a high purity Ge detector, resulting in a total dose rate value of 2.20±0.10 Gy/ka for Layer 6d, which is statistically identical to our data (2.14±0.07 Gy/ka). Dose rates increase with depth in the lower cave section and reach a maximum of 3.11±0.18 Gy/ka in Layer 30 which is approximately 1.35 m below the cave mouth section.

In contrast to the dose rates, D_e values in the cave increase continuously with depth without any remarkable deviation. Calculating final ages based on these data would lead to an age inversion, with the lower cave section being younger than the overlying layers of the cave mouth section. Since the D_e values for the lower cave section show consistently stable luminescence characteristics and are consistent with the other sections at Rhafas, the aforementioned problems in age calculation most likely originate from the abnormal increase in total dose rates observed in these sediments.

Our sedimentological investigations in the field as well as in the laboratory show no indication of a shift in the main accumulation processes between the two cave sections. The sedimentology of the cave sediments, however, displays major changes in the non-mobile elements (siliciclastic fractions) between the sections which indicate a shift in the sedimentary source over time. This may explain at least part of the increase of radioactive elements (Fig 3).

Although the observed differences in the grain size compositions of the layers in the two cave sections most likely reflect primarily the presence or absence of secondary carbonate cementation, the increasing clay content in the lower cave section may support our hypothesis for variability in sediment source. Clay concentrations of 20–30% in a predominantly aeolian cave deposit strongly indicate the presence of a second local sedimentological process which influenced the lower cave section. The clay is either a local weathering product of the dolomitic limestone which forms the cave or reflects past pedogenesis which is no longer preserved in the present-day profile.

Irrespective of clay origin in the lower cave section layers, it does not provide a comprehensive explanation for the substantial increase of potassium observed in these sediments (S10 Fig), and furthermore by the particular peak in ^{40}K and correspondingly low clay content within Layer 6d. A possible post-depositional decrease in total dose rates in carbonate cemented layers is also highly unlikely, since the dose rates of unconsolidated layers in the cave mouth and terrace section (1 and S2) are consistent with those of the cemented layers. Moreover, the high (60%) carbonate content in Layer 6d - comparable with the overlying Layer 4c from the cave mouth section–does not appear to influence the downward increase in total dose rates observed between these two layers.

The most likely explanation for the increase in dose rates below Layer 6d - beside the possible influence of a change in sediment source—is a post-depositional input of mobile radioactive elements to the lower cave sediments. Groundwater could easily percolate through the fracture network of the lithological unconformity between the meta-sediments and the dolomitic limestone (located 1–2 m below the cave mouth section), mobilising radioactive elements from the underlying meta-sediments and granodiorite and precipitating them in the lower part of the cave fill sequence. The prominent tufa/flowstone mound on the southwestern wall of the cave clearly indicates spring activity associated with Layer 6d which might have affected the subjacent sediments. While potassium is relatively immobile, it is soluble in water following feldspar weathering [67]. It is readily incorporated into clay mineral lattices, a process which might explain the high ^{40}K concentration in Layer 6d relative to the underlying sediment layers.

Unfortunately it is impossible to precisely determine the total amount and timing of precipitation of allochthonous radioactive elements in the individual sediment layers. Moreover, and particularly in the context of a dating study, the timing and flux of fluid activity in the cave is of particular relevance and renders these sediments effectively undateable despite stratigraphically consistent D_e values for the OSL samples. Therefore, we regard the age estimate for Layer 6d published by Mercier et al. [26] as an underestimate, and argue that, without further investigations, the lower cave section at Rhafas remains undateable.

Chronology of deposition

Fig 8 summarises the chronostratigraphy of the cave mouth and the terrace section at Rhafas based on single grain OSL age estimates obtained in this study, in comparison with previously published data by Mercier et al. [26]. Deposition of the sediments in the cave mouth section took place between 135 ka and 7.8 ka with a major unconformity between the MSA and the overlying Neolithic (Fig 8A). Although our OSL ages for the MSA Layers 3a and 3b are both slightly older than the corresponding TL age estimates by Mercier et al. [26], both datasets are consistent with each other within the given error ranges as well as with the expected age of the archaeological finds based on chronologies from other sites. OSL and ^{14}C age determinations for the Neolithic Layer 1 yielded results of 7.8±0.6 ka and 6.0±0.2 ka cal BP, respectively, which fall into the expected age range.

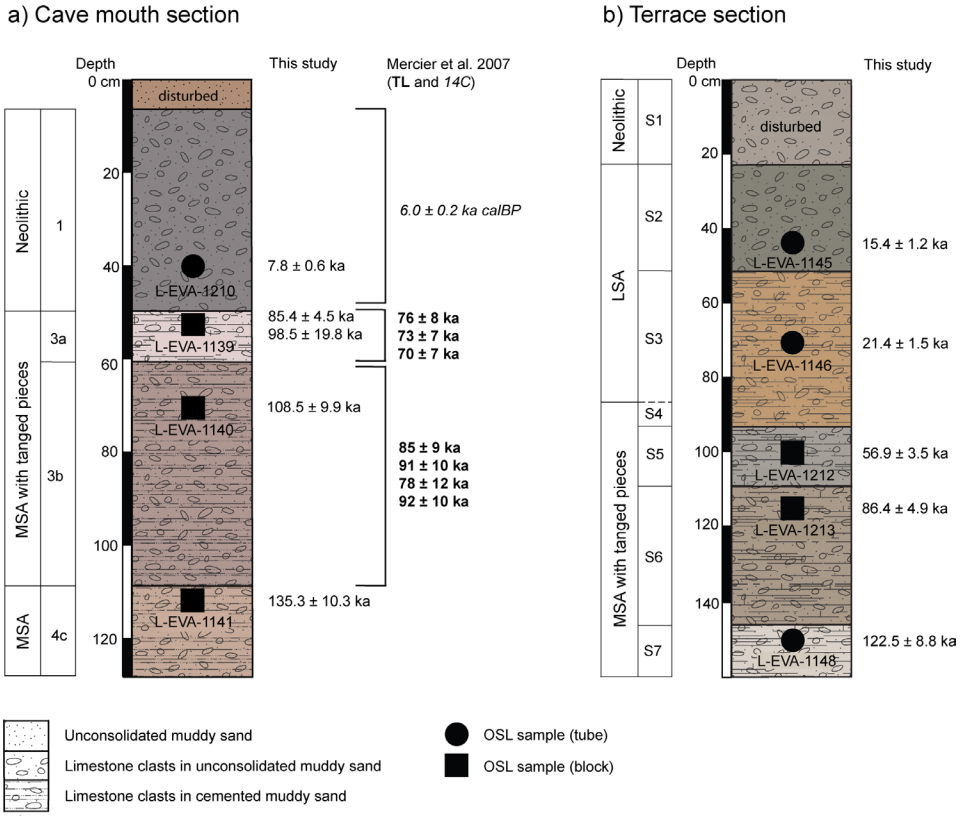

Fig 8. Chronostratigraphy of Rhafas. Determined single grain OSL ages and formerly published absolute age estimates by Mercier et al. 2007 [26] plotted against the stratigraphy of (a) the cave mouth and (b) the terrace section at Rhafas.

doi:10.1371/journal.pone.0162280.g008

There is evidence within the three cemented Layers 3a, 3b and 4c for a post-depositional phase where younger material was incorporated into those units around 56 ka. This process involved infiltration of younger grains into the older, still unconsolidated sediment layers, in diminishing concentrations down the stratigraphic profile as indicated by the proportion of younger grains within each sample. FMM analysis of the single grain D_e distributions clearly shows the presence of two age populations–an older, dominant population and a younger, minor population—in both Layers 3b and 4c (L-EVA-1140 and -1141). Indications of younger sediment infiltration into Layer 3a (L-EVA-1139), by contrast, are not as unequivocal, and consequently ages for Layer 3a were calculated using both CAM- and FMM-derived D_e values in order to interrogate the data before final interpretation of the age (Table 3). The CAM assumes a Gaussian single grain D_e distribution [64], and this holds for L-EVA-1139 and is further supported by its 23% overdispersion (Fig 6A). Layer 3a gives a CAM age of 85±5 ka. The FMM-derived D_e values, in comparison, result in major (58%) and minor component ages (42%) of 99±20 ka and 71±14 ka respectively (Fig 6B). The relatively similar proportions, and large uncertainties, of the two components of sample L-EVA-1139 can be used to argue that the FMM cannot clearly distinguish two discrete age populations and, therefore, that the FMM is

unsuitable. On the other hand, when the dating results from the two underlying Layers 3b and 4c are taken into consideration, there may have been one single post-depositional mixing event affecting all three layers at the same time (~56ka), since the proportions of the minor, younger age component—representing the mixing event—decrease from top (3a) to bottom (4c) and lie within the same age range (Table 3; S9 Fig). Given this interpretation, the FMM is in fact the most parsimonious age model for Layer 3a; the relatively similar proportions and large uncertainties of the two FMM components for this sample are most likely caused by the depositional events occurring within short temporal succession. There are doubtlessly strong arguments supporting the application of either the CAM or the FMM; however, as stratigraphic indications should be fundamental for any dating study, we consider the FMM age to be more conclusive. Regardless of this discussion, both models provide ages that are consistent with the archaeological finds as well as the cave stratigraphy and date to MIS 5.

The earliest deposition of sediments in the terrace section is dated to ~123 ka (Layer S7, Fig 8B). These sediments form a matrix between large dolomitic limestone boulders. The boulders are interpreted to originate from a former extension of the cave roof prior to 123 ka. The stratigraphy of the terrace section sediments is mostly undisturbed (except for Neolithic Layer S1) with no indications for post-depositional mixing or major unconformities. The most remarkable feature of this section is the prominent indurated duricrust that separates Layer S5 (~57 ka, MIS 3) from the overlying Layer S3 (~21 ka, MIS 2) and consists of numerous sublayers of calcretes, intergrade duricrusts and silcretes. The timing of duricrust formation must, therefore, fall in the range 57–21 ka. Since the age of post-depositional sediment incorporation into Layers 3b and 4c at the cave mouth section also dates to ~56 ka, during which time the layers were still sufficiently unconsolidated to allow infiltration of younger grains, pedogenesis (including carbonate induration) of those layers must postdate this process.

Environmental implications

Regionally, central North Africa has been dominated by C_4 vegetation and arid conditions over the last 190 ka, with some expansion of C_3 vegetation assemblages during wetter climatic phases [68]. Rhafas experiences a semi-arid Mediterranean climate (300 mm rainfall p.a.) and lies ~50 km from the present-day coastline (indicating a slight marine influence on both $\delta^{13}C$ and $\delta^{18}O$ values), resulting in a mixture of C_3 and C_4 plants. Westerlies currently bring winter rains to North Africa and are mainly controlled by the North Atlantic Oscillation [69, 70]. Summers are dry and hot due to the influence of the subtropical high pressure belt [69, 71]. Today, summer rains associated with the African or Indian monsoon do not penetrate far enough north to provide rain to the Sahara or the Maghreb. Climatic conditions in North Africa were, however, substantially different during "green Sahara" events when intensification and northward migration of the monsoonal systems led to enhanced humidity and expansion of subtropical savannah landscapes in the region [72]. While these "green Sahara" events were restricted to relatively short (<5–10 ka) time intervals, past glacial phases were characterised by comparatively cool and arid climatic conditions and interglacials by warmer average temperatures and enhanced monsoon rains. The long term climatic trend over the past several hundred thousand years in North Africa appears to be one of increased aridity [69, 72–74].

Our dating results show that sediment deposition and human occupation at Rhafas initiated at least in MIS 6, when climatic conditions were relatively dry in North Africa, interrupted only by a "green Sahara" event around 170 ka [72]. The sediments of the lower cave section predate 135 ka and show indications for evaporite enrichment (increasing Cl and S concentrations and a decreasing Na/Cl mol ratio, Fig 3). This most likely reflects deposition of the lower cave

sediments during relatively arid climatic conditions for the interval between 165 and 140 ka. This time period is also associated with an increased dust flux in the Sahara [72].

While the geochemistry of the sediments from the cave mouth and terrace section share the same characteristics, major differences can be observed in comparison to the lower cave section sediments (Fig 3, S6 Fig), especially in the siliciclastic fractions. Ti/Th, K/Al, Pb/Al, Rb/K and Ni/Al ratios reflect concentrations of primary non-soluble elements, which are unlikely to get introduced into sediment layers post-depositionally. The substantial changes in the siliciclastic ratios between the different sections at Rhafas can, therefore, be attributed to a change in sediment source towards the end of MIS 6/beginning of MIS 5. As north-western Morocco was primarily influenced by the westerlies, this change in sediment source is most likely linked to a shift in wind directions on a regional or local scale.

During MIS 5, climatic conditions were characterised by increasing humidity. "Green Sahara" events took place during substages 5a, 5c, with a particularly strong event around 125 ka (MIS 5e). Studies have shown that the north-eastern Sahara received at least 500 mm of annual rainfall during MIS 5e which enabled the widespread occurrence of wooded savannah landscapes inhabited by subtropical fauna [75, 76]. These conditions would also have facilitated human expansion across northern Africa and the Levant. With the end of the green Sahara event in MIS 5a and the beginning of MIS 4, climatic conditions became drier, leading to a proposed depopulation of the Sahara after 80 ka [70, 77]. Humans rapidly migrated into desert ecological refugia, coastal areas and sub-Saharan Africa [72, 75, 76, 78]. While MIS 5 sediments are present at Rhafas within the cave as well as on the flat terrace area in front of the cave entrance, including archaeological finds that prove intensive human occupation of the site between ~123 ka to ~86 ka, deposits from MIS 4 are not preserved throughout all section profiles. It is unlikely that sedimentation at Rhafas stopped during MIS 4, since glacial periods are commonly associated with increased aeolian reactivation and deposition [72]; rather, we propose that the absence of MIS 4 deposits is more likely linked to natural or anthropogenic erosion that predates the sedimentation of Layer S5 in the terrace section (~57 ka).

Humidity increased again during MIS 3 in North Africa but did not reach the intensity of MIS 5. Humid conditions intensified between ~45 ka and 30 ka. At this time, the western Sahara was covered by steppe-prairie vegetation [78–80]. Deposits from MIS 3 are present at Rhafas in the terrace section (Layer S5) as well as in the cave mouth section. Although almost all material was removed from the latter at some point after deposition, its former presence is still traceable as minor components that were mixed into the underlying sediment layers (3a-4c).

A prominent duricrust was formed on top of Layer S5 in the terrace section (S6 Fig). To obtain further information on the prevailing environmental conditions during their precipitation, stable isotope analyses of carbon and oxygen were undertaken on three distinct types of calcretes–micrite matrix, calcrete rich in organics and laminar calcrete (Fig 6A). The oxygen isotope ratios in the calcretes indicate a lack of significant evaporation, and the $\delta^{13}C$ mean value of -6.14 suggests a mix of C_3 and C_4 plants comparable with present day conditions. As there is no strong degree of covariance between $\delta^{13}C$ and $\delta^{18}O$, it is unlikely that the two sets of isotope ratios were controlled by the same environmental factor, which would have been an indicator for arid environments [81]. Thus it is more likely that the calcretes formed under semi-arid or seasonally arid conditions. The combined results of the duricrust fabrics, isotope ratios from the duricrust (S7 Table) and the abundance of organic matter are consistent with pedogenic calcretes. The $\delta^{13}C$ values from the dark organic layers within the calcrete—comprising carbonate, organic matter and oxides—suggest a greater abundance of C_4 plants (-2.03), indicating more arid conditions during its formation. The equivalent $\delta^{18}O$ values are depleted which suggests low evaporation rates (a key sign of aridity), and therefore appears to

contradict the $\delta^{13}C$ results from the same material. The $\delta^{13}C$ value (-9.12) of the laminar crust indicates an increased proportion of C_3 plants and perhaps more of a Mediterranean environmental influence.

Duricrust formation must have occurred between the deposition of Layer S5 (~57 ka) and S3 (~21 ka) during MIS 3 and MIS 2, respectively. The western Mediterranean climate during MIS 2 was characterised by semi-arid to arid conditions [82]. The faunal remains from Layer S3 at Rhafas suggest the presence of open, grassy landscapes at that time.

While humid conditions in northern Africa during MIS 3 might have been favourable for the formation of silcretes, calcretes on the contrary tend to form in semi-arid to arid, but not hyper-arid, conditions. The characterisation of the various components of the duricrusts, supported by the isotope results of the calcretes, suggest that the duricrust at Rhafas is most likely a product of formation under the range of climates that north-western Africa experienced over the last 57 ka rather than of one single climatic event of short duration.

During the early-middle Holocene (10–6 ka) another green Sahara period with increased humidity and expansion of savannah landscapes took place in northern Africa [72, 74]. Sediment deposition at Rhafas associated with the occupation of the site by Neolithic groups date to ~7.8 ka.

Archaeological chronologies and human occupation phases in the Maghreb

The new series of excavations undertaken in the terrace area in front of the cave of Rhafas yielded archaeological find horizons associated with the LSA and thereby help fill the occupational gap between the MSA and the Neolithic formerly reported for the site by Wengler [42]. Rhafas now represents one of the few sites in the Maghreb which provides a well dated archaeological sequence spanning multiple Palaeolithic technocomplexes (Fig 8).

The chronology presented here does suggest occupation of both the terrace and cave during the MSA with tanged pieces, with depositional ages for Layer 3a and S6, and 3b and S7 overlapping in time. The Neolithic Layers 1 and S1 also allow clear correlations between the two sections at that time. Layers from the LSA, while present in the terrace area, are either not present or have been removed from the cave mouth section.

Our revised chronostratigraphy from Rhafas contributes towards a rigorous investigation of evidence for human activity across the Maghreb during the Middle and Late Pleistocene. Here we compare our results with published chronological data from 25 MSA and LSA sites across western Morocco, northern Morocco, Algeria, Tunisia and western Libya (Figs 9 and 10; for site locations see Fig 1) [2, 3, 6, 10, 13–17, 26, 28, 31, 33, 34, 83–99]. In this analysis we consider only archaeological layers which can be clearly associated to a defined stone tool technology and have been reliably dated by absolute dating (^{14}C, TL, single aliquot OSL (SA-OSL), single grain OSL (SG-OSL), electron spin resonance (ESR) or U-series (Th/U)).

Our data corroborate previously published data and are used to catalyse a synthesis for stone tool assemblage chronologies across the Maghreb.

The first phase of occupation at Rhafas associated with the MSA started at least in late MIS 6 (~134 ka) or even earlier (since MSA is also found in the as yet undateable lower cave section). Its duration was at least 60,000 years and persisted into MIS 5 (Fig 9). Apart from Rhafas, evidence for occupation in the Maghreb in MIS 6 or earlier is limited to the sites of Jebel Irhoud [83], Abrigo de Benzù [31, 33], Ifri N'Ammar [10], El Akarit [92] and Ain Zargha in the Jebel Gharbi [95]. The oldest age is 254±17 ka, recorded at Benzú [31, 33]. The onset of the MIS 5 interglacial resulted in increasingly humid climatic conditions associated with an expansion of grassland habitats in northern Africa [68, 100–102]. These conditions most likely facilitated an

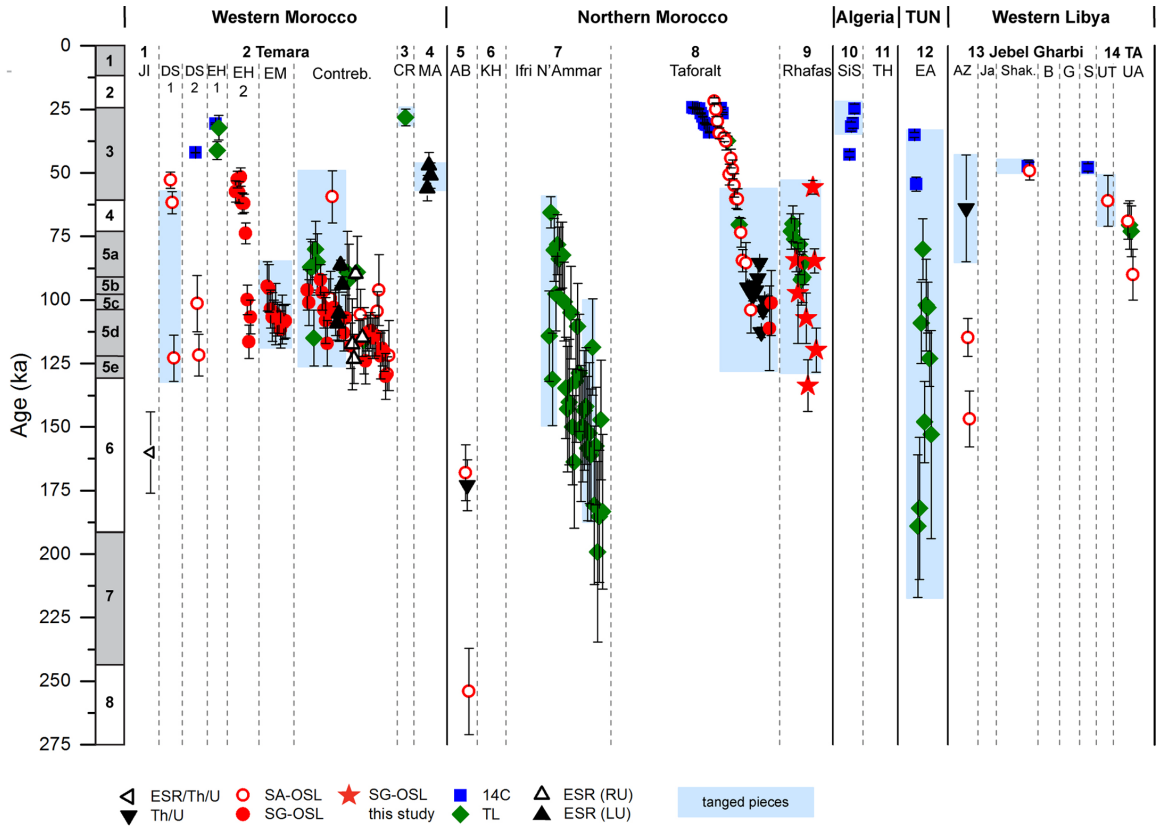

Fig 9. Synthesis of age estimates for MSA layers from archaeological sites in the Maghreb. Numbers in the headline correspond to numbers of the sites given in Fig 1.

doi:10.1371/journal.pone.0162280.g009

increase in human populations living in the region [1]. Occupation during the MIS 5—associated with the MSA—has been published for all parts of the Maghreb, with the exception of Algeria for which no absolute dates are available before MIS 3 (Fig 9). Particularly striking is this phase of settlement at the Atlantic coast of Morocco (Témara region) [3, 13, 14, 16, 17], the sites of Ifri N'Ammar [10], Taforalt [2, 6, 15, 103] and Rhafas in northern Morocco (this study; [26]), and at El Akarit in Tunisia [92].

There appears to be a hiatus in occupation at Rhafas during MIS 4. This may reflect less favourable, drier climatic conditions. However, during MIS 3 occupation associated with the MSA is evident across all areas of the Maghreb.

Some of the key questions relating to the MSA of North Africa refer to the Aterian, its characteristics, technological definition and timing (e.g. [8, 9]). The Aterian has been used to argue for cultural modernity associated with the dispersal of anatomically modern humans out of Africa [4, 6, 7]. There remains some debate over how to define and recognize the Aterian, particularly for MSA assemblages post-dating the earliest Aterian but lacking tanged pieces. There are also assemblages in need of renewed study in light of more recent studies on the non-tanged elements in Aterian assemblages. Consequently, we focus here on the least ambiguous

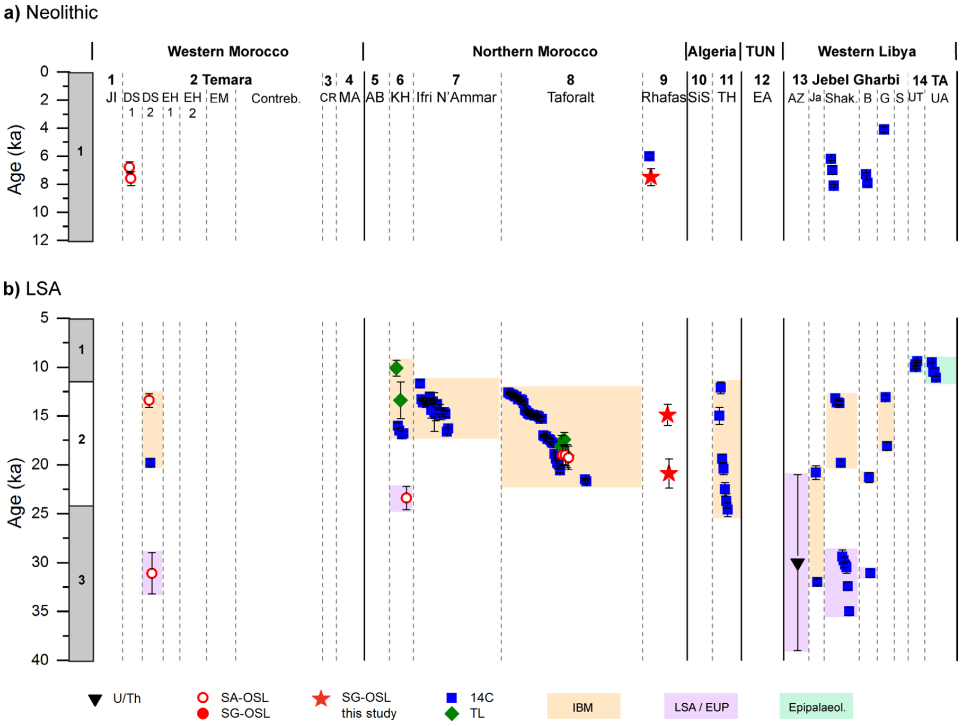

Fig 10. Synthesis of age estimates for Neolithic or LSA layers from archaeological sites in the Maghreb. (a) Neolithic and (b) LSA. Numbers in the headline correspond to numbers of the sites given in Fig 1. Highlighted are dates associated to the Epipalaeolithic, the Iberomaurusian and the LSA/EUP in green, orange and purple, respectively.

doi:10.1371/journal.pone.0162280.g010

indicator for the Aterian–namely tanged pieces–as an indicator of its temporal onset (Fig 9), while acknowledging that an Aterian without tanged pieces could be yet earlier Dates from archaeological layers containing regular occurrence of tanged pieces have been highlighted in blue (Fig 9). It is important to note that the ^{14}C dates of Betrouni [89] from Sidi Sa should be treated with caution. Likewise, the older TL ages from El Akarit may not be reliable due to problems with dose rate determination within the sediments [92]. The earliest reliably occurrence of tanged pieces is found at Ifri N'Ammar, and dated by TL to a weighted average of 145 ±9 ka [10]. Apart from Ifri N'Ammar, tanged pieces do not regularly occur within Moroccan archaeological assemblages until the onset of MIS 5e ~130 ka [2, 3, 6, 13–17, 26]. Tanged pieces occur even later in Algeria and western Libya: 43±1 ka at Sidi Sa [89], 64±21 ka at Ain Zargha [93], ~47 ka at Jebel Gharbi [93, 94] and 61±10 ka at Uan Tabu [98]. This may be, however, an artefact of the limited chronological dataset for sites in Algeria, Tunisia and western Libya. Tanged pieces persist in archaeological assemblages until at least ~47 ka in western Morocco (Mugharet el'Aliya [86]), northern Morocco (Rhafas, this study) and western Libya (Shakshuk [94]), and maybe until ~35 ka at El Akarit (Tunisia [92]) and ~25 ka at Sidi Sa (Algeria [89]). It is important to note that despite the widespread distribution of tanged pieces within the MSA across the Maghreb after 130 ka, other sites in the region have archaeological layers which do not contain tanged pieces (e.g. El Harhoura 1 [84, 85] and Taforalt [2]).

The youngest dates for the MSA overlap with the onset of the LSA between 30 and 35 ka (Fig 10B). The early LSA is particularly widespread in the archaeological assemblages of western Libya [93, 94]. By contrast, with the exception of Dar es-Soltan II [14], LSA records are not present in other parts of the Maghreb before ~24 ka [34, 91]. At Rhafas, the LSA Layers S2 and S3 date to 15±1 ka and 21±2 ka, respectively, and are consistent with the overall LSA dataset for the Maghreb. Here we follow Linstädter et al. [104] in dividing the LSA of the Maghreb into an early LSA (or EUP), the Iberomaurusian (IBM) and the Epipalaeolithic, as indicated in purple and orange and green in Fig 10B. This recent work at Rhafas has highlighted the exceptional nature and preservation of the LSA marked by one of the earliest appearances of the microlithic bladelet industries in North Africa. The earliest phase of the LSA (Layer S3) is characterised by microliths, bladelets and backed tool industries that occur in Algeria and Morocco around 20 ka [2, 91, 105] and are defined as Iberomaurusian. Elsewhere in Cyrenaica similar technology at Hua Fteah was dated to ~17 ka cal BP [106]. The late phase of the LSA at Rhafas (Layer S2) is typified by a high proportion of backed bladelets and the use of the microburin technique that also occur elsewhere in Algeria [107, 108] and Morocco [109].

The LSA ends with the onset of the Neolithic during the Holocene. In Fig 10A Neolithic age estimates from the MSA and LSA sites in the Maghreb are shown. The dates for Layer 1 from Rhafas fit within the commonly determined age range for the Neolithic and are consistent with the dates from Dar es-Soltan I in western Morocco [13, 14] and the Jebel Gharbi [93, 94]. However, there is still an age gap between the late LSA and the Neolithic at Rhafas. To further investigate the occupation history of the site and the palaeoenvironmental context of the late LSA and Neolithic, additional dating work focusing on the younger occupation phases should be conducted in the future.

Conclusion

This study presents a revised chronostratigraphy of the archaeological sequence at Rhafas spanning the MSA through to the Neolithic. We used a multidisciplinary approach, applying single grain OSL dating which elucidated post-depositional processes in several stratigraphic units (Layers 3a, 3b and 4c), combined with stratigraphic observations and sedimentological and geochemical analyses of sediments and duricrusts to investigate palaeoclimatic conditions. Our methods were placed within a classical archaeological framework to examine human-environmental interactions at the site during its long occupational history. Our results suggest changes in environmental conditions from arid to humid some time before 135 ka and a phase shortly after 57 ka that favoured carbonate cementation of parts of the archaeological sequences at the site. Detailed investigations of a duricrust layer from the terrace sequence demonstrated their pedogenic origin as well as variability in the climate of north-western Africa since MIS 3. The earliest readily dateable evidence for occupation of the site extends to MIS 6 (~135 ka); the lower deposits, containing comparable stone tool assemblages, remain undateable. Tanged pieces first occur at Rhafas at ~123 ka and continue until ~57 ka, which is consistent with the chronological dataset of the Maghreb for the Aterian. Archaeological layers associated with the LSA are dated to ~21 ka and ~15 ka; although it is unclear whether the site was periodically or continuously occupied during this phase, the nearby site of Taforalt suggests that the latter is possible [2].

Supporting Information

S1 Fig. Parent-daughter equilibrium plots for Rhafas. (a) $^{238}U/^{226}Ra$ (b) $^{226}Ra/^{210}Pb$. In each figure the solid line represents secular equilibrium. Samples from the lower section, the cave mouth section and the slope section are shown as black dots, grey squares and open triangles

respectively. Dashed lines represent 20% and dotted lines 50% of equilibrium.
(TIF)

S2 Fig. Results of OSL standard performance tests. (a) Preheat plateau test (b) Dose-recovery preheat plateau test for samples L-EVA-1139 (grey diamonds) and L-EVA-1146 (black circles) are shown. The solid line indicates the target value; dashed lines represent 10% deviation from unity.
(TIF)

S3 Fig. Radial plots showing the dose distributions of single grain values of samples from the terrace section. (a) L-EVA-1145, (b) L-EVA-1146, (c) L-EVA-1213 and (d) L-EVA-1148. The shaded bands in the radial plots correspond to the standard error deviation from the calculated De.
(TIF)

S4 Fig. Radial plots showing the dose distributions of single grain values of samples from the cave mouth section. (a) L-EVA-1210 and (b) L-EVA-1141. The shaded bands in the radial plots correspond to the standard error deviation from the calculated D_e for each identified component.
(TIF)

S5 Fig. Grain-size distributions of the OSL samples per section. Each stacked bar shows the percentage distribution of the grain-size classes for one sample (in total 100%).
(TIF)

S6 Fig. Sedimentological characteristics of the terrace section.
(TIF)

S7 Fig. XRF results showing correlations between Ca and Mg, Al and Ca, Fe and Ca, and Ca and gS. Layer 1 (blue square) and 6d (red dot) plot relatively far away from their groups, which indicates that they do not share the same sedimentological characteristics with the other layers of the cave mouth and the lower cave section, respectively.
(TIF)

S8 Fig. Thin section photographs. (a) micritic cement with corroded lithoclasts: around one of the clasts there is evidence of the dissolution of some of the calcite cement and replacement by silica cement (arrow); (b) stringer within the silcrete-calcretes showing the chalcedony crystals in greater detail; (c) preservation of the form of a replaced calcite shell by silicification; (d) mammillary structured quartz crystals showing micro-laminated opal as well as fibrous lussatite and chalcedony. Photographs were taken under cross-polarised light.
(TIF)

S9 Fig. Single grain OSL ages for the cave mouth section at Rhafas determined by applying the FMM. Major and minor age components are shown in green and red, respectively
(TIF)

S10 Fig. Correlation between ^{40}K and clay content at Rhafas.
(TIF)

S11 Fig. LM-OSL curve for L-EVA-1083, showing dominant OSL fast component.
(TIF)

S1 File. MSA/MP nomenclature in the Maghreb.
(PDF)

S2 File. Sediment and bedrock analyses.
(PDF)

S3 File. Duricrust characteristics.
(PDF)

S1 Table. Measured moisture contents, beta dose rates and chosen preheat/cutheat temperatures.
(PDF)

S2 Table. Summary of faunal remains.
(PDF)

S3 Table. Single grain characteristics.
(PDF)

S4 Table. Single grain dose recovery properties.
(PDF)

S5 Table. Grain size results.
(PDF)

S6 Table. XRF results and $CaCO_3$ content.
(PDF)

S7 Table. Summary of istope data.
(PDF)

S8 Table. FMM details.
(PDF)

Acknowledgments

The authors would like to thank the members of the Department of Human Evolution, Max Planck Institute for Evolutionary Anthropology, and especially Vera Aldeias, Steffi Hesse and Stefanie Stelzer for their great support during field work, sample preparation and OSL measurements in the laboratory as well as during the writing process. Special thanks go to Detlev Degering (VKTA Dresden) for performing the γ-ray spectrometry measurements. We would also like to thank El Hassan Talbi and Lahbib Boudchiche for providing invaluable assistance in understanding the local geology of the site and all members of the excavation team in Morocco for their dedicated and active cooperation during fieldwork. We would like to thank Zenobia Jacobs and the other anonymous reviewers for their insightful comments which improved our paper. Access and permission to collect samples in Rhafas was granted by l'Institut National des Sciences de l'Archéologie et du Patrimoine, Rabat, Morocco.

Author Contributions

Conceptualization: ND KEF AB SPM JJH.

Formal analysis: ND SJM CZ TES.

Investigation: ND SPM AB TES CZ SJM PD.

Methodology: ND KEF SJM TES CZ.

Project administration: ND.

Resources: CZ SJM AB JJH.

Supervision: KEF SPM JJH.

Validation: ND KEF CZ SJM TES.

Visualization: ND.

Writing – original draft: ND.

Writing – review & editing: KEF SJM PD AB SPM CZ TES.

References

1. Garcea EAA. Successes and failures of human dispersals from North Africa. Quaternary International. 2012; 270:119–28. doi: http://dx.doi.org/10.1016/j.quaint.2011.06.034.
2. Barton RNE, Bouzouggar A, Hogue JT, Lee S, Collcutt SN, Ditchfield P. Origins of the Iberomaurusian in NW Africa: New AMS radiocarbon dating of the Middle and Later Stone Age deposits at Taforalt Cave, Morocco. Journal of Human Evolution. 2013; 65(3):266–81. doi: http://dx.doi.org/10.1016/j.jhevol.2013.06.003. doi: 10.1016/j.jhevol.2013.06.003 PMID: 23891007
3. Dibble HL, Aldeias V, Alvarez-Fernández E, Blackwell BAB, Hallett-Desguez E, Jacobs Z, et al. New Excavations at the Site of Contrebandiers Cave, Morocco. Paleoanthropology. 2012:145–201.
4. McBrearty S, Brooks AS. The revolution that wasn't: a new interpretation of the origin of modern human behavior. Journal of Human Evolution. 2000; 39(5):453–563. doi: http://dx.doi.org/10.1006/jhev.2000.0435. PMID: 11102266
5. d'Errico F, Vanhaeren M, Barton N, Bouzouggar A, Mienis H, Richter D, et al. Additional evidence on the use of personal ornaments in the Middle Paleolithic of North Africa. Proceedings of the National Academy of Sciences. 2009; 106(38):16051–6.
6. Bouzouggar A, Barton N, Vanhaeren M, d'Errico F, Collcutt S, Higham T, et al. 82,000-Year-Old Shell Beads from North Africa and Implications for the Origins of Modern Human Behavior. Proceedings of the National Academy of Sciences of the United States of America. 2007; 104(24):9964–9. PMID: 17548808
7. Vanhaeren M, d'Errico F, Stringer C, James SL, Todd JA, Mienis HK. Middle Paleolithic Shell Beads in Israel and Algeria. Science. 2006; 312(5781):1785–8. PMID: 16794076
8. Bouzouggar A, Barton N. The identity and the timing of the Aterian in Morocco. In: Hublin J-J, McPherron SP, editors. Modern Origins: A North African Perspective New York: Springer; 2012. p. 93–105.
9. Dibble HL, Aldeias V, Jacobs Z, Olszewski DI, Rezek Z, Lin SC, et al. On the industrial attributions of the Aterian and Mousterian of the Maghreb. Journal of Human Evolution. 2013; 64(3):194–210. doi: http://dx.doi.org/10.1016/j.jhevol.2012.10.010. doi: 10.1016/j.jhevol.2012.10.010 PMID: 23399349
10. Richter D, Moser J, Nami M, Eiwanger J, Mikdad A. New chronometric data from Ifri n'Ammar (Morocco) and the chronostratigraphy of the Middle Palaeolithic in the Western Maghreb. Journal of Human Evolution. 2010; 59:672–9. doi: 10.1016/j.jhevol.2010.07.024 PMID: 20880568
11. Debénath A. Hommes et cultures matérielles de l'Atérien marocain. Anthropologie. 1992; 96:711–9.
12. Richter D, Moser J, Nami M. New data from the site of Infri n'Ammar (Morocco) and some remarks on the cronometric status of the Middle Paleolithic in the Maghreb. In: Hublin J-J, McPherron SP, editors. Modern Origins: A North African Perspective. New York: Springer; 2012. p. 61–78.
13. Barton RNE, Bouzouggar A, Collcutt SN, Schwenninger J- L, Clark-Balzan L. OSL dating of the Aterian levels at Dar es-Soltan I (Rabat, Morocco) and implications for the dispersal of modern Homo sapiens. Quaternary Science Reviews. 2009; 28:1914–31.
14. Schwenninger JL, Collcutt SN, Barton N, Bouzouggar A, Clark-Balzan L, El Hajraoui MA, et al. A new luminescence chronology for Aterian cave sites on the Atlantic coast of Morocco. In: Garcea EAA, editor. South-Eastern Mediterranean Peoples between 130,000 and 10,000 years ago. Oxford: Oxbow Books; 2010. p. 18–36.
15. Clark-Balzan LA, Candy I, Schwenninger J-L, Bouzouggar A, Blockley S, Nathan R, et al. Coupled U-series and OSL dating of a Late Pleistocene cave sediment sequence, Morocco, North Africa: Significance for constructing Palaeolithic chronologies. Quaternary Geochronology. 2012; 12(0):53–64. doi: http://dx.doi.org/10.1016/j.quageo.2012.06.006.
16. Jacobs Z, Meyer MC, Roberts RG, Aldeias V, Dibble H, El Hajraoui MA. Single-grain OSL dating at La Grotte des Contrebandiers ('Smugglers' Cave'), Morocco: improved age constraints for the Middle Paleolithic levels. Journal of Archaeological Science. 2011; 38(12):3631–43.

17. Jacobs Z, Roberts RG, Nespoulet R, El Hajraoui MA, Debénath A. Single-grain OSL chronologies for Middle Palaeolithic deposits at El Mnasra and El Harhoura 2, Morocco: Implications for Late Pleistocene humaneenvironment interactions along the Atlantic coast of northwest Africa. Journal of Human Evolution. 2012; 62:377–94. doi: 10.1016/j.jhevol.2011.12.001 PMID: 22245146

18. Iovita R. Shape Variation in Aterian Tanged Tools and the Origins of Projectile Technology: A Morphometric Perspective on Stone Tool Function. PLoS ONE. 2011; 6(12):e29029. doi: 10.1371/journal.pone.0029029 PMID: 22216161

19. Garcea EAA. The Lower and Upper Later Stone Age of North Africa. In: Garcea EAA, editor. South-Eastern Mediterranean Peoples Between 130,000 and 10,000 Years Ago. Oxford: Oxbow Books; 2010. p. 54–65.

20. Barton RNE, Bouzouggar A, Collcutt SN, Carrion MY, Clark-Balzan L, Debenham N, et al. Reconsidering the MSA to LSA transition at Taforalt Cave (Morocco) in the light of new multi-proxy dating evidence. Quaternary International. 2015:in press.

21. McBurney CMB. The Haua Fteah (Cyrenaica) and the Stone Age in the South-East Mediterranean. Cambridge: Cambridge Unitversity Press; 1967.

22. Ambrose SH. Chronology of the Later Stone Age and Food Production in East Africa. Journal of Archaeological Science. 1998; 25(4):377–92. doi: http://dx.doi.org/10.1006/jasc.1997.0277.

23. Villa P, Soriano S, Tsanova T, Degano I, Higham TFG, d'Errico F, et al. Border Cave and the beginning of the Later Stone Age in South Africa. Proceedings of the National Academy of Sciences. 2012; 109(33):13208–13.

24. Braham L, Mitchell P. The First Africans: African archaeology from the earliest toolmakers to most recent foragers. Cambridge: Cambridge University Press; 2008. 601 p.

25. Humphrey L, Bello SM, Turner E, Bouzouggar A, Barton N. Iberomaurusian funerary behaviour: Evidence from Grotte des Pigeons, Taforalt, Morocco. Journal of Human Evolution. 2012; 62:261–73. doi: 10.1016/j.jhevol.2011.11.003 PMID: 22154088

26. Mercier N, Wengler L, Valladas H, Joron J-L, Froget L, Reyss JL. The Rhafas Cave (Morocco): Chronology of the mousterian and aterian archaeological occupations and their implications for Quaternary geochronology based on luminescence (TL/OSL) age determinations. Quaternary Geochronology. 2007; 2:309–13.

27. Aitken MJ. An Introduction to Optical Dating. Oxford Oxford University Press; 1998.

28. Texier J-P, Huxtable J, Rhodes E, Miallier D, Ousmoi M. Nouvelles données sur la situation chronologique de l'Atérien du Maroc et leurs implications. Comptes Rendus de l'Académie des Sciences de Paris1988. p. 827–32.

29. Murray AS, Wintle AG. Luminescence dating of quartz using an improved single-aliquot regenerative-dose protocol. Radiation Measurements. 2000; 32(1):57–73. doi: http://dx.doi.org/10.1016/S1350-4487(99)00253-X.

30. Duller GAT, Bøtter-Jensen L, Murray AS, Truscott AJ. Single grain laser luminescence (SGLL) measurements using a novel automated reader. Nuclear Instruments and Methods in Physics Research BNuclear Instruments and Methods in Physics Research B. 1999; 155:506–14.

31. Ramos J, Bernal M, Domínguez-Bella S, Calado D, Ruiz B, Gil MJ, et al. The Benzu´ rockshelter: a Middle Palaeolithic site on the North African coast. Quaternary Science Reviews. 2008; 27:2230–8.

32. Rhodes EJ, Singarayer JS, Raynal J-P, Westaway KE, Sbihi-Alaoui FZ. New age estimates for the Palaeolithic assemblages and Pleistocene succession of Casablanca, Morocco. Quaternary Science Reviews. 2006; 25:2569–85.

33. Ramos Muñoz J, Bernal Casasola D, domínguez-Bella S, Calado D, Ruiz Zapata MB, Gil Garcia MJ, et al. El abrigo de Benzú (Ceuta)frecuentaciones humanas de un yacimiento con tecnología de modo 3 en el norte de África—The shelter of Benzú (Ceuta). Human occupations of a settlement with mode 3 technology in north Africa. Zephyrus, Revista de Prehistoria y Arqueología. 2007; 60:27–41.

34. Barton RNE, Bouzouggar A, Collcutt SN, Gale R, Higham TFG, Humphrey LT, et al. The Late Upper Palaeolithic Occupation of the Moroccan Northwest Maghreb during the Last Glacial Maximum. African Archaeological Review. 2005; 22(2):77–100.

35. Wallinga J. Optically stimulated luminescence dating of fluvial deposits: a review. Boreas. 2002; 31 (4):303–22.

36. Roberts RG, Galbraith RF, Olley JM, Yoshida H, Laslett GM. Optical dating of single and multiple grains of quartz from Jinmium rock shelter, northern Australia: part II, results and implications. Archaeometry. 1999; 41(2):365–95. doi: 10.1111/j.1475-4754.1999.tb00988.x

37. Jacobs Z, Wintle AG, Roberts RG, Duller GAT. Equivalent dose distributions from single grains of quartz at Sibudu, South Africa: context, causes and consequences for optical dating of archaeological deposits. Journal of Archaeological Science. 2008; 35:1808–20.

38. Lombard M, Wadley L, Jacobs Z, Mohapi M, Roberts RG. Still Bay and serrated points from Umhlatuzana Rock Shelter, Kwazulu-Natal, South Africa. Journal of Archaeological Science. 2010; 37:1773–84.

39. Jacobs Z, Roberts RG. Advances in Optically Stimulated Luminescence Dating of Individual Grains of Quartz from Archeological Deposits. Evolutionary Anthropology. 2007; 16:210–23.

40. Talbi EH, Boudchiche L. Report about the geology of the Rhafas zone. Oujda: Université Mohammed Premier, Oujda, 2012.

41. Roche J. L'Epipaléolithique Marocain. Lisbon: Fondation Calouste Gulbenkian; 1963.

42. Wengler L. Cultures préhistoriques et formations quaternaires au Maroc oriental. Relations entre comportements et paléoenvironments au Paléolithique moyen: Université de Bordeaux I; 1993.

43. Wengler L. La transition du Moustérien à l'Atérien. L'Anthropologie. 1997; 101(3):448–81.

44. Olley JM, Murray A, Roberts RG. The effects of disequilibria in the uranium and thorium decay chains on burial dose rates in fluvial sediments. Quaternary Science Reviews. 1996; 15(7):751–60. doi: http://dx.doi.org/10.1016/0277-3791(96)00026-1.

45. Olley JM, Roberts RG, Murray AS. Disequilibria in the uranium decay series in sedimentary deposits at Allen's cave, nullarbor plain, Australia: Implications for dose rate determinations. Radiation Measurements. 1997; 27(2):433–43. doi: http://dx.doi.org/10.1016/S1350-4487(96)00114-X.

46. Guérin G, Mercier N, Adamiec G. Dose-rate conversion factors: update. Ancient TL. 2011; 29:5–8.

47. Bøtter-Jensen L, Mejdahl V. Determination of potassium in feldspars by beta counting using a GM multicounter system. Nuclear Tracks and Radiation Measurements (1982). 1985; 10(4–6):663–6. doi: http://dx.doi.org/10.1016/0735-245X(85)90073-0.

48. Bøtter-Jensen L, Mejdahl V. Assessment of beta dose-rate using a GM Multicounter system. Radiation Measurements. 1988; 14(1/2):187–91.

49. Mejdahl V. Thermoluminescence dating: beta-dose attenuation in quartz grains. Archaeometry. 1979; 21(1):61–72. doi: 10.1111/j.1475-4754.1979.tb00241.x

50. Prescott JR, Hutton JT. Cosmic ray contributions to dose rates for luminescence and ESR dating: Large depths and long-term time variations. Radiation Measurements. 1994; 23(2–3):497–500. doi: http://dx.doi.org/10.1016/1350-4487(94)90086-8.

51. Bøtter-Jensen L, Bulur E, Duller GAT, Murray AS. Advances in luminescence instrument systems. Radiation Measurements. 2000; 32(5–6):523–8. doi: http://dx.doi.org/10.1016/S1350-4487(00)00039-1.

52. Bøtter-Jensen L. Luminescence techniques: instrumentation and methods. Radiation Measurements. 1997; 27(5–6):749–68. doi: http://dx.doi.org/10.1016/S1350-4487(97)00206-0.

53. Murray AS, Wintle AG. The single aliquot regenerative dose protocol: potential for improvements in reliability. Radiation Measurements. 2003; 37(4–5):377–81. doi: http://dx.doi.org/10.1016/S1350-4487(03)00053-2.

54. Duller GAT. Distinguishing quartz and feldspar in single grain luminescence measurements. Radiation Measurements. 2003; 37:161–5.

55. Wintle AG, Murray AS. A review of quartz optically stimulated luminescence characteristics and their relevance in single-aliquot regeneration dating protocols. Radiation Measurements. 2006; 41:369–91.

56. Ballarini M, Wallinga J, Wintle AG, Bos AJJ. A modified SAR protocol for optical dating of individual grains from young quartz samples. Radiation Measurements. 2007; 42(3):360–9. doi: http://dx.doi.org/10.1016/j.radmeas.2006.12.016.

57. Cunningham AC, Wallinga J. Optically stimulated luminescence dating of young quartz using the fast component. Radiation Measurements. 2009; 44(5–6):423–8. doi: http://dx.doi.org/10.1016/j.radmeas.2009.02.014.

58. Jacobs Z, Duller GAT, Wintle AG. Interpretation of single grainDe distributions and calculation of D_e. Radiation Measurements. 2006; 41:264–77.

59. Rodnight H. How many equivalent dose values are needed to obtain a reproducible distribution? Ancient TL. 2008; 26(1):3–9.

60. Wengler L, Wengler B, Bouzouggar A, El Azzouzi M, Bernoussi R, Elie Brochier J, et al., editors. Paléolithique moyen et Néolithique de l'Oriental marocain2006 2006: Archaeopress.

61. Michel P. Pour une meilleure connaissance du Quaternaire Continental Marocain: les vertébrés fossiles du Maroc Atlantique, Central et Oriental. L'Anthropologie. 1992; 96:643–56.

62. McLaren S, Nash DJ. Geochemical Sediments and Landscapes: general summary. In: Nash DJ, McLaren S, editors. Geochemical Sediments and Landscapes. Oxford: Blackwell; 2007. p. 443–7.

63. Grubbs FE. Sample Criteria for Testing Outlying Observations. 1950:27–58. doi: 10.1214/aoms/1177729885

64. Galbraith RF, Roberts RG, Laslett GM, Yoshida H, Olley JM. Optical dating of single and multiple grains of quartz from Jinmium rock shelter, northern Australia: Part I, experimental design and statistical models. Archaeometry. 1999; 41(2):339–64. doi: 10.1111/j.1475-4754.1999.tb00987.x

65. Roberts RG, Galbraith RF, Yoshida H, Laslett GM, Olley JM. Distinguishing dose populations in sediment mixtures: a test of single-grain optical dating procedures using mixtures of laboratory-dosed quartz. Radiation Measurements. 2000; 32(5–6):459–65. doi: http://dx.doi.org/10.1016/S1350-4487(00)00104-9.

66. Galbraith RF. Statistics for Fission Track Analysis. London: Chapman & Hall; 2005.

67. Brookins DG. Eh-pH diagrams for geochemistry. New York: Springer; 1988.

68. Castañeda IS, Mulitza S, Schefuß E, Lopes dos Santos RA, Sinninghe Damsté JS, Schouten S. Wet phases in the Sahara/Sahel region and human migration patterns in North Africa. Proceedings of the National Academy of Sciences. 2009; 106(48):20159–63.

69. Moreno A. A Multiproxy Palaeoclimate Reconstruction over the Last 250 kyr from Marine Sediments: The Northwest African Margin and the Western Mediterranean Sea. In: Hublin J-J, McPherron SP, editors. Modern Origins. New York: Springer; 2012. p. 3–17.

70. Whiting Blome M, S. Cohen A, Tryon CA, Brooks AS, Russell J. The environmental context for the origins of modern human diversity: A synthesis of regional variability in African climate 150,000–30,000 years ago. Journal of Human Evolution. 2012; 62:563–92. doi: 10.1016/j.jhevol.2012.01.011 PMID: 22513381

71. Smith JR. Palaeoenvironments of Eastern North Africa and the Levant in the Late Pleistocene. In: Garcea EAA, editor. South-Eastern Mediterranean Peoples Between 130,000 and 10,000 Years Oxford: Oxford Books; 2010. p. 6–17.

72. Larrosaña JC. Saharan Climate and Modern Human Origins. In: Hublin J-J, McPherron SP, editors. Modern Origins. New York: Springer; 2012. p. 19–34.

73. Moreno A, Cacho I, Canals M, Prins MA, Sánchez-Goñi M, amp, et al. Saharan Dust Transport and High-Latitude Glacial Climatic Variability: The Alboran Sea Record. Quaternary Research. 2002; 58 (3):318–28. doi: http://dx.doi.org/10.1006/qres.2002.2383.

74. Trauth MH, Larrasoaña JC, Mudelsee M. Trends, rhythms and events in Plio-Pleistocene African climate. Quaternary Science Reviews. 2009; 28(5–6):399–411. doi: http://dx.doi.org/10.1016/j.quascirev.2008.11.003.

75. Kowalski K, Neer Wv, Bocheński Z, Młynarski M, Rzebik-Kowalska B, Szyndlar Z, et al. A last interglacial fauna from the Eastern Sahara. Quaternary Research. 1989; 32(3):335–41. doi: http://dx.doi.org/10.1016/0033-5894(89)90099-9.

76. Wendorf F, Schild R, Close A. Egypt During the Last Interglacial. The Middle Paleolithic of Bir Tarfawi and Bir Sahara East. New York: Springer; 1993.

77. Garcea EAA. The Spread of Aterian Peoples in North Africa. In: Garcea EAA, editor. South-Eastern Mediterranean Peoples Between 130,000 and 10,000 Years Ago. Oxford: Oxbow Books; 2010. p. 37–53.

78. Smith JR. Spatial and Temporal Variation in the Nature of Pleistocene Pluvial Phase Environments Across North Africa. In: Hublin J-J, McPherron SP, editors. Modern Origins A North Afrian Perspective. New York: Springer; 2012. p. 35–47.

79. Wengler L, Weisrock A, Borchier J-E, Brugal J-P, Fontugne M, Magnin F. Enregistrement fluviatile et paleoenvironnements au Pleistocene superieur sur la bordure atlantique de l'Anti-Atlas (Oued Assaka, S-O marocain). Quaternaire. 2002; 13:179–92.

80. Giraudi C. Geology and the Palaeoenvironment. In: Barich BE, Garcea EAA, Giraudi C, Lucarini G, Mutri G, editors. The latest research in the Jebel Gharbi (Northern Libya): environment and Cultures from MSA to LSA and the First Neolithic Findings: Libya Antiqua, n.s.; 2010. p. 237–40.

81. Adamson K, Candy I, Whitfield L. Coupled micromorphological and stable isotope analysis of Quaternary calcrete development. Quaternary Research. 2015; 84(2):272–86. doi: http://dx.doi.org/10.1016/j.yqres.2015.05.002.

82. Prentice IC, Guiot J, Harrison SP. Mediterranean vegetation, lake levels and palaeoclimate at the Last Glacial Maximum. Nature. 1992; 360(6405):658–60.

83. Smith TM, Tafforeau P, Reid DJ, Grün R, Eggins S, Boutakiout M, et al. Earliest evidence of modern human life history in North Africa early *Homo sapiens*. PNAS. 2007; 104(15):6128–33. PMID: 17372199

84. Occhietti S, Raynal J-P, Pichet P, Texier J-P. Aminostratigraphie du dernier cycle climatique au Maroc atlantique, de Casablanca à Tanger. Comptes Rendus de l'Académie des Sciences de Paris1993. p. 1625–32.

85. Debénath A, Raynal J-P, Roche J, Texier JP, Ferembach D. Stratigraphie, habitat, typologie et devenir de l'Atérien marocain: données récentes. L'Anthropologie. 1986; 90(2):233–46.

86. Wrinn PJ, Rink WJ. ESR Dating of Tooth Enamel From Aterian Levels at Mugharet el 'Aliya (Tangier, Morocco). Journal of Archaeological Science. 2003; 30:123–33.

87. Moser J. La Grotte d'Ifri n'Ammar; Tome 1: L'Iberomaurusian. Aichwald: Lindensoft Verlag, 2003.

88. Bouzouggar A, Barton RNE, Blockley S, Bronk-Ramsey C, Collcutt SN, Gale R, et al. Reevaluating the Age of the Iberomaurusian in Morocco. African Archaeological Review. 2008; 25(1–2):3–19. doi: 10.1007/s10437-008-9023-3

89. Betrouni M. Le paléokarst de Sidi Said (Tipasa, Algérie) et la question du Paléolithique supérieur maghrébin. In: Fiullola JM, Soler N, editors. El món mediterrani despés del Pleniglacial (18000–12000 BP). Sèrie Monogràfica 17. Girona: Museu d'Arqueologia de Catalunya; 1997. p. 57–68.

90. Betrouni M. Le paleokarst de Sidi Said. Aspects chronoculturels In: CNRPAH, editor. L'homme maghrébin et son environnement depuis 100 000 ans. Alger: Centre national de recherches préhistoriques, anthropologiques et historiques; 2001. p. 101–12.

91. Saxon EC, Close A, Cluzel C, Morse V, Shackleton NJ. Results of recent investigations at Tamar Hat. Libyca. 1974; 22:49–91.

92. Roset J-P, Harbi-Riahi M. El Akarit: Un site archéologique du Paléolithique moyen dans le sud de la Tunisie. Paris, Editions Recherche sur les Civilisations2007.

93. Barich B, Garcea EA. Ecological Patterns in the Upper Pleistocene and Holocene in the Jebel Gharbi, Northern Libya: Chronology, Climate and Human Occupation. African Archaeological Review. 2008; 25(1–2):87–97. doi: 10.1007/s10437-008-9020-6

94. Garcea EAA, Giraudi C. Late Quaternary human settlement patterning in the Jebel Gharbi. Journal of Human Evolution. 2006; 51(4):411–21. doi: http://dx.doi.org/10.1016/j.jhevol.2006.05.002. PMID: 16911818

95. Garcea EAA. Modern Human Desert Adaptations: A Libyan Perspective on the Aterian Complex. In: Hublin J-J, McPherron SP, editors. Modern Origins A North African Perspective. New York: Springer; 2012. p. 127–42.

96. Garcea EAA. Aterian and "Early" and "Late Acacus" from the Uan Tabu rockshelter, Tadrart Acacus (Libyan Sahara). In: Cremaschi M, Di Lernia S, editors. Wadi Teshuinat—Palaeoenvironment and Prehistory in south-western Fezzan (Libyan Sahara). Firenze: All'Insegna del Giglio; 1998. p. 155–82.

97. Garcea EAA. The long sequence at Uan Tabu (Libyan Sahara): Aterian and Holocene deposit. In: Aumassip G, Clark JD, Mori F, editors. The prehistory of Africa, XIII Congress, UISPP, Colloquium XXX. 15. Forli1996. p. 183–93.

98. Martini M, Sibilia E, Zelaschi C, Troja SO, Forzese R, Gueli AM, et al. TL and OSL dating of fossil dune sand in the Uan Afuda and Uan Tabu rockshelters, Tadrart Acacus (Libyan Sahara). In: Cremaschi M, Di Lernia S, editors. Wadi Teshuinat—Palaeoenvironment and Prehistory in south-western Fezzan (Libyan Sahara). Firenze: All'Insegna del Giglio; 1998. p. 67–72.

99. Di Lernia S. Early Holocene pre-pastoral cultures in the Uan Afuda cave, Wadi Kessan, Tadrart Acacus (Libyan Sahara). In: Cremaschi M, Di Lernia S, editors. Wadi Teshuinat—Palaeoenvironment and Prehistory in south-western Fezzan (Libyan Sahara). Firenze: All'Insegna del Giglio 1998. p. 123–54.

100. Stoetzel E, Marion L, Nespoulet R, El Hajraoui MA, Denys C. Taphonomy and palaeoecology of the late Pleistocene to middle Holocene small mammal succession of El Harhoura 2 cave (Rabat-Témara, Morocco). Journal of Human Evolution. 2011; 60(1):1–33. doi: http://dx.doi.org/10.1016/j.jhevol.2010.07.016. doi: 10.1016/j.jhevol.2010.07.016 PMID: 21035833

101. Stoetzel E, Campmas E, Michel P, Bougariane B, Ouchaou B, Amani F, et al. Context of modern human occupations in North Africa: Contribution of the Témara caves data. Quaternary International. 2014; 320:143–61. doi: http://dx.doi.org/10.1016/j.quaint.2013.05.017.

102. Tjallingii R, Claussen M, Stuut J-BW, Fohlmeister J, Jahn A, Bickert T, et al. Coherent high- and low-latitude control of the northwest African hydrological balance. Nature Geoscience. 2008; 1:670–5.

103. Barton RNE, Bouzouggar A, Bronk Ramsey C, Collcutt S, Higham TFG, Humphrey LT, et al. Abrupt climatic change and chronology of the Upper Palaeolithic in northern and eastern Morocco. In: Mellars P, Boyle K, Bar-Yosef O, Stringer C, editors. Rethinking the human revolution: New behavioural and biological perspectives on the origins and dispersal of modern humans. Cambridge: Research Monographs of the Macdonald Institute; 2007. p. 177–86.

104. Linstädter J. The Epipalaeolithic-Neolithic-Transition in the Mediterranean region of Northwest Africa Quartär. 2008; 55:41–62.

105. Hogue JT, Barton N. New radiocarbon dates for the earliest Later Stone Age microlithic technology in Northwest Africa. Quaternary International.in press.

106. Douka K, Jacobs Z, Lane C, Grün R, Farr L, Hunt C, et al. The chronostratigraphy of the Haua Fteah cave (Cyrenaica, northeast Libya). Journal of Human Evolution. 2014; 66:39–63. doi: http://dx.doi.org/10.1016/j.jhevol.2013.10.001. doi: 10.1016/j.jhevol.2013.10.001 PMID: 24331954

107. Camps G. Les Civilisations préhistoriques de l'Afrique du Nord et du Sahara. Paris, Doin1974. 374 p.

108. Sari L. Technological change in Iberomaurusian culture: The case of Tamar Hat, Rassel and Columnata lithic assemblages (Algeria). Quaternary International. 2014; 320:131–42. doi: http://dx.doi.org/10.1016/j.quaint.2013.04.014.

109. Hogue JT. The origin and development of the Pleistocene LSA in Northwest Africa: A case study from Grotte des Pigeons (Taforalt), Morocco [unpublished PhD dissertation]: University of Oxford; 2014.

3. OSL dating of the Middle Pleistocene archaeological sites Thomas Quarry I and Rhino Cave, Morocco

Challenges and constraints for single-grain dating when using old quartz samples close to the upper OSL dating limit.

Unpublished case study.

Project members:

Nina Dörschner (MPI for Evolutionary Anthropology, Leipzig, Germany)
Kathryn E. Fitzsimmons (MPI for Chemistry, Mainz, Germany)
Jean-Jacques Hublin (MPI for Evolutionary Anthropology, Leipzig, Germany)
Abderrahim Mohib (INSAP, Rabat, Morocco)
Jean-Paul Raynal (Université Bordeaux, France)

3.1. Introduction

Although recent scientific debates on the origin of the first human populations colonising the European continent in the Early Pleistocene favour the Out of Asia hypothesis (Carbonell et al., 2005; 2008; Parés et al., 2006) and revealed that Africa most likely played a less important role than previously thought (Aguirre and Carbonell, 2001; Bar-Yosef and Belfer-Cohen, 2001), Morocco still occupies a strategic position in north-western Africa and is a key-region for examining potential ancient water crossings of the Strait of Gibraltar by past human populations and for studying the Acheulan far from its origins in eastern Africa (Raynal et al., 2010). Furthermore, Morocco yields an exceptional record of Pleistocene fossil hominins discovered at the sites of e.g. Jebel Irhoud, Salé and Thomas Quarry I (Hublin, 2001).

The Quaternary deposits around Casablanca, western Morocco (Fig. 3.1.1a), consist of a series of large barrier systems parallel to the present shoreline (Fig. 3.1.1b) and yield a rich archaeological record, including Middle Pleistocene human fossils (Daujeard et al., 2016; Ennouchi, 1969; Raynal et al., 2010). Stepped from 180 m above sea-level to the present shoreline, the Casablanca sequence is formed by successive cycles of deposition, each represented by an underlying marine unit covered by aeolian sediments (Texier et al., 2002; 1994). The sediments consist mostly of marine and aeolian calcarenites, strongly cemented by secondary carbonates (Texier et al., 2002). Erosional processes favoured the formation of small caves, which were later filled by aeolian sands and mud-flow deposits (Rhodes et al., 2006). The complete succession provides an exceptional record of past global sea-level fluctuations since the final Miocene and for the prevailing palaeoenvironmental conditions in the area at those times (Raynal et al., 1999).

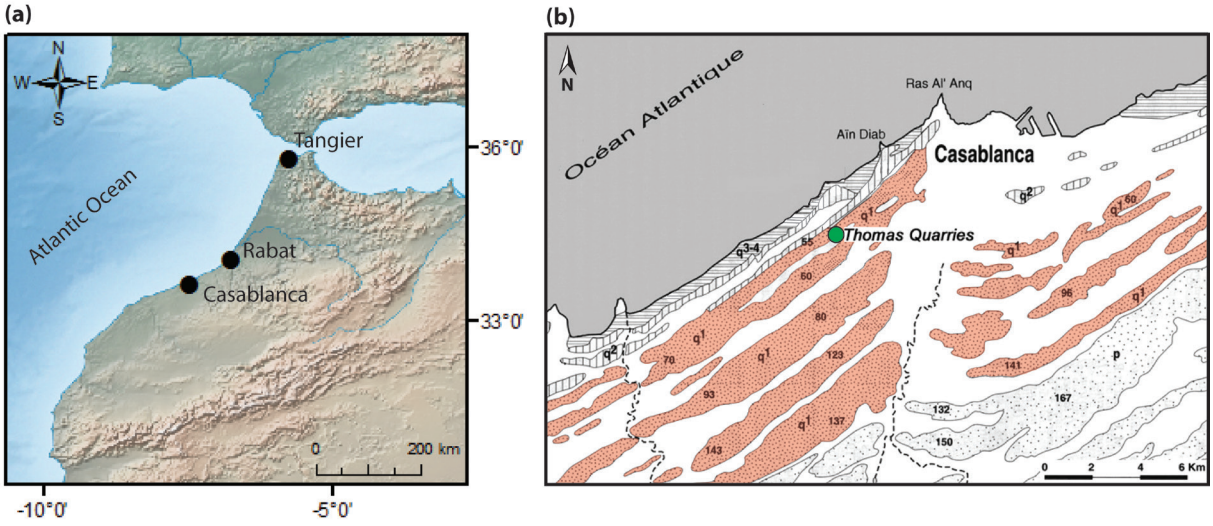

Figure 3.1.1 Location map of (a) Casablanca in western Morocco and (b) Plio-Pleistocene formations of the Casablanca area (q^{3-4} Upper Pleistocene and Holocene; q^2 Middle Pleistocene; q^1 Early Pleistocene; p Pliocene) modified after Raynal et al. (2010). Highlighted in light red are the Early Pleistocene morpho-stratigraphic units and as green dot the location of the Thomas Quarries (Thomas I, Thomas III and Oulad Hamida I Quarries).

The archaeological sites of Thomas Quarry I and Oulad Hamida I are both located within the Oulad Hamida morpho-stratigraphic unit (Fig. 3.1.1b), which consists of several marine-aeolian sedimentation cycles dated to the final Early and early Middle Pleistocene and contains the first evidence for human activity in the area (Raynal et al., 2001). Both quarries were part of the joint Moroccan-French research program 'Casablanca' which was started in 1978 and experienced intensive and still ongoing geological and archaeological investigations since then.

The site of Thomas Quarry I (Fig. 3.1.2a) – and especially the Hominid Cave therein – is famous for

containing hominin fossil remains. A human half-mandible was discovered in 1969 (Ennouchi, 1969, 1970) and assigned to *Homo rhodesiensis* (Hublin, 2001). Between 1994 and 2002 several isolated teeth and other hominin fossils were recovered from the Hominid Cave, Unit 4 (Fig. 3.1.2c), which also contains an Acheulian lithic assemblage and faunal remains (Daujeard et al., 2016; Raynal et al., 2010).

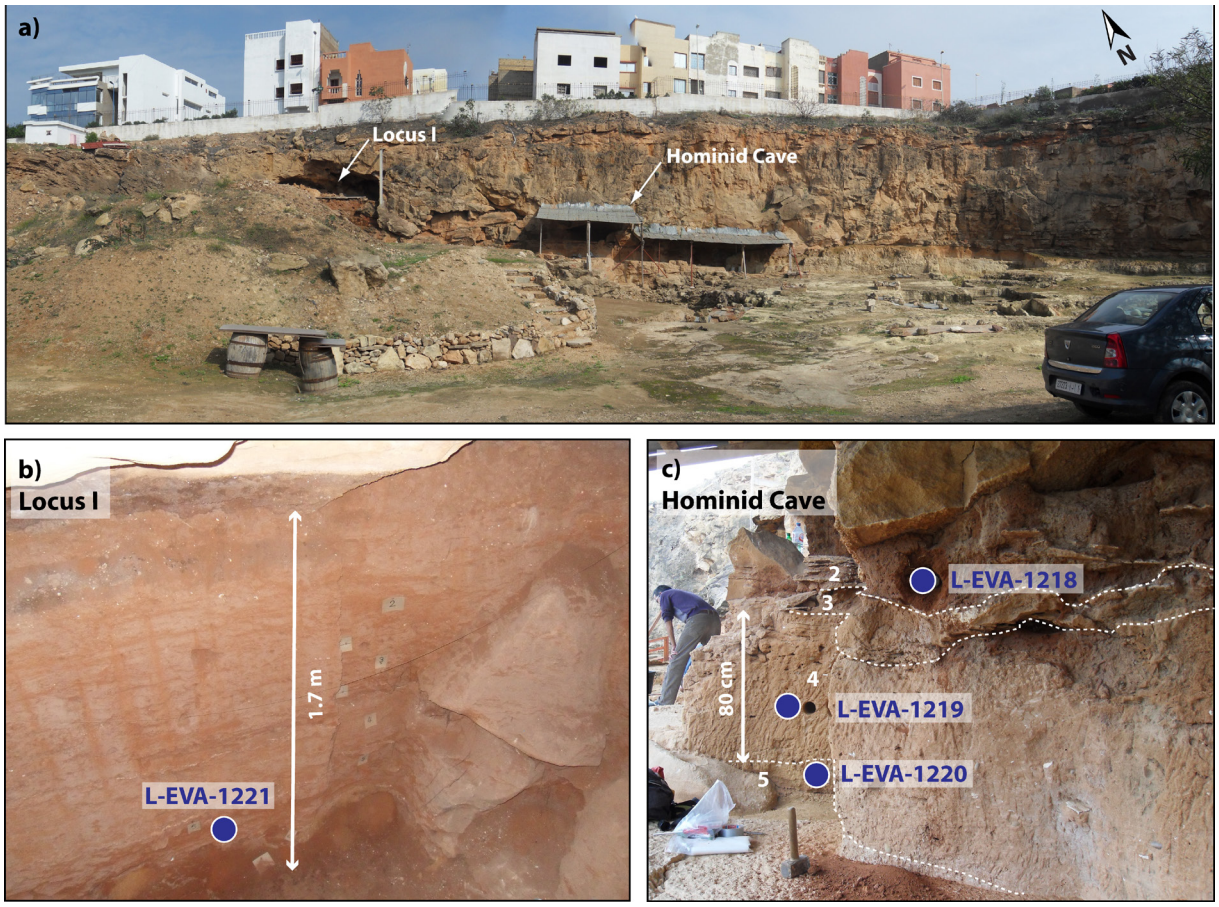

Figure 3.1.2 (a) The Thomas Quarry I site with the location of (b) Locus I and (c) the Hominid Cave. Collected OSL samples are indicated as blue dots.

Table 3.1.1 Previous chronological work at the Thomas Quarry I site (ages are shown in stratigraphic order).

Sample	Unit[a]	Dating method[b]	D_e (Gy)	Dose rate (Gy/ka)	Age (ka)	Reference
TQG	G	SAR OSL	327±83	0.86±0.05	382±100	(Rhodes et al., 2006)
		SAAD-SC OSL	377±24		440±38	(Rhodes et al., 2006)
TQN	N	SAR OSL	188±27	0.51±0.03	370±58	(Rhodes et al., 2006)
		SAR-CR OSL	209±12		412±35	(Rhodes et al., 2006)
TQC	C	SAR OSL	253±54	0.57±0.06	444±105	(Rhodes et al., 2006)
TQ-U1	-	U-series	-	-	409±88	(Rhodes et al., 2006)
Sediment	GH-4	OSL	n/a	n/a	420±34	(Raynal et al., 2010)
Enamel	GH-4	ICP-MS	-	-	501^{+94}_{-76}	(Raynal et al., 2010)
Sediment	GH-4	OSL	n/a	n/a	391±32	(Raynal et al., 2010)
TQQ	Q	SAR OSL	195±29	0.52±0.04	373±62	(Rhodes et al., 2006)
TQA	A	SAR OSL	288±59	0.80±0.04	359±76	(Rhodes et al., 2006)
TQL	L	SAR OSL	726±147	0.73±0.04	989±208	(Rhodes et al., 2006)
		SAR-CR OSL	696±438		948±599	(Rhodes et al., 2006)

[a] Abbreviation: GH - Hominid Cave.
[b] OSL protocol abbreviations: SAR – single-aliquot regenerative-dose; SAAD-SC – single-aliquot additive-dose slow component; SAR-CR - component-resolved SAR.

Previous dating studies at Thomas Quarry I used different methods to determine the age of the cave deposits and the archaeological finds therein (Table 3.1.1). The oldest dates for the site come from Unit L – which contains the most ancient lithics (Acheulian) known so far in the area - and revealed two depositional ages of 948 ± 599 ka and 989 ± 208 ka using OSL (Rhodes et al., 2006). The upper Units (N, G, C, Q and A) of the quarry are dated with OSL to between 359 ± 76 ka and 444 ± 105 ka (Rhodes et al., 2006) and are systematically younger than expected based on stratigraphical and lithological interpretations (Texier et al., 2002). H. Schwarcz determined a U-series date of 409 ± 88 ka for a speleothem capping the deposits within which the half-mandible was discovered (Rhodes et al., 2006). Ages for the Hominid Cave are up until now limited to one laser ablation ICP-MS date of a human premolar and two OSL samples from the embedding sediments of Unit 4 (Raynal et al., 2010). A combination of U-series and ESR yielded an age for the premolar of 501^{+94}_{-76} ka. The sediments revealed, although stratigraphically inverted, statistically identical ages of 420 ± 34 ka and 391 ± 32 ka (Table 3.1.1). The authors of this study, however, note that despite the absolute age estimates, bio- and lithostratigraphical evidence still point towards an even greater antiquity - much closer towards the Early Pleistocene - of Unit 4 (Raynal et al., 2010).

The Rhino Cave (Grotte des Rhinocéros; Fig. 3.1.3b) is located in the Oulad Hamida I Quarry in close proximity to Thomas Quarry I. The stratigraphical units at the cave comprise a Middle Pleistocene sequence with Acheulian artefacts and the richest faunal assemblage known for this period in North Africa (Daujeard et al., 2012; Geraads, 1993, 1994; Raynal et al., 1993). Characteristic for the macrofauna at the cave are the abundantly occurring white rhinoceros bones which also gave the site its name. Biostratigraphical investigations indicate a probably slightly more recent age for the Rhino Cave compared to the Hominid Cave at Thomas Quarry I (Daujeard et al., 2012). Absolute dates for the site are, however, limited to ESR estimates on the enamel of four rhinoceros teeth recovered from the lower stratigraphic section, which revealed mean ages of 435 ± 85 ka and 737 ± 129 ka, for early and linear uptake, respectively (Rhodes et al., 1994; Rhodes et al., 2006).

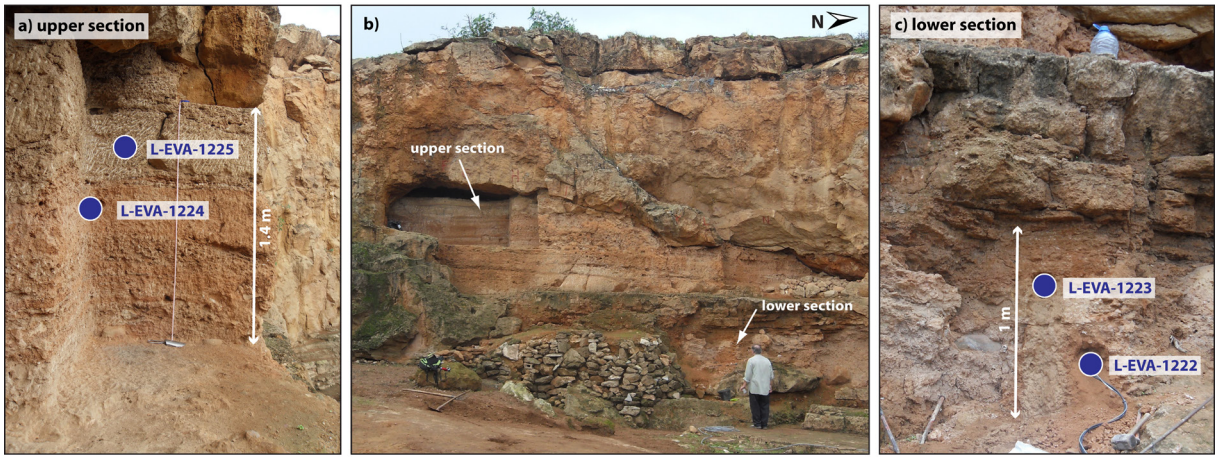

Figure 3.1.3 (b) The Rhino Cave site at Oulad Hamida I and location of the (a) upper and (c) lower cave sections. Collected OSL samples are indicated as blue dots.

Rhodes et al. (2006) performed a systematic OSL study on quartz samples from Thomas Quarry I and other sites in the Casablanca area using different measurement protocols (Table 3.1.1): a standard single-aliquot regenerative-dose (SAR; chapter 1.6.5), a component-resolved SAR (SAR-CR), a single-aliquot additive-dose slow component (SAAD-SC (Singarayer et al., 2000)) and a multiple aliquot additive-dose (MAAD) protocol (see e.g. Jain et al., 2003). The SAR-CR protocol is based on the linear modulation (LM) procedure (chapter 1.6.2) which allows isolation and quantification of the different luminescence signal components (Rhodes et al., 2006). The SAAD-SC protocol uses the slow signal component for dating

which has advantages over the fast and medium components due to a remarkable thermal stability and a high dose saturation level, it is, however, much harder to bleach (Singarayer et al., 2000). For the MAAD approach different aliquots of one sample are used to construct a dose response curve for equivalent dose (D_e) calculation (Jain et al., 2003) instead of just one used for single-aliquot dating techniques.

The authors showed that OSL signals from Thomas Quarry I are not fully saturated using the SAR protocol and that revealed age estimates of up to ~1 Ma are consistent with stratigraphic constraints and independent age control (Rhodes et al., 2006). Despite the chronological consistency, some of the dates for the younger units appeared to be underestimates based on the lithological interpretation of the site which places these deposits between MIS 18 and 22, approximately (Texier et al., 2002).

Building on the results of Rhodes et al. (2006), eight new sediment samples were collected during a field campaign in 2012 from Thomas Quarry I and Rhino Cave for single-grain OSL dating (Figs. 3.1.2 and 3.1.3). At Thomas Quarry I, three samples were collected from the Hominid Cave: two from the strongly cemented Units 4 and 5 and one from Unit 2 which is composed of unconsolidated fine grained red soils Fig. 3.1.2c. Acheulian artefacts and human fossils were recovered during past excavations from Unit 4, while the other units are archaeologically sterile. In addition, one OSL sample was taken from Locus I (Unit 5), a section characterised by unconsolidated red soils (Fig. 3.1.2b) intercalated with thin carbonate layers, for comparison with the stratigraphically older deposits of the Hominid Cave. At Rhino Cave sediments of both sections are diagenetically compacted to varying degrees. Two OSL samples were collected from the upper and the lower section, respectively (Fig. 3.1.3).

The aims of this project were to refine the absolute chronologies for both, the Thomas Quarry I and the Rhino Cave sites and to better understand the timing of human presence in the area. Moreover, the single-grain measurements at these sites allow detailed investigations of OSL signal characteristics from quartz samples close to saturation on an individual grain level, which can help to assess the reliability of OSL age estimates for samples of greater antiquity and to improve our understanding for the upper age limits of this dating method.

3.2. OSL DATING

OSL sample collection and chemical treatment in the red light laboratory were performed following standard procedures (chapter 1.6). Measurements were conducted on two automated Risø readers (TL/OSL DA-20 with single-grain attachment) using a SAR protocol with the same measurement parameters previously described for the site of Rhafas in chapter 2. Likewise, single-grain rejection criteria were chosen to be similar to those applied at Rhafas (test dose signal error >20%, recycling ratio >20%, recuperation >5%, IR depletion ratio >5%, D_e error >30%) and supplemented by the 2 D_0 criterion (Wintle and Murray, 2006) which rejects individual grains with D_es above signal saturation level.

3.2.1 Performance tests

Preheat plateau and dose recovery preheat plateau tests (with given doses close to the expected natural D_es, Table 3.2.1) at seven different preheat steps between 160°C and 280°C (chapter 1.6.6) were performed to determine the most appropriate preheat temperatures for single-grain D_e measurements (Murray and Wintle, 2003; Wintle and Murray, 2006). Three multiple-grain aliquots of 0.5 mm or 1 mm diameter were measured per preheat temperature, depending on the intensity of the luminescence signal stored in each sample. Figure 3.2.1 shows performance test results obtained from sample

L-EVA-1218 (Thomas Quarry I) and L-EVA-1224 (Rhino Cave). Preheat plateau tests for all samples in this study are unfortunately of little significance, as considerable amounts of the measured multiple-grain aliquots yield saturated quartz luminescence signals which effectively renders these aliquots unusable for D_e calculation (Fig. 3.2.1a). Moreover, even in samples for which D_es could be calculated at different preheat temperatures, results are largely scattered and no stable preheat plateaus were observed – except L-EVA-1220.

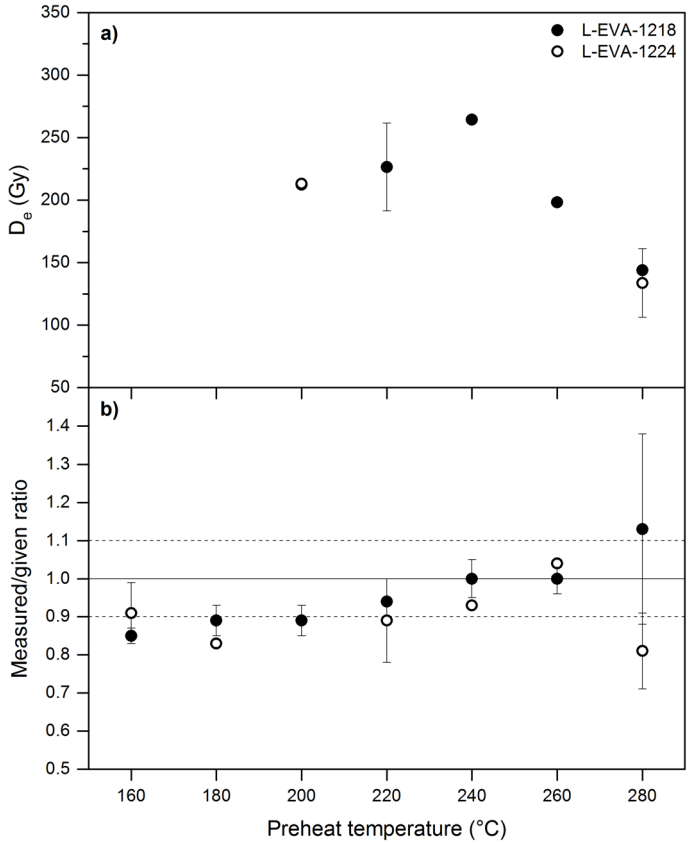

Figure 3.2.1 Results of standard performance tests: (a) preheat plateau test (b) dose recovery preheat plateau test for samples L-EVA-1218 (Thomas Quarry I, filled circles) and L-EVA-1224 (Rhino Cave, open circles). The solid line indicates the target value; dashed lines represent 10% deviation from unity.

Dose recovery preheat plateau tests yield more meaningful results (Fig. 3.2.1b). Although, measured/given ratios are relatively variable and often not consistent with unity at 280°C and for preheat temperatures below 220°C, all samples were found suitable to recover the laboratory given doses with sufficient accuracy and precision for at least one preheat temperature between 220°C and 260°C. According to these results, preheat and cutheat temperatures for single-grain D_e measurements were set to 220°C/180°C (L-EVA-1219, L-EVA-1223), 240°C/200°C (L-EVA-1220, L-EVA-1225) or 260°C/220°C (L-EVA-1218, L-EVA-1221, L-EVA-1222, L-EVA-1224).

To confirm the validity of the chosen preheat temperatures and to gather more information about single-grain luminescence characteristics and signal reproducibility, dose recovery tests were additionally performed for each sample on a single grain basis, again with given doses close to the expected natural D_es (Table 3.2.1). The results show, that i) the number of acceptable grains in single-grain dose recovery tests is relatively small (2-7%); ii) samples substantially underestimate dose recovery ratios by up to 19% and iii) overdispersion (σ_{OD}) values are higher (>12%) than expected from previous single-grain dose recovery studies (7-12% (Jacobs et al., 2006; Reimann et al., 2012; Thomsen et al., 2005)) and even reach 35% for sample L-EVA-1222 (Table 3.2.1). This data suggests that there is considerable variability in the ability of individual grains of some samples to accurately recover a known given dose, which might cause some serious issues for final D_e determination.

Table 3.2.1 Measured carbonate contents and results of single-grain dose recovery tests and determined D_es.

Sample	Unit[a]	Dose recovery				Equivalent dose		
		Given dose (Gy)	n[b]	Ratio[c]	σ_{OD}[d] (%)	n[b]	D_e[c] (Gy)	σ_{OD}[d] (%)
Thomas Quarry I								
L-EVA-1218	GH-2	180	52/1200	0.89±0.03	19±3	54/1400	126±9	47±5
L-EVA-1219	GH-4	250	68/1000	0.85±0.02	14±3	56/2200	193±10	35±4
L-EVA-1220	GH-5	130	47/2300	0.93±0.02	13±2	16/2300	-	-
L-EVA-1221	L1-5	205	42/600	0.81±0.02	15±3	62/1400	153±7	34±4
Rhino Cave								
L-EVA-1222	LS-bottom	350	52/2000	0.84±0.04	35±4	62/2000	180±9	38±4
L-EVA-1223	LS-top	270	76/1400	0.86±0.02	14±2	53/2500	200±11	36±4
L-EVA-1224	US-bottom	195	67/1600	0.90±0.02	16±3	58/3200	160±10	43±5
L-EVA-1225	US-top	200	12/600	0.83±0.05	12±6	3/600	-	-

[a] Abbreviations: GH - Hominid Cave; L1 - Locus 1; LS – lower section; US – upper section.
[b] Number of accepted/measured single grains.
[c] Determined using the Central Age Model (Galbraith et al., 1999).
[d] Overdispersion, determined using the Central Age Model (Galbraith et al., 1999).

3.2.2. Dosimetry

External dose rates were measured using high resolution germanium gamma spectrometry (HRGS) and the conversion factors by Guérin et al. (2011) were used to determine final estimates for the beta and gamma component from ^{238}U, ^{232}Th and ^{40}K contents of each sample (Table 3.2.2). Average life-time moisture contents were set to between 3 ± 2% and 10 ± 5% depending on the measurements of full saturation and in-situ moisture contents of each sample and incorporated into final dose rate calculations to account for attenuation. The cosmic dose rate was calculated according to Prescott and Hutton (1988, 1994), taking into account the altitude and geomagnetic latitude of the site, the burial depth and the density of the overburden.

Table 3.2.2 Results of radionuclide analysis and $CaCO_3$ contents.

Sample	Unit[a]	$CaCO_3$ (%)	Specific activities (Bq kg^{-1})		
			^{238}U	^{232}Th	^{40}K
Thomas Quarry I					
L-EVA-1218	GH-2	3	15.0±1.7	14.5±0.7	149±9
L-EVA-1219	GH-4	70	22.7±2.3	7±0.3	90±3
L-EVA-1220	GH-5	96	9.5±1.0	1.0±0.1	7.6±1
L-EVA-1221	L1-5	1.5	16.3±2.2	12.2±0.6	122±5
Rhino Cave					
L-EVA-1222	LS-bottom	55	20.5±2.3	12.6±0.6	167±10
L-EVA-1223	LS-top	68	18.3±2.1	6.3±0.3	95±5
L-EVA-1224	US-bottom	64	20.6±2.7	13.4±0.6	205±7
L-EVA-1225	US-top	87	7.9±1.2	2.2±0.1	31±2

[a] Abbreviations: GH - Hominid Cave; L1 - Locus 1; LS – lower section; US – upper section.

Total dose rates vary between 0.32 Gy/ka and 1.15 Gy/ka and between 0.40 Gy/ka and 1.36 Gy/ka at the sites of Thomas Quarry I and Rhino Cave, respectively (Table 3.2.3). Unit 5 at the Hominid Cave (L-EVA-1220, Thomas Quarry I) and the uppermost sample from Rhino Cave (L-EVA-1225) yield relatively low total dose rates which is most likely a consequence of their intensive secondary carbonate cementation ($CaCO_3$ contents >87%; Table 3.2.2). For these two samples, cosmic radiation contributes 23-25% to the total dose rate, while it is <10% for the remaining six samples which yield more consistent total dose rates between 0.87 Gy/ka and 1.36 Gy/ka.

Table 3.2.3 Dosimetric results.

Sample	Unit[a]	Moisture content (%)	Burial depth (m)	Dose rate (Gy/ka)			
				Beta[b]	Gamma[b]	Cosmic[b]	Total
Thomas Quarry I							
L-EVA-1218	GH-2	3±2	5±0.2	0.64±0.05	0.43±0.04	0.08±0.03	1.15±0.05
L-EVA-1219	GH-4	3±2	6±0.2	0.53±0.04	0.36±0.03	0.08±0.03	0.97±0.04
L-EVA-1220	GH-5	3±2	6±0.2	0.14±0.01	0.11±0.01	0.08±0.03	0.32±0.02
L-EVA-1221	L1-5	3±2	4±0.2	0.57±0.04	0.39±0.04	0.11±0.03	1.07±0.04
Rhino Cave							
L-EVA-1222	LS-bottom	5±3	7±0.2	0.71±0.05	0.47±0.05	0.07±0.02	1.25±0.07
L-EVA-1223	LS-top	5±3	7±0.2	0.48±0.03	0.32±0.03	0.07±0.02	0.87±0.05
L-EVA-1224	US-bottom	10±5	5±0.2	0.76±0.05	0.51±0.05	0.09±0.02	1.36±0.08
L-EVA-1225	US-top	3±2	5±0.2	0.18±0.02	0.12±0.01	0.09±0.02	0.40±0.04

[a] Abbreviations: GH - Hominid Cave; L1 - Locus 1; LS – lower section; US – upper section.
[b] Attenuated with respect to the moisture content.

In situ gamma spectrometry measurements could unfortunately not be realised during the time of sample collection at the sites. During a later excavation season, however, our colleague Christophe Falgueres (CNRS, Paris) performed in situ measurements - using a $LaBr_3$ detector - in the OSL sampling holes of the Hominid Cave Units 4 and 5 (L-EVA-1219 and L-EVA-1220) at Thomas Quarry I revealing gamma dose rates of 0.18 ± 0.09 Gy/ka and 0.30 ± 0.15 Gy/ka, respectively (C. Falgueres, pers. comment). For these two units, determined HRGS and in situ gamma dose rates are consistent with one another.

3.2.3. Equivalent doses and OSL ages

For this study, 15,600 individual grains from eight samples were measured for D_e determination (Table 3.2.1). All samples are generally characterised by highly sensitised quartz grains which exhibit single-grain decay curves with bright luminescence signals (see chapter 4). For two samples, however, the proportion of grains giving measurable luminescence signals that also pass all rejection criteria is so small (L-EVA-1220 and L-EVA-1225, 0.5% and 0.7%, respectively), that measurements were considered too costly and time consuming to be conducted. For the remaining six samples, between 1.8% (58/3200 grains) and 4.4% (62/1400 grains) of the measured individual grains were used for final D_e calculations (Table 3.2.1). The most frequent causes for discarding grains – in all eight samples - were i) absence of an initial luminescence signal significant above background and ii) sample saturation. While the former is quite common in single-grain OSL dating (not all individual grains exhibit measurable luminescence signals (Jacobs et al., 2006)), the latter once more emphasises the fact that these samples are close to the upper limit of quartz OSL dating.

Single grain D_e distributions are shown in Fig. 3.2.2 as radial plots. Final D_es were calculated using the Central Age Model (CAM, (Galbraith et al., 1999)) to determine the weighted mean D_es of the single grain populations and to statistically assess the scatter within the distributions (Table 3.2.1). The radial plots are centred on the CAM D_es and the shaded bands show the 95% confidence interval for the weighted means of the corresponding discrete populations (Fig. 3.2.2). For the Thomas Quarry I samples, CAM D_es vary between 126 ± 9 Gy and 193 ± 10 Gy, while overdispersions (σ_{OD}) range between 34% and 47%. Similar results were obtained for the Rhino Cave samples: CAM D_es between 160 ± 10 Gy and 200 ± 11 Gy and σ_{OD} between 36% and 43%. Probability density function (pdf) plots – which are an alternative way of displaying D_e distributions – show that none of the samples from the Thomas Quarries show D_e distributions of Gaussian shape (Fig. 3.2.3). Instead, distributions are relatively wide and not characterised by one major but often multiple smaller peaks, which, taken together, does not support the application of the CAM D_es for final age calculation.

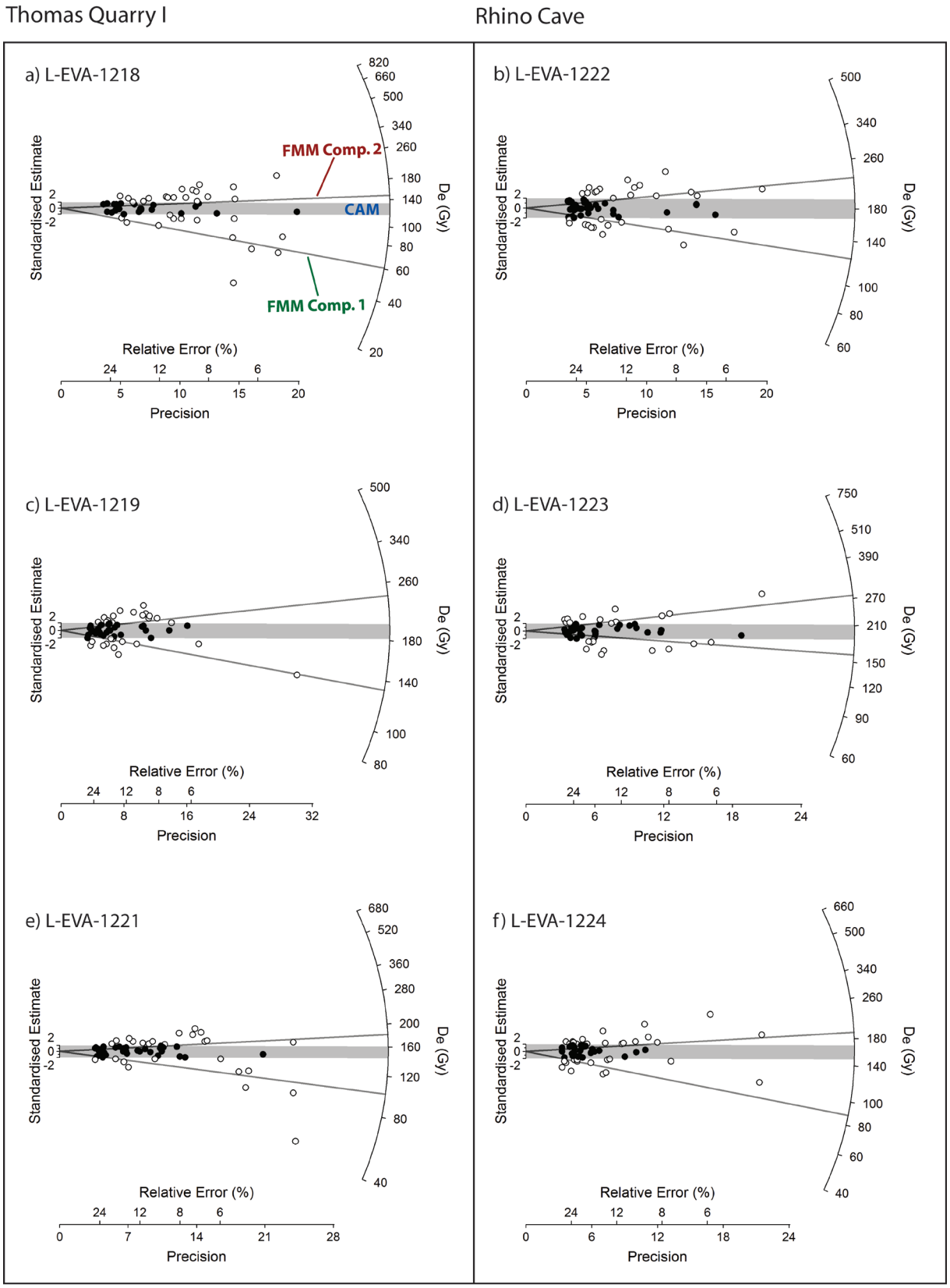

Fig. 3.2.2 Radial plots for the Thomas Quarry I (a,c,e) and Rhino Cave (b,d,f) samples. Radial plots are centred on the determined CAM D_es (shaded bands), FMM components are displayed as grey lines for comparison.

The samples from the Thomas Quarries show relatively large scatter within their D_e distributions (σ_{OD} 34-47%), which might indicate the presence multiple D_e populations. In the recent years, σ_{OD} values of

single-grain dose distributions were subject to scientific debates, as their interpretation is not always straightforward and judgements on the number of discrete D_e populations within one distribution exclusively based on σ_{OD} were questioned (Guérin et al., 2015; Jacobs et al., 2008; Olley et al., 2004; Thomsen et al., 2012). A common approach in the past was to use a threshold value for σ_{OD} of 20% to differentiate between one homogeneous D_e population and multiple D_e populations within one sample (Jacobs et al., 2008; Olley et al., 2004). Other authors, however, reported discrete age populations with σ_{OD} values of up to 62% (Guérin et al., 2015).

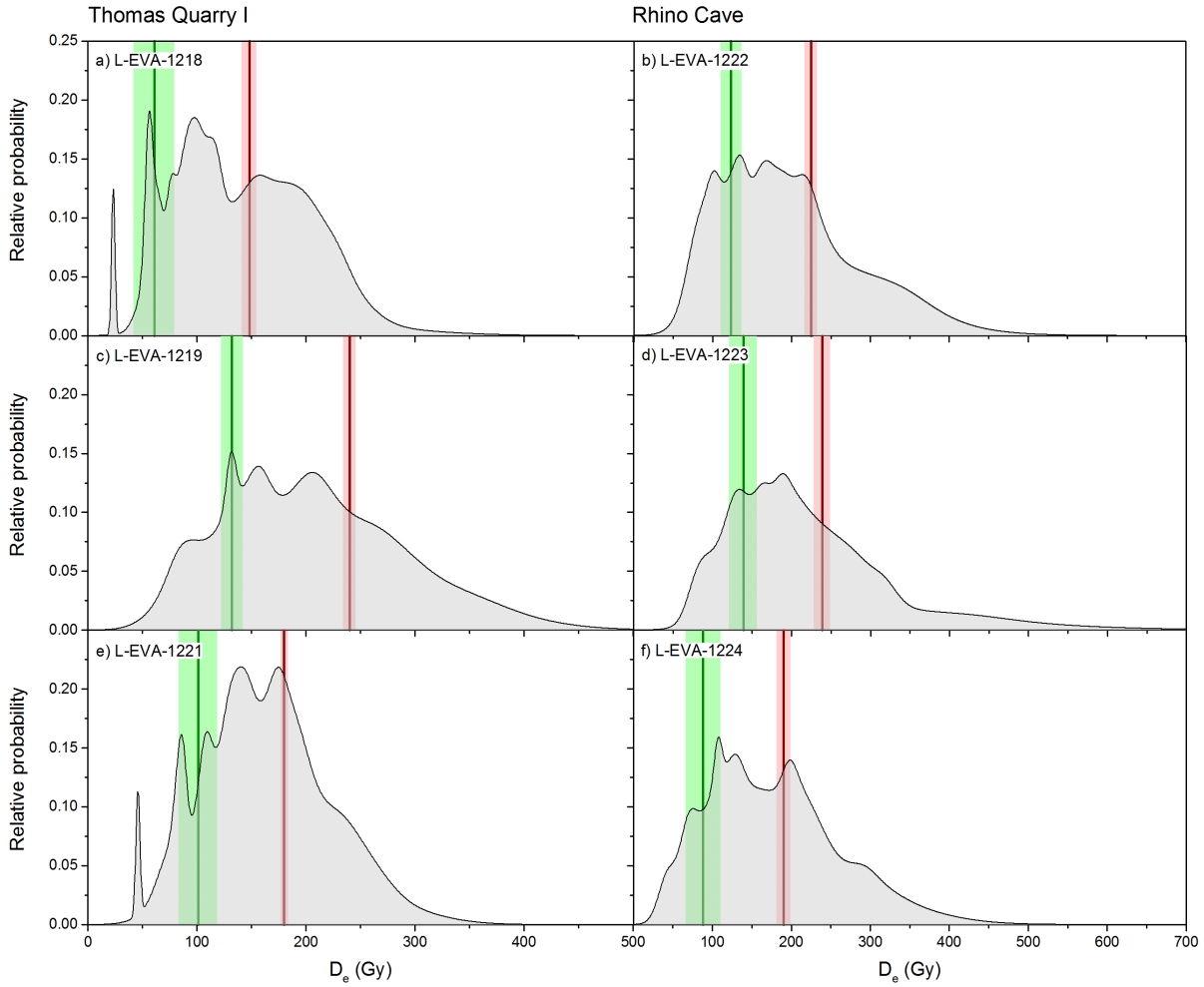

Fig. 3.2.3 Probability density function plots of single-grain D_e distributions of the Thomas Quarry I (a,c,e) and Rhino Cave (b,d,f) samples. FMM components are highlighted in green (minor component) and red (major component).

For this study, the Finite Mixture Model (FMM, (Galbraith et al., 1999; Roberts et al., 2000)) was applied additionally to the CAM to account for potential multiple depositional phases in the sedimentary units of the Thomas Quarries (Table 3.2.4). The FMM was run with 2-3 discrete components and σ_{OD} values between 15% and 30%. The Bayes Information Criterion (BIC) and values of maximum log likelihood were used to identify the number of supported discrete components (see also chapter 1.6.8 and chapter 2).

The FMM statistically supports two components for each sample from the Thomas Quarries, a major older grain population (63-95%) and a minor younger population (proportion: 5-37%) (Table 3.2.4) which are indicated as red and green lines in the pdf plots, respectively (Fig 3.2.3, see also grey lines in the radial plots (Fig 3.2.2)). These two D_e components are, however, not unambiguously recognisable neither in the pdf nor in the radial plots. Which is why, it must be noted that, in conclusion, none of

the D_es calculated by the two statistical age models (CAM and FMM) are conclusively supported by the visual shape of the D_e distributions for the Thomas Quarry I and Rhino Cave samples.

Single-grain OSL ages were calculated for both the CAM- and FMM-derived D_e values and the associated total dose rate for each sample (Table 3.2.5). CAM ages vary between 109 ± 9 ka and 198 ± 14 ka for Thomas Quarry I and 117 ± 10 ka and 231 ± 19 ka for the Rhino Cave samples. The ages of the major FMM populations revealed older ages for both sites: between 129 ± 9 ka and 246 ± 13 ka for Thomas Quarry I and between 139 ± 11 ka and 276 ± 21 ka for Rhino Cave. The minor single-grain populations are relatively variable in age at both sites. At the Hominid Cave (Thomas Quarry I), the age of the major component of Unit 2 (L-EVA-1218) is statistically indistinguishable from age of the minor component of Unit 4 (L-EVA-1219), which might indicate an intermixing of Unit 2 sediments into the underlying older, already accumulated material of Unit 4 (Table 3.2.5). A similar interpretation might be drawn from the ages of samples L-EVA-1224 (bottom sample of the upper section) and L-EVA-1223 (top sample of the lower section) at Rhino Cave. This scenario, however, appears to be less likely considering the stratigraphy of the site and the fact that both profile sections are vertically separated by several metres of sediments (Fig. 3.1.3).

Table 3.2.5 OSL dating results.

Sample	Unit[a]	Total dose	CAM[b]		FMM[c]			
		rate (Gy/ka)	Age (ka)	σ_{OD} (%)	C_1 age (ka)	Prop.	C_2 age (ka)	Prop.
Thomas Quarry I								
L-EVA-1218	GH-2	1.15±0.05	109±9.3	47±5	53±16.9	18.2	129±8.5	81.8
L-EVA-1219	GH-4	0.97±0.04	198±13.9	35±4	135±11.6	35.8	246±13.2	64.3
L-EVA-1221	L1-5	1.07±0.04	144±9.3	34±4	95±16.7	5.4	169±8.3	94.6
Rhino Cave								
L-EVA-1222	LS-bottom	1.25±0.07	144±11.1	38±4	98±11.8	36.7	180±12.4	63.3
L-EVA-1223	LS-top	0.87±0.05	231±19.1	36±4	160±22.5	33.8	276±21.0	66.2
L-EVA-1224	US-bottom	1.36±0.08	117±10.3	43±5	65±16.3	22.4	139±10.7	77.6

[a] Abbreviations: GH - Hominid Cave; L1 - Locus 1; LS – lower section; US – upper section.
[b] Determined using the Central Age Model (Galbraith et al., 1999). Age and overdispersion are given.
[c] Determined using the Finite Mixture Model (Galbraith et al., 1999; Roberts et al., 2000). Ages and relative proportions (%) are given for component 1 and 2.

3.3. Discussion and conclusion

In this chapter of the thesis, the first single-grain OSL dating results for two of the Early to Middle Pleistocene archaeological sites - Thomas Quarry I and Rhino Cave - in the Casablanca area were presented. Despite the promising outcomes of an earlier OSL study by Rhodes et al. (2006), who successfully dated the sediments at Thomas Quarry I up to ~1 Ma using that method, this study encountered greater difficulties throughout the whole dating process.

3.3.1. Assessment of general luminescence characteristics

Initial multiple-grain performance tests yielded bright, but unfortunately saturated OSL signals for a considerable number of the measured aliquots in all samples. In the following single-grain dose recovery tests and final D_e measurements, a similar pattern was observable: the D_es of many individual grains could not be determined due to saturation of the natural quartz luminescence signal. As a consequence, large quantities of individual grains had to be measured to reveal statistically significant numbers for final D_e calculation. For two of the collected eight samples (L-EVA-1220 and L-EVA-1225), the proportion of acceptable grains was less than 1% in D_e measurements, which effectively renders

these samples unsuitable for single-grain OSL dating. Interestingly, these two samples are not only exceptional for their low number of acceptable grains, but also for their intensive post-depositional carbonate cementation ($CaCO_3$ content >87%) and, thus, remarkably low total dose rates <0.4 Gy/ka. Cosmic radiation significantly contributes to the total dose rate of these two samples (23-25%) and, therefore, potential variability in burial depth or changes in the cosmic dose rate through time might have had significant impact on the annual radiation received by the individual quartz grains in these sediment layers. Consequently, present day measurements might not accurately reflect the average burial-time dose rate of L-EVA-1220 and L-EVA-1225. The remaining six samples yield more variable carbonate contents between 1.5% and 70% and total dose rates between 0.87 Gy/ka and 1.36 Gy/ka. For these samples, there is no correlation between high carbonate contents and low total dose rates.

The performed single-grain dose recovery tests for the Thomas Quarry I and Rhino Cave samples underestimate the given laboratory dose significantly by up to 19%, which is in great contrast to the conducted dose recovery preheat plateau tests on multiple-grain aliquots that proved their suitability for OSL dating using the SAR protocol under a sample-specific preheat temperature. From the single-grain results, it can be inferred that there are considerable numbers of individual grains in the samples that – although passing standard acceptance criteria – are not able to recover laboratory given doses with a sufficient accuracy which in turn casts some serious doubts on the reliability of any age determination using the SAR protocol for these samples.

Notwithstanding the above, the question remains as to why multiple-grain dose recovery test do not reflect similar results as the single-grain data. For both experiments, the same protocols were measured; beta sources were used for irradiation in the machine and given doses were close to the expected natural D_es of each sample. The only modifications between the two dose recovery measurements, thus, concerned i) light source (blue LEDs and green laser) and ii) aliquot size (multiple-grain aliquots and single-grains). While a change in the light stimulation source is unlikely to have any greater effect on dose recovery test results, individual grains naturally show different luminescence behaviour compared to averaged signals derived from multiple-grain aliquots (Duller et al., 1999).

Additional sources of uncertainty may derive from the bleaching treatment in the machines during dose recovery tests, which is not comparable to bleaching by sunlight exposure during natural transport and accumulation processes and might considerably influence luminescence characteristics of the quartz grains. σ_{OD} values in single-grain dose recovery test are, furthermore, high (12-35%); in theory, these values should be comparatively small, as they originate solely from intrinsic factors (e.g. counting statistics, instrument reproducibility, thermal transfer (Thomsen et al., 2007)), while extrinsic factors (mixing, incomplete bleaching, dose rate heterogeneity) which significantly enlarge the scatter in D_e distributions are excluded in laboratory experiments. Up until now, it remains unclear what might cause these unusually wide spreads in single-grain dose recovery distributions in the Thomas Quarry I and Rhino Cave samples.

In conclusion, a definite statement regarding the suitability of these samples for OSL dating using the SAR protocol remains challenging and further laboratory tests are needed to understand the luminescence characteristics of the sediments in greater detail and to allow an assessment of their suitability for future OSL projects at the two sites. Therefore, in a first attempt, a series of single grain dose recovery tests were performed – chapter 4 - on two samples from Thomas Quarry I using different bleaching sources and laboratory given doses and results are compared to those obtained from one sample from Rhafas and two samples of Australian quartz from Lake Mungo.

3.3.2. Reliability of single-grain ages

Single-grain ages were calculated for the Thomas Quarry I and Rhino Cave samples using CAM- and FMM-derived D_es and the final results are displayed in stratigraphically correct order in Figs. 3.3.1 and 3.3.2 (see also Table 3.2.5). Irrespective of the statistical model used for D_e calculation, there is no stratigraphical consistency in the determined ages for both sites. While at Thomas Quarry I (Fig. 3.3.1), one could potentially argue that at least the two samples from the Hominid Cave are in stratigraphic correct order (L-EVA-1218 and L-EVA-1219) and the overlying unit containing sample L-EVA-1221 is roughly contemporaneous to L-EVA-1218, there is simply no conclusive interpretation for the determined ages at Rhino Cave (Fig. 3.3.2).

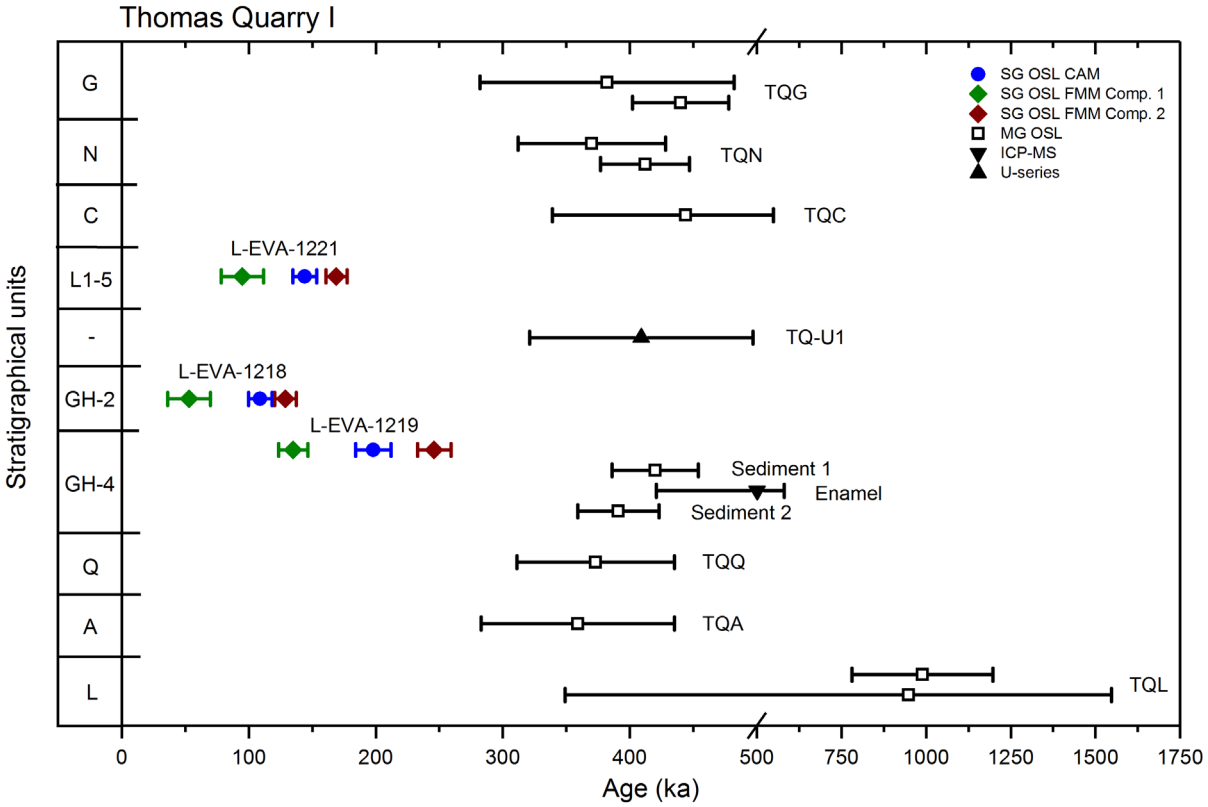

Fig. 3.3.1 Summary of the dating results from the Thomas Quarry I site. Single-grain OSL CAM-derived ages, minor FMM component ages and major FMM component ages from this study are displayed in blue, green and red, respectively. Previously published ages (Table 3.1.1) determined using multiple-grain OSL, U-series and ICP-MS (combined U-series/ESR) dating (Raynal et al., 2010; Rhodes et al., 2006) are shown in black.

All calculated single-grain OSL ages additionally suffer from tremendous age underestimations, given previously determined absolute ages (ESR, ICP-MS, OSL, U-series, Raynal et al., 2010; Rhodes et al., 2006) for these two sites which serve as independent age control. Even when assuming that the oldest FMM components correctly reflect the depositional age of the sediment units, ages are still around half the estimates determined by the other dating methods in the same stratigraphical units (Figs. 3.3.1 and 3.3.2) and are inconsistent with bio- and lithostratigraphical evidence (Raynal et al., 2010; Rhodes et al., 1994; Rhodes et al., 2006; Texier et al., 2002). Consequently, any further discussions about the validity of the two statistical age models are redundant, as standard single-grain OSL appears to be an inadequate technique for the absolute dating of the sediments at Thomas Quarry I and Rhino Cave. The calculated results can, therefore, only serve as minimum age constraints for the stratigraphic units at the two sites.

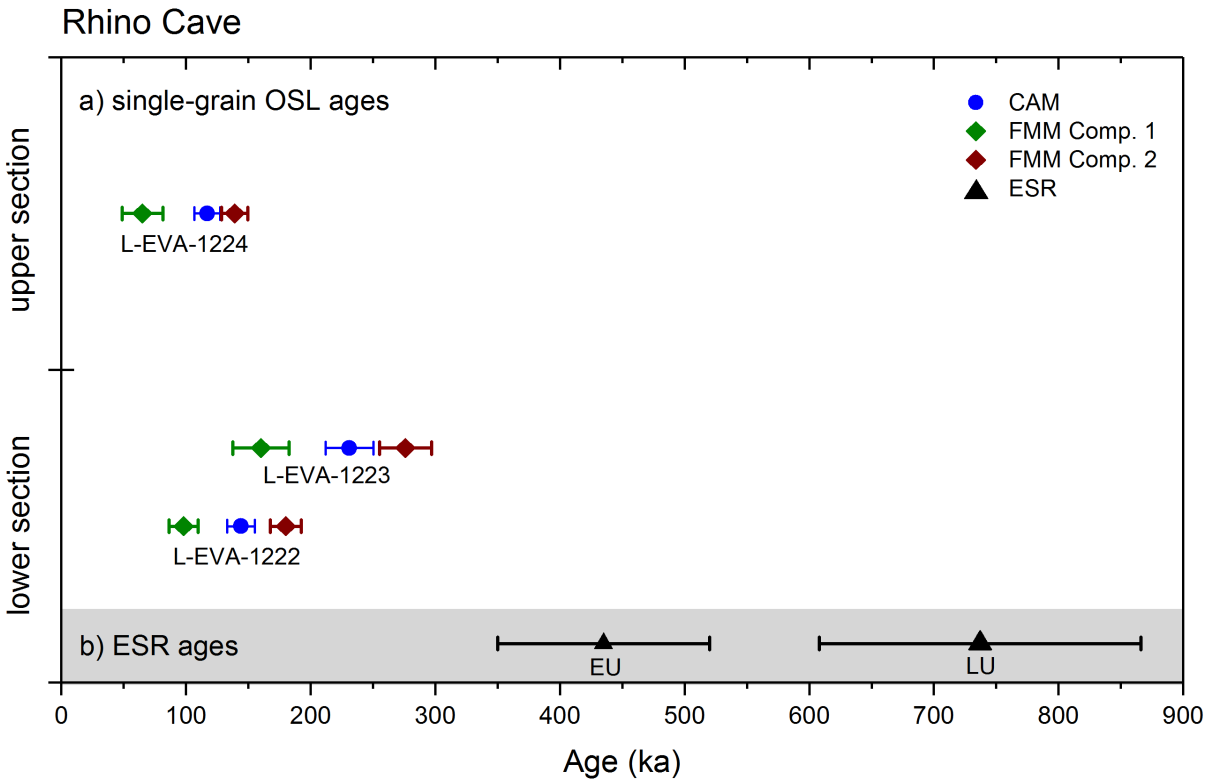

Fig. 3.3.2 Summary of the dating results from Rhino Cave. (a) Single-grain OSL ages from this study with CAM-derived ages, minor FMM component ages and major FMM component ages displayed in blue, green and red, respectively. (b) Previously published mean ESR ages (early and late uptake, Rhodes et al., 2006) from four rhinoceros teeth collected from the lower section at Rhino Cave.

Despite the fact that no reliable depositional ages could be calculated in this chapter for the Thomas Quarries sediments, it remains important to emphasise that considerable numbers of the measured individual quartz grains were not in saturation. Emitted luminescence signals are bright and reasonable numbers of individual grains pass standard rejection criteria which underlines the general suitability of these sediments for OSL dating as previously reported by Rhodes et al. (2006). It might well be possible to obtain reliable and conclusive age estimates – maybe even on a single-grain level (Arnold and Demuro, 2015; Arnold et al., 2013) - for the samples at Thomas Quarry I and Rhino Cave when different OSL techniques e.g. thermally transferred OSL (TT-OSL) or violet stimulated luminescence (VSL) are applied (Jain, 2009; Wang et al., 2006). Both approaches measure the luminescence stored in traps that are different to those used for standard quartz OSL. While TT-OSL and VSL signals are harder to bleach, they are also characterised by signal saturation limits significantly higher than the fast bleaching component used for OSL dating in this study. Both techniques, therefore, have the potential to reveal the true depositional age of the Thomas Quarry I and Rhino Cave units. It is, however, highly recommended to further investigate the general luminescence characteristics of these sediments in greater detail before additional attempts are made to actually date them.

References

Aguirre, E., Carbonell, E., 2001. Early human expansions into Eurasia: The Atapuerca evidence. Quaternary International 75, 11-18.

Arnold, L.J., Demuro, M., 2015. Insights into TT-OSL signal stability from single-grain analyses of known-age deposits at Atapuerca, Spain. Quaternary Geochronology.

Arnold, L.J., Demuro, M., Navazo, M., Benito-Calvo, A., Pérez-González, A., 2013. OSL dating of the Middle Palaeolithic Hotel California site, Sierra de Atapuerca, north-central Spain. Boreas 42, 285-305.

Bar-Yosef, O., Belfer-Cohen, A., 2001. From Africa to Eurasia — early dispersals. Quaternary International 75, 19-28.

Carbonell, E., Bermúdez de Castro, J.M., Arsuaga, J.L., Allue, E., Bastir, M., Benito, A., Cáceres, I., Canals, T., Díez, J.C., van der Made, J., Mosquera, M., Ollé, A., Pérez-González, A., Rodríguez, J., Rodríguez, X.P., Rosas, A., Rosell, J., Sala, R., Vallverdú, J., Vergés, J.M., 2005. An Early Pleistocene hominin mandible from Atapuerca-TD6, Spain. Proceedings of the National Academy of Sciences of the United States of America 102, 5674-5678.

Carbonell, E., Bermudez de Castro, J.M., Pares, J.M., Perez-Gonzalez, A., Cuenca-Bescos, G., Olle, A., Mosquera, M., Huguet, R., van der Made, J., Rosas, A., Sala, R., Vallverdu, J., Garcia, N., Granger, D.E., Martinon-Torres, M., Rodriguez, X.P., Stock, G.M., Verges, J.M., Allue, E., Burjachs, F., Caceres, I., Canals, A., Benito, A., Diez, C., Lozano, M., Mateos, A., Navazo, M., Rodriguez, J., Rosell, J., Arsuaga, J.L., 2008. The first hominin of Europe. Nature 452, 465-469.

Daujeard, C., Geraads, D., Gallotti, R., Lefèvre, D., Mohib, A., Raynal, J.-P., Hublin, J.-J., 2016. Pleistocene Hominins as a Resource for Carnivores: A c. 500,000-Year-Old Human Femur Bearing Tooth-Marks in North Africa (Thomas Quarry I, Morocco). PLOS ONE 11, e0152284.

Daujeard, C., Geraads, D., Gallotti, R., Mohib, A., Raynal, J.-P., 2012. Carcass acquisition and consumption by carnivores and hominins in Middle Pleistocene sites of Casablanca (Morocco). Journal of Taphonomy 10, 349-372.

Duller, G.A.T., Bøtter-Jensen, L., Murray, A.S., Truscott, A.J., 1999. Single grain laser luminescence (SGLL) measurements using a novel automated reader. Nuclear Instruments and Methods in Physics Research BNuclear Instruments and Methods in Physics Research B 155, 506-514.

Ennouchi, E., 1969. Découvertes d'un Pithécanthropien au Maroc. Comptes Rendus de l'Académie des Sciences de Paris 269, 763-765.

Ennouchi, E., 1970. Un nouvel archanthropien au Maroc. Annales de Paléontologie (Vertébrés) 56, 95-107.

Galbraith, R.F., Roberts, R.G., Laslett, G.M., Yoshida, H., Olley, J.M., 1999. Optical dating of single and multiple grains of quartz from Jinmium rock shelter, northern Australia: Part I, experimental design and statistical models. Archaeometry 41, 339-364.

Geraads, D., 1993. Middle Pleistocene Crocidura (Mammalia, Insectivora) from Oulad Hamida 1, Morocco, and their phylogenetic relationships. Proceedings of the Koninklijke Nederlandse Akademie Van Wetenschappen 96, 281-294.

Geraads, D., 1994. Rongeurs et Lagomorphes du Pléistocène moyen de la "Grotte des Rhinocéros", carrière Oulad Hamida 1, à Casablanca, Maroc. Neues Jahrbuch für Geologie and Paläontologie 191, 147-172.

Guérin, G., Combès, B., Lahaye, C., Thomsen, K.J., Tribolo, C., Urbanova, P., Guibert, P., Mercier, N., Valladas, H., 2015. Testing the accuracy of a Bayesian central-dose model for single-grain OSL, using known-age samples. Radiation Measurements 81, 62-70.

Guérin, G., Mercier, N., Adamiec, G., 2011. Dose-rate conversion factors: update. Ancient TL 29, 5-8.

Hublin, J.-J., 2001. Northwestern African Middle Pleistocene hominids and their bearing on the emergence of Homo sapiens, in: Braham, L., Robson-Brown, K. (Eds.), Human Roots. Africa and Asia in the Middle Pleistocene. Western Academic and Specialist Press Ltd, Bristol.

Jacobs, Z., Duller, G.A.T., Wintle, A.G., 2006. Interpretation of single grainDe distributions and calculation of De. Radiation Measurements 41, 264-277.

Jacobs, Z., Roberts, R.G., Galbraith, R.F., Deacon, H.J., Grün, R., Mackay, A., Mitchell, P., Vogelsang, R., Wadley, L., 2008. Ages for the Middle Stone Age of Southern Africa: Implications for Human Behavior and Dispersal. Science 332, 733-735.

Jain, M., 2009. Extending the dose range: Probing deep traps in quartz with 3.06 eV photons. Radiation Measurements 44, 445-452.

Jain, M., Bøtter-Jensen, L., Singhvi, A.K., 2003. Dose evaluation using multiple-aliquot quartz OSL: test of methods and a new protocol for improved accuracy and precision. Radiation Measurements 37, 67-80.

Murray, A.S., Wintle, A.G., 2003. The single aliquot regenerative dose protocol: potential for improvements in reliability. Radiation Measurements 37, 377-381.

Olley, J.M., Pietsch, T., Roberts, R.G., 2004. Optical dating of Holocene sediments from a variety of geomorphic settings using single grains of quartz. Geomorphology 60, 337-358.

Parés, J.M., Pérez-González, A., Rosas, A., Benito, A., Bermúdez de Castro, J.M., Carbonell, E., Huguet, R., 2006. Matuyama-age lithic tools from the Sima del Elefante site, Atapuerca (northern Spain). Journal of Human Evolution 50, 163-169.

Prescott, J.R., Hutton, J.T., 1988. Cosmic ray and gamma ray dosimetry for TL and ESR. International Journal of Radiation Applications and Instrumentation. Part D. Nuclear Tracks and Radiation Measurements 14, 223-227.

Prescott, J.R., Hutton, J.T., 1994. Cosmic ray contributions to dose rates for luminescence and ESR dating: Large depths and long-term time variations. Radiation Measurements 23, 497-500.

Raynal, J.-P., Lefevre, D., Geraads, D., El Graoui, M., 1999. Contribution du site paléontologique de Lissafa (Casablanca, Maroc) à une nouvelle interprétation du Mio-Pliocène de la Méseta. Comptes Rendus de l'Académie des Sciences de Paris, Sciences de la terre et de planètes 329, 617-622.

Raynal, J.-P., Magoga, L., Sbihi-Alaoui, F.Z., Geraads, D., 1993. La grotte des Rhinocéros (Carrière Oulad Hamida I, anciennnment Thomas III, Casablanca), nouveau site acheuléen du Maroc atlantique. Comptes Rendus de l'Académie des Sciences de Paris série II 316, 1477-1483.

Raynal, J.-P., Sbihi-Alaoui, F.-Z., Geraads, D., Magoga, L., Mohi, A., 2001. The earliest occupation of North-Africa: the Moroccan perspective. Quaternary International 75, 65-75.

Raynal, J.-P., Sbihi-Alaoui, F.-Z., Mohib, A., El Graoui, M., Lefèvre, D., Texier, J.-P., Geraads, D., Hublin, J.-J., Smith, T., Tafforeau, P., Zouak, M., Grün, R., Rhodes, E.J., Eggins, S., Daujeard, C., Fernandes, P., Gallotti, R., Hossini, S., Queffelec, A., 2010. Hominid Cave at Thomas Quarry I (Casablanca, Morocco): Recent findings and their context. Quaternary International 223-224, 369-382.

Reimann, T., Lindhorst, S., Thomsen, K.J., Murray, A.S., Frechen, M., 2012. OSL dating of mixed coastal sediment (Sylt, German Bight, North Sea). Quaternary Geochronology 11, 52-67.

Rhodes, E.J., Raynal, J.-P., Geraads, D., Sbihi-Alaoui, F.Z., 1994. Premières dates RPE pour l'Acheuléen du Maroc atlantique (Grotte des Rhinocéros, Casablanca). Comptes Rendus de l'Académie des Sciences de Paris série II 319, 1109-1115.

Rhodes, E.J., Singarayer, J.S., Raynal, J.-P., Westaway, K.E., Sbihi-Alaoui, F.Z., 2006. New age estimates for the Palaeolithic assemblages and Pleistocene succession of Casablanca, Morocco. Quaternary Science Reviews 25, 2569-2585.

Roberts, R.G., Galbraith, R.F., Yoshida, H., Laslett, G.M., Olley, J.M., 2000. Distinguishing dose populations in sediment mixtures: a test of single-grain optical dating procedures using mixtures of laboratory-dosed quartz. Radiation Measurements 32, 459-465.

Singarayer, J.S., Bailey, R.M., Rhodes, E.J., 2000. Potential of the slow component of quartz OSL for age determination of sedimentary samples. Radiation Measurements 32, 873-880.

Texier, J.-P., Lefèvre, D., Raynal, J.-P., El Graoui, M., 2002. Lithostratigraphy of the littoral deposits of the last one million years in the Casablanca region (Morocco). Quaternaire 13, 23-41.

Texier, J.P., Lefevre, D., Raynal, J.-P., 1994. Contribution pour un nouveau cadre stratigraphique des formations littorales quaternaires de la région de Casablanca. Comptes Rendus de l'Académie des Sciences de Paris série II 318, 1247-1253.

Thomsen, K.J., Murray, A., Jain, M., 2012. The dose dependency of the over-dispersion of quartz OSL single grain dose distributions. Radiation Measurements 47, 732-739.

Thomsen, K.J., Murray, A.S., Bøtter-Jensen, L., 2005. Sources of variability in OSL dose measurements using single grains of quartz. Radiation Measurements 39, 47-61.

Thomsen, K.J., Murray, A.S., Bøtter-Jensen, L., Kinahan, J., 2007. Determination of burial dose in incompletely bleached fluvial samples using single grains of quartz. Radiation Measurements 42, 370-379.

Wang, X.L., Wintle, A.G., Lu, Y.C., 2006. Thermally transferred luminescence in fine-grained quartz from Chinese loess: Basic observations. Radiation Measurements 41, 649-658.

Wintle, A.G., Murray, A.S., 2006. A review of quartz optically stimulated luminescence characteristics and their relevance in single-aliquot regeneration dating protocols. Radiation Measurements 41, 369-391.

4. Sources of variability in single grain dose recovery experiments: insights from Moroccan and Australian samples

A methodological study on the characteristics of single quartz grains from different environmental contexts during OSL dose recovery experiments.

Doerschner, N., Hernandez, M., Fitzsimmons, K.E.

Published in Ancient TL (2016, Volume 34)

Ancient TL

Sources of variability in single grain dose recovery experiments: Insights from Moroccan and Australian samples

Nina Doerschner[1]*, Marion Hernandez[1], Kathryn E. Fitzsimmons[1]

[1] Department of Human Evolution, Max Planck Institute for Evolutionary Anthropology
Deutscher Platz 6, D-04103 Leipzig, Germany

*Corresponding Author: nina_doerschner@eva.mpg.de

Received: April 12, 2016; in final form: June 10, 2016

Abstract

In our study, we investigate the quartz single-grain dose recovery characteristics of five aeolian samples from three archaeological sites in Australia and Morocco. Comparatively small (20 – 49 Gy) and high (180 – 208 Gy) doses were applied to sand-sized quartz grains of each sample. Samples were bleached by green laser, sunlight and solar simulator stimulation. We observed a primary dependency of the results on the size of the administered dose, but also observed sample-specific responses to the chosen dose recovery measurement parameters.

The Australian samples originate from an open-air archaeological site and consist of highly sensitized quartz grains with comparatively small equivalent doses. By contrast, the Moroccan samples originate from two cave sites known to be affected by heterogeneous dose rates and post-depositional mixing to varying degrees; this material is generally less sensitive, and expected equivalent doses are >180 Gy, while single-grain quartz weighted average signal saturation levels ($2D_0$) exceed 235 Gy.

Single grains from all sites, with one exception, recover small applied laboratory doses. These fall within 5 % of unity irrespective of the bleaching method. However, when applied doses are high, dose recovery test results vary substantially depending on how individual samples respond to the bleaching treatment prior to the given dose. The lowest dose recovery ratios and highest overdispersion values were observed in samples bleached in the solar simulator. Our results highlight the importance of investigating dose recovery characteristics at single grain level, and indicate additional sources of complexity in understanding the luminescence characteristics of quartz.

Keywords: OSL, single grain, quartz, SAR, dose recovery test, artificial bleaching, overdispersion

1. Introduction

In recent years, dating of single sand-sized grains of quartz using optically stimulated luminescence (OSL) has been frequently applied in geological and archaeological contexts. By reducing the aliquot size for equivalent dose (D_e) determination from multigrain aliquots to individual grain level, better resolution of dose distributions can be obtained.

The overdispersion value (σ_{OD}) allows quantification of the variability observed in single grain dose distributions (Galbraith et al., 1999), comprising both extrinsic (dose rate heterogeneity, incomplete bleaching and post depositional mixing) and intrinsic factors, such as counting statistics, instrument reproducibility, thermal transfer or other sample-specific OSL characteristics (Thomsen et al., 2007). Especially when dating material from highly complex settings such as cave sites, σ_{OD} of an individual sample can yield significant insight into, for example, the depositional history of sediments, thereby improving the reliability of age determinations (Jacobs et al., 2012).

Dose recovery experiments are one of the standard performance tests in quartz OSL dating, and are commonly assumed to represent a useful check of the suitability of mea-

surement protocol parameters and the reliability of natural D_e estimates (Murray & Wintle, 2003).

In dose recovery experiments, known laboratory doses, which are recommended to be close to the expected natural D_e of a certain sample (Murray & Wintle, 2003), are administered either to artificially bleached or modern analogous samples. Their ability to recover this given dose within acceptable ranges – calculated as a ratio normalized to the applied dose – is assessed. Thomsen et al. (2012) have shown that the size of the administered dose is of considerable importance in dose recovery tests for single grains as well as for multiple grain aliquots. They found that, their quartz samples recovered relatively small given doses within unity, but at higher administered doses of 103 and 208 Gy, dose recovery was substantially underestimated by 10 – 15 %. As dose recovery tests are by definition laboratory-based experiments, the observed σ_{OD} in resulting single grain dose distributions only reflects the intrinsic variability in the individual sample and is not influenced by extrinsic factors, as is the case for natural samples (Thomsen et al., 2007). Furthermore, Guérin et al. (2015) recently found no correlation between dose recovery ratios and accuracy for obtained ages in 19 single-grain samples with independent age control. These observations cast doubt on the standard dose recovery test as a check for sample reliability, and highlight a need to investigate dose recovery tests in greater depth.

Given the complex nature of many cave-based archaeological sediments, dose recovery tests are often undertaken by resetting the natural signal rather than using modern analogues. Resetting can be achieved by various light sources which simulate natural bleaching conditions. The most commonly used bleaching sources are natural sunlight, solar simulators (SOL2), and stimulation in the OSL reader by green lasers or blue light emitting diodes (LEDs) (e.g. Aitken & Smith, 1988; Ballarini et al., 2007; Kang et al., 2012; Li & Wintle, 1991, 1992). Solar simulators (SOL2) have recently been shown to cause inaccuracies in dose recovery tests on multigrain aliquots (Choi et al., 2009; Wang et al., 2011). Thomsen et al. (2016) on the other hand, observed no significant systematic differences in dose recovery test results after SOL2 and blue LED bleaching for both, single grains and multigrain aliquots.

As yet it is unclear whether experimental dose recovery tests using artificial bleaching sources can accurately recover dose for all samples, especially in single grains, since generally dose recovery tests are undertaken on multigrain aliquots – even in a number of single grain dating studies (e.g. Arnold & Demuro, 2015; Demuro et al., 2012; Jacobs et al., 2008).

In this study we undertook single grain dose recovery tests (e.g. natural D_es, signal intensities) on five sand-sized quartz samples from three different environmental settings from archaeological sites in Australia and Morocco. We investigate the dose recovery characteristics of these samples following different bleaching methods and after administering doses of different magnitude. We discuss the potential impact of experimental design and sample luminescence properties on the obtained results.

2. Instrumentation and sample characteristics

2.1. Instrumentation

All OSL measurements were undertaken using an automated Risø TL-DA-20 reader with a single grain attachment (Bøtter-Jensen et al., 2003), equipped with a calibrated $^{90}Sr/^{90}Y$ beta irradiation source (Bøtter-Jensen et al., 2000), and fitted with a 7.5 nm Hoya U-340 filter (Bøtter-Jensen, 1997). Individual grains were mounted on single grain sample discs containing 100 holes (300 µm diameter) on a 10 x 10 grid. Optical stimulation was provided by 10 mW 532 nm solid-state green laser beams for 1 s at 125 °C (90 % power, ∼50 W/cm^2 power density (Duller et al., 1999) and infrared LEDs (875 nm wavelength, ∼130 mW/cm^2 power density).

2.2. Samples

We investigated five samples from archaeological sites that were deposited by eolian processes. We used quartz of the 180 – 212 µm sand-size fraction. Samples were extracted by a combination of wet and dry sieving, followed by chemical treatment (HCl, H_2O_2, density separation and HF) under subdued red light.

Three samples originate from two archaeological cave sites in Morocco. L-EVA-1083 was collected at the inland site of Rhafas (Doerschner et al., in revision; Mercier et al., 2007; Wengler, 1993), and L-EVA-1218 and L-EVA-1221 from Thomas Quarry I (TQ I), located in aeolianite in Casablanca city on the Atlantic coast (Rhodes et al., 2006). Both sites are caves filled with Pleistocene sediments that were affected by post-depositional carbonate cementation and dose rate heterogeneity of varying degrees. The proportions of individual grains emitting detectable luminescence signals for natural D_e determination are 23 – 66 % for Rhafas and 6.8 – 31 % for TQ I samples (proportions reflect full suite of samples collected at Rhafas and TQ I). Furthermore, these samples yield particularly high D_0 values which allow reliable determination of natural D_e between 126 and 216 Gy (using the Central Age Model (CAM) proposed by Galbraith et al., 1999), with σ_{OD} reaching up to 47 % (Table 1).

We compare these samples with two dune samples from the open-air archaeological site at Lake Mungo (LM), Australia (L-EVA-1010 and -1012; Fitzsimmons et al., 2014). These two samples yield CAM-derived natural D_e values of 42 and 21 Gy respectively, and σ_{OD} of less than 25 % (Table 1). Although previous work has already demonstrated that these samples exhibit bright, rapidly decaying OSL signals typical of highly sensitive quartz and are therefore well suited to OSL dating (Fitzsimmons, 2011; Fitzsimmons et al., 2014), it has also been reported that variations in microdosimetry in sediments from this region might induce relatively high σ_{OD} values in natural D_e distributions (Lomax et al., 2007).

To examine the different sensitivity characteristics of the individual samples, the sensitivity of the first test dose response T_N (in counts/seconds/Gy) of each single grain, obtained after measurement of the natural signal, was plotted

Table 1. Results of natural D_e determination and dose recovery tests.

Sample	Natural equivalent dose				Given dose (Gy)	Test dose (Gy)	Dose recovery green laser				Dose recovery sunbleached				Dose recovery SOL2			
	n^1 (%)	D_e[2] (Gy)	σ_{OD}[2] (%)	D_0[3] (Gy)			n^1 (%)	recovery ratio[2]	σ_{OD}[2] (%)	D_0[3] ((Gy)	n^1 (%)	recovery ratio[2]	σ_{OD}[2] (%)	D_0[3] ((Gy)	n^1 (%)	recovery ratio[2]	σ_{OD}[2] (%)	D_0[3] ((Gy)
Lake Mungo																		
L-EVA-1010	16.7	42±1	24±2	65±3	49	10	24.0	0.95±0.01	7±1	67±3	18.2	0.96±0.01	6±1	65±4	18.7	0.95±0.01	10±1	63±6
					185	36	16.7	0.80±0.02	18±2	115±5	14.0	0.79±0.01	12±1	116±7	12.2	0.81±0.02	14±2	118±5
L-EVA-1012	9.0	21±1	24±3	73±9	20	4	21.5	0.96±0.01	6±1	72±3	18.5	0.97±0.01	9±1	53±3	10.1	0.94±0.01	11±1	63±7
					185	36	17.8	0.67±0.02	25±2	104±4	9.8	0.86±0.02	12±2	131±8	12.7	0.68±0.03	35±3	111±5
Rhafas																		
L-EVA-1083	4.1	216±12	36±4	208±16	20	4	11.2	0.97±0.01	9±1	51±5	6.3	0.83±0.02	22±2	76±11	6.5	0.99±0.02	10±2	59±7
					208	42	7.0	0.94±0.02	9±2	167±13	5.0	0.87±0.02	6±2	161±8	7.2	0.75±0.03	25±3	148±6
Thomas Quarry I																		
L-EVA-1218	3.9	126±9	47±5	118±7	20	4	16.7	0.93±0.01	5±1	47±3	4.1	0.91±0.02	8±2	40±3	7.5	1.04±0.02	7±2	75±5
					180	36	4.3	0.89±0.03	19±3	132±7	5.5	0.85±0.02	7±3	130±6	6.4	0.75±0.03	27±3	116±8
L-EVA-1221	4.4	153±7	34±4	149±6	20	4	16.8	0.95±0.01	6±1	49±3	4.3	0.93±0.02	9±2	59±6	11.2	0.97±0.01	9±1	59±5
					205	42	7.0	0.81±0.02	15±3	132±5	7.1	0.78±0.02	15±2	138±6	7.3	0.76±0.02	19±2	148±9

[1]Percentage of accepted grains.
[2]Determined using the Central Age Model (Galbraith et al., 1999).
[3]Weighted average D_0 value of the accepted D_es and standard error of the mean.

Table 2. Single grain characteristics of dose recovery experiments.

Sample	Given dose (Gy)	n^1	detectable signal[2] (100 %)	accepted grains (%)	No L_N/T_N intersection (%)	Remaining grains (100 %)	Dim grains[3] (%)	Recuperation > 5 % (%)	Recycling ratio (> 20 %) (%)	Depletion by IR (%)	D_e error > 30 % (%)	Grubbs test[4] (%)	$D_e > 2D0$ (%)
Lake Mungo													
L-EVA-1010	49	1800	1483 (82 %)	24.6	3.1	1072	17.0	0.8	57.8	19.5	4.3	0.1	0.6
	185	1800	1494 (83 %)	17.1	18.4	963	13.6	2.8	33.2	17.6	22.8	0.3	9.7
L-EVA-1012	20	2100	1504 (72 %)	22.2	0.2	1170	24.2	0.9	54.4	19.9	0.6	0.1	0.0
	185	2000	1525 (76 %)	17.5	18.9	972	18.6	4.4	31.0	19.7	18.3	0.1	7.8
Rhafas													
L-EVA-1083	20	2900	1447 (50 %)	14.7	0.3	1230	34.3	2.0	47.0	14.4	2.1	0.2	0.0
	208	2500	1343 (54 %)	11.9	14.2	990	22.3	22.1	34.1	9.6	7.5	0.2	4.1
Thomas Quarry I													
L-EVA-1218	20	2500	1451 (58 %)	14.1	0.3	1242	44.1	0.0	42.0	11.8	1.6	0.5	0.0
	180	2800	1884 (67 %)	7.9	25.8	1241	27.4	1.0	45.1	8.8	14.3	0.0	3.3
L-EVA-1221	20	2400	1530 (64 %)	14.8	0.4	1303	38.2	0.2	47.7	12.0	1.5	0.4	0.0
	205	3000	2309 (77 %)	9.3	23.3	1492	24.2	1.4	46.2	10.5	13.2	0.1	4.2

[1]Total number of grains measured per sample.
[2]Percentage of grains yielding an initial luminescence signal above background, and for which interpolation of the sensitivity-corrected natural signal using a single saturating exponential dose response curve resulted in finite dose estimates.
[3]Percentage of grains rejected due to insufficient test-dose signal.
[4]Percentage of grains identified as statistical outliers (Grubbs, 1950).

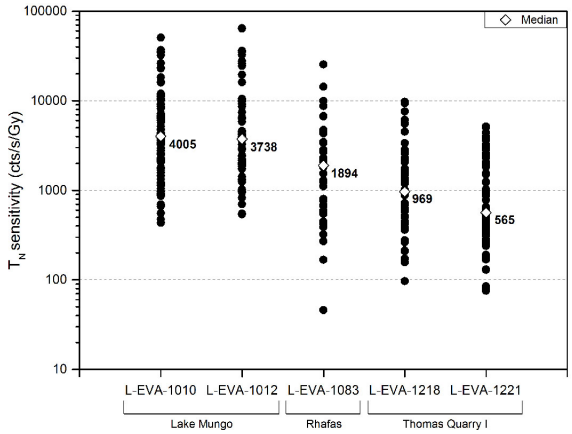

Figure 1. Luminescence sensitivity of single grains calculated from the OSL signal arising from the test dose immediately following natural D_e measurement (T_N) for all samples in this study (note logarithmic scale). Median values are indicated as open diamonds. Individual background corrected T_N signals were multiplied by 28.75 (1/0.035, integration in seconds) and then divided by the given test dose (Table S1) for comparability between samples.

(Fig. 1). Only individual grains accepted for natural D_e determination were incorporated to this figure; the test doses as applied to the samples using the single-aliquot regenerative-dose (SAR) protocol are listed in Table S1. The Australian samples yield high proportions of very bright grains ($> 10^4$ cts/s/Gy) and few grains emitting signal intensities of less than 10^3 cts/s/Gy. The samples from TQ I consistently yield single grain signal intensities in the range of $10^2 - 10^4$ cts/s/Gy. The sample L-EVA-1083 from Rhafas exhibits the most variable grain sensitivity; its calculated median sensitivity value is half that observed for the Australian samples.

In order to visualize the dominant OSL signal components in the samples, we undertook linearly-modulated OSL (LM-OSL) measurements on small (1 mm) aliquots at 125 °C using LEDs (470 nm, ∼40 mW/cm^2), following the procedure described by Bulur (1996). After preheating at 260 °C for 10 s, light intensity was increased from 0 to 90 % power over 500 s. The LM-OSL curves illustrate that all samples are dominated by the fast OSL signal component (Fig. S1). Single grain decay and growth curves of sample L-EVA-1221 (TQ I) and L-EVA-1010 (LM) also show that the samples are characterised by individual quartz grains with bright luminescence signals (Fig. 2). Weighted average D_0 values are higher in the Moroccan than the Australian samples. The determined D_e values – obtained using single saturating exponential curve fitting of the single grain dose response curves – for all samples in this study lie well below signal saturation levels (Table 1).

3. Dose recovery test – experimental details

Dose recovery tests on single grains were performed using the standard SAR protocol (Murray & Wintle, 2000, 2003) with a preheat temperature of 260 °C for 10 s, and a cutheat temperature of 220 °C. Preheat temperatures were determined based on the results of standard preheat plateau tests as well as combined dose recovery preheat plateau tests, in which seven different preheats (160 – 280 °C, data not shown) were applied to 1 mm multigrain aliquots (Murray & Wintle, 2003; Wintle & Murray, 2006). Potential feldspar contamination was tested at the end of each protocol by measuring the IR depletion of the OSL signal (Duller, 2003).

OSL signals were summed over the first 0.035 s of stimulation and corrected for background using the subsequent 0.035 s (Ballarini et al., 2007; Cunningham & Wallinga, 2009). Laboratory dose response curves were fitted using a single saturating exponential passing through the origin. Single grains were accepted for final analyses only when interpolation of the sensitivity-corrected natural signal on the dose response curve: 1) resulted in a finite dose estimate; 2) uncertainty on the natural test dose response was less than 20 % (test doses are given in Table 1); 3) were not affected by equivalent dose error > 30 %; and 4) passed the recuperation- (< 5 %), recycling- (< 20 %) and IR-depletion ratio tests (< 5 %). In addition, grains were rejected when exhibiting D_e signals exceeded saturation level (2 D_0) as suggested by Wintle & Murray (2006). Average dose recovery test ratios were calculated using the CAM.

Dose recovery tests were undertaken for each sample by applying two different laboratory doses and three different types of light exposure for bleaching. One applied dose was chosen to be close to the natural D_e (Murray & Wintle, 2003) and varied – depending on the sample – between 20 and 208 Gy (Table 1). A second set of dose recovery tests were performed for comparison using a laboratory dose of 185 Gy for the Australian samples (L-EVA-1010 and -1012) and 20 Gy for the Moroccan samples (L-EVA-1083, -1218 and -1221). Single grains from each sample were bleached by 1) the green laser (1 s at room temperature) in the OSL reader, 2) sunlight on the window sill (> 7 days, behind glass and therefore not entirely analogous to natural bleaching conditions), and 3) SOL2 at a lamp/sample distance of 60 cm. Stimulation in the Hönle solar simulator (equipped with a Hönle H2 filter, transmission range > 295 nm) by SOL2 was performed for 5 min to make sure that the individual grains were completely bleached while also avoiding underestimation of the recovered dose, as has been demonstrated for exposure times exceeding 1 hour (Choi et al., 2009). The total amount of individual grains measured for each dose recovery experiment is listed in Table S1.

4. Results

4.1. Acceptance and rejection of individual grains

Detailed information about the rejection of single grains for the different dose recovery experiments is listed in Ta-

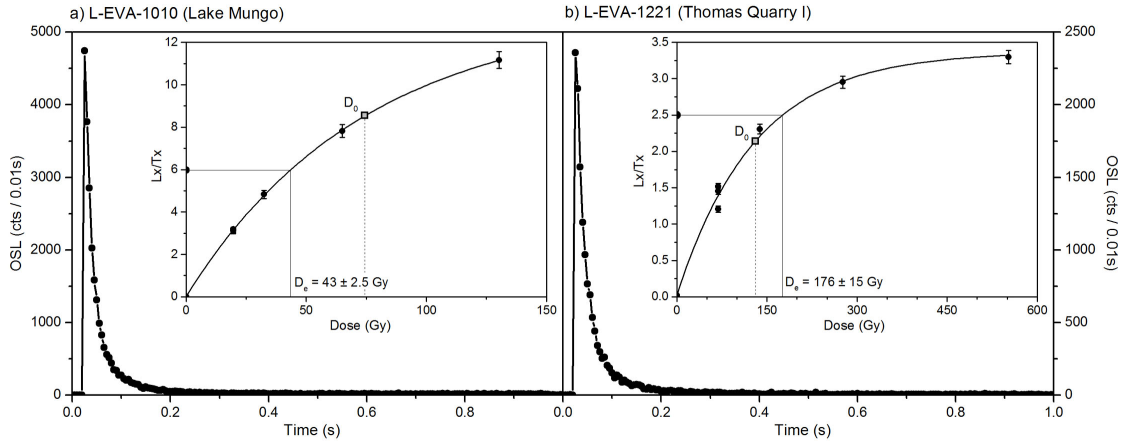

Figure 2. Natural OSL single grain decay and (as inset) dose-response curves for samples (a) L-EVA-1010 and (b) L-EVA-1221.

ble 2. Australian samples are more likely to give detectable luminescence signals for the chosen test doses (Table 1) than the Moroccan samples (LM 72 – 83 %, Rhafas 50 – 54 %, TQ I: 58 – 77 %, Table 2). This arises from the variability in intrinsic luminescence properties; the Australian samples generally comprise higher proportions of bright grains than the Moroccan samples (Fig. 1). Out of the grains exhibiting detectable luminescence signals, 14 to 26 % were rejected due to oversaturation (grains showing a L_n/T_n ratio well above maximum L_x/T_x value of the generated dose response curve) when administered doses are high (180 – 208 Gy), while this is only the case for 0.3 – 3.1 % of grains when administered doses are small (20 – 49 Gy). Sample L-EVA-1083 (Rhafas) yields the lowest rejection rate due to oversaturation at high given doses. This is most likely a consequence of its high signal saturation level after administration of a high dose, revealing weighted average D_0 values $>$ 148 Gy in our dose recovery experiments (Table 1).

D_0 values calculated for all samples are consistent between bleaching types (Table 1). They do, however, show large variability depending on the given dose, with D_0 values arising from low administered doses yielding significantly smaller values than those arising from high doses. This is most likely caused by the different regeneration doses of the dose recovery measurements (Table S2). Maximum regeneration doses are considerably smaller after low given doses in comparison with high given doses. These results indicate that D_0 can presumably only be accurately determined when dose response curves are taken up to large doses.

Oversaturated grains were excluded from further analyses of rejection criteria in Table 2 to avoid statistical bias between dose recovery experiments with high and low given doses. As previously mentioned, regeneration doses vary in dose recovery experiments depending on the size of the given dose (Table S2). Therefore, observed differences in criteria causing rejection of individual grains between low and high given doses might partly be caused by those different measurement parameters. Depending on the sample site, individual grains are more likely to be rejected after a low administered dose due to poor recycling ratios (LM), insufficient test dose signals (TQ I) or a combination of both (Rhafas). While TQ I samples at high given doses only show a significant increase in rejection rates due to D_e errors exceeding 30 %, samples from LM are additionally affected by single grains failing the $2D_0$ criterion. Single grains from Rhafas increasingly fail due to recuperation values of $>$ 5 %.

The number of individual grains passing all rejection criteria for dose determination varies considerably between sampling locations (LM: 10 – 24 %, Rhafas: 5 – 11 % and TQ I: 4 – 17 %; Table 1, Fig. 3a). Although a large number of single grains were rejected due to oversaturation solely when given doses were high, there is no clear correlation – with the exception of sample L-EVA-1010 (LM) – between the proportion of accepted grains and the size of the given dose. It is interesting to note that exceptionally high acceptance rates (11 – 24 %) were achieved for all samples when low doses were applied following green laser bleaching (Fig. 3a).

4.2. Differences observed in dose recovery ratios

Figure 3b summarizes the results of the measured/given ratios for each sample in the dose recovery experiment. The Australian samples from LM (L-EVA-1010 and -1012) and sample L-EVA-1221 from TQ I (Morocco) yield dose recovery ratios within 7 % of unity after low given doses, regardless of bleaching type (Fig. 3b, Table 1). By contrast, when given doses are high, these samples underestimate the measured/given ratios by 14 – 33 %. For the remaining Moroccan samples from Rhafas (L-EVA-1083) and TQ I (L-EVA-1218), recovery ratios vary between 1 – 17 % and 6 – 25 % of unity following low and high applied doses, respectively.

The type of bleaching source appears to influence dose recovery ratios for the Moroccan samples (Rhafas and TQ I). SOL2 stimulation at small given doses consistently results in values with the lowest (1 – 4 %) deviation from unity. Bleaching by sunlight results in the highest (7 – 17 %) devi-

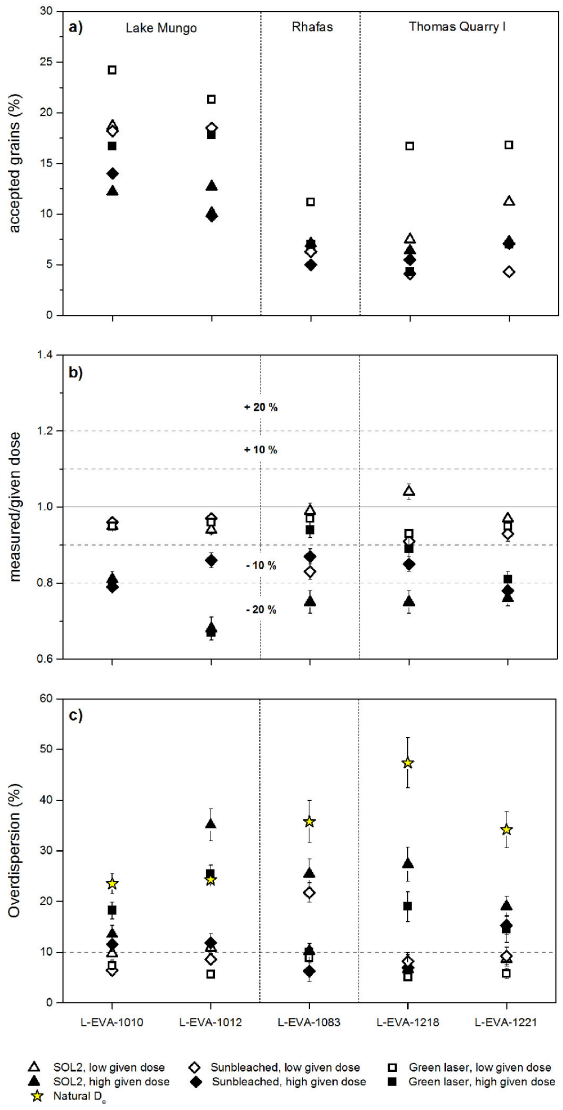

Figure 3. Results of single grain dose recovery experiments: (a) number of accepted grains after applying rejection criteria, (b) measured/given dose ratios and (c) calculated σ_{OD} values. Individual grains from each sample were bleached with green laser (squares), natural sunlight (diamonds) and SOL2 (triangles) prior to administering low (open symbols) or high (filled symbols) doses. Overdispersion values determined for the natural D_es are indicated by yellow stars.

ation of dose recovery from unity. Conversely, when given doses are high, green laser bleaching results in the most accurate (6 – 19 %) and SOL2 the least accurate (25 – 26 %) measured/given ratios. The Australian sample L-EVA-1012 (LM), however, yields consistent values of underestimation after high given doses for both, SOL2 and green laser bleaching (32 – 33 %).

To examine potential correlation between the degree of grain sensitivity and the accuracy of the dose recovery test results, measured/given ratios were plotted as a function of the corresponding single grain L_N signal intensities (Fig. S2). Individual grains from all samples emitting high intensity signals yield measured/given ratios close to unity when given doses are small. This characteristic decreases with decreasing signal intensity (Fig. S2a-e). The shape of the dose distributions, however, varies between samples. Individual grains from Rhafas (L-EVA-1083, Fig. S2c) are more widely scattered than LM or TQ I samples, whose distributions are relatively narrow. These results indicate a stronger correlation between signal intensity and accuracy of the dose recovery ratio. Similar single grain distributions following dose recovery experiments have also been observed in other studies (Duller et al., 2000; Jacobs et al., 2006; Thomsen et al., 2007). By contrast, when given doses are high, samples from all three sites exhibit a different behaviour. Single grains inconsistently over- and under-estimate the measured/given ratios, independently of L_N signal intensity (Fig. S2f-j).

The insets of Figure S2 show a correlation between measurement precision and L_N signal intensities for all samples. This is expected, as the impact of counting statistics decreases with increasing signal brightness (Duller et al., 2000).

4.3. Overdispersion variability in recovered doses

It has been shown that even under the controlled laboratory conditions of dose recovery tests, whereby all extrinsic factors can be excluded, σ_{OD} values of 7 – 12 % are nevertheless observed in single grain dose distributions (Jacobs et al., 2006; Reimann et al., 2012; Thomsen et al., 2005). This intrinsic σ_{OD} is caused by luminescence characteristics inherent within sand grains from a sample.

We calculated the σ_{OD} values for each single grain dose recovery test. The results, together with the σ_{OD} values from the natural D_es, are plotted in Figure 3c (see also Table 1). The behaviour of the Australian material (LM) and sample L-EVA-1221 (TQ I) differs from the other Moroccan samples by consistently revealing intrinsic σ_{OD} values of ∼10 % when administered doses are small, and substantially increased σ_{OD} values of up to 35 % following larger given doses.

For samples L-EVA-1083 (Rhafas) and L-EVA-1218 (TQ I), σ_{OD} values of 5-10 % (Table 1) are observed for almost all dose recovery test parameters. This is consistent with intrinsic σ_{OD} values reported in previous studies. A remarkable increase in σ_{OD}, however, can be observed for L-EVA-1083 when a small dose was given after sunlight bleaching (22 %), for L-EVA-1218 when a high administered dose was combined with green laser stimulation (19 %), and for both samples when high given doses and SOL2 were used (25 – 27 %).

Applying SOL2 stimulation prior to a high given dose results in the highest σ_{OD} (19 – 35 %) in all samples, except L-EVA-1010 (LM). For the sake of completeness, it should be noted that for sample L-EVA-1012 (LM) the intrinsic σ_{OD} following green laser (25 %) and SOL2 bleaching (35 %) at

high given doses exceeds the value determined from the natural D_e (24 %, Fig. 3c). Those values are, however, not entirely comparable, since the given dose (185 Gy) is considerably higher than the natural D_e estimate (∼21 Gy) and, therefore, intersection of the sensitivity-corrected natural signal of the individual grains occurs along different parts of the dose response curves. Intrinsic σ_{OD} after sunlight stimulation of the material prior to a high given dose (12 %) is entirely comparable to the σ_{OD} obtained for all bleaching treatments and small administered doses (6 – 11 %).

Given the highly variable results of our dose recovery experiments, we cannot confidently specify the proportion of intrinsic σ_{OD} within the natural D_e σ_{OD} for most samples. Comparisons of the internal σ_{OD} from the dose recovery experiments close to the expected natural D_es with the measured σ_{OD} from the natural D_es of each sample indicate that considerable proportions of the σ_{OD} value are caused by extrinsic factors. As neither post depositional mixing, nor incomplete bleaching is likely for any of our samples (Doerschner et al., in revision; Fitzsimmons et al., 2014; Rhodes et al., 2006), high extrinsic σ_{OD} most likely results from heterogeneous dose rates (Lomax et al., 2007). Autoradiography was undertaken at the University of Bern to verify this assumption by highlighting spatially resolved radiation inhomogeneities in our samples following the procedure described in Rufer & Preusser (2009). Autoradiographs are shown in Figure S3; high-radiation emitters are visible as black hotspots and indicate dose rate heterogeneity, thereby explaining the high values obtained for external σ_{OD}. Furthermore, visual inspection under a microscope indicates that carbonate shielding of quartz grains, which could introduce further variation in microdosimetry by reducing the dose rate received by individual grains (Olley et al., 1997), might additionally affect L-EVA-1083 (Rhafas). This effect is, however, absent from LM and TQ I samples.

5. Discussion

5.1. Dose recovery and overdispersion

In this study the dose recovery characteristics of single quartz grains of archaeological samples from two Moroccan (Rhafas and TQ I) and one Australian (LM) site were examined.

The Australian samples consist of highly sensitized, bright quartz grains which are able to recover a small laboratory given dose (close to their natural D_e) within 6 % of unity and homogeneously (σ_{OD} 6 – 11 %) over a large number of individual grains. By contrast, when administered doses are high (185 Gy), the total number of single grains passing rejection criteria decreases (Table 1), while σ_{OD} increases (12 – 35 %) and the measured/given dose ratio is systematically underestimated by up to 33 %.

For the Moroccan samples, the results are variable. The samples originate from two cave sites and consist of individual quartz grains significantly less bright than the Australian samples. These results suggest that the Moroccan material underwent comparatively fewer sensitization cycles (cycles of dose and light exposure) than the Australian samples (Moska & Murray, 2006; Pietsch et al., 2008). Dose recovery ratios and σ_{OD} values in sample L-EVA-1083 (Rhafas) and L-EVA-1218 (TQ I) are highly variable (Fig. 3). Single grains from these samples recover low administered doses with similar accuracy (1 – 17 %) and precision (σ_{OD} 5 – 22 %) as high doses (within 6 – 25 % of unity, σ_{OD} 6-27 %). They also do not show significant dependency on the bleaching treatment. Therefore, it seems most likely that the results reflect a sample-specific response to the chosen dose recovery test parameters (bleaching type and size of administered dose).

For sample L-EVA-1221 (TQ I), however, measured/given dose ratios and σ_{OD} values are clearly dependent on the magnitude of the given dose. Consequently, our results suggest that the SAR protocol would have to be declared as unsuitable for dating sample L-EVA-1221, in the case where a standard dose recovery test with a given dose close to the expected natural D_e (205 Gy) is applied. L-EVA-1221, however, passes a SAR suitability check when applied doses are low (20 Gy). Interestingly, L-EVA-1218 (TQ I) and L-EVA-1083 (Rhafas) pass standard SAR suitability checks when green laser bleaching is applied, yet fail after sunlight or SOL2 treatment, when given doses are close to their expected natural D_e (180 and 208 Gy, respectively).

Our contradictory results raise questions as to the validity of dose recovery tests in general, and more particularly as to the adequate choice of test parameters to interrogate the suitability of the SAR protocol. The Moroccan material is in general less sensitive than the Australian samples. While single grain signal intensity in all samples correlates positively with accuracy of measured/given ratio when given doses are small, even bright grains are not necessarily able to reproduce a given dose $>$ 180 Gy with any accuracy. The observed variability in intrinsic σ_{OD} in our samples is alarming, particularly when considering that the correct assessment of natural σ_{OD} is critical for reliable age determination. Underestimation of the intrinsic, and thereby overestimation of the extrinsic, σ_{OD} might result in misinterpretation of single grain dose distributions and/or selection of inappropriate statistical age models. Autoradiographs suggest that increased values of extrinsic σ_{OD} in all samples result from variations in their microdosimetry.

5.2. Single grain rejection criteria

Application of single grain rejection criteria significantly reduces the amount of acceptable grains in each dose recovery experiment presented in this study. The justification of single grain standard rejection criteria (recycling, IR depletion and recuperation) has been recently questioned in several studies (e.g. Geach et al. 2015; Guérin et al. 2015; Thomsen et al. 2012; Zhao et al. 2015. Thomsen et al. (2016) reported that standard rejection criteria for single grains "do not result in significant changes in either dose or overdispersion of the single grain distributions" in the samples that they investigated. To investigate the impact of the chosen single

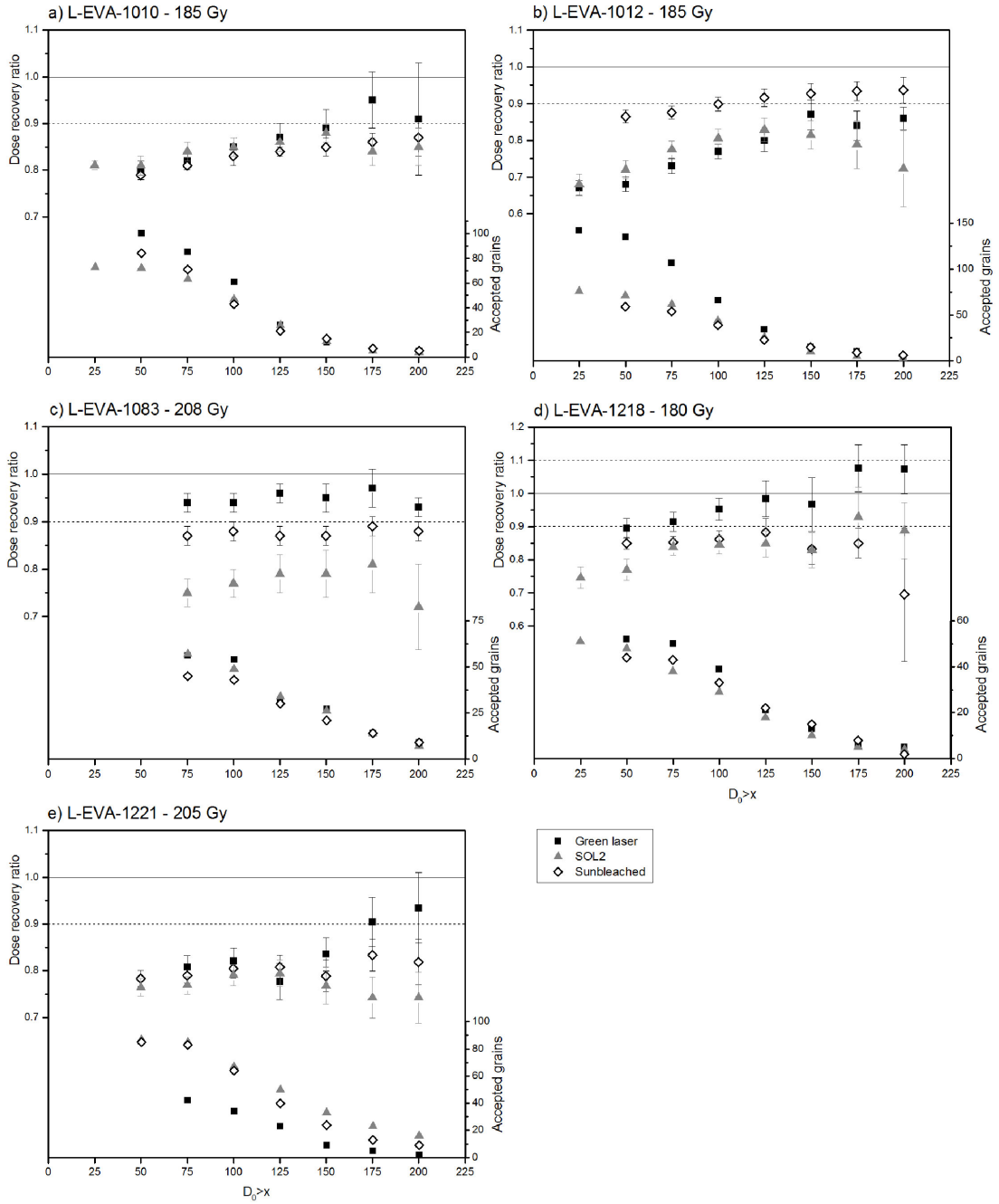

Figure 4. Dose recovery ratio and total amount of accepted grains as a function of single grain D_0 values in dose recovery experiments, with high given doses for each sample in this study.

grain rejection criteria in our dose recovery experiments, we compared dose recovery ratios and σ_{OD} values both before and after application of single grain rejection criteria (Table 1 and Table S3). The dose recovery ratios prior and subsequent to application of rejection criteria are – with the exception of L-EVA-1218 following green laser bleaching and a low given dose – indistinguishable from one another within the given error ranges. σ_{OD} values, however, were reduced considerably (up to 12 %) following application of rejection criteria in 15 out of the 30 dose recovery experiments. We, therefore,

argue that rejection of individual grains due to the chosen criteria reduces σ_{OD} values significantly in our experiments.

We further investigated the impact of applying the $D_e > 2D_0$ and the D_e error $< 30\,\%$ criteria in our samples. We undertook this exercise in response to the argument that those criteria are more likely to reject individual grains with high dose estimates rather than low dose estimates, and may consequently bias our single grain dose distributions toward underestimated dose recovery ratios and reduced σ_{OD} values. We calculated dose recovery ratios and σ_{OD} for each experiment in this study using all rejection criteria listed in Section 3, with the exception of $D_e > 2D_0$ and D_e error $< 30\,\%$ (Table S4). Our results from this exercise indicate that application of those two rejection criteria has no significant impact on dose recovery ratios and σ_{OD} values, in 29 out of 30 experiments. Only in sample L-EVA-1083 following green laser bleaching and a high given dose, do dose recovery ratios improve and σ_{OD} is significantly reduced. We then compared dose recovery test results prior to application of rejection criteria (Table S3), with results when all rejection criteria, except the $D_e > 2D_0$ and the D_e error $< 30\,\%$ were applied (Table S4). This comparative exercise shows that σ_{OD} values are still significantly reduced for 14 out of 30 dose recovery experiments, and for only one dose recovery ratio. Our findings suggest that there is no clear justification for the assumption that application of $D_e > 2D_0$ and D_e error $< 30\,\%$ criteria bias single grain dose distributions in our samples. Furthermore, our results also do not indicate that those two rejection criteria cause the apparent reduction of σ_{OD} observed prior and subsequent to application of rejection criteria – at least in the case of the samples analysed in this study.

5.3. Bleaching methods

The impact of different bleaching methods on the dose recovery characteristics of individual grains is almost negligible when given doses are small (Fig. 3, Table 1). With the exception of L-EVA-1083 following sunlight bleaching, all measured/given ratios lie within unity and σ_{OD} ranges from $5-11\,\%$. It is, however, interesting to note that a combination of green laser stimulation and low given doses consistently yields the highest proportions of acceptable grains in all samples.

When given doses exceed 180 Gy in the dose recovery experiments, variability in dose recovery ratios and σ_{OD} increases substantially compared to results following low administered doses. No obvious pattern can be observed when comparing results following sunlight and green laser bleaching, leading to the conclusion that there is most likely an additional factor influencing dose recovery results that is best described as a sample-specific response to dose recovery test parameters. This assumption is supported by the fact that both the proportion of accepted single grains, as well as the specific rejection criteria, show dependency on the sampling location.

SOL2 bleaching results – with the exception of L-EVA-1010 – considerably underestimate dose recovery ratios ($25-32\,\%$) and oversee a substantial increase in σ_{OD} ($19-35\,\%$) for all samples. In their study, Choi et al. (2009) observed an underestimation of the given dose (10 – 150 Gy) by $\sim$20 % after SOL2 treatment (> 1 h) as a consequence of sensitisation of the quartz signal during or after the first OSL measurement. Although we chose a relatively short SOL2 stimulation time (5 min) in our experiments, and sample L-EVA-1010 seemed not to be affected at all, we cannot rule out that sensitisation of the material might have taken place either during bleaching treatment or preheating prior to the first OSL signal measurement.

5.4. Administered dose

In our experiments, the most conspicuous factor driving dose recovery characteristics and especially σ_{OD} is the size of the administered dose, as has previously been argued by Thomsen et al. (2012). Determined measured/given ratios and their associated σ_{OD} in three out of five samples are undeniably dependent on the given dose, as is the oversaturation criterion for rejection of single grains.

Thomsen et al. (2016) showed that the dependency of dose recovery ratio and σ_{OD} on the administered dose can be eliminated in dose recovery experiments (with given doses > 30 Gy) by excluding individual grains with D_0 values greater or equal the given dose. They argue that underestimation of dose recovery ratio is related to the inclusion of grains with comparatively small D_0 values, and that by applying the D_0 selection criterion one is likely to discard saturated grains that might otherwise bias dose recovery test results. Following the procedure described in Thomsen et al. (2016), we plotted dose recovery ratios for our experiments with high given doses (> 180 Gy) as a function of $x > D_0$, with x ranging from 0 – 200 Gy (Fig. 4, Table S5). In addition, we show the total amount of accepted grains that pass all rejection criteria for each $x > D_0$. Our observations are similar to those made by Thomsen et al. (2016); dose recovery ratios generally increase with increasing D_0 value. At a threshold value of $D_0 > 125-175$ Gy (depending on the sample), however, dose recovery ratios appear to decrease. This is probably linked to the small quantity of individual grains passing D_0 rejection criterion > 125 Gy (Table S5), which may be too few to allow reliable statistical age modelling. Although both dose recovery ratios and σ_{OD} improve in most of our experiments when the D_0 exceeds the given dose criterion is applied (Thomsen et al., 2016), the dose recovery ratios falling closest to unity in most of our samples occurred when $D_0 > 125-175$ Gy. This is the case even though not all recovery ratios lie close to unity, as was shown by Thomsen et al. (2016). The total amount of accepted grains from our samples are, however, significantly reduced to fewer than 15 grains (for 10 out of 15 experiments). Thus, we conclude that while rejection of individual grains based on their D_0 values can significantly improve dose recovery ratios and the associated σ_{OD}, it also reduces the quantity of accepted grains overall. This might present problems for statistical age modelling.

6. Conclusion

Our results demonstrate that while the main driving factor influencing beta dose recovery test ratios and σ_{OD} on single quartz grains is the size of the administered dose, sample-specific responses to chosen test parameters (size of the given dose, bleaching type) can also significantly alter the obtained results. High variability in dose recovery test results was observed that is unlikely to be derived solely from the size of the administered dose, particularly for the less sensitized Moroccan samples. Therefore, caution is advised when performing dose recovery tests on samples which are likely to have undergone relatively few sensitization cycles. We conclude that further studies are required to improve our understanding of the range of effects that irradiation time and laboratory bleaching method might have on individual samples.

Acknowledgments

This research was funded by the Max Planck Institute for Evolutionary Anthropology. The Moroccan samples were collected with the assistance of our project partners, Abdeljalil Bouzouggar, Jean-Paul Raynal and Abderrahim Mohib. Research on the Australian samples was undertaken with the permission of the Elders' Council and the Technical and Scientific Advisory Committee of the Willandra Lakes Region World Heritage Area (WLRWHA); sampling was funded by an Australian Research Council (ARC) Discovery Project (DP1092966) and assisted in the field by the project's Cultural Heritage Officer, Daryl Pappin. The authors wish to thank Steffi Hesse for her support during sample preparation and OSL measurements in the laboratory, and Daniel Rufer from the University of Bern for performing the autoradiography. The constructive comments of Kristina Thomsen substantially improved the paper.

References

Aitken, M. J. and Smith, B. W. *Optical dating: Recuperation after bleaching*. Quaternary Science Reviews, 7(34): 387–393, 1988. doi: http://dx.doi.org/10.1016/0277-3791(88)90034-0.

Arnold, L. J. and Demuro, M. *Insights into TT-OSL signal stability from single-grain analyses of known-age deposits at Atapuerca, Spain*. Quaternary Geochronology, 2015. doi: http://dx.doi.org/10.1016/j.quageo.2015.02.005.

Ballarini, M., Wallinga, J., Wintle, A. G., and Bos, A. J. J. *A modified SAR protocol for optical dating of individual grains from young quartz samples*. Radiation Measurements, 42(3): 360–369, 2007. doi: http://dx.doi.org/10.1016/j.radmeas.2006.12.016.

Bøtter-Jensen, L., Bulur, E., Duller, G. A. T., and Murray, A. S. *Advances in luminescence instrument systems*. Radiation Measurements, 32(56): 523–528, 2000. doi: http://dx.doi.org/10.1016/S1350-4487(00)00039-1.

Bøtter-Jensen, L., Andersen, C. E., Duller, G. A. T., and Murray, A. S. *Developments in radiation, stimulation and observation facilities in luminescence measurements*. Radiation Measurements, 37(45): 535–541, 2003. doi: http://dx.doi.org/10.1016/S1350-4487(03)00020-9.

Bøtter-Jensen, L. *Luminescence techniques: instrumentation and methods*. Radiation Measurements, 27(56): 749–768, 1997. doi: http://dx.doi.org/10.1016/S1350-4487(97)00206-0.

Bulur, E. *An alternative technique for optically stimulated luminescence (OSL) experiment*. Radiation Measurements, 26(5): 701–709, 1996. doi: http://dx.doi.org/10.1016/S1350-4487(97)82884-3.

Choi, J. H., Murray, A. S., Cheong, C. S., and Hong, S. C. *The dependence of dose recovery experiments on the bleaching of natural quartz OSL using different light sources*. Radiation Measurements, 44(56): 600–605, 2009. doi: http://dx.doi.org/10.1016/j.radmeas.2009.02.018.

Cunningham, A. C. and Wallinga, J. *Optically stimulated luminescence dating of young quartz using the fast component*. Radiation Measurements, 44(56): 423–428, 2009. doi: http://dx.doi.org/10.1016/j.radmeas.2009.02.014.

Demuro, M., Froese, D. G., Arnold, L. J., and Roberts, R. G. *Single-grain OSL dating of glaciofluvial quartz constrains Reid glaciation in NW Canada to MIS 6*. Quaternary Research, 77(2): 305–316, 2012. doi: http://dx.doi.org/10.1016/j.yqres.2011.11.009.

Doerschner, N., Fitzsimmons, K. E., Ditchfield, P., McLaren, S. J., Steele, T. E., Zielhofer, C., McPherron, S. P., Bouzouggar, A., and Hublin, J.-J. *A new chronology for Rhafas, northeast Morocco, spanning the North African Middle Stone Age through to the Neolithic*. PLoS ONE, in revision.

Duller, G. A. T., Bøtter-Jensen, L., and Murray, A. S. *Optical dating of single sand-sized grains of quartz: sources of variability*. Radiation Measurements, 32(56): 453–457, 2000. doi: http://dx.doi.org/10.1016/S1350-4487(00)00055-X.

Duller, G. *Distinguishing quartz and feldspar in single grain luminescence measurements*. Radiation Measurements, 37: 161–165, 2003.

Duller, G. A., Bøtter-Jensen, L., Murray, A. S., and Truscott, A. J. *Single grain laser luminescence (SGLL) measurements using a novel automated reader*. Nuclear Instruments and Methods in Physics Research BNuclear Instruments and Methods in Physics Research B, 155: 506–514, 1999.

Fitzsimmons, K. E. *An assessment of the luminescence sensitivity of Australian quartz with respect to sediment history*. Geochronometria, 38(3): 199–208, 2011. doi: 10.2478/s13386-011-0030-9.

Fitzsimmons, K. E., Stern, N., and Murray-Wallace, C. V. *Depositional history and archaeology of the central Lake Mungo lunette, Willandra Lakes, southeast Australia*. Journal of Archaeological Science, 41: 349–364, 2014. doi: http://dx.doi.org/10.1016/j.jas.2013.08.004.

Galbraith, R. F., Roberts, R. G., Laslett, G. M., Yoshida, H., and Olley, J. M. *Optical dating of single and multiple grains of quartz*

from Jinmium rock shelter, northern Australia: Part I, experimental design and statistical models. Archaeometry, 41(2): 339–364, 1999. doi: 10.1111/j.1475-4754.1999.tb00987.x.

Geach, M. R., Thomsen, K. J., Buylaert, J. P., Murray, A. S., Mather, A. E., Telfer, M. W., and Stokes, M. *Single-grain and multi-grain OSL dating of river terrace sediments in the Tabernas Basin, SE Spain.* Quaternary Geochronology, 30: 213–218, 2015.

Grubbs, F. E. *Sample Criteria for Testing Outlying Observations*. pp. 27–58, 1950. doi: 10.1214/aoms/1177729885.

Guérin, G., Combés, B., Lahaye, C., Thomsen, K. J., Tribolo, C., Urbanova, P., Guibert, P., Mercier, N., and Valladas, H. *Testing the accuracy of a Bayesian central-dose model for single-grain OSL, using known-age samples*. Radiation Measurements, 81: 62–70, 2015. doi: http://dx.doi.org/10.1016/j.radmeas.2015.04.002.

Jacobs, Z., Duller, G. A., and Wintle, A. G. *Interpretation of single grainDe distributions and calculation of De*. Radiation Measurements, 41: 264–277, 2006.

Jacobs, Z., Roberts, R. G., Galbraith, R. F., Deacon, H. J., Grn, R., Mackay, A., Mitchell, P., Vogelsang, R., and Wadley, L. *Ages for the Middle Stone Age of Southern Africa: Implications for Human Behavior and Dispersal*. Science, 332: 733–735, 2008.

Jacobs, Z., Roberts, R. G., Nespoulet, R., El Hajraoui, M. A., and Debnath, A. *Single-grain OSL chronologies for Middle Palaeolithic deposits at El Mnasra and El Harhoura 2, Morocco: Implications for Late Pleistocene humaneenvironment interactions along the Atlantic coast of northwest Africa*. Journal of Human Evolution, 62: 377–394, 2012.

Kang, S. G., Wang, X. L., and Lu, Y. C. *The estimation of basic experimental parameters in the fine-grained quartz multiple-aliquot regenerative-dose OSL dating of Chinese loess*. Radiation Measurements, 47(9): 674–681, 2012. doi: http://dx.doi.org/10.1016/j.radmeas.2012.01.009.

Li, S.-H. and Wintle, A. G. *Luminescence sensitivity change due to bleaching of sediments*. Radiation Measurements, 20(4): 567–573, 1992. doi: http://dx.doi.org/10.1016/1359-0189(92)90006-H.

Li, S.-H. and Wintle, A. G. *Sensitivity changes of luminescence signals from colluvial sediments after different bleachung procedures*. Ancient TL, 9(3): 50–53, 1991.

Lomax, J., Hilgers, A., Twidale, C. R., Bourne, J. A., and Radtke, U. *Treatment of broad palaeodose distributions in OSL dating of dune sands from the western Murray Basin, South Australia*. Quaternary Geochronology, 2(14): 51–56, 2007. doi: http://dx.doi.org/10.1016/j.quageo.2006.05.015.

Mercier, N., Wengler, L., Valladas, H., Joron, J.-L., Froget, L., and Reyss, J. *The Rhafas Cave (Morocco): Chronology of the mousterian and aterian archaeological occupations and their implications for Quaternary geochronology based on luminescence (TL/OSL) age determinations*. Quaternary Geochronology, 2: 309–313, 2007.

Moska, P. and Murray, A. S. *Stability of the quartz fast-component in insensitive samples*. Radiation Measurements, 41(78): 878–885, 2006. doi: http://dx.doi.org/10.1016/j.radmeas.2006.06.005.

Murray, A. S. and Wintle, A. G. *Luminescence dating of quartz using an improved single-aliquot regenerative-dose protocol*. Radiation Measurements, 32(1): 57–73, 2000. doi: http://dx.doi.org/10.1016/S1350-4487(99)00253-X.

Murray, A. S. and Wintle, A. G. *The single aliquot regenerative dose protocol: potential for improvements in reliability*. Radiation Measurements, 37(45): 377–381, 2003. doi: http://dx.doi.org/10.1016/S1350-4487(03)00053-2.

Olley, J. M., Roberts, R. G., and Murray, A. S. *Disequilibria in the uranium decay series in sedimentary deposits at Allen's cave, nullarbor plain, Australia: Implications for dose rate determinations*. Radiation Measurements, 27(2): 433–443, 1997. doi: http://dx.doi.org/10.1016/S1350-4487(96)00114-X.

Pietsch, T. J., Olley, J. M., and Nanson, G. C. *Fluvial transport as a natural luminescence sensitiser of quartz.* Quaternary Geochronology, 3(4): 365–376, 2008. doi: http://dx.doi.org/10.1016/j.quageo.2007.12.005.

Reimann, T., Lindhorst, S., Thomsen, K. J., Murray, A. S., and Frechen, M. *OSL dating of mixed coastal sediment (Sylt, German Bight, North Sea)*. Quaternary Geochronology, 11(0): 52–67, 2012. doi: http://dx.doi.org/10.1016/j.quageo.2012.04.006.

Rhodes, E. J., Singarayer, J., Raynal, J.-P., Westaway, K., and Sbihi-Alaoui, F. *New age estimates for the Palaeolithic assemblages and Pleistocene succession of Casablanca, Morocco*. Quaternary Science Reviews, 25: 2569–2585, 2006.

Rufer, D. and Preusser, F. *Potential of autoradiography to detect spatially resolved radiation patterns in the context of trapped charge dating*. Geochronometria, 34: 1–13, 2009.

Thomsen, K. J., Murray, A. S., Buylaert, J. P., Jain, M., Hansen, J. H., and Aubry, T. *Testing single-grain quartz OSL methods using sediment samples with independent age control from the Bordes-Fitte rockshelter (Roches d'Abilly site, Central France)*. Quaternary Geochronology, 31: 77–96, 2016. doi: http://dx.doi.org/10.1016/j.quageo.2015.11.002.

Thomsen, K. J., Murray, A. S., and Bøtter-Jensen, L. *Sources of variability in OSL dose measurements using single grains of quartz*. Radiation Measurements, 39: 47–61, 2005.

Thomsen, K. J., Murray, A. S., Bøtter-Jensen, L., and Kinahan, J. *Determination of burial dose in incompletely bleached fluvial samples using single grains of quartz*. Radiation Measurements, 42: 370–379, 2007.

Thomsen, K. J., Murray, A., and Jain, M. *The dose dependency of the over-dispersion of quartz OSL single grain dose distributions*. Radiation Measurements, 47: 732–739, 2012.

Wang, X. L., Wintle, A. G., Du, J. H., Kang, S. G., and Lu, Y. C. *Recovering laboratory doses using fine-grained quartz from Chinese loess*. Radiation Measurements, 46(10): 1073–1081, 2011. doi: http://dx.doi.org/10.1016/j.radmeas.2011.07.022.

Wengler, L. *Cultures prhistoriques et formations quaternaires au Maroc oriental. Relations entre comportements et paloenvironments au Palolithique moyen*. Thesis, 1993.

Wintle, A. and Murray, A. *A review of quartz optically stimulated luminescence characteristics and their relevance in single-aliquot regeneration dating protocols*. Radiation Measurements, 41: 369–391, 2006.

Zhao, Q. Y., Thomsen, K. J., Murray, A. S., Wei, M. J., Pan, B. L., Zhou, R., Zhao, X. H., and Chen, H. Y. *Quartz single-grain OSL dating of debris flow deposits from Miyun, north east Beijing in China.* Quaternary Geochronology, 30: 320–327, 2015.

Reviewer

Kristina Thomsen

5. Chronology of the Late Pleistocene archaeological sequence at Vanguard Cave, Gibraltar

A case study of single and multiple grain OSL dating for the Palaeolithic site of Vanguard Cave.

Doerschner, N.[a], Fitzsimmons, K.E.[a, b], Blasco, R.[c], Finlayson, G.[d, e], Rodríguez-Vidal, J.[f], Rosell, J.[g, h], Hublin, J.-J.[a], Finlayson, C.[d, e, i]

Accepted for publication in Quaternary International, February, 16th 2018

[a] Department of Human Evolution, Max Planck Institute for Evolutionary Anthropology, DeutscherPlatz 6 04103 Leipzig, Germany

[b] Research Group for Terrestrial Palaeoclimates, Max Planck Institute for Chemistry, Hahn-Meitner-Weg 1, 55128 Mainz, Germany

[c] Centro Nacional de Investigación sobre la Evolución Humana (CENIEH), Paseo Sierra de Atapuerca 3, 09002 Burgos, Spain

[d] The Gibraltar Museum, 18-20 Bomb House Lane, Gibraltar

[e] Institute of Life and Earth Sciences, The University of Gibraltar, Gibraltar Museum Associate Campus, 18-20 Bomb House Lane, Gibraltar

[f] Departamento de Ciencias de la Tierra / Earth Sciences, Facultad de Ciencias Experimentales, Universidad de Huelva, Campus del Carmen, Av. Tres de Marzo s/n, 21071 Huelva, Spain

[g] Àrea de Prehistòria, Universitat Rovira i Vigili (URV), Avenida de Catalunya 35, 43002 Tarragona, Spain

[h] IPHES, Institut Català de Paleoecologia Humana I Evolució Social, Zona Educacional 4, Campus Sescelades URV (Edifici W3), 43007 Tarragona, Spain

[i] Department of Anthropology, University of Toronto at Scarborough, 1265 Military Trail, Toronto, Ontario M1C 1A4, Canada

Keywords: Optically stimulated luminescence, quartz single grains, multi-grain aliquots, Vanguard Cave, Gibraltar, Middle Palaeolithic

Abstract

Vanguard Cave is an archaeological site located on the shoreline of the Rock of Gibraltar at the south-western extreme of the Iberian Peninsula. It is part of a limestone cave system facing the adjacent Governor's Beach on the south-eastern coast of Gibraltar and has been filled to the roof with more than 17 m of sedimentary deposits. Due to its long stratified sequence, comprising rich palaeoenvironmental and faunal records as well as multiple Palaeolithic occupation layers, Vanguard Cave provides valuable information for our understanding of human behaviour and dispersal across south-eastern Iberia in general and particularly about the strategic role of the promontory of Gibraltar for past human populations. The development of a reliable absolute chronology for the sedimentary sequence at Vanguard Cave is therefore of great importance in this context.

In this study, we applied optically stimulated luminescence dating to sand-sized quartz grains from the uppermost ~4 m of the Vanguard Cave deposits, as well as from the Hyaena Cave sediments – a small niche adjacent to the main cave chamber. We use single-grain and multiple-grain dating to clarify the depositional history of the sedimentary sequence, as well as to assess the reliability of the two dating approaches and their potential for future chronological studies at the site. The single-grain and multi-grain ages are consistent with one another and indicate no partial bleaching or post-depositional mixing of the sediments. Our results suggest that Vanguard Cave experienced continuous sediment accumulation probably since the last sea-level highstand in MIS 5, and was completely filled by ~43 ka (MIS 3). The eastern side of the Rock of Gibraltar faced an exposed coastal shelf covered with savannah and an active coastal dune system during MIS 3. Our results indicate that similar environmental conditions are likely to have persisted also during MIS 4 and large parts of MIS 5.

1. Introduction

Current data suggest that the disappearance of Neanderthals in the Iberian Peninsula was more complex than previously thought (Finlayson et al., 2006; Higham et al., 2014). While the timing of Neanderthal persistence in southern Iberia is still a matter of ongoing scientific debate, general consensus exists that there was a temporal overlap between anatomically modern human (AMH) and Neanderthal populations on the European continent (e.g. Finlayson et al., 2006; Higham et al., 2014; Mellars, 2006; Wood et al., 2013). Recent genetic studies have showed that these two human groups even interbred outside Africa (Green et al., 2010), which contradicts a rapid replacement of Neanderthals by AMHs and supports the more complex model of a population mosaic during the Middle to Upper Palaeolithic transition in Europe (Finlayson et al., 2006; Higham et al., 2014).

Central to understanding the process of Neanderthal replacement by, and their interaction with, AMHs in Europe are robust chronological frameworks, coupled with palaeoenvironmental contexts for the conditions under which the contact between the two human groups took place. High resolution archives can be obtained from sites with long stratigraphic sequences yielding indications of long-term occupation by humans in the territory. The archaeological sites of Gibraltar present a unique opportunity to assess the persistence of the last Neanderthals in the same geographical setting as the first AMHs.

The Vanguard Cave (VC) site of Gibraltar contains evidence of Middle Palaeolithic human occupation within a >17 m thick sedimentary sequence. The site is located on the south-eastern coast of the peninsula in close vicinity to the better known Gorham's Cave. Unlike Gorham's – which was discovered in 1907 by A. Gorham and has experienced a long history of academic research since then – the first series of excavations at VC was conducted much more recently (1995-1998) as part of the Gibraltar Caves Project (Barton et al., 2013; Stringer et al., 2000). Despite its later discovery, investigation at VC has had the benefit of more sophisticated analytical methods and the systematic integration of modern sedimentological, archaeological and geochronological data (Table S1).

Up until now, 16 ages provide a chronological overview of VC, but their usefulness and reliability is limited. Seven radiocarbon dates published by Pettitt and Bailey (2000) showed that the cave deposits accumulated close to or beyond the limit of that dating method, and therefore that VC had probably filled to its present level by ~45 thousand years ago (ka). These results were confirmed by the results of multiple(multi-)-grain optically stimulated luminescence (OSL) dating – also often referred to as single aliquot dating - on three sediment samples ranging in age from 46 ± 3 ka to 112 ± 10 ka (Pettitt and Bailey, 2000). Later work, however, indicated a much earlier depositional age for VC of Marine Isotope Stage (MIS) 5 (~74-133 ka, Table S1), based on an OSL chronology comprising one single-grain and six multi-grain age estimates (Rhodes, 2013). Despite conflicting dating results, both studies were further limited by small sample numbers, and provide the age for only a few layers from the >17 m sequence at VC.

Clearly, then, a more careful investigation of the VC sequence and its chronology was in order. Recent renewed archaeological excavations by the Gibraltar Museum at the VC site made such a study possible (Finlayson et al., 2014).

In this paper, we provide a high resolution chronology based on 15 OSL samples collected from the uppermost ~4 m of the recently excavated VC profile and 3 additional samples from Hyaena Cave (HC, previously referred to as the Northern Alcove), a small niche adjacent to the north side of the main cave chamber, and compare both single-grain and multi-grain dating techniques for all samples. A direct correlation between the recently excavated VC section and the previously published stratigraphy

(Macphail et al., 2013) remains a matter of ongoing archaeological work, which is why comparisons between our new OSL chronology with the dating results from Pettitt and Bailey (2000) and Rhodes (2013) are based on absolute sample positions in the profile.

Luminescence dating of mineral grains – such as quartz and feldspar – offers advantages over other chronometric dating methods, particularly at this site, since the datable material is ubiquitous within the sediments; unlike heated lithics required for thermoluminescence dating, and the fact that the organic matter preserved at the site is likely to be older than the upper limits of the radiocarbon technique. OSL dating measures the time elapsed since mineral grains were last exposed to sunlight, with quartz and feldspar grains acting as natural dosimeters for the surrounding environmental radiation (Aitken, 1998). Technical improvements in recent years have enabled the refinement of measurement protocols (Murray and Wintle, 2000) as well as the measurement of luminescence arising from individual grains (Bøtter-Jensen et al., 2000; Duller et al., 1999; Jacobs and Roberts, 2007). Single-grain OSL dating of quartz enables – unlike dating of multi-grain aliquots - the identification of potential problems such as incomplete signal resetting, post-depositional mixing or beta dose rate heterogeneity in sediment samples (Jacobs and Roberts, 2007). Quartz single-grain dating is increasingly adopted for archaeological sites in particular, where these sorts of issues are relatively common and need to be identified (e.g. Doerschner et al., 2016; Fitzsimmons et al., 2014; Jacobs et al., 2012; Tribolo et al., 2010). The measurement of multi-grain aliquots remains advantageous over single-grains when i) each of the aforementioned factors that may bias the real depositional age of a sediment layer can be excluded, since measurement and analyses time is reduced; and ii) luminescence signal intensities of individual grains are comparatively low and difficult to measure, so an aggregate signal can be measured. According to what we know from previous studies, the sediments at VC should have been completely bleached and not subject to post-depositional mixing; nevertheless this is important to test. Consequently, VC provides an excellent context for comparing single-grain with multi-grain dating results, and so we undertake both sets of measurements in this study. Our new, high resolution dual chronology for the uppermost part of the VC sequence and HC aims not only to clarify the timing of sediment deposition and human occupation in the cave, but also to assess the reliability of single-grain vs. multi-grain ages and their suitability for future dating of the lower stratigraphic units at VC. Finally, we place our chronological results in the context of existing Late Pleistocene archaeological and palaeoenvironmental data for the region.

2. Regional setting

The Gibraltar promontory is located at the southernmost tip of the Iberian Peninsula (Fig. 1), forming the northern shoreline of the Strait of Gibraltar which connects the Mediterranean Sea with the Atlantic Ocean. VC (36°7’17’’N, 5°20’30’’W) is part of a complex of limestone caves (which includes Bennett’s, Gorham’s, Vanguard, Hyaena and Boat Hoist among others) close to the present sea-level, facing onto Governor’s Beach which is situated at the south-eastern part of the promontory (Fig. 1). The present beach is dominated by fine limestone blast debris from military tunnelling operations and cemented beach-rock deposits, presumably accumulated during MIS 5 (Jiménez-Espejo et al., 2013; Rodríguez-Vidal et al., 2004; Stringer, 2000). Geomorphic studies of the Rock of Gibraltar have shown that it underwent significant stages of tectonic uplift and eustatic sea-level fluctuations during the Pleistocene (Rodríguez-Vidal et al., 2004; Rodríguez-Vidal et al., 2013). Although the neighbouring caves at Governor’s Beach are currently at sea-level, they faced an emerged coastal shelf with a widespread savannah landscape for most of the last glacial cycle (MIS 5d-2) (Carrión et al., 2008; Finlayson and Carrión, 2007; Rodríguez-Vidal et al., 2013). Substantial aeolian deposits accumulated at Gorham’s

Cave in MIS 3 – during which maximum distance from the caves to the shoreline was up to 5 km (Rodríguez-Vidal et al., 2013) – indicate an actively migrating transgressive dune system in the direct vicinity of the caves at that time (Jiménez-Espejo et al., 2013). As with the other caves, VC preserves a rich stratigraphic sequence comprising more than 17 m of sediment deposits, which have filled the entire cave up to its roof presumably by 45 ka.

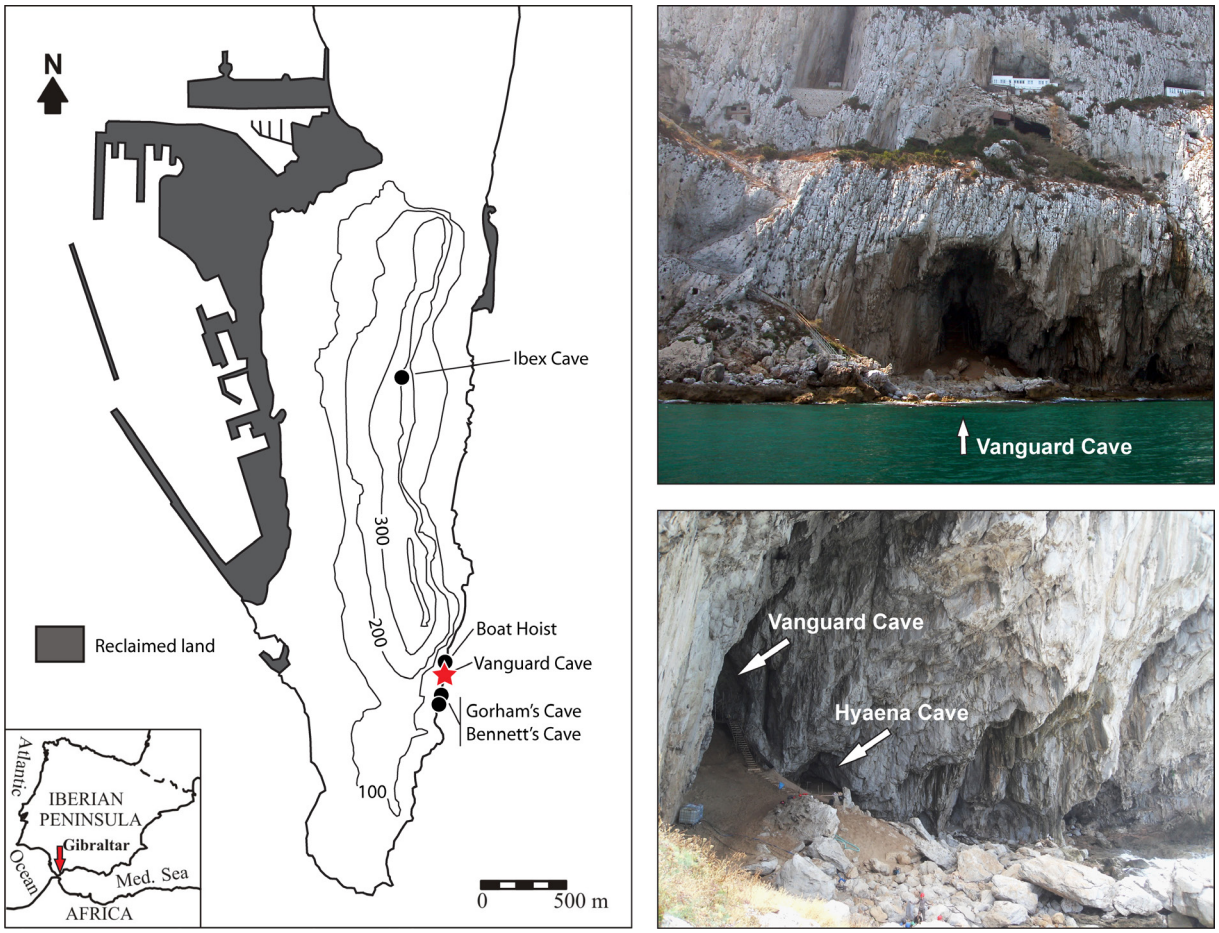

Fig. 1. Location of the Vanguard Cave site, Gibraltar, southern Iberia.

2.1. Cave stratigraphy and sampling context

VC features a stratigraphic sequence composed mainly of massive, coarse-to-medium sands intermixed with tabular-to-lenticular units of silts and silty sands (Macphail and Goldberg, 2000). In the upper excavation area of the cave - uppermost ~5 m of the VC sequence - the sands are interdigitated with black humic clays, showing evidence of phosphatisation (Macphail et al., 2013).

Stratigraphic studies, including comparison of our stratigraphy from the recent excavations with previously published work (Macphail et al., 2013), are still underway. OSL samples were collected by driving stainless steel tubes (4 cm diameter, 10 cm long) horizontally into the freshly excavated profile walls (Fig. 2). Hereafter, since stratigraphic correlation is ongoing, we will use the following summary of the main characteristics of the excavated sediment sections (Table 1):

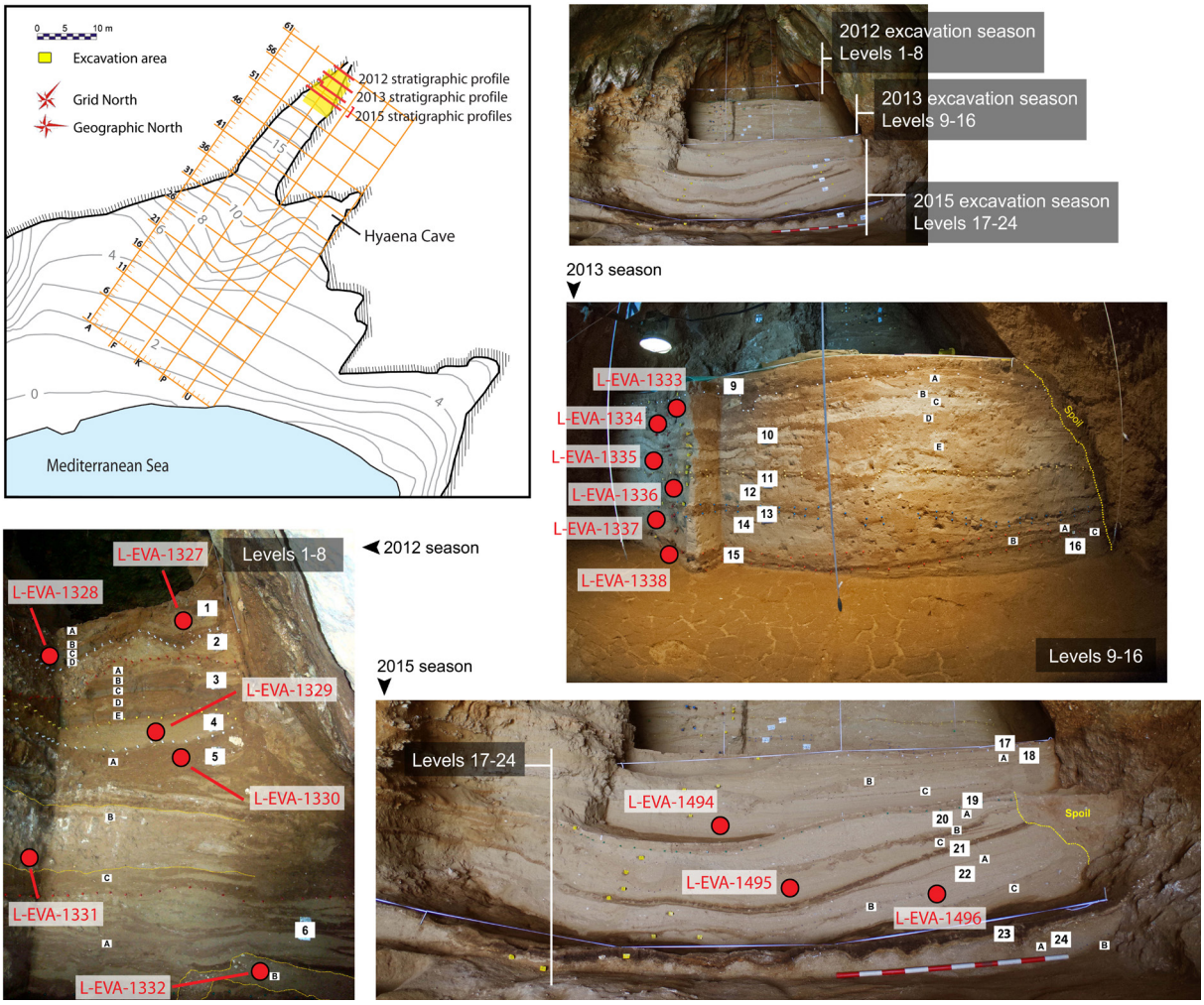

Fig. 2. Plan view map of the Vanguard Cave site and photographs showing the section profiles excavated during the 2012, 2013 and 2015 seasons. Indicated are layer boundaries and positions of the OSL samples.

2015 exposed profile:

The sediments exposed during the 2015 excavation are mainly dominated by sands and clays. The section displays an overall homogeneity within the sedimentary units due to the regular alternation of >20 cm thick sand deposits with 2-10 cm thick palaeoponds (Table 1, Fig. 2). The sand Layers 24, 22 and 18 were subdivided into several sublevels to account for their slightly varying clay contents. Shell fragments and micro-charcoals are present in Layers 19 and 18a, respectively. A cemented crust of red sand was recovered in Layer 24, which is likely to correspond to context 54 described by Macphail et al. (2013).

In Layer 19 a lagomorph in anatomical connection was documented; a circumstance that can be linked to natural intrusions and perturbations in form of burrows. This finding indicates that post-depositional processes clearly affected parts of the sedimentary sequence. The excellent preservation of the clay-rich palaeoponds and their morphology, however, reflect that biological activity and bioturbation (e.g. by trampling) did not dominate the sequence.

Layers 22, 20 and 18 contained Middle Palaeolithic stone tools together with evidences for cut marks, burning and other intentional impacts on bones to access marrow. The faunal assemblage from the 2015 section profile is dominated by small vertebrates – mainly rabbits and birds – but also ungulates appear on a regular basis. Furthermore, one hyaena bone was identified at Layer 18, which, together with a coprolite from Layer 20, indicates that the cave was used by carnivores.

Table 1. Summary of the Vanguard Cave stratigraphy from the 2012-2015 excavations.

Stratigraphic layer	Thickness (cm)	Description	OSL samples (L-EVA-)
2012 exposed profile			
1	15	Brown clay with cemented sand.	1327, 1328
2	15	Whitish sand with limestone gravel.	-
3 (a-e)	15-30	Slightly cemented reddish clay alternated with small amounts of whitish sand. The roof of the layer is eroded by the previous Layer 2.	-
4	15	Disintegrated whitish sand. Not compacted, crumbles easily.	1329
5 (a-c)	60	Mainly composed of alternating strips of cemented clay and sand. 5a is very even and has a high clay content. 5b has the most sand and a browner colour. 5c is similar to 5a. They all display interdigitation	1330, 1331
6 (a,b)	45	Alternating whitish sand and small red clay lenses. 6b has a higher clay and gravel content. Charcoal.	1332
7	10	Reddish clay with sand.	-
8	~2	Clay with greater purity. The layer roof includes abundant dried mud pellets, which can clearly be seen in natural soil that is undisturbed in the archaeological sense of the term.	-
2013 exposed profile			
9	10	Reddish clay with a high sand content.	-
10 (a-e)	25	Alternating whitish sand and red clay lenses.	1333-1335
11	~2	Palaeopond	-
12	10-15	Pure whitish sand.	1336
13	~2	Palaeopond	-
14	15-20	Pure whitish sands with surface irregularities.	1337
15 (a,b)	>2	Palaeopond that splits into two different palaeoponds towards grid E, with a strip of white sand between them.	1338
16	10-15	Pure whitish sand.	-
2015 exposed profile			
17	2-4	Palaeopond that served as the final excavation's palaeosurface. Clay with very low sand content.	-
18 (a-c)	70	Very fine white sand and disintegrated sand. Two very thin clay lenses separate the three sub-layers. The lenses are not continuous over the entire surface of the Layer. 18a corresponds to the roof of the deposit and consists of an even layer (30 cm) of very fine sand filled with shell micro-fragments. 18b (15 cm) contains coarser sand with higher clay content. In the grid E sector, there is a cut-and-fill phenomenon produced by dissolution, pressure or large-scale bioturbation. 18c (20-30 cm) consist of whitish sands without shell micro-fragments.	1494
19	5	Palaeopond with prismatic shaped clay and micro-charcoals. Saved as palaeosurface.	-
20 (a-c)	25	Fine whitish sand interrupted by a homogeneous shale deposit that covers the entire surface of the excavation sector.	1495
21	4-5	Palaeopond.	-
22 (a,b)	35-40	Even, fine, whitish sand. 22b has a higher clay content. It is not continuous throughout the sector and attached to the creeping base of the subjacent layer.	1496
23	3-10	Palaeopond of blackish clay. Thickness is higher in the centre of the excavation area and decreases towards the cave walls. Separated from Layer 24 by a cemented crust of red sand with a very high content of iron oxides. Likely corresponds to context 54 in Macphail et al. (2013).	-
24 (a,b)	35-40	Fine whitish sand similar to Layer 22, with high purity on the ceiling (24a) and higher clay content on the wall (24b).	-

2013 exposed profile:

The stratigraphical Layers 16-9 were exposed during the 2013 excavation season and are, similarly to the underlying sedimentological layers, characterised by alternating thin palaeoponds (~2 cm) with thicker homogeneous sand deposits (Table 1, Fig. 2). Human presence is indicated by a few Middle Palaeolithic stone tools in Layers 16-14 and 12-9. Among the faunal remains, rabbits and birds continue to dominate, the proportion of ungulate bones decreases.

2012 exposed profile:

The uppermost stratigraphical units at VC - Layers 5-1 - are, again, mainly characterised by sands and clays. The layers of this section profile are, however, to varying degrees affected by post-depositional cementation and, compared with the underlying sediments of the VC sequence, relatively heterogeneous due to regularly appearing clay lenses and pockets of cemented sand and gravels (Table 1).

Barton (2013) reported a small number of blades and blade fragments, and a single undiagnostic bladelet, near and above ~40 cm below the top of the sedimentary sequence, respectively. The single bladelet also represents the lowermost Upper Palaeolithic record at VC (Barton, 2013). Of the limited archaeological material that was recovered during the recent excavations, only a few undiagnostic stone tools and charcoal fragments – from Layers 6 and 5 - indicated human presence in the cave. There is clearly a need for further archaeological research in the uppermost parts of the VC profile to learn more about human occupation of the site at that time and to unambiguously verify their cultural affiliation within the Palaeolithic.

The faunal assemblage recovered from the uppermost stratigraphic section at VC is again dominated by small vertebrates, including rabbits and birds. Many of them were semi-articulated and show no biostratinomic modifications, which suggests that they intruded naturally into the cave. Investigations of coprolites and hyaena bones preserved within the sediments (especially Layer 5) reaffirm that hominids and carnivores alternated occupation of the cave. The vertical position of the uppermost layers close to the cave ceiling (Fig. 2) suggests a low entrance that gradually became smaller as the cave filled with sediment.

Hyaena Cave:

The sediments in HC are characterised by massive sands punctuated by numerous clay and silt stringers that thin outwards from cracks in the cave walls, which suggests that they were washed into the cave chamber along joints and fissures of the bedrock (Macphail et al., 2013). Human presence is documented in HC by an oval-shaped hearth and numerous lithic artefacts, including flakes (Barton, 2013). The faunal remains (hyaena and brown bear bones, as well as coprolites) may indicate intensive carnivore denning activities (Currant et al., 2013).

HC was not subject to excavations in recent field seasons. Three pilot OSL samples were collected from homogeneous sand-rich deposits located at the western entrance wall of the chamber to allow general temporal classification of the deposits therein using luminescence dating (Fig. S1).

3. Luminescence dating - Methods

3.1. Sample preparation

Opening of the sampling tubes and sample preparation was undertaken in the luminescence laboratory of the Max Planck Institute for Evolutionary Anthropology (Leipzig, Germany) under subdued red light conditions. Coarse grain quartz (90-300 µm) was extracted from the sediment by a combination of wet and dry sieving, acid cleaning with HCl (10%), H_2O_2 (30%), heavy liquid separation (at both 2.62 g cm^{-3} and 2.68 g cm^{-3} densities) and etching with HF (40%) for 60 min for purification and to remove the outer alpha-irradiated layer. After HF-etching, quartz grains were rinsed with HCl, dried and re-sieved again to extract the 180-212 µm sand fraction, which was used for equivalent dose (D_e) determination.

Multi-grain aliquots of 1 mm diameter (containing ~30 individual grains) were prepared by mounting quartz grains on stainless steel discs using silicon oil and a mask of 1 mm. Single-grain discs were loaded by sweeping individual grains over aluminium discs containing 100 holes with a small brush.

3.2. Experimental details

D_e measurements were made on two automated readers (Risø TL/OSL DA-20 with single-grain attachment), both equipped with calibrated $^{90}Sr/^{90}Y$ beta sources and fitted with 7.5 mm Hoya U-340 detection filters (Bøtter-Jensen, 1997). Light stimulation was performed with infrared diodes (875 nm) and blue LEDs emitting at 470 nm for the multi-grain aliquots, and IR diodes and a 10mW Nd:YVO_4 solid-state green laser (90% power) emitting at 532 nm for the single-grains (Bøtter-Jensen et al., 2000).

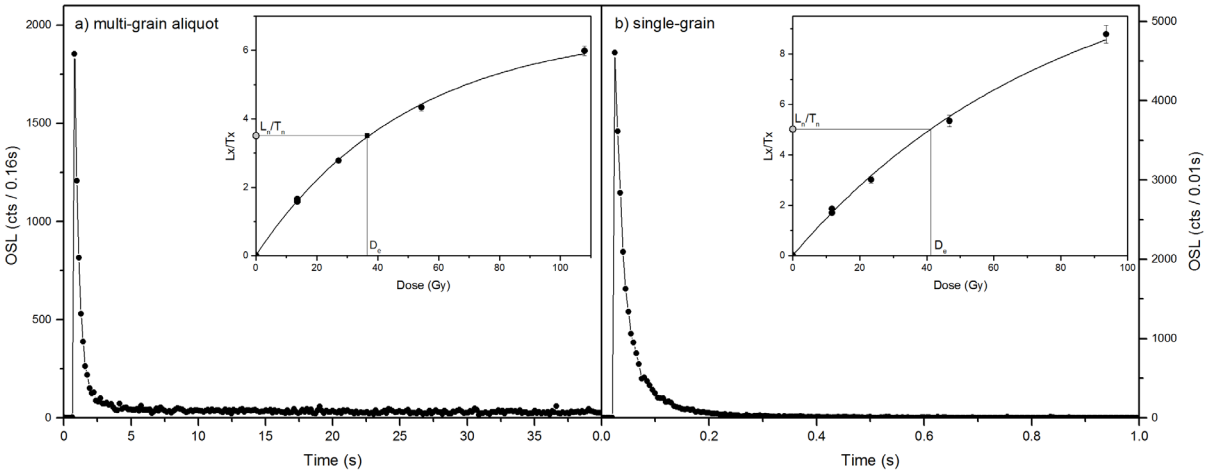

Fig. 3. Representative natural decay curves and (as insets) dose response curves of a (a) multi-grain aliquot, and (b) single-grain of sample L-EVA-1332.

The single-aliquot regenerative-dose (SAR) protocol (Murray and Wintle, 2000, 2003) was applied for performance tests and measurement of the D_es (Tables S2 and S3). In addition to the recycling ratio and recuperation test recommended by Wintle and Murray (2006), we also measured the IR depletion ratio following Duller (2003) to identify potential feldspar contamination in our quartz samples. Early background subtraction was used for D_e determination (Ballarini et al., 2007; Cunningham and Wallinga, 2009). OSL signals were integrated over the first 0.8 s/0.035 s and corrected for background using the subsequent 1.6 s/0.035 s for multi-grain aliquots/single-grains, respectively. Doses were derived by interpolating the natural sensitivity corrected signal (Ln/Tn) from the laboratory generated dose response curve using a single saturating exponential curve fit. Dose estimates were only accepted

for final age determination when (i) showing a Ln/Tn ratio below maximum Lx/Tx of the laboratory measured dose response curve, (ii) the relative uncertainty on the first (natural) test dose signal was less than 10% (15%) for multi-grain aliquots (single-grains), (iii) recuperation was less than 5% and (iv) the recycling ratio and IR depletion ratio were both consistent with unity within 2 standard deviations (details on the single-grain characteristics are given in Table S4).

For each sample, we measured 44 multi-grain aliquots and between 1200 and 2400 individual grains until at least 50 single-grain D_e values passed rejection criteria, as suggested by Rodnight (2008). Two representative signal decay and SAR dose response curves for a multi-grain aliquot and a single grain from VC (sample L-EVA-1332) are shown in Fig. 3.

3.3. Performance tests: assessment of reliability of the samples for dating

Preheat plateau and dose recovery tests using seven different preheat temperatures in 20°C increments (160-280°C) were carried out with a fixed cutheat at 160°C on multi-grain aliquots from all samples to select the most appropriate thermal treatment for each individual sample (Murray and Wintle, 2003; Wintle and Murray, 2006). The variety of performance test results observable in the samples is illustrated in Fig. 4. While sample L-EVA-1332 shows relative thermal stability, L-EVA-1328 is more variable and reaches preheat plateau only at higher temperatures (220-280°C). Dose recovery test ratios, determined based on a given laboratory dose, appear to be unaffected by the selected preheat temperature and lie close to unity (Table S5). According to the results of our performance tests, preheat/cutheat temperatures of 260°C/220°C or 240°C/200°C appeared to be most suitable for our samples and were selected for the final D_e measurement protocols (Table S5).

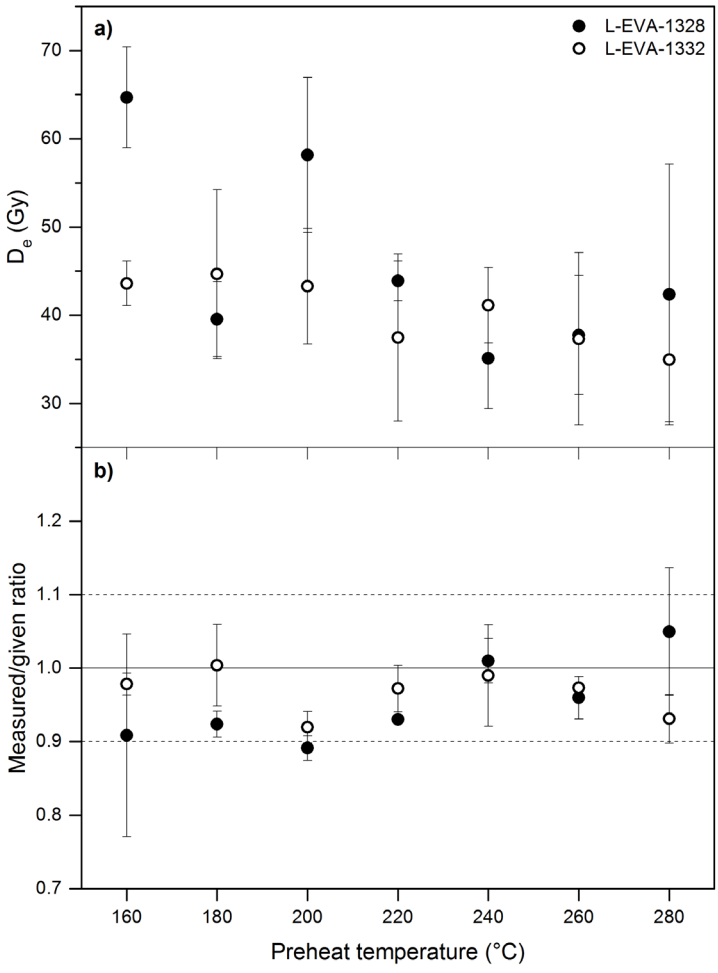

Fig. 4. Results of standard performance tests: (a) preheat plateau test, (b) dose-recovery preheat plateau test for samples L-EVA-1328 (filled circles) and L-EVA-1332 (open circles). The solid line indicates the target values; dashed lines represent 10% deviation from unity.

3.4. Dose rate measurements

External dose rates were calculated using a combination of in situ gamma–ray spectrometry and low-level beta counting (Table 2). Material from the ends of each OSL-sampling tube was dried, milled and homogenised for beta dose rate measurements with a Risø GM-25-5 beta counter (Bøtter-Jensen and Mejdahl, 1985; Bøtter-Jensen and Mejdahl, 1988). For each sample, gamma rays were measured in situ with a portable $LaBr_3$ (Ce) gamma spectrometer. This approach accounts for any spatial heterogeneity in the gamma radiation field surrounding a sample. Gamma dose rates were then determined using the so-called threshold technique (Mercier and Falguères, 2007). The state of secular equilibrium in the ^{238}U and ^{232}Th decay series - which contribute 22-37% and 21-27% to the determined dose rates of the sediments in this study, respectively (Table S6) - was assessed by high resolution germanium gamma spectrometry (HRGS) measurements at the low-radiation background laboratory of the Felsenkeller (VKTA, Dresden/Germany). This method allows identification of potential radioactive disequilibrium resulting from dissolution and transport of soluble daughter products within the ^{238}U and ^{232}Th decay chains (Olley et al., 1996; Olley et al., 1997). Comparisons of daughter-parent isotopic concentrations indicate that both radioactive decay chains are secular equilibrium (Fig. S2), and therefore it is assumed that dose rates have remained constant with time. The cosmic dose rate was calculated according to Prescott and Hutton (1994) from the altitude and geomagnetic latitude of the site, burial depth, and density of the overburden. Due to the sheer magnitude of the Rock of Gibraltar rising up to >400 m above sea-level (a.s.l.), the cosmic dose rate determined for the VC samples - assuming an effective burial depth of 50 m - is reduced to an almost negligible level (Table 2). An additional 0.03 ± 0.01 Gy/ka was added to the final dose rate calculation to account for internal dose rate of the quartz grains (Bowler et al., 2003; Jacobs et al., 2006; Vandenberghe et al., 2008).

Table 2. Dosimetric results.

Sample	Layer	Depth (cm)	Moisture content (%)	Dose rate (Gy/ka)			
				Beta[1]	Gamma[1]	Cosmic[1]	Total
Vanguard Cave							
L-EVA-1327	1	27	5±3	0.38±0.02	0.21±0.02	0.003±0.001	0.62±0.04
L-EVA-1328	1c	43	5±3	0.55±0.02	0.27±0.03	0.003±0.001	0.86±0.04
L-EVA-1329	4	76	5±3	0.31±0.02	0.37±0.04	0.003±0.001	0.71±0.05
L-EVA-1330	5a	90	5±3	0.67±0.02	0.37±0.04	0.003±0.001	1.07±0.05
L-EVA-1331	5c	145	5±3	0.56±0.03	0.33±0.03	0.003±0.001	0.93±0.09
L-EVA-1332	6b	175	5±3	0.23±0.02	0.31±0.03	0.003±0.001	0.57±0.10
L-EVA-1333	10a-c	218	5±3	0.34±0.03	0.30±0.03	0.003±0.001	0.67±0.06
L-EVA-1334	10a-c	230	5±3	0.28±0.01	0.25±0.03	0.003±0.001	0.56±0.06
L-EVA-1335	10d-e	251	5±3	0.29±0.02	0.22±0.02	0.003±0.001	0.54±0.04
L-EVA-1336	12	273	5±3	0.24±0.02	0.24±0.02	0.003±0.001	0.52±0.05
L-EVA-1337	14	296	5±3	0.24±0.02	0.24±0.02	0.003±0.001	0.51±0.05
L-EVA-1338	15	310	5±3	0.40±0.03	0.27±0.03	0.003±0.001	0.71±0.04
L-EVA-1494	18c	345	5±3	0.30±0.02	0.24±0.02	0.003±0.001	0.57±0.04
L-EVA-1495	20c	390	5±3	0.30±0.02	0.22±0.02	0.003±0.001	0.54±0.04
L-EVA-1496	22b	408	5±3	0.28±0.02	0.21±0.02	0.003±0.001	0.51±0.04
Hyaena Cave							
L-EVA-1339	top	82	5±3	0.39±0.03	0.24±0.02	0.003±0.001	0.66±0.06
L-EVA-1340	middle	128	5±3	0.36±0.02	0.25±0.03	0.003±0.001	0.64±0.06
L-EVA-1341	bottom	164	5±3	0.34±0.03	0.25±0.03	0.003±0.001	0.62±0.05

[1] Attenuaded with respect to the moisture content.

An average life-time moisture content of 5 ± 3% was assumed to represent a reasonable average for these well-drained sandy sediments (Table S6). These values were incorporated into dose rate calculations to account for attenuation (Mejdahl, 1979). Full saturation moisture values were estimated

as the ratios of absorbed water to dry weights and vary between 17.0 and 20.2%. Field moisture content was determined by averaging moisture content values from the OSL samples and the sealed plastic bags containing the surrounding sediment (0.1-5.1%).

4. Results

4.1. Single-grain D_e values

Of the 28,400 individual quartz grains measured in this study, only 1295 grains (4.6%) passed all rejection criteria and were used for final D_e determination. The most frequent causes for discarding individual grains (Table S4) were i) absence of an initial luminescence signal significantly above background (73.3-87.5%) and ii) an insufficient test-dose signal (5.8-17.6%). Only small numbers of grains were rejected due to saturation of the natural signal, feldspar contamination, poor recycling ratios or elevated recuperation doses.

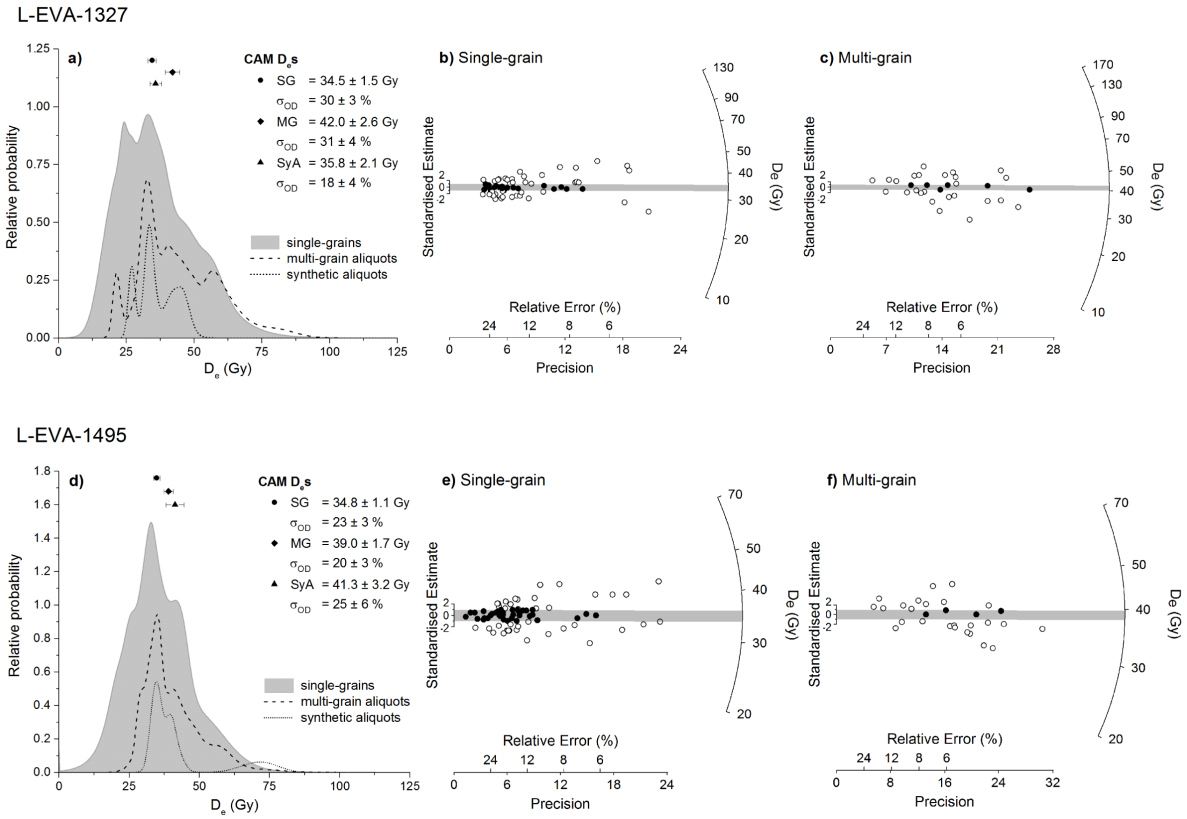

Fig. 5. D_e distributions of sample L-EVA-1327 and L-EVA-1495: (a,d) probability density function plots of single-grains, multi-grain aliquots and synthetic aliquots, (b,e) single-grain radial plots and (c,f) multi-grain radial plots, respectively.

Representative single-grain D_e distributions for samples L-EVA-1327 and L-EVA-1495 are shown in Fig. 5; those for the remaining samples are given in the supplementary material (Figs. S3-S8). All D_e distributions are displayed as probability density function (pdf) plots as well as radial plots and appear to be generally Gaussian, indicating unmixed sediments for which OSL signals were completely reset prior to deposition. Almost all samples, however, yield overdispersion (σ_{OD}) values exceeding 20% (σ_{OD} range: 18-35%, Table 3). Such values are often considered too high to represent a population of well-bleached single quartz grains (Jacobs et al., 2011; Jacobs et al., 2008a; Olley et al., 2004). More recent studies (Guérin et al., 2015; Thomsen et al., 2012), on the other hand, convincingly argue that there

is no justification for a 20% limit on σ_{OD} - which can reach up to 62% (Guérin et al., 2015) - for well-bleached single-grain samples. Based on the latter arguments, combined with our observations of Gaussian D_e distributions, we used the Central Age Model (CAM, Galbraith et al., 1999) to calculate the D_e for all samples (Table 3).

Synthetic aliquots were generated from the single-grain dataset by summing the luminescence signals emitted from every grain per single-grain disc (each containing 100 grains). The determined D_e distributions are shown in the probability density plots of Figs. 5 and S3-S5 in order to compare with the single-grain and multi-grain data (also see Table S5). The pdf plots of synthetic aliquots agree with the results of single-grain measurements. The resulting CAM D_es from the synthetic aliquots are generally consistent but tend to slightly overestimate at 1-sigma compared to single-grains in 9 out of the 18 samples (Table S5), in particular when the D_es are close to or exceed 40 Gy. Calculation of age estimates based on synthetic aliquots was omitted because of the limited number of aliquots available per sample.

4.2. Multi-grain D_e values

Multi-grain D_es were determined based on between 26 and 41 aliquots per sample (Table S5). Pdf and radial plots show relatively narrow, Gaussian multi-grain D_e distributions (Figs. 5, S3-S5 and S9-S11). This is to be expected considering that they represent averaged luminescence signals derived from 30-40 individual grains. Critically, the main peaks closely match the dose distributions derived from the single-grain and synthetic aliquot data (Figs. 5 and S3-S5). σ_{OD} values range between 15-31% - except in the case of sample L-EVA-1496 (σ_{OD}: 40%) - and CAM derived D_es are overall in good agreement with the single-grain D_es (see age ratio in Table 3). When comparing multi-grain and synthetic aliquot results at 1-sigma, it is striking that multi-grain D_es are systematically lower than those derived from artificially created aliquots in 8 out of 18 samples in this study (synthetic aliquot/multi-grain D_e ratios >1.10, Table S5). For sample L-EVA-1327, however, single-grains and synthetic aliquots reveal consistent D_e values around 35 Gy, while multi-grain aliquots yield a CAM D_e of 42.0 ± 2.6 Gy.

4.3. Dosimetry

The dose rates for samples in this study are relatively low and range from 0.51 ± 0.04 to 1.07 ± 0.05 Gy/ka (Table 2). While dose rates are consistent from Layer 6b to Layer 22b and in HC (0.51 ± 0.04 - 0.71 ± 0.04 Gy/ka), substantial variability – mainly in the beta dose component - occurs within the uppermost 120 cm of the VC profile (Layer 1 to 5c). Layers 1 (L-EVA-1327) and 4 (L-EVA-1329) yield comparatively low dose rates (0.62 ± 0.04 Gy/ka and 0.71 ± 0.05 Gy/ka, respectively), in Layers 1c (L-EVA-1328), 5a (L-EVA-1330) and 5c (L-EVA-1331) dose rates increase up to 1.07 ± 0.05 Gy/ka. Increasing concentrations of radioactive minerals (Table S6) are most likely responsible for this growth.

4.4. Ages

The OSL ages for single-grain and multi-grain measurements were calculated from the CAM-derived D_e values and the associated total dose rates for each sample (Table 3). The stratigraphically oldest excavated sediment layers from the VC sequence and the three samples from HC were deposited during the transitional period between the end of MIS 5 and the onset of MIS 4 (Fig. 6a,b). Sample L-EVA-1496 (VC Layer 22b) dates to 66 ± 6 ka and 65 ± 7 ka and sample L-EVA-1341 (bottom sample HC) to 73 ± 7 ka and 62 ± 6 ka, based on single-grain and multi-grain measurements, respectively. Ages

Table 3. OSL dating results.

Sample	Layer	Total dose rate (Gy/ka)	Single-grains			Multi-grain aliquots			Age ratio (SG/MG)
			n[1]	Age[2] (ka)	σOD[2] (%)	n1	Age[2] (ka)	σOD[2] (%)	
Vanguard Cave									
L-EVA-1327	1	0.62±0.04	63/1400	55.6±4.2	30±3	31/44	67.7±5.8	31±4	0.82±0.08
L-EVA-1328	1c	0.86±0.04	61/1200	43.0±2.7	25±3	32/44	43.1±2.7	19±3	0.99±0.06
L-EVA-1329	4	0.71±0.05	71/2000	54.6±4.2	20±3	28/44	51.3±4.3	23±3	1.06±0.08
L-EVA-1330	5a	1.07±0.05	69/2200	51.1±3.3	32±3	28/44	43.0±3.0	25±4	1.19±0.07
L-EVA-1331	5c	0.93±0.09	71/1900	50.2±5.4	23±3	30/44	44.6±4.9	19±3	1.13±0.11
L-EVA-1332	6b	0.57±0.10	74/1200	60.4±11.0	32±3	37/44	60.8±11.0	19±3	0.99±0.18
L-EVA-1333	10a-c	0.67±0.06	93/1200	52.7±5.3	22±2	41/44	58.2±5.9	20±2	0.91±0.10
L-EVA-1334	10a-c	0.56±0.06	69/1200	63.8±7.0	18±3	37/44	64.2±7.1	18±2	0.99±0.11
L-EVA-1335	10d-e	0.54±0.04	67/1200	66.3±5.5	29±3	33/44	67.6±5.3	17±2	0.98±0.08
L-EVA-1336	12	0.52±0.05	68/1200	65.6±6.9	25±3	28/44	65.1±7.0	20±3	1.01±0.11
L-EVA-1337	14	0.51±0.05	90/1200	65.1±6.8	26±3	40/44	66.1±6.8	15±2	0.99±0.11
L-EVA-1338	15	0.71±0.04	78/2200	57.1±3.9	28±3	29/44	57.2±3.9	17±3	0.99±0.07
L-EVA-1494	18c	0.57±0.04	77/1200	60.1±4.6	28±3	26/44	65.3±5.7	28±4	0.92±0.08
L-EVA-1495	20c	0.54±0.04	73/1200	64.5±4.9	23±3	29/44	72.3±5.7	20±3	0.89±0.08
L-EVA-1496	22b	0.51±0.04	65/1200	65.6±5.7	35±4	30/44	64.6±6.6	40±5	1.02±0.09
Hyaena Cave									
L-EVA-1339	top	0.66±0.06	72/2400	70.0±6.9	27±3	31/44	65.3±6.5	21±3	1.07±0.10
L-EVA-1340	middle	0.64±0.06	69/2200	70.3±7.0	31±3	30/44	61.5±5.9	18±3	1.14±0.10
L-EVA-1341	bottom	0.62±0.05	65/2100	73.1±7.0	30±3	36/44	62.4±5.7	16±2	1.17±0.10

[1] Number of accepted/measured grains or aliquots.
[2] Determined using the Central Age Model (Galbraith et al., 1999). All age errors represent 1-sigma confidence levels.

decrease up the sequence between Layer 22b and Layer 6b (L-EVA-1332, ~60 ka) (Fig. 6a) and indicate relatively rapid sediment accumulation during MIS 4 at the site (>2 m in less than 10 ka). There appears to be a depositional hiatus of several thousand years between Layer 6b and the overlying layers 5c-1 (L-EVA-1331 - L-EVA-1327), which yield – with the exception of Layer 1 - stratigraphically consistent single-grain ages of ~55-43 ka and multi-grain ages of ~51-43 ka (MIS 3). Finally, sample L-EVA-1327 collected from the uppermost Layer 1 of the VC sequence – which is located in direct vicinity to cave wall and ceiling – date to 56 ± 4 ka and 68 ± 6 ka using single-grains and multi-grain aliquots, respectively. L-EVA-1327 is the only sample in this study that yields stratigraphically inconsistent ages. This sample appears to be significantly older than the underlying sediment layers, and furthermore the single- and multi-grain results do not fall within error of one another (Fig 6a).

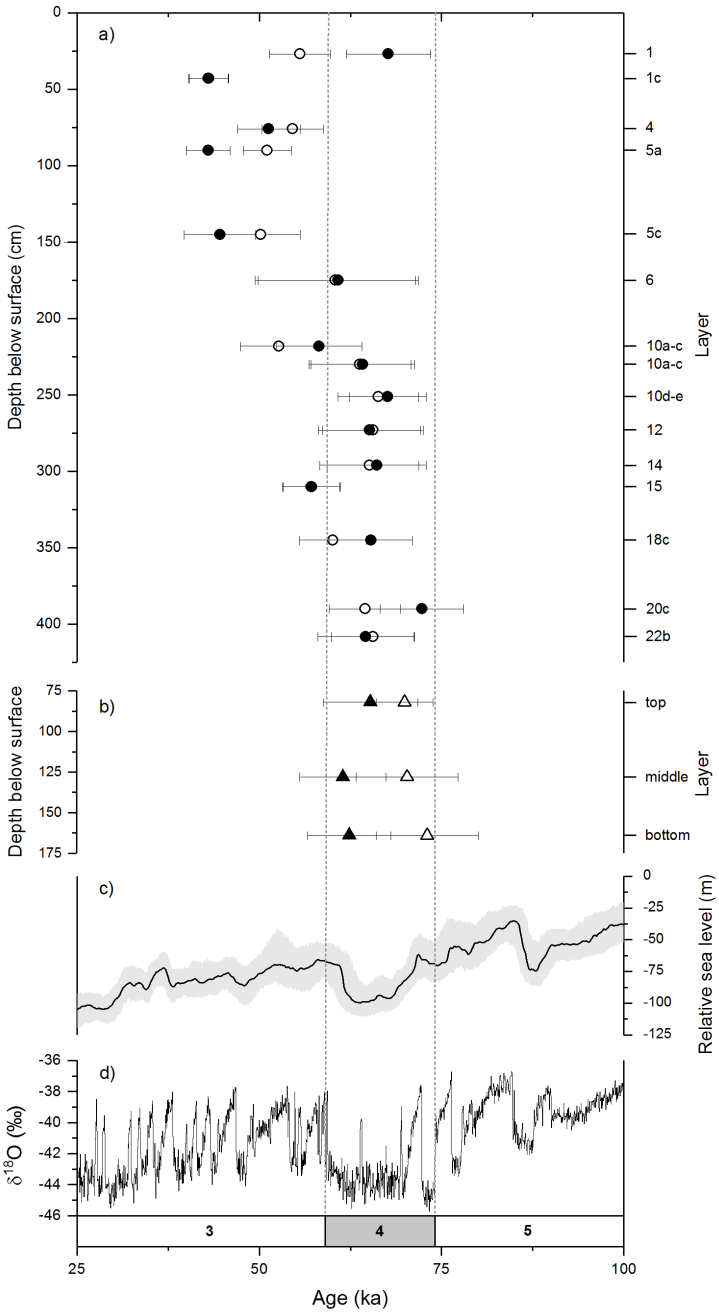

Fig. 6. Age-depth profile of (a) Vanguard Cave and (b) Hyaena Cave using OSL dating on single-grains (open circles) and multi-grain aliquots (filled circles); (c) Red Sea relative sea-level record (probability maximum, black; 95% confidence interval, light grey) (Grant et al., 2014) and (d) NGRIP GICC05 oxygen isotope record (Rasmussen et al., 2014; Seierstad et al., 2014).

5. Discussion

5.1. Reliability of single-grain and multi-grain ages

In Fig. 7, single-grain ages are plotted against their paired multi-grain ages. Ages derived from the two OSL techniques for this site are consistent with one another and fall well within 10% of the 1:1 line. The median ratios of single-grain to multi-grain age are 0.936 and 1.126 for the VC and HC samples, respectively (see also Table 3 for age ratios of each sample). This suggests that while single-grain ages tend to be slightly younger than the associated multi-grain ages in the VC sequence, the opposite appears to be the case for sediments in HC. Fig 6a shows that there is - apart from this general trend - some variability observable in the age estimates for the VC samples; single-grains yield sometimes older (Layers 1, 10a-c, 18c, 20c) and sometimes younger (Layers 4, 5a, 5c) ages than the corresponding multi-grain aliquots. This variability nevertheless lies – except for Layer 1 and 5a - within given error ranges and can be considered natural. Less clear is whether the systematically younger single-grain ages relative to multi-grain aliquots is truly valid for HC sediments (Fig. 6b), given small sample size and the consistency within error margins. Additional sample collection and OSL dating at HC would be necessary to further investigate this trend and its potential causes. Nevertheless, the overall good agreement between the two applied OSL dating techniques (Fig. 7), together with the Gaussian D_e distributions (Figs. 5 and S3-S5), emphasises the well-bleached and unmixed nature of all sediments from VC site.

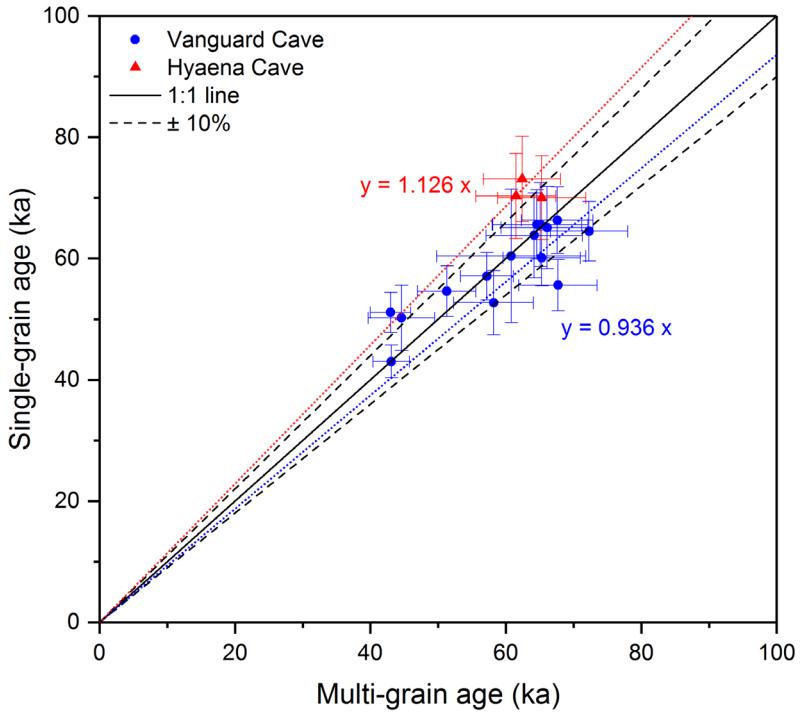

Fig. 7. Single-grain OSL ages as a function of multi-grain OSL ages for all Vanguard Cave (blue circles) and Hyaena Cave (red triangles) samples in this study. Error bars indicate age uncertainties at 1σ. (For interpretation of the references to colour in this figure legend, the reader is referred to the online version of this article.)

There are only two samples in this study for which the calculated age estimates using single-grains and multi-grain aliquots do not overlap within given error margins (Table 3, Fig. 6a): sample L-EVA-1327 (Layer 1) and L-EVA-1330 (Layer 5a). Both samples were collected from the uppermost 150 cm of the VC profile, which are characterised by rather inhomogeneous sand and clay deposits intercalated

with numerous small lenses of either clay- or carbonate-rich materials. This complex stratigraphy is reflected in the variable dose rates determined for different layers in these parts of the profile (Tables 1, S6). Dose rate variability in the laminated sediments is not surprising, since clays typically have high potassium concentrations and carbonates reduce the overall dose rate (Murray and Roberts, 1997; Olley et al., 1997). Variations in microdosimetry are also likely to influence the resulting D_es of sediments in this part of the profile at single-grain level for the same reason.

Layer 5a (L-EVA-1330) consists of comparatively clay-rich material and yields the highest total dose rate determined for sediments in this study (1.07 Gy/ka). Single-grain data show a relatively wide but nevertheless Gaussian distribution (Fig. S3c) which strongly suggests heterogeneity in the beta dose rates (Lomax et al., 2007). Multi-grain aliquot D_es are unaffected by this effect due to dose averaging. In this case we felt that single-grain results more closely reflected the true situation and therefore favoured the single-grain age for Layer 5a.

By contrast, Layer 1 (L-EVA-1327, Fig. 5) had experienced post-depositional cementation by carbonates which are likely to have altered the environmental dose rate of the sediments through time. Furthermore, this sample was collected in close vicinity to cave wall and ceiling, and may have been affected by the incorporation of carbonate fragments and larger clasts derived from the limestone bedrock which serve as low-radioactivity cold spots in sandy or clayey sediments and cause variations in beta microdosimetry (Jacobs et al., 2008a; Jacobs et al., 2008b; Olley et al., 1997). The dose rate at single-grain level of Layer 1 will consequently vary through both space and time; the resulting of which will be obscured through averaging in multi-grain D_e distributions. We therefore recommend that any dating results from this layer should be treated with caution. Our measured total dose rates derive from present day conditions and may not accurately reflect dose rates through time, potentially resulting in an underestimation of the true burial-time dose rate of the sediment. Calculated final ages for sample L-EVA-1327 therefore only serve as maximum ages for the deposition of Layer 1.

Studies suggest that the majority (90-95%) of an emitted luminescence signal commonly derives from 5-10% (or less) of the grains within a given sample (Duller et al., 2000; Jacobs et al., 2003). Measurements of small multi-grain aliquots (1-2 mm) - especially in samples which are characterised by small amounts of grains yielding sufficient luminescence signals to allow D_e determination - are, therefore, likely to be dominated by the signal of just a few individual grains (Duller, 2008). In this study, the proportion of grains exhibiting luminescence signals below background, and for which the relative uncertainty on the natural test-dose signal is more than 15%, varies between 86.7% and 93.3% (Table S4). Consequently, multi-grain aliquots - consisting of ~30 individual sand grains - on average contain only 2-4 grains that are suitable for D_e determination. Taking all quality criteria for single-grains applied in this study into account, the amount of individual grains acceptable for D_e determination is further reduced to 3.1-7.8% (Table S4) or – in other words – 1-2 individual grains per multi-grain aliquot. As a consequence of the relatively few grains from the VC and HC sediments yielding luminescence signals for dating, the averaging effect in multi-grain aliquots is reduced, and it is this which is responsible for the observed consistency between single-grain and multi-grain ages. On the other hand, D_es from synthetic aliquots, for which luminescence signals of 100 grains are summed, are more likely to be dominated by just a few bright grains yielding significantly above-average D_e values. The presence of small numbers of this type of individual grains and their increasing effect on determined D_es of synthetic aliquots in the sediments was proven in a methodological exercise on the luminescence signal characteristics of individual grains (for further details see Appendix C in the supplementary material). As a consequence of the difference in single-grain luminescence characteristics in our samples, D_es of synthetic aliquots are considerably higher than approximately half of the D_es calculated based on single-grains and multi-grain aliquots (Table S5).

Despite overall good agreement, single-grain ages in this study are considered to be more reliable then multi-grain ages not only because they are not subject to any averaging effects but also due to their larger sample size - 61-93 individual grains in contrast to 26-41 aliquots per sample - which improves our understanding of the timing of sediment deposition. Notwithstanding the above, both OSL dating techniques yield reliable results in this study and can, therefore, be safely recommended for future dating projects at the site.

5.2. Comparison with previous chronological work

Here we present the first high resolution OSL chronology for the recently excavated uppermost ~4 m of the VC profile (Fig. 6). Previous work so far yielded eleven OSL and six radiocarbon dates (for a summary see Table S1), and mainly focussed on age constraint of sediment layers further down the 17 m profile (Pettitt and Bailey, 2000; Rhodes, 2013). This, unfortunately, limits the direct comparison of our OSL chronology to previously published ages to one multi-grain OSL age (X730, (Rhodes, 2013)) and three radiocarbon dates (OxA-7389, OxA-6998 and OxA-7191 (Pettitt and Bailey, 2000)) from ~40 cm, ~170 cm and ~400-420 cm below the top of the sedimentary sequence, respectively (Fig. 14.1 in Rhodes, 2013). As already outlined, a direct correlation between the published VC stratigraphy (Macphail et al., 2013) and the one developed during recent excavations remains incomplete. Rather we compare the ages of the aforementioned four samples with our chronology based on their absolute position below the top of VC's sedimentary sequence.

Sample X730 was collected 40 cm below the sequence top and dated using multi-grain aliquots (5 mm diameter, ~300 grains) to 73.7 ± 5.3 ka (Rhodes, 2013). Given what we know of the luminescence characteristics of the sediments at VC (Section 5.1 and Appendix C in the supplementary material), age overestimation due to biasing effects of a few extremely bright grains is even more likely for multi-grain aliquots (containing ~300 individual grains each) than for the synthetic aliquots in our study (summed signal from 100 grains each). Hence, it is not surprising that sample X730 is significantly older than any of our single-grain ages from the uppermost 150 cm of the VC profile. The age is, however, consistent with the multi-grain age of Layer 1 (L-EVA-1327, 67.7 ± 5.8 ka). Given that the dose rate surrounding L-EVA-1327 is likely to have varied in the past due to post-depositional carbonate cementation of the sediments (Section 5.1), a similar sedimentological history can be assumed for sample X730 since it originates from "brecciated deposits adhering to the rock wall" (Barton and Collcutt, 2013). It remains unclear whether the apparent age overestimation in sample X730 is solely a result of aliquot size, variable dose rate with time, or a combination of both. Additional measurements on the original sample material using single-grains would be necessary for further clarifications.

Pettitt and Bailey (2000) provided a date from a charcoal sample (OxA-7389) collected from ~170 cm below the sequence top of 49.1 ± 3.0 ky cal BP (45.2 ± 2.4 ky BP). The stratigraphically closest OSL sample from our study is L-EVA-1332 (Layer 6b) which yields a statistically consistent - due to large uncertainties - single-grain age of 60.4 ± 11.0 ka. Two additional ^{14}C samples, OxA-6998 (charcoal) and OxA-7191 (bone), collected from ~400-420 cm below the sequence top, roughly correspond to our Layer 22 (single-grain: 65.6 ± 5.7 ka), and yielded dates of 45.5 ± 1.5 ky cal BP (41.8 ± 1.4 ky BP) and 11.8 ± 0.3 ky cal BP (10.2 ± 0.1 ky BP), respectively. The latter age (OxA-7191) was argued to be an underestimate due to limited preserved collagen (Pettitt and Bailey, 2000). Caution is also required when assessing the validity of the five remaining radiocarbon dates for the VC sequence (Table S1), since they yield values at the upper limit of this dating technique and lack stratigraphic consistency. Consequently, it seems reasonable to consider these dates as providing minimum constraints on the deposition of the associated sedimentological layers.

In addition to the chronological work performed on the main VC sequence, Pettitt and Bailey (2000) dated a charcoal fragment from a hearth in HC to >47.6 ky cal BP (>44.1 ky BP, OxA-7078). This minimum date is considerably younger than, but therefore not inconsistent with, the three OSL samples from our study which were collected from the western entrance wall of the chamber and yielded single-grain ages between ~70 ka and ~73 ka. Additional dating work in the inner part of HC is required to clarify the depositional history of the sediments and the age of the hearth therein.

5.3. Archaeological and palaeoenvironmental implications

The >17 m sedimentological sequence at VC is mainly composed of aeolian sand deposits overlying a fossilized marine beach which formed during the MIS 5 sea-level highstand (Rodríguez-Vidal et al., 2004). The uppermost ~4 m of the cave sequence represents a broadly continuous sediment deposition between the onset of MIS 4 (~66 ka) and MIS 3 (~43 ka), with a potential accumulation hiatus of a few thousand years between ~60 ka and ~50 ka – Layer 6b and 5c, respectively (Fig. 6).

Human activity at VC can be traced throughout the recently excavated sections in the form of, for example, Palaeolithic stone tools, cut-marked bones and evidence of burning, which indicates repeated and intentional occupation of the site. While the stone tools recovered from Layers 9-22 are diagnostic of Middle Palaeolithic industries made by Neanderthals, lithic assemblages in the uppermost layers of the cave fill sequence are more ambiguous, despite previous links to the Upper Palaeolithic (Barton, 2013). Not only are artefacts in these layers sparsely scattered (n=7 artefacts during the 2012 excavations), they are also largely undiagnostic. We argue that further work in new excavation areas is required to reliably attribute cultural classification to the finds.

Intensive research has been conducted in recent years to reconstruct the landscape, climatic conditions and ecological environment of south-eastern Iberia between MIS 5 and MIS 2 (e.g. Blain et al., 2013; Carrión et al., 2008; Finlayson, 2006; Finlayson and Carrión, 2007; Finlayson et al., 2006; Jiménez-Espejo et al., 2013; Rodríguez-Vidal et al., 2013; Zilhão et al., 2016). Of particular importance for understanding the depositional history of the VC sediments is the presence of an extensive, now submerged, coastal shelf at the east side of the Rock, directly in front of the caves' entrances at Governor's Beach during MIS 3 when sea-level was significantly lower (Fig. 6). At that time, the shoreline was up to 5 km away (Rodríguez-Vidal et al., 2013) and the coastal plain was covered with savannah and sand dunes formed by easterly winds. These dunes provided the main sediment source for the Catalan Bay sand ramp – a >300 m thick dune complex at the east side of the Rock with Ibex Cave (290 m) roughly indicating its highest elevation a.s.l., although it may have reached higher as parts were removed by the military in the 18th Century (Fig. 1) – and for the caves' infills (Jiménez-Espejo et al., 2013; Rodríguez-Vidal et al., 2013).

Studies on the faunal record of Gorham's and VC indicate a mild and sub-humid Mediterranean climate during times of Neanderthal occupation at Gibraltar (MIS 5-3), similar to that found in southern Iberia today (Blain et al., 2013; Finlayson, 2006; Stringer et al., 2008). While winters were colder in MIS 3, summers and mean annual precipitation rates were similar to present day conditions (Blain et al., 2013; Finlayson, 2006). The geomorphic evidence from the long, homogeneous sequence at VC, extending from ~43-73 ka, strengthens the view that relatively stable palaeoenvironmental conditions with strong easterly winds persisted from MIS 5 to MIS 3 in the region (Carrión et al., 2008; Finlayson, 2006; Finlayson and Carrión, 2007; Finlayson et al., 2006; Rodríguez-Vidal et al., 2013), when sea-level was between 30 m and 100 m lower than today (Grant et al., 2014). Although large portions of the sequence have never been excavated, the results from our recent and former investigations (Barton et al., 2013; Stringer et al., 2000) indicate that the VC deposits provide an archaeological and palaeoenvironmental

record of that time at a high resolution, due to relatively high accumulation rates.

Intensive research has been carried out at Gorham's Cave in the last years which greatly improved our knowledge about the ecological and climatic conditions in south-eastern Iberia during MIS 3 and MIS 2 (e.g. Blain et al., 2013; Carrión et al., 2008; Fa et al., 2016; Jiménez-Espejo et al., 2013) – a time which is critical to understand the eventual replacement of Neanderthals by AMHs in Europe – and about the way human groups interacted with the prevailing environment (e.g. Blasco et al., 2016; Finlayson et al., 2012, 2016; Rodríguez-Vidal et al., 2014). With a sedimentological sequence preceding the deposits recovered at Gorham's Cave, VC bears future potential to shed light on a less well understood time range (MIS 4-5) in the history of human populations in the area and to provide a baseline for environmental conditions that persisted during a time of Neanderthal dominance and before AMHs arrived in the region.

6. Conclusion

This study presents a chronostratigraphy for the uppermost part of the VC sequence, Gibraltar, suggesting that the cave comprises a sedimentary record at high resolution overlying MIS 5 marine terrace which sits at the present sea-level. The VC sequence was continuously deposited until the cave was completely filled to its roof at ~43 ka (MIS 3). While sediments in the uppermost 150 cm of the VC profile are relatively variable, a continuous alternation of sand layers and palaeoponds continues further down the sedimentary sequence. Human – most likely Neanderthal - presence in the cave can be traced throughout most of its depositional history and indicates repeated occupation phases during the Late Pleistocene. Although only parts of the >17 m sedimentary profile have been excavated, the site offers the great potential for current and future studies to investigate human-environmental interactions in south-eastern Iberia from MIS 5 to MIS 3, over a period when sea-level was significantly lower than today and the cave faced an emerged coastal shelf.

A comparison between single- and multi-grain OSL dating was implemented with the aim of creating a reliable dual chronology for the uppermost part of the VC sequence and to examine the suitability of the different methodological approaches for future dating projects at the site. The good agreement between the two OSL methods is a result of the luminescence characteristics of the VC sediments (low proportion of grains suitable for D_e determination) and the size of multi-grain aliquots (1 mm) used in this study. Both factors contribute towards a reduction of averaging effects in multi-grain measurements. The VC sediments consist, moreover, of substantial amounts of relatively bright grains which are likely to superimpose the signals of dimmer grains. OSL dating using multi-grain aliquots larger than 1 mm is, consequently, highly likely to produce dates that significantly overestimate the true burial age of the sediments. Therefore, small multi-grain aliquots or preferably dating of individual grains is recommended to reliably date the lower part of the >17 m stratigraphical sequence at VC or sediments of similar depositional origin at Gibraltar.

Acknowledgements

This research was funded by the Max Planck Institute for Evolutionary Anthropology (MPI-EVA). Excavations at Vanguard Cave were funded by H.M. Government of Gibraltar. J. Rosell and R. Blasco develop their work within the Spanish MINECO projects CGL2015-65387-C3-1-P (J. Rosell) and CGL2015-68604-P (R. Blasco), the Generalitat de Catalunya-AGAUR projects 2014 SGR 900 and 2014/100573, and the SéNeCa Foundation project 19434/PI/14. The authors would like to thank the members of the Department of Human Evolution (MPI-EVA) and especially Steffi Hesse for her valuable support during sample preparation and OSL measurements in the laboratory as well as during the writing process. We thank Norbert Mercier (Université Bordeaux Montaigne) and Marion Hernandez for their support with the $LaBr_3$(Ce) gamma spectrometer setup. Special thanks go to the excavation team from Vanguard Cave for their dedicated and active cooperation during fieldwork and to Detlev Degering (VKTA Dresden) for performing the γ-ray spectrometry measurements on the OSL samples. The authors also wish to thank the three anonymous reviewers for their constructive and helpful comments on earlier versions of this article.

References

Aitken, M.J., 1998. An Introduction to Optical Dating. Oxford University Press, Oxford

Ballarini, M., Wallinga, J., Wintle, A.G., Bos, A.J.J., 2007. A modified SAR protocol for optical dating of individual grains from young quartz samples. Radiation Measurements 42, 360-369.

Barton, R.N.E., 2013. The lithic artefact assemblage of Vanguard Cave, in: Barton, R.N.E., Stringer, C.B., Finlayson, J.C. (Eds.), Neanderthals in Context. A report of the 1995-1999 excavations at Gorham's and Vanguard Caves, Gibraltar. Oxford University School of Archaeology Oxford, pp. 243-252.

Barton, R.N.E., Collcutt, S.N., 2013. Vanguard Cave Summary, in: Barton, R.N.E., Stringer, C.B., Finlayson, J.C. (Eds.), Neanderthals in Context. A report of the 1995-1998 excavations at Gorham's and Vanguard Caves, Gibraltar. Oxford University School of Archaeology, Oxford, pp. 277-278.

Barton, R.N.E., Stringer, C.B., Finlayson, J.C., 2013. Neanderthals in Context. A report of the 1995-1998 excavations at Gorham's and Vanguard Caves, Gibraltar. Oxford University School of Archaeology, Oxford, p. 328.

Blain, H.-A., Gleed-Owen, C.P., López-García, J.M., Carrión, J.S., Jennings, R., Finlayson, G., Finlayson, C., Giles-Pacheco, F., 2013. Climatic conditions for the last Neanderthals: Herpetofaunal record of Gorham's Cave, Gibraltar. Journal of Human Evolution 64, 289-299.

Blasco, R., Rosell, J., Rufà, A., Sánchez Marco, A., Finlayson, C., 2016. Pigeons and choughs, a usual resource for the Neanderthals in Gibraltar. Quaternary International.

Bøtter-Jensen, L., 1997. Luminescence techniques: instrumentation and methods. Radiation Measurements 27, 749-768.

Bøtter-Jensen, L., Bulur, E., Duller, G.A.T., Murray, A.S., 2000. Advances in luminescence instrument systems. Radiation Measurements 32, 523-528.

Bøtter-Jensen, L., Mejdahl, V., 1985. Determination of potassium in feldspars by beta counting using a GM multicounter system. Nuclear Tracks and Radiation Measurements (1982) 10, 663-666.

Bøtter-Jensen, L., Mejdahl, V., 1988. Assessment of beta dose-rate using a GM Multicounter system. Radiation Measurements 14, 187-191.

Bowler, J.M., Johnston, H., Olley, J.M., Prescott, J.R., Roberts, R.G., Shawcross, W., Spooner, N.A., 2003. New ages for human occupation and climatic change at Lake Mungo, Australia. Nature 421, 837-840.

Carrión, J.S., Finlayson, C., Fernández, S., Finlayson, G., Allué, E., López-Sáez, J.A., López-García, P., Gil-Romera, G., Bailey, G., González-Sampériz, P., 2008. A coastal reservoir of biodiversity for Upper Pleistocene human populations: palaeoecological investigations in Gorham's Cave (Gibraltar) in the context of the Iberian Peninsula. Quaternary Science Reviews 27, 2118-2135.

Cunningham, A.C., Wallinga, J., 2009. Optically stimulated luminescence dating of young quartz using the fast component. Radiation Measurements 44, 423-428.

Currant, A.P., Fernández-Jalvo, Y., Price, C., 2013. The large mammal remains from Vanguard Cave, in: Barton, R.N.E., Stringer, C.B., Finlayson, J.C. (Eds.), Neanderthals in Context. A report of the 1995-1998 excavations at Gorhma's and Vanguard Caves, Gibraltar. Oxford University School of Archaeology, Oxford, pp. 236-239.

Doerschner, N., Fitzsimmons, K.E., Ditchfield, P., McLaren, S.J., Steele, T.E., Zielhofer, C., McPherron, S.P., Bouzouggar, A., Hublin, J.-J., 2016. A New Chronology for Rhafas, Northeast Morocco, Spanning the North African Middle Stone Age through to the Neolithic. PLoS ONE 11, e0162280.

Duller, G.A.T., 2003. Distinguishing quartz and feldspar in single grain luminescence measurements. Radiation Measurements 37, 161-165.

Duller, G.A.T., 2008. Single-grain optical dating of Quaternary sediments: why aliquot size matters in luminescence dating. Boreas 37, 589-612.

Duller, G.A.T., Bøtter-Jensen, L., Murray, A.S., 2000. Optical dating of single sand-sized grains of quartz: sources of variability. Radiation Measurements 32, 453-457.

Duller, G.A.T., Bøtter-Jensen, L., Murray, A.S., Truscott, A.J., 1999. Single grain laser luminescence (SGLL) measurements using a novel automated reader. Nuclear Instruments and Methods in Physics Research BNuclear Instruments and Methods in Physics Research B 155, 506-514.

Fa, D.A., Finlayson, J.C., Finlayson, G., Giles-Pacheco, F., Rodríguez-Vidal, J., Gutiérrez-López, J.M., 2016. Marine mollusc exploitation as evidenced by the Gorham's Cave (Gibraltar) excavations 1998–2005: The Middle–Upper Palaeolithic transition. Quaternary International 407, Part B, 16-28.

Finlayson, C., 2006. Climate, Vegetation and Biodiversity - a multiscale study of the south of the Iberian Peninsula. Anglia Ruskin University, Cambridge.

Finlayson, C., Blasco, R., Rodríguez-Vidal, J., Giles Pacheco, F., Finlayson, G., Gutiérrez, J.M., Jennings, R., Fa, D.A., Rosell, J., Carrión, J.S., Sánchez Marco, A., Finlayson, S., Bernal, M.A., 2014. Gibraltar excavations with particular reference to Groham's and Vanguard Caves, in: Sala Ramos, R. (Ed.), Pleistocene and Holocene Hunter-Gatherers in Iberia and the Gibraltar Strait. The Current Archaeological Record. Universidad de Burgos, Burgos.

Finlayson, C., Brown, K., Blasco, R., Rosell, J., Negro, J.J., Bortolotti, G.R., Finlayson, G., Sánchez Marco, A., Giles Pacheco, F., Rodríguez Vidal, J., Carrión, J.S., Fa, D.A., Rodríguez Llanes, J.M., 2012. Birds of a Feather: Neanderthal Exploitation of Raptors and Corvids. PLoS ONE 7, e45927.

Finlayson, C., Carrión, J.S., 2007. Rapid ecological turnover and its impact on Neanderthal and other human populations. Trends in Ecology & Evolution 22, 213-222.

Finlayson, C., Finlayson, S., Giles Guzman, F., Sánchez Marco, A., Finlayson, G., Jennings, R., Giles Pacheco, F., Rodriguez Vidal, J., 2016. Using birds as indicators of Neanderthal environmental quality: Gibraltar and Zafarraya compared. Quaternary International 421, 32-45.

Finlayson, C., Giles Pacheco, F., Rodriguez-Vidal, J., Fa, D.A., Maria Gutierrez Lopez, J., Santiago Perez, A., Finlayson, G., Allue, E., Baena Preysler, J., Caceres, I., Carrion, J.S., Fernandez Jalvo, Y., Gleed-Owen, C.P., Jimenez Espejo, F.J., Lopez, P., Antonio Lopez Saez, J., Antonio Riquelme Cantal, J., Sanchez Marco, A., Giles Guzman, F., Brown, K., Fuentes, N., Valarino, C.A., Villalpando, A., Stringer, C.B., Martinez Ruiz, F., Sakamoto, T., 2006. Late survival of Neanderthals at the southernmost extreme of Europe. Nature 443, 850-853.

Fitzsimmons, K.E., Stern, N., Murray-Wallace, C.V., 2014. Depositional history and archaeology of the central Lake Mungo lunette, Willandra Lakes, southeast Australia. Journal of Archaeological Science 41, 349-364.

Galbraith, R.F., Roberts, R.G., Laslett, G.M., Yoshida, H., Olley, J.M., 1999. Optical dating of single and multiple grains of quartz from Jinmium rock shelter, northern Australia: Part I, experimental design and statistical models. Archaeometry 41, 339-364.

Grant, K.M., Rohling, E.J., Ramsey, C.B., Cheng, H., Edwards, R.L., Florindo, F., Heslop, D., Marra, F., Roberts, A.P., Tamisiea, M.E., Williams, F., 2014. Sea-level variability over five glacial cycles. Nature Communications 5, 5076.

Green, R.E., Krause, J., Briggs, A.W., Maricic, T., Stenzel, U., Kircher, M., Patterson, N., Li, H., Zhai, W., Fritz, M.H.-Y., Hansen, N.F., Durand, E.Y., Malaspinas, A.-S., Jensen, J.D., Marques-Bonet, T., Alkan, C., Prüfer, K., Meyer, M., Burbano, H.A., Good, J.M., Schultz, R., Aximu-Petri, A., Butthof, A., Höber, B., Höffner, B., Siegemund, M., Weihmann, A., Nusbaum, C., Lander, E.S., Russ, C., Novod, N., Affourtit, J., Egholm, M., Verna, C., Rudan, P., Brajkovic, D., Kucan, Ž., Gušic, I., Doronichev, V.B., Golovanova, L.V., Lalueza-Fox, C., de la Rasilla, M., Fortea, J., Rosas, A., Schmitz, R.W., Johnson, P.L.F., Eichler, E.E., Falush, D., Birney, E., Mullikin, J.C., Slatkin, M., Nielsen, R., Kelso, J., Lachmann, M., Reich, D., Pääbo, S., 2010. A Draft Sequence of the Neandertal Genome. Science 328, 710.

Guérin, G., Combès, B., Lahaye, C., Thomsen, K.J., Tribolo, C., Urbanova, P., Guibert, P., Mercier, N., Valladas, H., 2015. Testing the accuracy of a Bayesian central-dose model for single-grain OSL, using known-age samples. Radiation Measurements 81, 62-70.

Higham, T., Douka, K., Wood, R., Ramsey, C.B., Brock, F., Basell, L., Camps, M., Arrizabalaga, A., Baena, J., Barroso-Ruiz, C., Bergman, C., Boitard, C., Boscato, P., Caparros, M., Conard, N.J., Draily, C., Froment, A., Galvan, B., Gambassini, P., Garcia-Moreno, A., Grimaldi, S., Haesaerts, P., Holt, B., Iriarte-Chiapusso, M.-J., Jelinek, A., Jorda Pardo, J.F., Maillo-Fernandez, J.-M., Marom, A., Maroto, J., Menendez, M., Metz, L., Morin, E., Moroni, A., Negrino, F., Panagopoulou, E., Peresani, M., Pirson, S., de la Rasilla, M., Riel-Salvatore, J., Ronchitelli, A., Santamaria, D., Semal, P., Slimak, L., Soler, J., Soler, N., Villaluenga, A., Pinhasi, R., Jacobi, R., 2014. The timing and spatiotemporal patterning of Neanderthal disappearance. Nature 512, 306-309.

Jacobs, Z., Duller, G.A.T., Wintle, A.G., 2003. Optical dating of dune sand from Blombos Cave, South Africa: II—single grain data. Journal of Human Evolution 44, 613-625.

Jacobs, Z., Duller, G.A.T., Wintle, A.G., Henshilwood, C.S., 2006. Extending the chronology of deposits at Blombos Cave, South Africa, back to 140 ka using optical dating of single and multiple grains of quartz. Journal of Human Evolution 51, 255-273.

Jacobs, Z., Meyer, M.C., Roberts, R.G., Aldeias, V., Dibble, H., El Hajraoui, M.A., 2011. Single-grain OSL dating at La Grotte des Contrebandiers ('Smugglers' Cave'), Morocco: improved age constraints for the Middle Paleolithic levels. Journal of Archaeological Science 38, 3631-3643.

Jacobs, Z., Roberts, R.G., 2007. Advances in Optically Stimulated Luminescence Dating of Individual Grains of Quartz from Archeological Deposits. Evolutionary Anthropology 16, 210-223.

Jacobs, Z., Roberts, R.G., Galbraith, R.F., Deacon, H.J., Grün, R., Mackay, A., Mitchell, P., Vogelsang, R., Wadley, L., 2008a. Ages for the Middle Stone Age of Southern Africa: Implications for Human Behavior and Dispersal. Science 332, 733-735.

Jacobs, Z., Roberts, R.G., Nespoulet, R., El Hajraoui, M.A., Debénath, A., 2012. Single-grain OSL chronologies for Middle Palaeolithic deposits at El Mnasra and El Harhoura 2, Morocco: Implications for Late Pleistocene humaneenvironment interactions along the Atlantic coast of northwest Africa. Journal of Human Evolution 62, 377-394.

Jacobs, Z., Wintle, A.G., Roberts, R.G., Duller, G.A.T., 2008b. Equivalent dose distributions from single grains of quartz at Sibudu, South Africa: context, causes and consequences for optical dating of archaeological deposits. Journal of Archaeological Science 35, 1808-1820.

Jiménez-Espejo, F.J., Rodríguez-Vidal, J., Finlayson, C., Martínez-Ruiz, F., Carrión, J.S., García-Alix, A., Paytan, A., Giles Pacheco, F., Fa, D.A., Finlayson, G., Cortés-Sánchez, M., Rodrigo Gámiz, M., González-Donoso, J.M., Linares, M.D., Cáceres, L.M., Fernández, S., Iijima, K., Martínez Aguirre, A., 2013. Environmental conditions and geomorphologic changes during the Middle–Upper Paleolithic in the southern Iberian Peninsula. Geomorphology 180–181, 205-216.

Lomax, J., Hilgers, A., Twidale, C.R., Bourne, J.A., Radtke, U., 2007. Treatment of broad palaeodose distributions in OSL dating of dune sands from the western Murray Basin, South Australia. Quaternary Geochronology 2, 51-56.

Macphail, R.I., Goldberg, P., 2000. Geoarchaeological investigation of sediments from Gorham's and Vanguard Caves, Gibraltar: Microstratigraphical (soil micromorphological and chemical) signatures. , in: Stringer, C.B., Barton, R.N.E., Finlayson, J.C. (Eds.), Neanderthals on the Edge. Oxbow Books, Oxford, pp. 183-200.

Macphail, R.I., Goldberg, P., Barton, R.N.E., 2013. Vanguard Cave sediments and soil micromorphology, in: Barton, R.N.E., Stringer, C.B., Finlayson, J.C. (Eds.), Neanderthals in Context. A report of the 1995-1998 excavations at Gorham's and Vanguard Caves, Gibraltar. Oxford University School of Archaeology, Oxford, pp. 193-210.

Mejdahl, V., 1979. Thermoluminescence dating: beta-dose attenuation in quartz grains. Archaeometry 21, 61-72.

Mellars, P., 2006. A new radiocarbon revolution and the dispersal of modern humans in Eurasia. Nature 439, 931-935.

Mercier, N., Falguères, C., 2007. Field gamma dose-rate measurement with a NaI(Tl) detector: re-evaluation of the "threshold" technique. Ancient TL 25.

Murray, A.S., Roberts, R.G., 1997. Determining the burial time of single grains of quartz using optically stimulated luminescence. Earth and Planetary Science Letters 152, 163-180.

Murray, A.S., Wintle, A.G., 2000. Luminescence dating of quartz using an improved single-aliquot regenerative-dose protocol. Radiation Measurements 32, 57-73.

Murray, A.S., Wintle, A.G., 2003. The single aliquot regenerative dose protocol: potential for improvements in reliability. Radiation Measurements 37, 377-381.

Olley, J.M., De Deckker, P., Roberts, R.G., Fifield, L.K., Yoshida, H., Hancock, G., 2004. Optical dating of deep-sea sediments using single grains of quartz: a comparison with radiocarbon. Sedimentary Geology 169, 175-189.

Olley, J.M., Murray, A., Roberts, R.G., 1996. The effects of disequilibria in the uranium and thorium decay chains on burial dose rates in fluvial sediments. Quaternary Science Reviews 15, 751-760.

Olley, J.M., Roberts, R.G., Murray, A.S., 1997. Disequilibria in the uranium decay series in sedimentary deposits at Allen's cave, nullarbor plain, Australia: Implications for dose rate determinations. Radiation Measurements 27, 433-443.

Pettitt, P.B., Bailey, R.M., 2000. AMS Radiocarbon and Luminescence Dating of Gorham's and Vanguard Caves, Gibraltar, and Implications for the Middle to Upper Palaeolithic Transition in Iberia, in: Stringer, C.B., Barton, R.N.E., Finlayson, J.C. (Eds.), Neanderthals on the Edge. Oxbow Books, Oxford, pp. 155-162.

Prescott, J.R., Hutton, J.T., 1994. Cosmic ray contributions to dose rates for luminescence and ESR dating: Large depths and long-term time variations. Radiation Measurements 23, 497-500.

Rasmussen, S.O., Bigler, M., Blockley, S.P., Blunier, T., Buchardt, S.L., Clausen, H.B., Cvijanovic, I., Dahl-Jensen, D., Johnsen, S.J., Fischer, H., Gkinis, V., Guillevic, M., Hoek, W.Z., Lowe, J.J., Pedro, J.B., Popp, T., Seierstad, I.K., Steffensen, J.P., Svensson, A.M., Vallelonga, P., Vinther, B.M., Walker, M.J.C., Wheatley, J.J., Winstrup, M., 2014. A stratigraphic framework for abrupt climatic changes during the Last Glacial period based on three synchronized Greenland ice-core records: refining and extending the INTIMATE event stratigraphy. Quaternary Science Reviews 106, 14-28.

Rhodes, E.J., 2013. OSL age estimates from Vanguard Cave, in: Barton, R.N.E., Stringer, C.B., Finlayson, J.C. (Eds.), Neanderthals in Context. A report of the 1995-1998 excavations at Gorham's and Vanguard Caves, Gibraltar. Oxford University School of Archaeology, Oxford, pp. 211-217.

Rodnight, H., 2008. How many equivalent dose values are needed to obtain a reproducible distribution? Ancient TL 26, 3-9.

Rodríguez-Vidal, J., Cáceres, L.M., Finlayson, J.C., Gracia, F.J., Martínez-Aguirre, A., 2004. Neotectonics and shoreline history of the Rock of Gibraltar, southern Iberia. Quaternary Science Reviews 23, 2017-2029.

Rodríguez-Vidal, J., d'Errico, F., Giles Pacheco, F., Blasco, R., Rosell, J., Jennings, R.P., Queffelec, A., Finlayson, G., Fa, D.A., Gutiérrez López, J.M., Carrión, J.S., Negro, J.J., Finlayson, S., Cáceres, L.M., Bernal, M.A., Fernández Jiménez, S., Finlayson, C., 2014. A rock engraving made by Neanderthals in Gibraltar. Proceedings of the National Academy of Sciences.

Rodríguez-Vidal, J., Finlayson, G., Finlayson, C., Negro, J.J., Cáceres, L.M., Fa, D.A., Carrión, J.S., 2013. Undrowning a lost world — The Marine Isotope Stage 3 landscape of Gibraltar. Geomorphology 203, 105-114.

Seierstad, I.K., Abbott, P.M., Bigler, M., Blunier, T., Bourne, A.J., Brook, E., Buchardt, S.L., Buizert, C., Clausen, H.B., Cook, E., Dahl-Jensen, D., Davies, S.M., Guillevic, M., Johnsen, S.J., Pedersen, D.S., Popp, T.J., Rasmussen, S.O., Severinghaus, J.P., Svensson, A., Vinther, B.M., 2014. Consistently dated records from the Greenland GRIP, GISP2 and NGRIP ice cores for the past 104 ka reveal regional millennial-scale δ18O gradients with possible Heinrich event imprint. Quaternary Science Reviews 106, 29-46.

Stringer, C., 2000. Gibraltar and the Neanderthals 1848-1998, in: Stringer, C.B., Barton, R.N.E., Finlayson, J.C. (Eds.), Neanderthals on the Edge. Oxbom Books, Oxford, pp. 133-137.

Stringer, C.B., Barton, R.N.E., Finlayson, J.C., 2000. Neanderthals on the Edge. Oxbow, Oxford, p. 267.

Stringer, C.B., Finlayson, J.C., Barton, R.N.E., Fernández-Jalvo, Y., Cáceres, I., Sabin, R.C., Rhodes, E.J., Currant, A.P., Rodríguez-Vidal, J., Giles-Pacheco, F., Riquelme-Cantal, J.A., 2008. Neanderthal exploitation of marine mammals in Gibraltar. Proceedings of the National Academy of Sciences 105, 14319-14324.

Thomsen, K.J., Murray, A., Jain, M., 2012. The dose dependency of the over-dispersion of quartz OSL single grain dose distributions. Radiation Measurements 47, 732-739.

Tribolo, C., Mercier, N., Rasse, M., Soriano, S., Huysecom, E., 2010. Kobo 1 and L'Abri aux Vaches (Mali, West Africa): Two case studies for the optical dating of bioturbated sediments. Quaternary Geochronology 5, 317-323.

Vandenberghe, D., De Corte, F., Buylaert, J.P., Kučera, J., Van den haute, P., 2008. On the internal radioactivity in quartz. Radiation Measurements 43, 771-775.

Wintle, A.G., Murray, A.S., 2006. A review of quartz optically stimulated luminescence characteristics and their relevance in single-aliquot regeneration dating protocols. Radiation Measurements 41, 369-391.

Wood, R.E., Barroso-Ruíz, C., Caparrós, M., Jordá Pardo, J.F., Galván Santos, B., Higham, T.F.G., 2013. Radiocarbon dating casts doubt on the late chronology of the Middle to Upper Palaeolithic transition in southern Iberia. Proceedings of the National Academy of Sciences 110, 2781-2786.

Zilhão, J., Ajas, A., Badal, E., Burow, C., Kehl, M., López-Sáez, J.A., Pimenta, C., Preece, R.C., Sanchis, A., Sanz, M., Weniger, G.-C., White, D., Wood, R., Angelucci, D.E., Villaverde, V., Zapata, J., 2016. Cueva Antón: A multi-proxy MIS 3 to MIS 5a paleoenvironmental record for SE Iberia. Quaternary Science Reviews 146, 251-273.

6. Conclusion

The purpose of this thesis was to establish reliable chronostratigraphies for Palaeolithic cave sites in the western Mediterranean. The data produced by this work was then combined with archaeological, geological and sedimentological evidence from the sites to gain insights into hominin subsistence strategies, as well as hominin interaction with changing palaeoenvironments throughout the Pleistocene. Consistent application of single-grain quartz OSL to sites of varying antiquity addresses two main themes. The first is investigation of the general suitability of these quartz grains as luminescence chronometers and how variable their luminescence properties are on site and regional scale. The second informs us how the timing and geographical distribution of changes in Palaeolithic human behaviour and occupation patterns in the region might be linked to the different population dispersal events within Africa and into Europe that took place over the last ~2 Ma. OSL dating of individual sand-sized grains provides valuable information on the sedimentary history of sampled deposits that contribute to an improved understanding of local site formation processes and past palaeoclimatic variability in the area.

6.1. Quartz luminescence dating

Quartz OSL dating has increasingly been used to determine the burial age of sediments at Palaeolithic cave sites in the western Mediterranean over the past two decades. Most of those studies applying multiple-grain dating approaches (e.g. Álvarez-Alonso et al., 2016; Barton et al., 2009; Galván et al., 2014; Ramos et al., 2008; Rhodes et al., 2006; Schwenninger et al., 2010). Single-grain dating of sand-sized quartz grains at archaeological sites in the region, on the other hand, was primarily adopted to small subsets of samples to supplement the results of other radiometric dating techniques - e.g. at Taforalt (Clark-Balzan et al., 2012), Morocco, or Cuevá Anton (Zilhão et al., 2016) and Gorham's Cave (Rhodes, 2013), both in southern Iberia. Complete chronostratigraphies have so far only been generated for three coastal sites in the Témara region, Morocco (Jacobs et al., 2011; Jacobs et al., 2012). Consequently, our knowledge on how individual grains of quartz from these areas behave during luminescence dating is limited. Single-grain data elucidate the potential of multiple-grain measurements to under- or overestimate the true age. The luminescence characteristics of the deposited sediment itself or locally occurring site-specific processes, like i.e. post depositional intrusion of grains or carbonate cementation – had yet to be studied systematically at single-grain level.

Within this thesis, the investigated individual quartz grains from three western Mediterranean archaeological cave sites were shown to exhibit generally bright, fast-component-dominated luminescence signals. Initial standard OSL performance tests proved the material generally suitable for measurements using the SAR protocol and single grain rejection criteria were successfully applied to discard aberrant grains from the D_e datasets.

Despite showing promising prerequisites for OSL dating, there are also some considerable differences recognisable in the luminescence characteristics of the sediments between sites. Among these are the low proportions of individual grains from Vanguard Cave, Gibraltar (chapter 5), exhibiting luminescence signals suitable for D_e determination (7–15%) compared to the Moroccan sediments (12-62%). The majority of grains from Vanguard Cave giving measurable luminescence signals also pass other rejection criteria, which contrasts with the grains investigated at Rhafas (chapter 2) and Thomas Quarries (chapter 3). The latter regularly fail quality criteria due to signal saturation, poor recycling ratios, or feldspar contamination. Luminescence characteristics of the sediments in this thesis, furthermore, vary through time at a given site. Although a few extremely bright grains with above-average D_e values occur in low proportions in some samples from Vanguard Cave and might have an impact on determined ages when using multiple-grain aliquots, the sediments are overall characterised by homogeneous luminescence behaviours. This is the opposite of what was observed at Rhafas, where causes for individual grain rejection are highly layer-dependent. Quartz grains from the Thomas Quarries are not only affected by luminescence signal saturation. Single-grain dose recovery tests from that site yielded substantial dose recovery ratio underestimations and high intrinsic overdispersion (σ_{OD}) values. These results question the ability of the material to recover known laboratory doses, as well as the applicability of dose recovery tests which are commonly based on multiple-grain measurements.

In chapter 4 of this thesis, we examine whether dose recovery tests are a useful check for i) the suitability of the measured SAR protocol and ii) the reliability of natural D_e estimates in single-grain dating of archaeological sediments. Recently, some authors have cast doubt on the significance of such tests. They found no correlation between dose recovery ratios and accuracy of single-grain age estimates (Guérin et al., 2015) and showed that the size of the given dose in such experiments has considerable impact on the test results (Thomsen et al., 2012). Dose recovery characteristics of samples from Thomas Quarry I and Rhafas (natural D_es >180 Gy) following different bleaching methods (sunlight, green laser beams and solar simulator) and sizes of administered doses were systematically investigated. The results were compared to those derived from highly sensitised, well-bleached Australian quartz sand with comparatively small natural D_es from the site of Lake Mungo (Fitzsimmons et al., 2014) using the same test parameters. While the Australian samples show primary dependencies of dose recovery ratios and σ_{OD} on the size of the given dose, the Moroccan samples yield more variable results. No obvious correlations exist between the bleaching treatments or the size of the given dose, and the accuracy and precision of recovered doses in two out of three Moroccan samples. Thus we concluded that – in addition to administered dose size - sample-specific responses to chosen test parameters can significantly influence single-grain dose recovery test ratios and σ_{OD} values, particularly in less sensitised archaeological cave sediments like Thomas Quarry I and Rhafas. Performing a dose recovery test to assess the validity of the chosen SAR protocol parameters in these samples can lead to highly controversial results depending on the size of the given dose and on the bleaching source used. It remains doubtful as to which extent such tests can serve as quality check of the measurement protocol and the reliability of final age estimates.

The overdispersion value, which quantifies the spread in D_e distributions, is commonly used as an argument to justify the application of specific statistical age models in single-grain dating studies. Olley et al. (2004) stated that single-grain D_es of well-bleached natural samples are typically overdispersed by 9-22%, while σ_{OD} values vary between 7-12% during laboratory-based dose recovery tests, whereby all extrinsic factors influencing the spread of natural D_e distributions are excluded (Jacobs et al., 2006; Reimann et al., 2012; Thomsen et al., 2007). Intrinsic σ_{OD} in dose recovery experiments in this thesis (chapter 4) is highly variable for both Australian and Moroccan samples – 5-27% and 6-35%, respectively. These values may even exceed the value determined for the natural D_e of a sample. Thus, definite

statements as to the amount of intrinsic σ_{OD} in natural D_e distributions and a correct assessment of the extrinsic component – which is usually associated to dose rate heterogeneity, incomplete bleaching or post depositional mixing – cannot be reliably made for our samples. Examples like these and studies like Guérin et al. (2015) or Thomsen et al. (2012) raise questions concerning the implication of σ_{OD} values, the impact of natural and/or experimental factors influencing them and whether they can serve as arguments justifying the use of statistical age models in single-grain dating. Consequently, decisions regarding the application of CAM or FMM for the samples from Vanguard Cave, Rhafas and the Thomas Quarries were primarily made based on the shape of single-grain D_e distributions, as well as sedimentological and stratigraphical observations in field, rather than σ_{OD} values.

Challenges for single-grain dating at the investigated cave sites are predominantly a result of sediment composition and local site formation processes that lead to heterogeneous dose rates and post-depositional mixing in the stratigraphical layers. Partial bleaching of the luminescence signal stored in the sand grains was not observed at any of the three sites. While at Rhafas (chapter 2), a single mixing event significantly affects D_e distributions of three layers in the cave mouth section. One main source of uncertainty for reliable age determination at all sites relates to correct assessments of the environmental dose rates of each layer. At Vanguard Cave (chapter 5), patches and small layers of potassium-rich clays, which are known to increase dose rates, commonly occur throughout the stratigraphical profile. Carbonates, on the other hand, which decrease the dose rate of a sediment layer, are present at all sites in form of exogenic carbonate fragments from local limestone bedrock, crusts/layers/lenses of pure carbonate, and post-depositional cementation of sediment layers. Consequently, stratigraphical profiles at these cave sites are characterised by inhomogeneous sediment layers with highly variable beta and gamma dose rates. Variations in microdosimetry are, furthermore, likely to influence equivalent dose at single grain level. Moreover, introduction of allochthonous radioactive elements via groundwater after sediment deposition was identified for the lower cave section at Rhafas and renders these layers undateable using standard quartz OSL dating. An upcoming project will clarify whether subtraction dating (Feathers, 2002) or isochron dating (Li et al., 2008) can overcome those dose rate issues and determine the age of the lower cave section sediments at Rhafas.

In conclusion, for western Mediterranean cave sites, it is highly recommended to analyse site formation and sediment composition in great detail and to use multiple methods for dose rate determination – including in-situ measurements – to identify potential mixing processes and to be able to assess the dose rate of each dated layer.

6.2. Implications for Palaeolithic human behaviour and dispersal

In this thesis, single-grain OSL dating was successfully used to establish reliable chronological frameworks for stratigraphical profiles at two Palaeolithic cave sites in the western Mediterranean: Rhafas (chapter 2) and Vanguard Cave (chapter 5).

For the sites of Thomas Quarry I and Rhino Cave near Casablanca (chapter 3), however, standard quartz OSL dating of individual grains did not yield conclusive results for age determination. Large numbers of single-grains at Casablanca are affected by luminescence signal saturation; others pass all established quality criteria, while still failing to correctly recover known laboratory doses. D_e distributions are widely scattered and calculated absolute ages lack stratigraphical consistency, irrespective of the applied statistical age model. While the latter could at least partially result from the fact that present-day dose rates do not correctly reflect average burial-time dose rates within the sampled layers - since large parts of the stratigraphical profiles experienced intensive post-depositional cementation by

carbonates – the former reinforces doubts as to the general suitability of these sediments for standard quartz single-grain dating. Comparison with independent age control available for the Thomas Quarries shows that calculated single-grain ages suffer from substantial age underestimation. Given the successful OSL dating results from Rhodes et al. (2006) and the dose recovery experiments performed in this thesis (chapter 4), it can be stated that luminescence dating is not necessarily an inadequate technique for age determination of the Thomas Quarries sediments. While individual grain dating using a standard SAR protocol did not result in reliable ages for both sites, sediments are nevertheless extremely promising for future research focussing on other luminescence approaches such as thermally transferred or violet stimulated OSL. The single-grain dating study performed at the Thomas Quarries in this thesis, unfortunately, does not allow any conclusions regarding the role of northern African populations in the emergence of the European Acheulian or in the debate of potential ancient human crossings of the Strait of Gibraltar during the Early Pleistocene. It nevertheless highlights once more the fundamental importance of cross-checks between different Quaternary dating techniques for reliable age determination of Palaeolithic caves sites.

The long stratified sequence at Rhafas (chapter 2) covers a time period from >135 ka to the Neolithic (~7.8 ka), during which two important human dispersal events from Africa into Europe took place: Out of Africa 2a and 2b, in MIS 5 and MIS 3, respectively. The archaeological record of the site comprises classical MSA, Aterian, LSA as well as Neolithic industries spread over three sections within the cave itself and on a flat terrace area in front of the cave opening. Evidence for human occupation of the Maghreb during the Middle Pleistocene predating MIS 5 is extremely sparse and limited to a few sites in Morocco, Tunisia and western Libya. Recent studies at Jebel Irhoud, western Morocco, emphasise the significance of this region for understanding the emergence of the human lineage in Africa by presenting reliable evidence for early *homo sapiens* fossil remains (Hublin et al., 2017) associated with MSA lithic artefacts as early as 315 ± 34 ka at the site (Richter et al., 2017). The archaeological record from Jebel Irhoud, therefore, predates the earliest appearance of MSA assemblages in the Maghreb – formerly associated with the Benzù rockshelter at 254 ± 17 ka in northern Morocco (Ramos et al., 2008; Ramos Muñoz et al., 2007) - by ~60.000 years. Its fossil remains, together with the partial cranium from Florisbad (Grün et al., 1996), South Africa, now represent the earliest known representatives of the *homo sapiens* clade. Archaeological finds proving human presence in the Maghreb become more frequent with the onset of MIS 6, when climatic conditions in Northern Africa were relatively dry. At Rhafas this time period is reflected by evaporite enriched sediments in the lower cave section containing MSA stone tools predating 135 ka. With the onset of MIS 5, humidity generally increased in Northern Africa, facilitating AMH expansions in the region, especially during the 'green Sahara' events in MIS 5a, 5c and 5e. Rapid peopling of all parts of the Maghreb can be easily traced through the substantial increase of archaeological sites ~130 ka, which is around the same time when hominin groups started to settle out of the African continent again (Out of Africa 2a). While a long-term colonisation of the Levant by AMHs failed, the Maghreb became permanently inhabited. MIS 5 deposits at Rhafas firstly reflect a change in sediment source compared to the underlying MIS 6 layers, which is likely to be linked to a regional shift in prevailing wind directions and, secondly, witness the transition from classical MSA to Aterian through the regular appearance of pedunculated tools after 123 ka. This lithic technocomplex is typically interpreted as indicator for behavioural modernity – a potential key factor to understand the evolutionary success of our lineage over Neanderthals - in AMH populations of the Maghreb. Its earliest reliable occurrence dates to 145 ± 9 ka at Ifri N'Ammar (Richter et al., 2012), northern Morocco.

A regional comparison of the data available today from dated archaeological sites in the Maghreb shows i) that tanged pieces became a widespread feature in archaeological assemblages with the onset of MIS 5e in Morocco, while being present in Algeria, Tunisia and western Libya not before ~65 ka,

and ii) that MSA and Aterian lithic assemblages coexisted in the region over a long time until they got eventually replaced by LSA industries in MIS 3. Future research must clarify whether the technological innovations of the Aterian truly emerged in Morocco or whether this temporal signal in the regional comparison is simply an artefact of the limited chronological data available for archaeological sites in other parts of the Maghreb. Likewise still unresolved questions which require further investigations in the region concern i) the debate as to whether the Aterian represents a phase within the MSA or has to be seen as separate entity in North Africa (Dibble et al., 2013; Iovita, 2011) and ii) the clarification of the role of Aterian people in the successful Out of Africa event 2b that took place after 60 ka.

The site of Rhafas (chapter 2), additionally, yields evidence for an intensive phase of human occupation between 21 ± 2 ka and 15 ± 1 ka associated with LSA lithic industries and for the prevailing palaeoclimate during MIS 3 and MIS 2. Climatic conditions at that time favoured intensive carbonate formation at the site including beside cementation of sediment layers in the cave mouth section a prominent duricrust in the terrace section. Detailed investigations of the duricrust fabric suggests that its formation took place over a longer period of time and under various climatic conditions ranging from relatively humid to arid but not hyper arid, just as Northern Africa experienced over MIS 3 and MIS 2. While the LSA appears in lithic assemblages – especially in South Africa – before 42 kcal BP at some sites (Ambrose, 1998; Villa et al., 2012), it occurs relatively late in the Maghreb. The regional comparison shows that early LSA assemblages are particularly widespread in western Libya between 35-30 ka, while they are not present – with the exception of Dar es-Soltan II, Morocco (Schwenninger et al., 2010) – in other parts of the Maghreb before ~24 ka. While the origins of the LSA in Africa are still matter of ongoing scientific debate, there also remains the question whether this technocomplex was brought to the Maghreb by AMH populations traveling through Northern Africa from the East to the West.

In chapter 5 of this thesis, a high-resolution dual chronostratigraphy for the uppermost ~4 m of the >17 m sedimentary sequence at Vanguard Cave, Gibraltar, was established using single-grain and multiple-grain OSL dating. Located at the present-day shoreline of the Mediterranean Sea and accumulated on top of a MIS 5 fossilized marine terrace, the site contains evidence for repeated occupation by Neanderthals at a time before AMHs arrived in Southern Iberia. Due to the fact that relatively few individual grains at Vanguard Cave emit sufficient luminescence signals for dating, averaging effects in 1 mm multiple-grain aliquots are almost negligible, resulting in an excellent correspondence between their dating results with those obtained using single-grains. Dated to between 66 ± 6 ka and 43 ± 3 ka, the uppermost ~4 m of the sedimentary profile are a reliable proof of the rapid aeolian accumulation that took place during MIS 3 and MIS 4 at the site, and which is likely to have also persisted throughout MIS 5.

Recent studies from Gibraltar indicate mild and sub-humid Mediterranean climatic conditions for the time of Neanderthal occupation, MIS 5-3 (Blain et al., 2013; Stringer et al., 2008), and the presence of an extensive – now submerged – coastal shelf on the east side of the Rock, directly in front of the Vanguard Cave entrance, covered with savannah and aeolian sand dunes during MIS 3 (Rodríguez-Vidal et al., 2013). Geomorphic evidence from the site presented in this thesis, indicates similar palaeoenvironmental conditions in the region with strong easterly winds throughout the entire depositional history of the sedimentary sequence. Ongoing and future research on the Vanguard Cave record coupled with the reliable chronostratigraphic framework offers great potential to significantly improve our understanding of climatic and environmental conditions as well as Neanderthal lifestyle in southern Iberia during MIS 5-3. Detailed analyses of the stone tools recovered from the uppermost layers of the cave fill sequence – previously described as Upper Palaeolithic (Barton et al., 2013) - must clarify their cultural affiliation within the Palaeolithic.

In conclusion, this thesis underlines that dating of archaeological cave sites using OSL remains a

highly complex task. In the western Mediterranean region, where luminescence characteristics of sediments are diverse and variable climatic conditions throughout the Pleistocene can largely affect sedimentological profiles post-depositionally, the use of individual grain dating is highly recommended, although even this method comes with caveats. Palaeoenvironmental signals can be stored at cave sites in the region enabling conclusive statements regarding climatic changes on local or regional scales. Reliable chronologies for Palaeolithic cave sites are crucial to understand human behaviour and dispersal patterns. They are, however, only one part of a complex picture and need to be complemented by archaeological, geological and sedimentological investigations to achieve their highest possible information value.

References

Álvarez-Alonso, D., de Andrés-Herrero, M., Díez-Herrero, A., Medialdea, A., Rojo-Hernández, J., 2016. Neanderthal settlement in central Iberia: Geo-archaeological research in the Abrigo del Molino site, MIS 3 (Segovia, Iberian Peninsula). Quaternary International.

Ambrose, S.H., 1998. Chronology of the Later Stone Age and Food Production in East Africa. Journal of Archaeological Science 25, 377-392.

Barton, R.N.E., Bouzouggar, A., Collcutt, S.N., Schwenninger, J.-L., Clark-Balzan, L., 2009. OSL dating of the Aterian levels at Dar es-Soltan I (Rabat, Morocco) and implications for the dispersal of modern Homo sapiens. Quaternary Science Reviews 28, 1914-1931.

Barton, R.N.E., Stringer, C.B., Finlayson, J.C., 2013. Neanderthals in Context. A report of the 1995-1998 excavations at Gorham's and Vanguard Caves, Gibraltar. Oxford University School of Archaeology, Oxford, p. 328.

Blain, H.-A., Gleed-Owen, C.P., López-García, J.M., Carrión, J.S., Jennings, R., Finlayson, G., Finlayson, C., Giles-Pacheco, F., 2013. Climatic conditions for the last Neanderthals: Herpetofaunal record of Gorham's Cave, Gibraltar. Journal of Human Evolution 64, 289-299.

Clark-Balzan, L.A., Candy, I., Schwenninger, J.-L., Bouzouggar, A., Blockley, S., Nathan, R., Barton, R.N.E., 2012. Coupled U-series and OSL dating of a Late Pleistocene cave sediment sequence, Morocco, North Africa: Significance for constructing Palaeolithic chronologies. Quaternary Geochronology 12, 53-64.

Dibble, H.L., Aldeias, V., Jacobs, Z., Olszewski, D.I., Rezek, Z., Lin, S.C., Alvarez-Fernández, E., Barshay-Szmidt, C.C., Hallett-Desguez, E., Reed, D., Reed, K., Richter, D., Steele, T.E., Skinner, A., Blackwell, B., Doronicheva, E., El-Hajraoui, M., 2013. On the industrial attributions of the Aterian and Mousterian of the Maghreb. Journal of Human Evolution 64, 194-210.

Feathers, J.K., 2002. Luminescence Dating in Less Than Ideal Conditions: Case Studies from Klasies River Main Site and Duinefontein, South Africa. Journal of Archaeological Science 29, 177-194.

Fitzsimmons, K.E., Stern, N., Murray-Wallace, C.V., 2014. Depositional history and archaeology of the central Lake Mungo lunette, Willandra Lakes, southeast Australia. Journal of Archaeological Science 41, 349-364.

Galván, B., Hernández, C.M., Mallol, C., Mercier, N., Sistiaga, A., Soler, V., 2014. New evidence of early Neanderthal disappearance in the Iberian Peninsula. Journal of Human Evolution 75, 16-27.

Grün, R., Brink, J.S., Spooner, N.A., Taylor, L., Stringer, C.B., Franciscus, R.G., Murray, A.S., 1996. Direct dating of Florisbad hominid. Nature 382, 500-501.

Guérin, G., Combès, B., Lahaye, C., Thomsen, K.J., Tribolo, C., Urbanova, P., Guibert, P., Mercier, N., Valladas, H., 2015. Testing the accuracy of a Bayesian central-dose model for single-grain OSL, using known-age samples. Radiation Measurements 81, 62-70.

Hublin, J.-J., Ben-Ncer, A., Bailey, S.E., Freidline, S.E., Neubauer, S., Skinner, M.M., Bergmann, I., Le Cabec, A., Benazzi, S., Harvati, K., Gunz, P., 2017. New fossils from Jebel Irhoud, Morocco and the pan-African origin of Homo sapiens. Nature 546, 289-292.

Iovita, R., 2011. Shape Variation in Aterian Tanged Tools and the Origins of Projectile Technology: A Morphometric Perspective on Stone Tool Function. PLoS ONE 6, e29029.

Jacobs, Z., Duller, G.A.T., Wintle, A.G., 2006. Interpretation of single grainDe distributions and calculation of De. Radiation Measurements 41, 264-277.

Jacobs, Z., Meyer, M.C., Roberts, R.G., Aldeias, V., Dibble, H., El Hajraoui, M.A., 2011. Single-grain OSL dating at La Grotte des Contrebandiers ('Smugglers' Cave'), Morocco: improved age constraints for the Middle Paleolithic levels. Journal of Archaeological Science 38, 3631-3643.

Jacobs, Z., Roberts, R.G., Nespoulet, R., El Hajraoui, M.A., Debénath, A., 2012. Single-grain OSL chronologies for Middle Palaeolithic deposits at El Mnasra and El Harhoura 2, Morocco: Implications for Late Pleistocene humaneenvironment interactions along the Atlantic coast of northwest Africa. Journal of Human Evolution 62, 377-394.

Li, B., Li, S.-H., Wintle, A.G., Zhao, H., 2008. Isochron dating of sediments using luminescence of K-feldspar grains. Journal of Geophysical Research: Earth Surface 113, F02026.

Olley, J.M., De Deckker, P., Roberts, R.G., Fifield, L.K., Yoshida, H., Hancock, G., 2004. Optical dating of deep-sea sediments using single grains of quartz: a comparison with radiocarbon. Sedimentary Geology 169, 175-189.

Ramos, J., Bernal, M., Domínguez-Bella, S., Calado, D., Ruiz, B., Gil, M.J., Clemente, I., Durán, J.J., Vijande, E., Chamorro, S., 2008. The Benzu´ rockshelter: a Middle Palaeolithic site on the North African coast. Quaternary Science Reviews 27, 2230-2238.

Ramos Muñoz, J., Bernal Casasola, D., domínguez-Bella, S., Calado, D., Ruiz Zapata, M.B., Gil Garcia, M.J., Clemente Conte, I., Durán Valsero, J.J., Vijande Vila, E., Chamorro Moreno, S., 2007. El abrigo de Benzú (Ceuta) frecuentaciones humanas de un yacimiento con tecnología de modo 3 en el norte de África - The shelter of Benzú (Ceuta). Human occupations of a settlement with mode 3 technology in north Africa. Zephyrus, Revista de Prehistoria y Arqueología 60, 27-41.

Reimann, T., Lindhorst, S., Thomsen, K.J., Murray, A.S., Frechen, M., 2012. OSL dating of mixed coastal sediment (Sylt, German Bight, North Sea). Quaternary Geochronology 11, 52-67.

Rhodes, E.J., 2013. OSL dating of sediments from the lower part of Gorham's Cave, in: Barton, R.N.E., Stringer, C.B., Finlayson, J.C. (Eds.), Neanderthals in Context. A report of the 1995-1998 excavations at Gorham's and Vanguard Caves, Gibraltar. Oxford University School of Archaeology, Oxford, pp. 77-88.

Rhodes, E.J., Singarayer, J.S., Raynal, J.-P., Westaway, K.E., Sbihi-Alaoui, F.Z., 2006. New age estimates for the Palaeolithic assemblages and Pleistocene succession of Casablanca, Morocco. Quaternary Science Reviews 25, 2569-2585.

Richter, D., Grün, R., Joannes-Boyau, R., Steele, T.E., Amani, F., Rué, M., Fernandes, P., Raynal, J.-P., Geraads, D., Ben-Ncer, A., Hublin, J.-J., McPherron, S.P., 2017. The age of the hominin fossils from Jebel Irhoud, Morocco, and the origins of the Middle Stone Age. Nature 546, 293-296.

Richter, D., Moser, J., Nami, M., 2012. New data from the site of Infri n'Ammar (Morocco) and some remarks on the cronometric status of the Middle Paleolithic in the Maghreb, in: Hublin, J.-J., McPherron, S.P. (Eds.), Modern Origins: A North African Perspective. Springer, New York, pp. 61-78.

Rodríguez-Vidal, J., Finlayson, G., Finlayson, C., Negro, J.J., Cáceres, L.M., Fa, D.A., Carrión, J.S., 2013. Undrowning a lost world — The Marine Isotope Stage 3 landscape of Gibraltar. Geomorphology 203, 105-114.

Schwenninger, J.L., Collcutt, S.N., Barton, N., Bouzouggar, A., Clark-Balzan, L., El Hajraoui, M.A., Nespoulet, R., Debénath, A., 2010. A new luminescence chronology for Aterian cave sites on the Atlantic coast of Morocco, in: Garcea, E.A.A. (Ed.), South-Eastern Mediterranean Peoples between 130,000 and 10,000 years ago. Oxbow Books, Oxford, pp. 18-36.

Stringer, C.B., Finlayson, J.C., Barton, R.N.E., Fernández-Jalvo, Y., Cáceres, I., Sabin, R.C., Rhodes, E.J., Currant, A.P., Rodríguez-Vidal, J., Giles-Pacheco, F., Riquelme-Cantal, J.A., 2008. Neanderthal exploitation of marine mammals in Gibraltar. Proceedings of the National Academy of Sciences 105, 14319-14324.

Thomsen, K.J., Murray, A., Jain, M., 2012. The dose dependency of the over-dispersion of quartz OSL single grain dose distributions. Radiation Measurements 47, 732-739.

Thomsen, K.J., Murray, A.S., Bøtter-Jensen, L., Kinahan, J., 2007. Determination of burial dose in incompletely bleached fluvial samples using single grains of quartz. Radiation Measurements 42, 370-379.

Villa, P., Soriano, S., Tsanova, T., Degano, I., Higham, T.F.G., d'Errico, F., Backwell, L., Lucejko, J.J., Colombini, M.P., Beaumont, P.B., 2012. Border Cave and the beginning of the Later Stone Age in South Africa. Proceedings of the National Academy of Sciences 109, 13208-13213.

Zilhão, J., Ajas, A., Badal, E., Burow, C., Kehl, M., López-Sáez, J.A., Pimenta, C., Preece, R.C., Sanchis, A., Sanz, M., Weniger, G.-C., White, D., Wood, R., Angelucci, D.E., Villaverde, V., Zapata, J., 2016. Cueva Antón: A multi-proxy MIS 3 to MIS 5a paleoenvironmental record for SE Iberia. Quaternary Science Reviews 146, 251-273.

Summary

The western Mediterranean is a key region to understand human dispersal events within and out of the African continent as well as for the eventual replacement of Neanderthals by anatomically modern humans during the Pleistocene. Palaeolithic cave sites safely store records of hominin presence and lifestyle at a certain time in a certain region and can, furthermore, yield useful information about past environmental conditions. Central to any conclusive interpretation of archaeological and palaeoclimatic datasets is the establishment of a reliable chronostratigraphic framework for the investigated site.

Optically stimulated luminescence (OSL) dating provides an estimate of the time elapsed since quartz or feldspar minerals were last exposed to sunlight. The technique, therefore, enables determination of the burial age of sediments at geoscientific and archaeological sites. Single-grain OSL dating is of particular importance in the latter context, as stratigraphical layers at those sites are regularly affected by e.g. post-depositional mixing due to natural or anthropogenic processes, which can result in significant over- or underestimation of the true burial age when using multiple-grain dating approaches.

In this thesis, single-grain OSL dating was used to investigate the general luminescence characteristics of the sedimentary deposits at three Palaeolithic cave sites in the western Mediterranean - the Thomas Quarries and Rhafas, both Morocco, and Vanguard Cave, Gibraltar - and to identify potential factors that might falsely alter their determined burial ages to eventually provide reliable chronologies for those sites. Dating results were coupled with archaeological, sedimentological and geological proxy data to allow conclusive statements regarding the timing of human occupation phases and the appearance of technological innovations at the sites, local site formation processes and palaeoenvironmental conditions in the region in the past.

Individual grains from all three sites generally exhibit bright and fast component dominated luminescence signals. Challenges for OSL dating of the samples primarily arise from i) single grains affected by signal saturation, ii) individual grains unable to recover known laboratory doses with sufficient accuracy, iii) heterogeneous dose rates or changes in dose rates over time, and iv) post-depositional mixing of sediment layers.

OSL chronologies were developed for stratigraphical sequences at Rhafas and Vanguard Cave, while single-grain dating turned out to be an inadequate technique for age determination of the Thomas Quarries sediments. Rhafas covers a time period from >135 ka to the Neolithic, including a technological shift from classical MSA to Aterian after 123 ka, LSA industries dated to ~21 ka and ~15 ka and evidence of climatic conditions that favoured intensive carbonate formation during MIS 3 and MIS 2 at the site. Vanguard Cave preserves a record of rapid aeolian sedimentation between MIS 5 and ~43 ka with evidence for repeated occupation by Neanderthals. The sedimentary record of the site suggests that relatively stable mild and sub-humid Mediterranean climatic conditions persisted in the area throughout its entire depositional history.

Samenvatting

De westelijke Middellandse Zee is een belangrijke regio voor ons begrip van de menselijke verspreiding in en vanuit Afrika, met inbegrip van de aflossing van Neandertalers door anatomisch moderne mensen in het Pleistoceen. Paleolitische vindplaatsen bevatten overblijfselen van de aanwezigheid en het gedrag van mensachtigen in het verleden op een specifiek moment en kunnen daarbij ook informatie leveren over vroegere klimaatsomstandigheden. Centraal voor dergelijke archeologische and paleoclimatologische datasets is de vaststelling van een betrouwbare chronostratigrafie voor de onderzochte vindplaats.

Optisch gestimuleerde luminescentie (OSL) datering geeft een ouderdomsbepaling vanaf het moment dat een zandkorrel kwarts of veldspaat voor het laatst blootgesteld was aan zonlicht. De methode maakt het daarmee mogelijk de ouderdom te bepalen van geologische of archeologische sedimenten. OSL toegepast of individuele zandkorrels ("single-grain") is van essentieel belang bij de bestudering van archeologische vindplaatsen omdat de stratigrafische lagen op deze vindplaatsen vaak te maken hebben met postdepositionele vermenging door natuurlijke of menselijke processen. Zulke processen kunnen leiden tot grote verschillen tussen de gemeten ouderdom en de correcte ouderdom in OSL op conventionele , "multiple-grain", monsters.

In deze dissertatie is single-grain OSL datering gebruikt om de luminescentiekenmerken te bepalen van sedimenten afkomstig van drie Paleolitische vindplaatsen rond de westelijke Middellandse Zee – de Thomas Quarries en Rhafas, beiden in Marokko, en Vanguard Cave, in Gibraltar – en vervolgens de factoren te identificeren die mogelijkerwijs tot een valse ouderdomsbepaling konden leiden. Dateringen werden daarna gekoppeld aan archeologische, sedimentaire en geologische proxies om conclusies te kunnen trekken over het moment van menselijke aanwezigheid alsmede het verschijnen van nieuwe technologische innovaties, lokale sedimentarie processen, en regionale klimaatsreconstructies.

Individuele grains van alle drie de vindplaatsen worden over het algemeen gedomineerd door de heldere, snelle luminescentie-component. OSL op dergelijke single-grains wordt bemoeilijkt door: i) luminescentieverzadiging van individuele grains, ii) single-grains die de overdosis niet met voldoende nauwkeurigheid reproduceren, iii) heterogene dosistempos binnen de sedimenten, of verschillen in dosistempo gedurende de begravingsduur, iv) postdepositionele vermenging van sedimentlagen.

OSL chronologieën konden hiermee worden verkregen voor Rhafas en Vanguard Cave, terwijl single-grain datering niet in staat bleek een datering te verkrijgen voor de sedimenten van Thomas Quarries. Rhafas omvat de tijdsperiode van >135 ka tot het Neolithicum, waarin de belangrijke technologische verschuiving valt van het MSA naar het Aterian na 123 ka, LSA technologie rond 21 ka en 15 ka, en de aanwezigheid van klimaatsfactoren die de aanwas van grote carbonaatdeposities tijdens MIS 3 en MIS 2 bevorderden. Vanguard Cave preserveert een serie snelle windafzettingen tussen MIS 5 en 43 ka met bewijs voor de herhaalde aanwezigheid van Neanderthalers. De sedimenten van Vanguard Cave suggereren daarmee dat een relatief stabiel, humide Mediterraans klimaat aanwezig was in de regio gedurende de gehele depositionele geschiedenis.

Acknowledgements

In summer 2005, just a couple of weeks before starting my first semester at the university, I visited my grandmother, Hanna Dörschner, who made a huge effort during my stay to tentatively talk me out of studying geography, in favour of a more grounded degree programme. She never got mad at me because I refused to follow her advice back then, and although she kept being sceptical about the career path I decided to follow, she supported me unconditionally and got more and more excited about it with every little step I took on my way to this PhD. I feel sad that she wasn't given the chance to see it finally coming to this happy ending, but am more than grateful for almost thirty years of encouragement and support.

Crucial to the realisation of my dissertation and articles has been the help of my supervisors. I would like to thank Jean-Jacques Hublin for his unwavering support and his valuable advices in many aspects of my work over the past years. Kathryn Fitzsimmons guided me through the complexities of this PhD, whether it concerned field work, luminescence dating, palaeoenvironmental reconstructions or scientific writing, she always helped me make sense of my data and opened new lines of thoughts when I felt lost.

The publications featured in this dissertation could not have been realised without the support of my co-authors, who spent hours in collecting research data and in writing on and correcting these articles. Thanks so much, Ruth Blasco, Abdeljalil Bouzouggar, Peter Ditchfield, Geraldine and Clive Finlayson, Sue McLaren, Shannon McPherron, Joaquín Rodríguez-Vidal, Jordi Rosell, Teresa Steele and Christoph Zielhofer for your support during field work and for providing me with essential data in the fields of archaeology, geology, sedimentology, micromorphology and isotope analyses. My special thanks belong to Shannon McPherron who also provided much-needed assistance on the various aspects of Palaeolithic archaeology and gave critical, but always friendly, comments which significantly improved my work. Many thanks to Marion Hernandez for introducing me to the solar simulator and for valuable discussions on the setup and results of dose recovery test experiments. I would also like to acknowledge my colleagues from the Casablanca project, Jean-Paul Raynal and Abderrahim Mohib, and thank them for our fruitful cooperation, which will hopefully result in a satisfactory chronostratigraphic framework for this outstanding Palaeolithic site in the coming years.

This research was made possible financially by the Max Planck Society and greatly supported by my colleagues from the Department of Human Evolution at the Max Planck Institute for Evolutionary Anthropology. I would like to thank all of you for commenting on test runs of presentations or poster drafts and for helping me solve the small problems in the everyday life of a PhD student. Thank you, Vera Aldeias, for intensive geoscientific discussions. Special thanks also go to Steffi Hesse for her

invaluable help not only in the luminescence lab and to Marjolein Bosch, Debra Colarossi, Tobias Lauer, Simon Neubauer and especially Stefanie Stelzer for their moral support during spontaneous coffee breaks when my head was overloaded with work. You all became close friends over the years and it has been a great pleasure to work with you.

My family, in particular my parents, Etta and Michael Dörschner, and my close friends, Katrin Krüger, Julia Burda, Anja and Ingmar Nitze and Jens Hartwich, have always been extremely supportive during the ups and downs of this PhD, irrespective of the spatial distance that separated us from time to time.

Finally, and most importantly, I would like to thank Thorsten Dörschner, my lovely husband, for supporting me unconditionally since now more than fourteen years. You are a source of boundless patience and encouragement which helped me to never give up. You had my back at any time over the past years and gave me the strength and self-confidence to start the biggest adventure of our lives. Having a baby right in the middle of my PhD has been challenging for both of us, still neither of us has ever regretted this decision for a single moment. We were rewarded with the most beautiful and precious little gift, our beloved daughter Eliza, who joyfully brought chaos into our daily routine. Who would have thought that hours over hours of sorting beads or watching sharks in the zoo swim in circles could be such delightful and satisfying experiences? You both taught me new perspectives on life and keep inspiring and me every single day.

Curriculum vitae

The author of this dissertation, Nina Dörschner, was born on the twenty-sixth of March in 1986, in Berlin, Germany. After receiving her Abitur in 2005, she followed the Bachelor of Science program in geographical sciences at the Freie Universität, Berlin, from which she graduated in 2008. Her growing interest on the chronometric dating of sediments initially aroused while working on her Bachelor thesis, which focussed on the geomorphology and timing of glacial and post-glacial landforms in north-eastern Germany, and made her decide to continue her studies at the Freie Universität. She undertook a Master program in geography specialising in terrestrial systems and obtained her degree (M.Sc.) in 2011, with a thesis on the reconstruction of the Holocene evolution of a coastal dune system, Fulong Beach, in north-eastern Taiwan using luminescence dating. Her master project was granted by the DAAD (Deutscher Akademischer Austausch Dienst) and included beside field work in Taiwan also OSL sample preparation and dating at the LIAG (Leibniz Institute for Applied Geophysics), Hannover. The results of her master thesis were published in 2012 as part of the Special Issue “Late Quaternary morphodynamics in East Asia” in Quaternary International. In 2011 she started her PhD on the OSL dating of Palaeolithic cave sites and their environmental context in the western Mediterranean under the supervision of Dr. habil. Kathryn E. Fitzsimmons and Prof. Dr. Jean-Jacques Hublin. During her PhD she conducted active research in Morocco and Gibraltar, published her research in several peer-reviewed international journals and presented her work at archaeological, geoscientific and luminescence dating conferences.

Appendix A

Supplementary information of Doerschner et al. (2016), PLoS ONE

S1 File

MSA/MP nomenclature in the Maghreb.

The Maghreb (comprising Morocco, Algeria, Tunisia and western Libya) is geographically located in the transition zone between the Middle/Upper Paleolithic (MP/UP) industries of western Eurasia and the African MSA/LSA [1]. The geographical position and characteristics of stone tool morphologies of the Maghreb inevitably raise the question regarding nomenclature for the Palaeolithic technocomplexes in the region. Although recent papers invest much effort into resolving the ongoing scientific debate by providing critical reviews on the characteristics of these stone tool assemblages [2, 3], an overall accepted terminology for the Palaeolithic industries from the Maghreb has yet to be agreed upon. Dibble et al. [2] pointed out that the attribution of many assemblages from Morocco to the MP seem to have happened largely due to historical reasons, and that they moreover share closer affinity to other MSA industries from the African continent. For our paper, we decided to use the African terminology and consequently use the terms MSA and LSA for the respective Palaeolithic industries from the Maghreb.

References

1. Garcea EAA. The Spread of Aterian Peoples in North Africa. In: Garcea EAA, editor. South-Eastern Mediterranean Peoples Between 130,000 and 10,000 Years Ago. Oxford: Oxbow Books; 2010. p. 37-53.

2. Dibble HL, Aldeias V, Jacobs Z, Olszewski DI, Rezek Z, Lin SC, et al. On the industrial attributions of the Aterian and Mousterian of the Maghreb. Journal of Human Evolution. 2013;64(3):194-210. doi: http://dx.doi.org/10.1016/j.jhevol.2012.10.010.

3. Linstädter J, Eiwanger J, Mikdad A, Weniger G-C. Human occupation of Northwest Africa: A review of Middle Palaeolithic to Epipalaeolithic sites in Morocco. Quaternary International. 2012;274:158-74.

S2 File: Sediment and bedrock analyses

Grain size

Subsamples of 10 g (<2 mm diameter) were treated with hydrogen peroxide (50 ml, 35%) overnight and heated during the next day to remove any organic matter. Afterwards, the samples were dispersed using sodium pyrophosphate solution (10 ml, 0.4 N) and ultrasonic treatment for 45 minutes. Carbonates were not dissolved, in order to retain the original grain sizes of each sample. Particle-size analysis of the sand fraction was carried out by dry-sieving with screens of 63, 125, 200 and 630 µm. The subfractions of silt and clay were determined by X-ray granulometry using a SediGraph IIITM with MasterTech 052 AutosamplerTM (Micrometrics) [1].

XRF analysis

XRF analyses were applied to sediment samples and bedrock materials to obtain their elemental compositions. Concentrations of specific elements and their ratios can serve as indicators for sediment provenience and weathering processes.

Bedrock materials were put in a steel cylinder, closed with a steel pin and crushed manually by hammering on the steel pin. The crushed bedrock samples and subsamples of the air-dried sediments (8 g, <2 mm diameter) were homogenised and milled to fine powder (<30 µm) using a vibration mill MM 200 (Retsch) for 10 min at 30 Hz). 4 g of the milled powder was mixed and homogenised with a binder (1 g Cereox Licowax). Subsequently, the mixture was filled into a die and pressed to pellets by a Vaneox press (20 t for 2 min). Analyses were carried out with a Spectro Xepos X-ray fluorescence analyser under a He gas atmosphere. Contents of the elements from sodium (11) to uranium (92) were simultaneously determined.

Thin sections

For the preparation of thin sections, samples were first impregnated with araldite glue and then placed in a vacuum (-20 in Hg) overnight. After being oven dried, both the samples and the glass slides were ground down to create flat surfaces using a Metaserv 2000 grinder. The samples were mounted onto the slides before being cut and then ground down using the diamond wheel on a PetroThin machine until a uniform thickness of 30 µm was achieved. Visual examinations were performed under a Nikon polarizing microscope using both plane-polarized and cross-polarized light (see the sections on micromorphological characteristics in Nash and McLaren [2] and the references therein).

Stable isotopes

For stable isotope analysis hand specimens were ground in a mortar using a pestle and then powdered in a ball mixer mill. About 1.5 mg per sample were flushed with He to remove air and then acidified with ~0.2 ml phosphoric acid (100%). CO_2 gas from the acidified samples was obtained using a Gilson autosampler system. Measurements were conducted using a SERCON Hydra 20-20 continuous flow isotope ratio mass spectrometer, calibrated via IAEA calcite standard CO8. The precision of carbonate analysis based on replicate investigation of the laboratory standard is better than 0.2‰ for both $\delta^{18}O$ and $\delta^{13}C$. Isotope values are reported per mil (‰) vs V-PDB.

References

1. Zielhofer C, Clare L, Rollefson G, Wächter S, Hoffmeister D, Bareth G, et al. The decline of the early Neolithic population center of 'Ain Ghazal and corresponding earth-surface processes, Jordan Rift Valley. Quaternary Research. 2012;78(3):427-41. doi: http://dx.doi.org/10.1016/j.yqres.2012.08.006.

2. Nash DJ, McLaren SJ, editors. Geochemical Sediments and Landscapes. Oxford: Blackwell; 2007.

Supplementary Tables

S1 Table
Measured moisture contents, beta dose rates and chosen preheat/cutheat temperatures.

Sample	Unit	Depth	Moisture content (%)		Attenuated beta dose rate (Gy/ka)		Preheat/Cutheat
		(cm)	Full saturation	Present day	Beta counter	HRGS[b]	
Cave mouth section							
L-EVA-1210	1	40	19.8	5.5[a]	0.90±0.02	0.70±0.02	260/220
L-EVA-1139	3a	55	22.9	0.9	0.73±0.01	0.74±0.01	260/220
L-EVA-1140	3b	70	22.4	1.1	0.69±0.03	0.40±0.02	260/220
L-EVA-1141	4c	110	19.2	2.2	0.68±0.01	0.56±0.01	240/200
Lower cave section							
L-EVA-1142	6d	185	24.3	1.9	1.49±0.02	2.55±0.05	260/220
L-EVA-1143	16	210	24.3	5.5	1.74±0.05	1.71±0.03	260/220
L-EVA-1083	30	260	26.8	9.3	2.32±0.05	1.99±0.04	260/220
L-EVA-1084	39	300	25.2	9.5	1.87±0.03	1.71±0.04	260/220
L-EVA-1085	55	375	26.7	5.2	1.81±0.03	1.50±0.03	260/220
L-EVA-1144	55	375	26.7	5.5	1.72±0.04	1.58±0.03	260/220
Terrace section							
L-EVA-1145	S2	45	25.0	12.1[a]	0.76±0.02	0.89±0.02	260/220
L-EVA-1146	S3	70	24.5	4.1[a]	0.79±0.01	0.73±0.02	260/220
L-EVA-1212	S5	100	19.4	4.1[a]	0.62±0.01	0.49±0.01	260/220
L-EVA-1213	S6	115	17.0	3.6[a]	0.93±0.02	0.51±0.02	260/220
L-EVA-1148	S7	150	23.8	8.1[a]	0.81±0.02	0.84±0.02	260/220

[a]Samples were collected after a rain event.
[b]High resolution gamma spectrometry.

S2 Table

Summary of faunal remains.

Linnaean Names	Vernacular Names	MIS 1	MIS 2		MIS 3		MIS 5			MIS 6			Wengler's
		1[a]	S2[a]	S3[a]-S4[b]	S5[a]	3a[a]	S6[a]	3b[a]	S7[a]	4ab[b]	4c[a]	5[b]	Unit III[b]
Hystrix cristata	crested porcupine	2											
Lepus sp.	hare	1		1									
Felis cf. *caracal*	cf. caracal	1											
Canis sp.	dog or jackal	1											1
Equus sp.	indet. equid	13	35	5	1	1		2	10	2	3	4	24
Rhinocerotidae gen. et sp. indet.	rhinoceros	1						1			1		2
Suidae gen. et sp. indet.	pig(s)	3											
Sus sp.	pig	3											
Phacochoerus africanus	warthog						1						
Gazella sp.	gazelle	5	6	1							1		1
Caprini	sheep/goat	6											
Ammotragus lervia	Barbary sheep/aoudad		1										
Alcelaphini gen. et sp. indet.	hartebeest/wildebeest	19	21										14
Bovini gen. et sp. indet.	bovine	1	4						1				1
	Small bovid(s)	35	23		2	2							4
	Small-medium bovid(s)	92	55	2	1		1		1		1	1	10
	Large-medium bovid(s)	38	66	4		2					2	3	38
	Large bovid(s)	9	11				1	2			2		16
NISP		230	222	13	4	5	3	5	12	2	10	8	115
	Coprolite											2	4
Aves	Bird												1
Struthio camelus	Ostrich eggshell	18	6							1			3
	Terrestrial tortoise	18	4		1		1						1
	Terrestrial mollusk	122	8	2	4				2				

[a]Layer dated in this study.

[b]Chronological position is undetermined.

S3 Table

Single grain characteristics.

Sample	n[a]	No signal[b]	T_N signal <3x BG	No L_N/T_N intersection	Dim grains[c]	Recuperation >5%	Poor recycling ratio (>20%)	Depletion by IR	D_e error >30%	Grubbs test[d]	accepted grains	
	(100%)	(%)	(%)	(%)	(%)	(%)	(%)	(%)	(%)	(%)	total	(%)
Cave mouth section												
L-EVA-1210	4100	76.2	0.2	3.2	12.1	0.1	3.1	3.4	0.2	0.1	54	1.3
L-EVA-1139	1000	47.9	0	7.1	14.6	0.4	9.0	11.7	2.4	0.2	67	6.7
L-EVA-1140	900	54.0	0	5.8	14.4	0.2	7.3	9.4	1.7	0.2	62	6.9
L-EVA-1141	1000	52.5	0.2	17.9	4.3	2.2	5.7	10.1	0.5	0	66	6.6
Terrace section												
L-EVA-1145	1200	57.9	0.2	1.3	16.9	0.4	8.5	9.8	0.1	0.1	58	4.8
L-EVA-1146	1300	69.1	0.2	1.9	11.5	0.6	4.9	6.5	0.2	0	68	5.2
L-EVA-1212	1400	66.3	0	2.4	9.9	0.2	6.1	9.6	0.8	0	64	4.6
L-EVA-1213	1500	67.3	0.3	7.9	7.3	0.4	4.5	7.2	1.1	0	59	3.9
L-EVA-1148	800	33.9	0.1	19.3	13.0	1.9	7.8	13.5	2.8	0	63	7.9

[a]Total number of grains measured per sample.

[b]Percentage of grains not emitting any detectable luminescence signal.

[c]Percentage of grains rejected due to insufficient test-dose signal.

[d]Percentage of grains identified as statistical outliers [1].

1. Grubbs FE. Sample Criteria for Testing Outlying Observations. 1950:27-58. doi: 10.1214/aoms/1177729885.

S4 Table
Single grain dose recovery properties.

Sample	Unit	accepted/measured grains	given dose (Gy)	measured D_e [a] (Gy)	Overdispersion (%)	recovery ratio
Cave mouth section						
L-EVA-1210	1	51/1600	11.2	10.9	2±4	0.97±0.04
L-EVA-1139	3a	86/1000	78.5	72.2	7±1	0.92±0.05
L-EVA-1140	3b	58/900	98.5	90.6	14±2	0.92±0.06
L-EVA-1141	4c	97/800	105.0	100.8	5±1	0.96±0.05
Terrace section						
L-EVA-1145	S2	88/1200	21.5	20.9	7±1	0.97±0.05
L-EVA-1146	S3	86/1400	23.9	22.9	7±1	0.96±0.05
L-EVA-1212	S5	61/900	67.2	63.8	6±1	0.95±0.05
L-EVA-1213	S6	63/900	118.3	111.2	14±2	0.94±0.07
L-EVA-1148	S7	89/800	135.2	124.4	9±1	0.92±0.05

[a]Determined using the Central Age Model (Galbraith et al., 1999).

S5 Table

Grain size results.

Sample	Layer	Grain size fractions (%)												
		fT	mT	gT	fU	mU	gU	fS	mS	gS	Total clay (T)	Total silt (U)	Total sand(S)	classified as [1, 2]
Cave mouth section														
L-EVA-1210	1	8.4	3.7	8.0	6.9	9.4	8.4	20.8	18.3	16.0	20.1	24.7	55.2	muddy Sand
L-EVA-1139	3a	4.3	1.1	2.9	2.9	3	2.9	8.0	12.9	62.0	8.3	8.8	82.9	muddy Sand
L-EVA-1140	3b	-[a]	-[a]	-[a]	-[a]	-[a]	-[a]	-[a]	-[a]	-[a]	-[a]	-[a]	-[a]	-[a]
L-EVA-1141	4c	6.8	2.4	7.1	6.7	4.4	4.5	13.7	15.8	38.6	16.3	15.6	68.1	muddy Sand
Lower cave section														
L-EVA-1142	6d	9.7	4.4	6.3	8.9	6.1	5.3	13.2	14.5	31.6	20.4	20.3	59.3	muddy Sand
L-EVA-1143	16	13.9	6.6	8.3	11.3	8.4	10.0	19.4	8.8	13.3	28.8	29.7	41.5	sandy Mud
L-EVA-1083	30	7.9	3.3	22.1	15.1	9.6	9.6	16.2	7.1	9.1	33.3	34.3	32.4	sandy Mud
L-EVA-1084	39	12.9	10.2	7.3	9.5	7.6	11.7	22.4	11.2	7.2	30.4	28.8	40.8	sandy Mud
L-EVA-1085	55	15.8	6.3	6.6	6.4	5.8	10.1	25.9	14.7	8.4	28.7	22.3	49.0	sandy Mud
L-EVA-1144	55	14.6	7.0	6.6	5.7	5.1	9.3	25.5	14.7	11.6	28.2	20.1	51.7	muddy Sand
Terrace section														
L-EVA-1145	S2	6.2	4.8	8.0	7.0	5.0	7.3	26.2	23.9	11.6	19.0	19.3	61.7	muddy Sand
L-EVA-1146	S3	10.1	7.6	9.4	7.0	5.1	6.9	21.8	17.3	14.9	27.1	19.0	53.9	muddy Sand
L-EVA-1212	S5	9.3	6.2	9.3	6.4	4.5	4.0	15.9	22.5	22.0	24.8	14.9	60.3	muddy Sand
L-EVA-1213	S6	11.7	5.2	7.0	6.2	4.5	4.4	16.3	20.7	24.0	23.9	15.1	61.0	muddy Sand
L-EVA-1148	S7	9.6	6.2	9.0	7.5	4.9	5.5	20.5	22.7	14.1	24.8	17.9	57.3	muddy Sand

[a]Not enough sample material for grain size determination available.

1. Folk RL. The distinction between grain size and mineral composition in sedimentary rocks. Journal of Geology. 1954;62:344-59.
2. Folk RL. Petrology of Sedimentary Rocks. Austin, TX: Hemphill Publishing; 1980. 184 p.

S6 Table

XRF results and $CaCO_3$ content.

Sample	S	Cl	Mg	Ca	Al	Fe	Na/Cl 10^0	Pb/Al 10^{-3}	Rb/K 10^{-3}	Ni/Al 10^{-3}	Ti/Th 10^3	K/Al 10^0	$CaCO_3$
	(g/kg)						mol ratio						(%)
Cave mouth section													
L-EVA-1210	0.56	0.20	32.0	207	20.3	15.0	52.4	3.36	3.15	0.97	0.27	0.42	56
L-EVA-1139	0.65	0.16	20.5	273	14.8	9.8	67.0	2.48	3.91	3.12	0.21	0.39	78
L-EVA-1140	0.55	0.23	20.2	261	14.9	9.9	41.4	2.88	3.86	2.71	0.22	0.39	89
L-EVA-1141	0.52	0.20	19.7	254	18.7	11.7	46.7	1.57	3.81	1.37	0.23	0.35	62
Lower cave section													
L-EVA-1142	2.18	4.59	27.7	197	23.5	14.9	3.3	0.96	1.54	0.93	0.30	0.93	61
L-EVA-1143	2.92	0.96	25.6	130	44.5	23.9	10.5	0.77	2.82	0.63	0.41	0.42	33
L-EVA-1083	3.21	11.3	42.3	92	40.2	23.9	1.7	1.17	2.13	0.70	0.38	0.61	26
L-EVA-1084	2.62	4.09	29.6	88	47.7	25.0	5.0	1.09	2.54	0.66	0.39	0.45	19
L-EVA-1085	0.44	1.86	25.5	61	53.9	26.9	5.8	0.82	2.43	0.55	0.44	0.41	34
L-EVA-1144	0.88	1.02	26.3	85	49.9	26.1	12.9	0.87	2.50	0.57	0.46	0.40	21
Terrace section													
L-EVA-1145	0.64	0.19	29.0	168	31.3	17.3	69.4	12.18	3.37	0.67	0.32	0.30	35
L-EVA-1146	0.34	0.11	20.9	207	28.0	16.4	61.0	2.50	4.00	0.80	0.30	0.29	45
L-EVA-1212	0.30	0.11	20.9	240	18.3	10.7	77.1	1.93	3.85	0.89	0.25	0.29	79
L-EVA-1213	0.30	0.10	19.9	186	33.2	19.0	90.3	1.14	3.73	0.89	0.34	0.27	66
L-EVA-1148	0.21	0.12	20.4	191	33.7	17.9	79.5	0.93	3.62	0.81	0.36	0.27	34

S7 Table
Summary of istope data.

Sample	$\delta^{13}C$ (‰)	$\delta^{18}O$ (‰)
Calcrete		
2iii	-7.65	-5.03
3i	-6.67	-6.61
3iii	-6.79	-6.33
4ii	-6.56	-6.23
5i	-4.31	-6.84
5ii	-4.87	-7.31
mean	**-6.14**	**-6.39**
standard deviation	**1.16**	**0.70**
Organic layer		
3iii	-2.85	-8.16
4i	-1.21	-9.48
mean	***-2.03***	***-8.82***
standard deviation	***1.64***	***0.66***
Laminar crust		
5iii	-9.12	-5.33

S8 Table

FMM details.For L-EVA-1139 and L-EVA-1140 BIC and llik continuously increase and decrease, respectively, when Overdispersion values further increase. The chosen combination of Overdispersion and number of components used for age determination of each sample are shaded in grey.

Sample	k	σ_{OD}[1]	K1		K2		K3		BIC	llik
			D_e±error	Proportion	D_e±error	Proportion	D_e±error	Proportion		
L-EVA-1210	2	15	3.2±0.1	7.1%	10.9±0.3	92.9%			62.1	-25.09
	2	20	3.0±0.1	6.3%	10.8±0.4	93.7%			54.2	-21.13
	2	25	2.7±0.1	4.8%	10.7±0.5	95.2%			52.7	-20.36
	2	30	1.8±0.5	2.4%	10.4±1.0	97.6%			53.6	-20.81
	3	15	1.6±0.1	1.9%	5.9±0.6	14.8%	11.4±0.6	83.3%	53.0	-16.47
	3	20	1.6±0.3	1.9%	5.5±0.7	10.7%	11.2±0.4	87.4%	53.6	-16.84
	3	25	1.6±0.3	1.9%	5.0±0.8	6.9%	10.9±0.4	91.2%	56.6	-18.35
	3	30	1.6±0.4	2.0%	4.8±1.1	3.6%	10.7±0.5	94.4%	60.7	-20.39
L-EVA-1139	2	15	71.3±14.1	42.2%	99.4±19.7	57.6%			23.0	-5.20
	2	20	72.3±30.0	28.3%	92.4±23.7	71.7%			24.5	-5.93
	3	15	51.3±24.3	3.5%	77.3±8.9	54.3%	103.7±9.2	42.2%	30.3	-4.64
	3	20	69.7±20.7	20.4%	89.5±NaN	45.5%	92.87±57.1	37.2%	30.9	-4.93
L-EVA-1140	2	15	57.2±3.4	25.9%	105.8±7.5	74.1%			55.9	-21.76
	2	20	56.7±4.6	23.1%	104.2±8.5	76.9%			51.4	-19.51
	2	25	57.1±13.5	19.9%	101.6±9.3	80.1%			53.0	-20.29
	3	15	53.4±7.7	19.3%	91.3±10.5	48.8%	122.9±12.5	31.9%	59.1	-19.23
	3	20	56.0±10.7	21.9%	97.0±12.2	38.1%	110.0±5.0	40.1%	59.6	-19.48
L-EVA-1141	2	15	59.1±2.4	21.6%	137.7±3.2	78.4%			133.0	-60.20
	2	20	56.7±3.0	18.6%	135.7±4.0	81.4%			106.2	-46.80
	2	25	55.2±3.4	16.4%	134.0±8.3	83.6%			96.1	-41.77
	2	30	53.6±7.3	13.7%	131.4±9.4	86.3%			99.3	-45.37
	3	15	50.8±7.5	14.3%	114.9±4.5	60.8%	191.6±7.9	24.9%	109.0	-44.03
	3	20	51.7±10.1	14.3%	118.2±6.0	65.4%	195.3±13.0	20.3%	103.0	-41.04
	3	25	51.9±13.9	13.5%	120.8±9.3	69.4%	188.1±23.1	17.1%	101.9	-40.46
	3	30	51.8±22.8	12.1%	115.6±NaN	35.1%	140.4±NaN	52.8%	101.6	-40.34

[1]Overdispersion used running the FMM.

Supplementary Figures

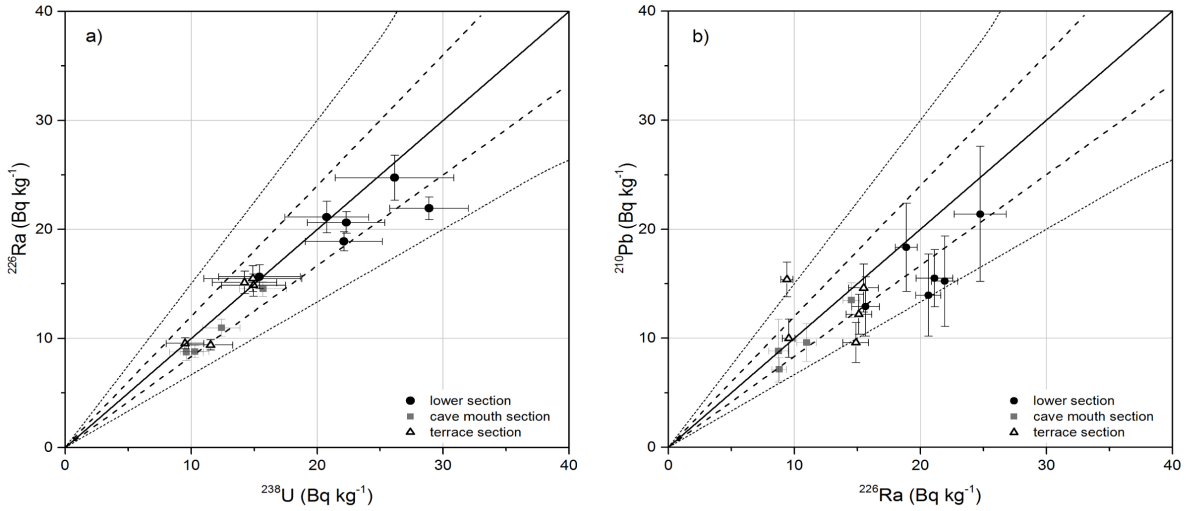

S1 Fig. Parent-daughter equilibrium plots for Rhafas. (a) 238U/226Ra (b) 226Ra/210Pb. In each figure the solid line represents secular equilibrium. Samples from the lower section, the cave mouth section and the slope section are shown as black dots, grey squares and open triangles respectively. Dashed lines represent 20% and dotted lines 50% of equilibrium.

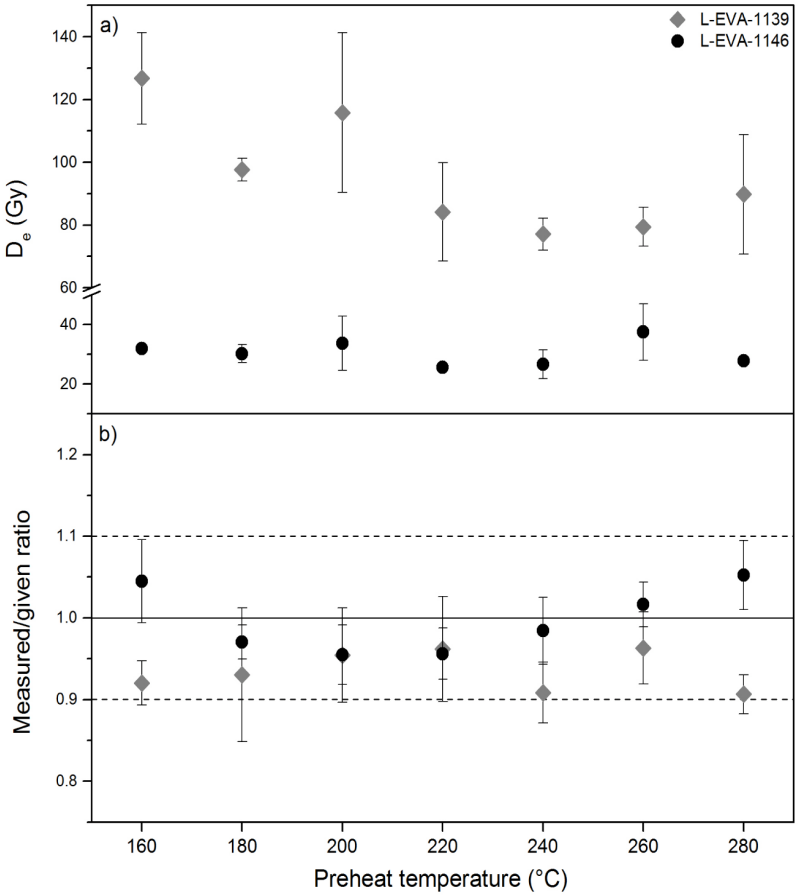

S2 Fig. Results of OSL standard performance tests. (a) Preheat plateau test (b) Dose-recovery preheat plateau test for samples L-EVA-1139 (grey diamonds) and L-EVA-1146 (black circles). The solid line indicates the target value; dashed lines represent 10% deviation from unity.

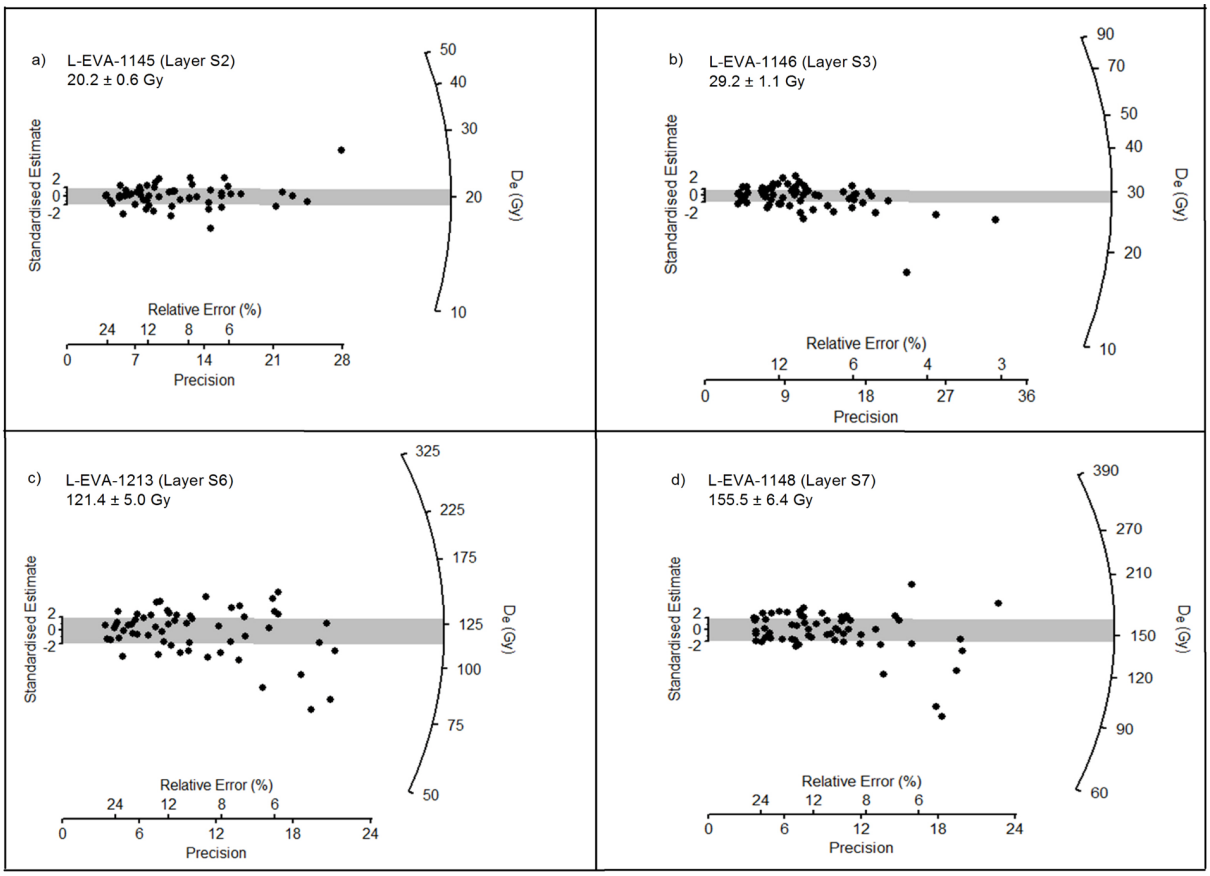

S3 Fig. Radial plots showing the dose distributions of single grain values of samples from the terrace section. (a) L-EVA-1145, (b) L-EVA-1146, (c) L-EVA-1213 and (d) L-EVA-1148. The shaded bands in the radial plots correspond to the standard error deviation from the calculated De.

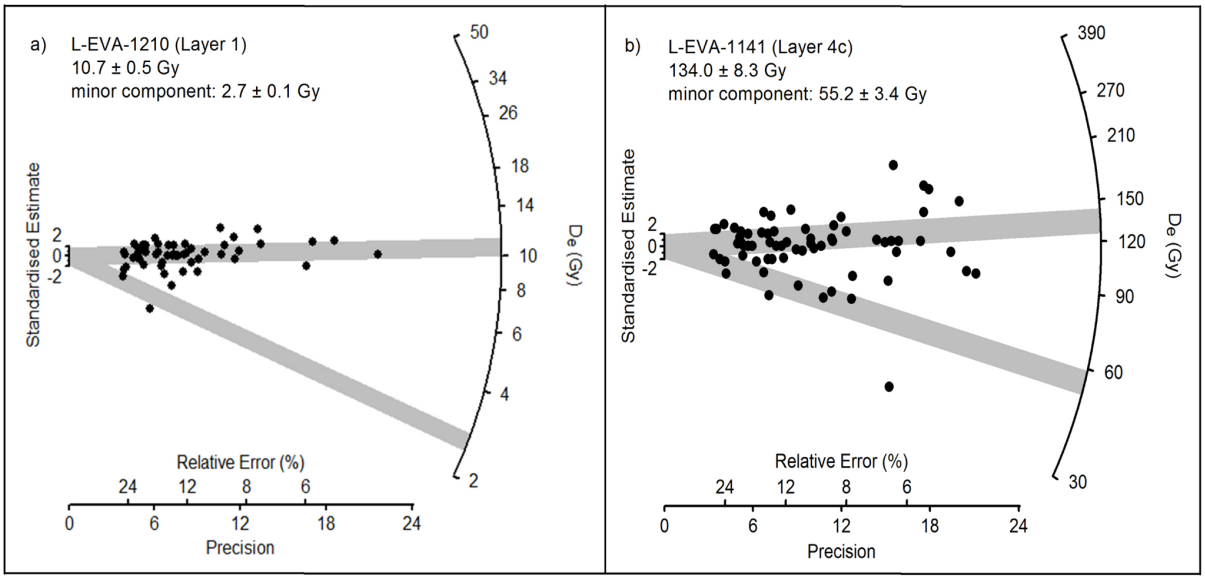

S4 Fig. Radial plots showing the dose distributions of single grain values of samples from the cave mouth section. (a) L-EVA-1210 and (b) L-EVA-1141. The shaded bands in the radial plots correspond to the standard error deviation from the calculated De for each identified component.

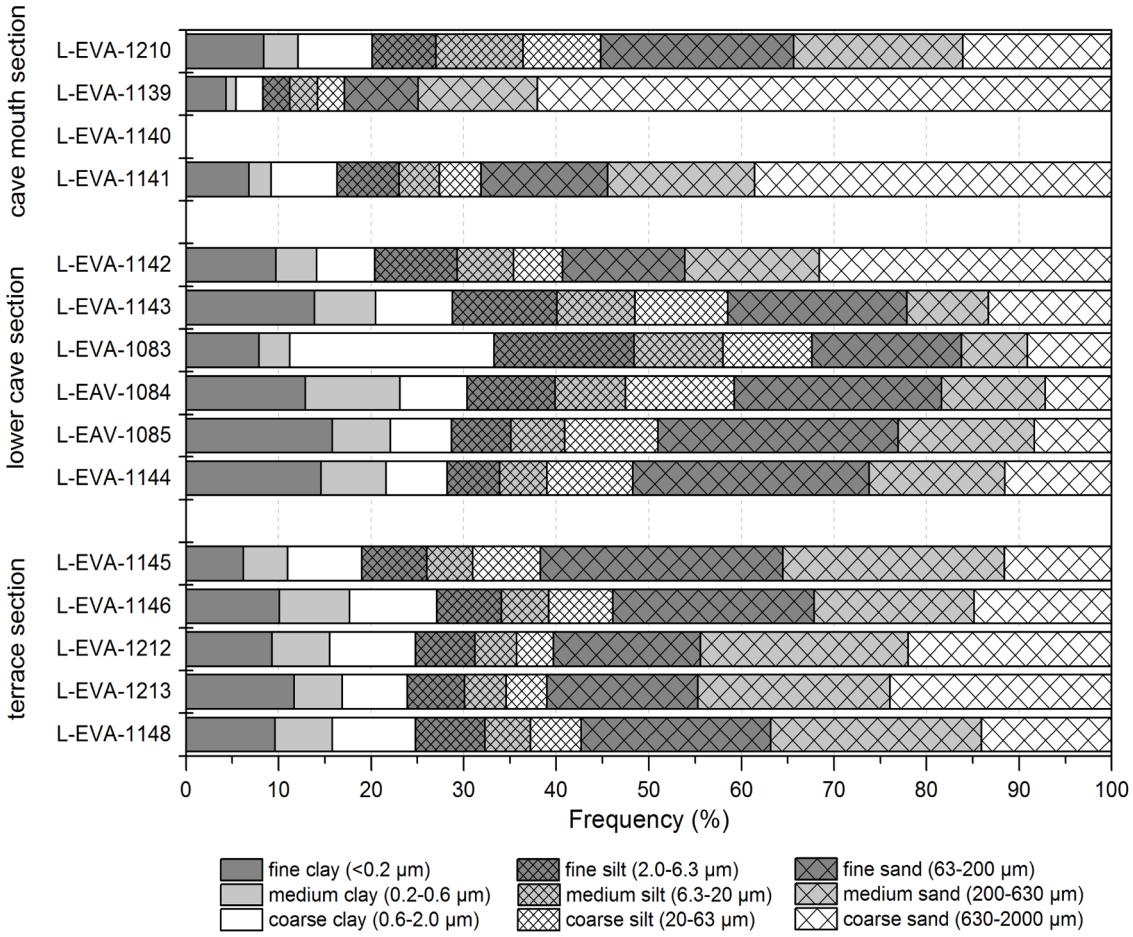

S5 Fig. Grain-size distributions of the OSL samples per section. Each stacked bar shows the percentage distribution of the grain-size classes for one sample (in total 100%).

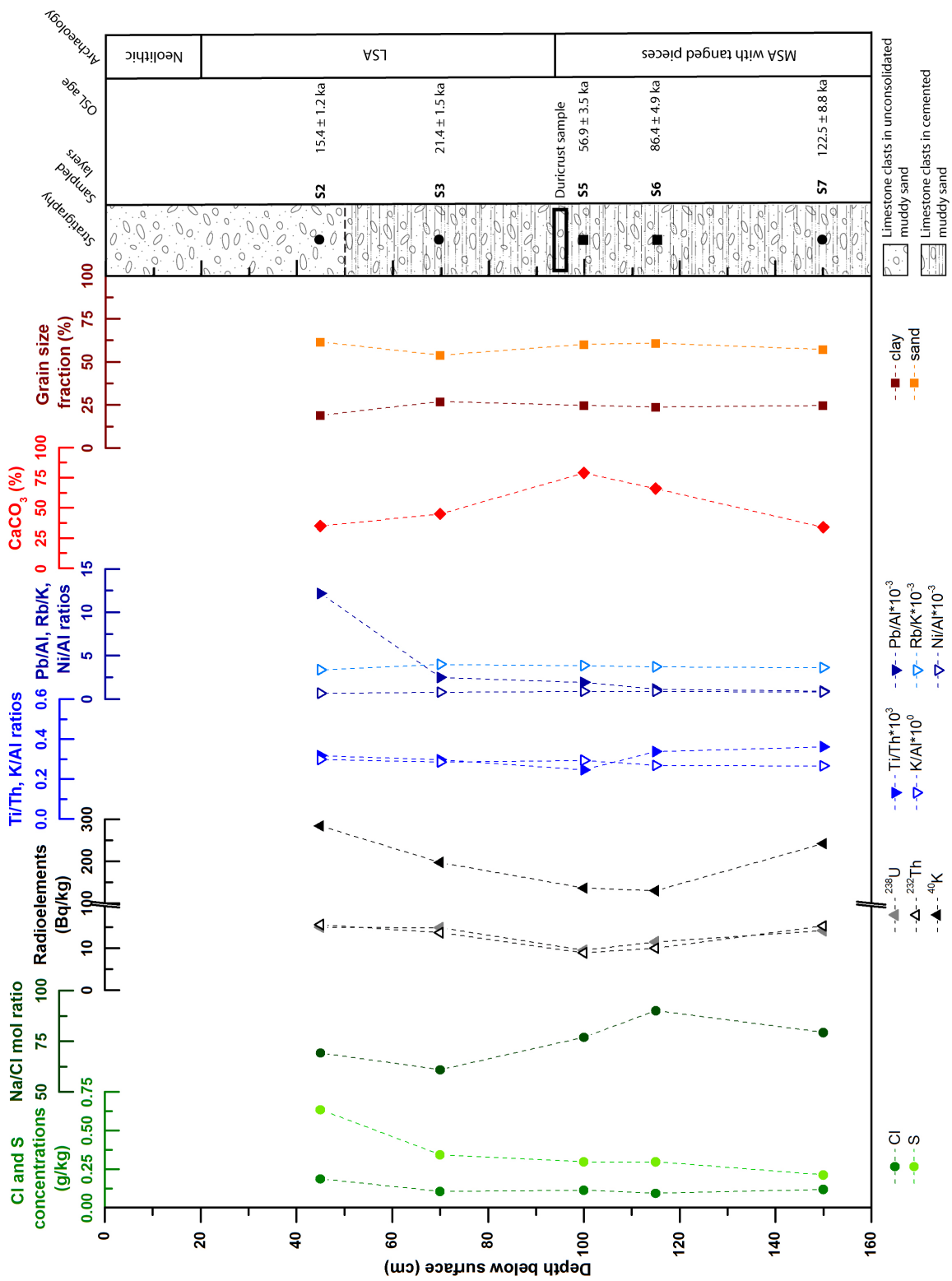

S6 Fig. Sedimentological characteristics of the terrace section.

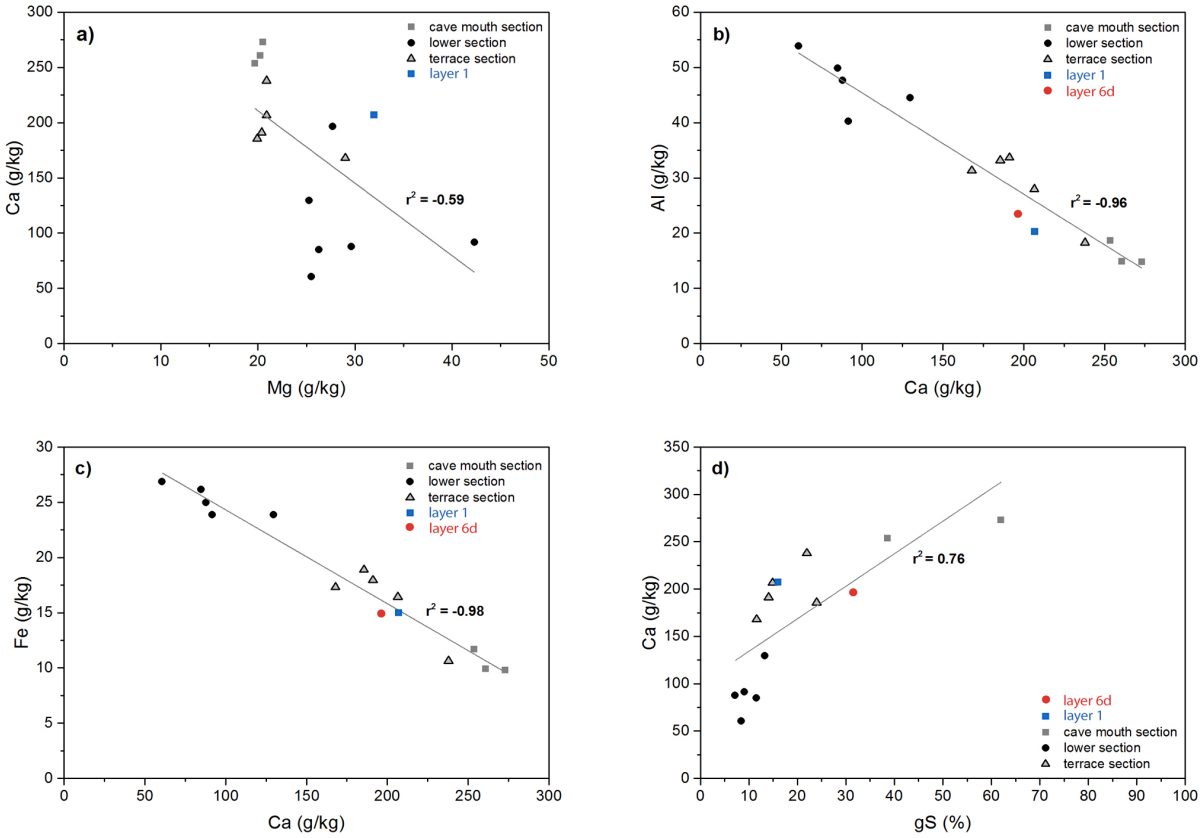

S7 Fig. XRF results showing correlations between Ca and Mg, Al and Ca, Fe and Ca, and Ca and gS. Layer 1 (blue square) and 6d (red dot) plot relatively far away from their groups, which indicates that they do not share the same sedimentological characteristics with the other layers of the cave mouth and the lower cave section, respectively.

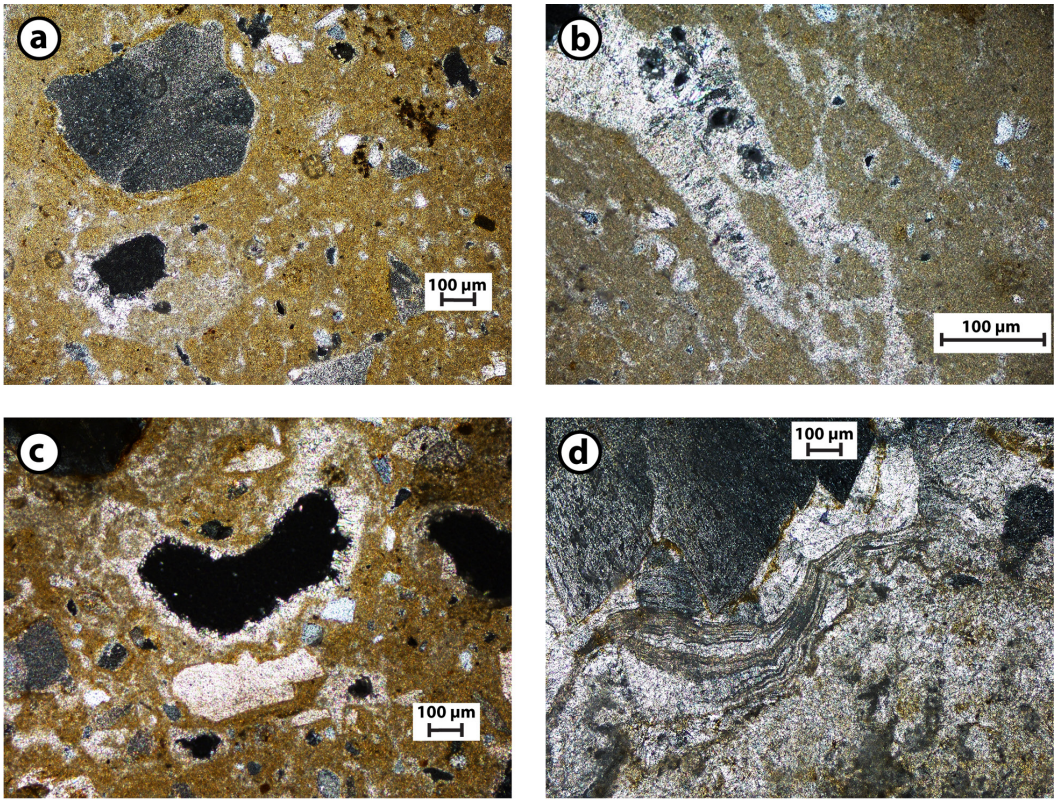

S8 Fig. Thin section photographs. (a) micritic cement with corroded lithoclasts: around one of the clasts there is evidence of the dissolution of some of the calcite cement and replacement by silica cement (arrow); (b) stringer within the silcrete-calcretes showing the chalcedony crystals in greater detail; (c) preservation of the form of a replaced calcite shell by silicification; (d) mammillary structured quartz crystals showing micro-laminated opal as well as fibrous lussatite and chalcedony. Photographs were taken under cross-polarised light.

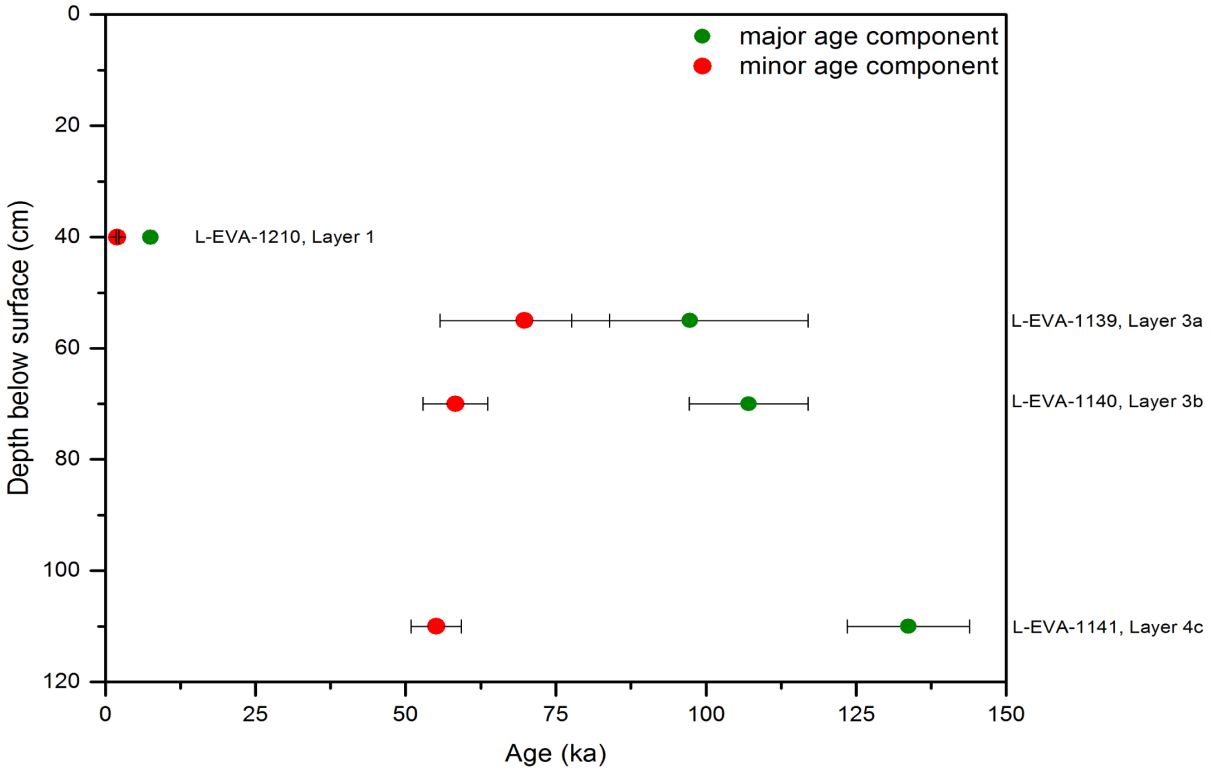

S9 Fig. Single grain OSL ages for the cave mouth section at Rhafas determined by applying the FMM. Major and minor age components are shown in green and red, respectively

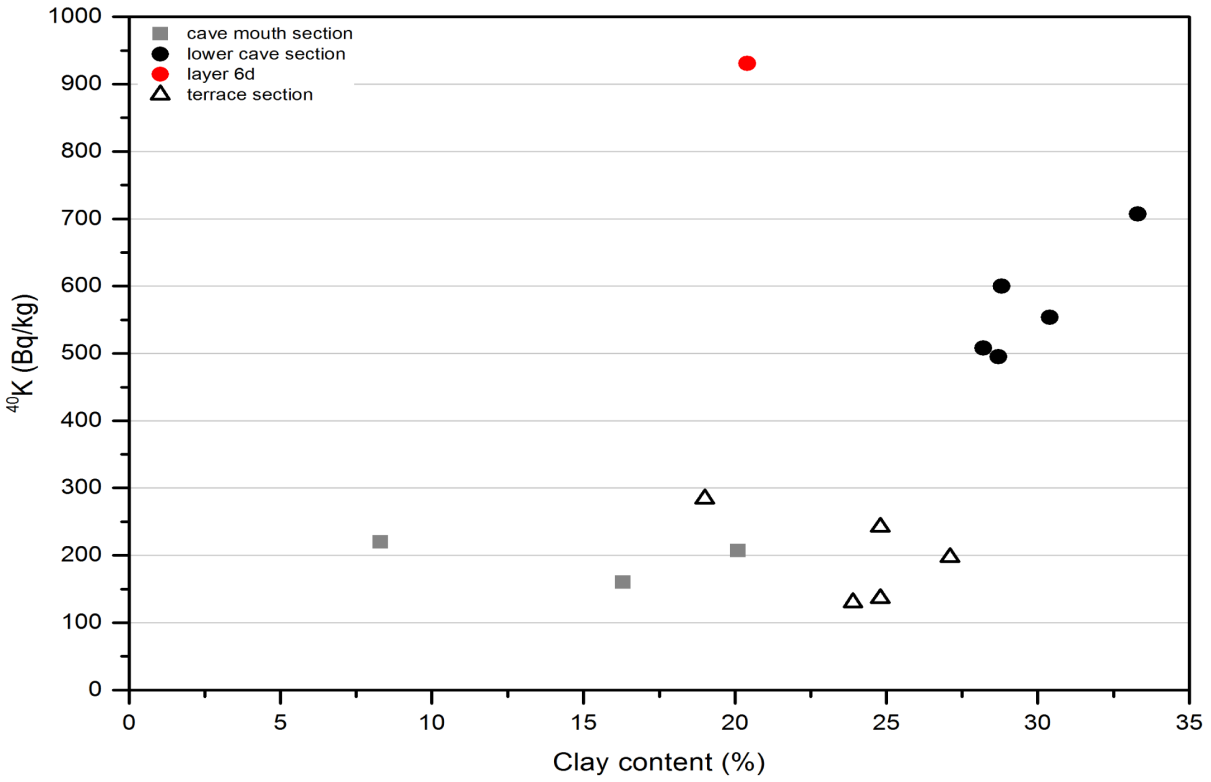

S10 Fig. Correlation between 40K and clay content at Rhafas.

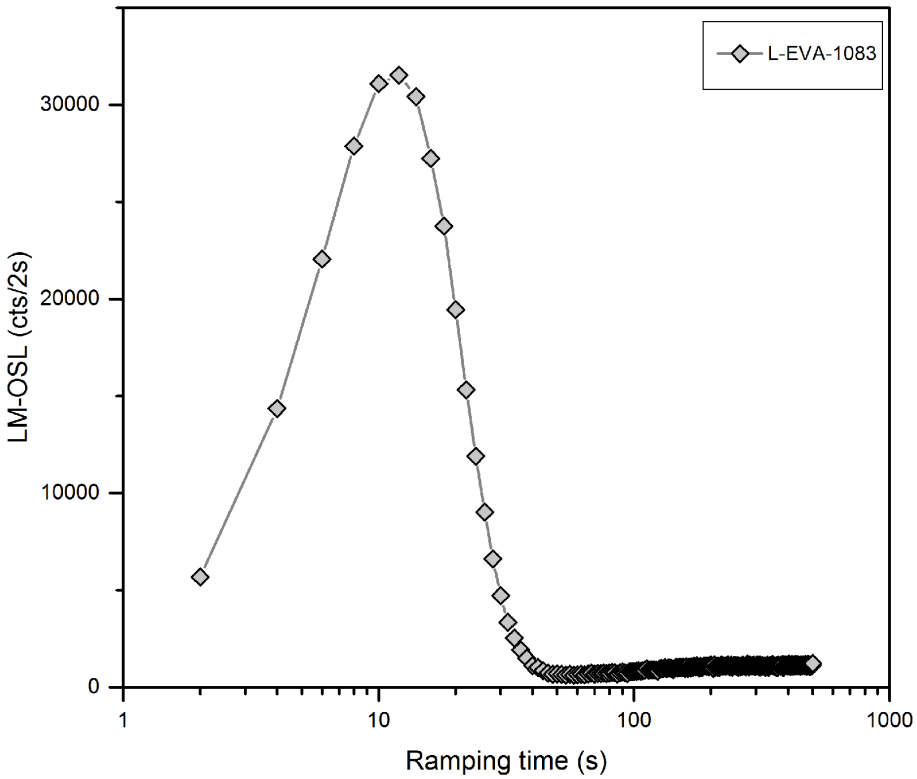

S11 Fig. LM-OSL curve for L-EVA-1083, showing dominant OSL fast component.

Appendix B

Supplementary information of Doerschner et al. (2016), Ancient TL

Supplementary tables

Table S1. Total number of individual grains measured for equivalent dose determination and dose recovery tests for each sample in this study.

Sample	Equivalent dose		Given dose (Gy)	n[1] (dose recovery)		
	n[1]	Test dose (Gy)		green laser	sunbleached	SOL2
Lake Mungo						
L-EVA-1010	600	10	49	600	600	600
			185	600	600	600
L-EVA-1012	600	4	20	600	600	900
			185	800	600	600
Rhafas						
L-EVA-1083	1100	40	20	600	1500	800
			208	800	900	800
Thomas Quarry I						
L-EVA-1218	1400	36	20	600	1100	800
			180	1200	800	800
L-EVA-1221	1400	43	20	600	1200	600
			205	600	1200	1200

[1]Total number of grains measured per sample

Table S2. Measurement details of dose recovery experiments.

Sample	Given dose (Gy)	Test dose (Gy)	Regeneration doses						
			Cycle 1 (Gy)	Cycle 2 (Gy)	Cycle 3 (Gy)	Cycle 4 (Gy)	Recuperation (Gy)	Recycling (Gy)	IR deplition (Gy)
Lake Mungo									
L-EVA-1010	49	10	18	30	60	120	0	18	18
	185	36	57	113	227	454	0	57	57
L-EVA-1012	20	4	7	14	28	56	0	7	7
	185	36	57	113	227	454	0	57	57
Rhafas									
L-EVA-1083	20	4	7	14	28	56	0	7	7
	208	42	70	140	280	560	0	70	70
Thomas Quarry I									
L-EVA-1218	20	4	7	14	28	56	0	7	7
	180	36	62	125	250	500	0	62	62
L-EVA-1221	20	4	7	14	28	56	0	7	7
	205	42	65	130	260	520	0	65	65

Table S3. Dose recovery test results prior to application of rejection criteria (apart from the uncertainty on the natural test dose response <20% criterion, which was also applied here). Highlighted in bold are values which significantly improve when rejection criteria are used (see Table 1 for comparison).

Sample	Given dose (Gy)	Dose recovery green laser			Dose recovery sunbleached			Dose recovery SOL2		
		n[1]	recovery ratio[2]	σ_{OD}^2 (%)	n[1]	recovery ratio[2]	σ_{OD}^2 (%)	n[1] (%)	recovery ratio[2]	σ_{OD}^2 (%)
Lake Mungo										
L-EVA-1010	49	505	0.94±0.01	**11±1**	485	0.97±0.01	**10±1**	447	0.96±0.01	**13±1**
	185	432	0.81±0.01	19±1	423	0.78±0.01	**16±1**	365	0.79±0.01	**21±1**
L-EVA-1012	20	506	0.97±0.01	7±1	459	0.97±0.01	10±1	536	0.96±0.01	**14±1**
	185	554	0.67±0.01	27±1	345	0.82±0.02	**23±2**	350	0.72±0.02	39±2
Rhafas										
L-EVA-1083	20	406	0.99±0.01	11±1	643	0.86±0.01	21±1	394	0.99±0.01	**14±1**
	208	338	0.96±0.02	**21±2**	366	0.87±0.01	**12±1**	444	0.80±0.01	25±2
Thomas Quarry I										
L-EVA-1218	20	508	**0.89±0.01**	**8±1**	506	0.93±0.01	10±1	433	1.00±0.01	**14±1**
	180	544	0.91±0.02	**30±2**	402	0.84±0.01	12±2	442	0.74±0.02	31±2
L-EVA-1221	20	484	0.96±0.01	7±1	582	0.95±0.01	**13±1**	457	0.96±0.01	8±1
	205	395	0.80±0.01	19±2	709	0.77±0.01	**21±1**	602	0.78±0.01	21±1

[1]Total number of grains measured per sample
[2]Determined using the Central Age Model (Galbraith et al., 1999)

Table S4. Dose recovery test results without application of the rejection criteria: $D_e>2D_0$ and D_e error <30%. Highlighted in bold are values which show significant differences to when all rejection criteria are used (see Table 1 for comparison).

Sample	Given dose (Gy)	Dose recovery green laser			Dose recovery sunbleached			Dose recovery SOL2		
		n[1]	recovery ratio[2]	σ_{OD}^2 (%)	n[1]	recovery ratio[2]	σ_{OD}^2 (%)	n[1] (%)	recovery ratio[2]	σ_{OD}^2 (%)
Lake Mungo										
L-EVA-1010	49	150	0.95±0.01	7±1	118	0.96±0.01	6±1	125	0.96±0.01	10±1
	185	168	0.82±0.01	18±1	126	0.79±0.01	12±1	96	0.82±0.02	14±2
L-EVA-1012	20	129	0.96±0.01	6±1	111	0.97±0.01	9±1	93	0.94±0.01	11±1
	185	181	0.68±0.03	26±2	94	0.89±0.02	15±2	109	0.73±0.03	35±3
Rhafas										
L-EVA-1083	20	67	0.97±0.01	9±1	95	0.83±0.02	22±2	54	0.99±0.02	10±2
	208	85	**0.99±0.02**	**17±2**	64	0.88±0.01	5±2	84	0.79±0.02	23±2
Thomas Quarry I										
L-EVA-1218	20	100	0.93±0.01	5±1	47	0.91±0.02	8±2	64	1.03±0.02	7±2
	180	113	0.93±0.03	20±3	91	0.87±0.02	9±2	86	0.79±0.03	27±3
L-EVA-1221	20	104	0.95±0.01	6±1	56	0.93±0.02	9±2	69	0.97±0.01	9±1
	205	76	0.84±0.02	14±2	148	0.80±0.02	15±2	170	0.78±0.02	19±2

[1]Total number of grains measured per sample
[2]Determined using the Central Age Model (Galbraith et al., 1999).

Tale S5. CAM dose recovery test results after high given doses as a function of single grain D_0 values. Highlighted in bold are obtained dose recovery values closest to unity for the different bleaching treatments for each sample.

D_0	green laser			sunbleached			SOL2		
	n^1	recovery ratio[2]	σ_{OD}^2	n^1	recovery ratio[2]	σ_{OD}^2	n^1	recovery ratio[2]	σ_{OD}^2
L-EVA-1010 (given dose: 185 Gy)									
D_0 range		50-395 Gy			52-463 Gy			40-309 Gy	
all	100	0.80±0.02	18±2	84	0.79±0.01	12±1	73	0.81±0.01	10±1
>50 Gy	-	-	-	-	-	-	72	0.81±0.02	11±2
>75 Gy	85	0.82±0.02	15±2	71	0.81±0.01	10±2	63	0.84±0.02	11±2
>100 Gy	61	0.85±0.02	14±2	43	0.83±0.02	11±2	47	0.85±0.02	11±2
>125 Gy	26	0.87±0.03	15±3	21	0.84±0.01	3±3	26	0.86±0.02	5±2
>150 Gy	12	0.89±0.04	13±3	15	0.85±0.02	2±3	13	**0.88±0.02**	5±3
>175 Gy	6	**0.95±0.06**	14±5	7	0.86±0.02	4±3	5	0.84±0.03	0
>200 Gy	5	0.91±0.12	12±5	5	**0.87±0.04**	6±4	4	0.85±0.04	0
$>D_{given}$	6	0.91±0.12	12±5	7	0.86±0.02	4±3	4	0.85±0.04	0
L-EVA-1012 (given dose: 185 Gy)									
D_0 range		45-305 Gy			59-367 Gy			23-276 Gy	
all	142	0.67±0.02	25±2	59	0.86±0.02	12±2	76	0.68±0.03	35±3
>50 Gy	135	0.68±0.02	25±2	-	-	-	71	0.72±0.03	27±3
>75 Gy	107	0.73±0.02	21±3	54	0.88±0.02	12±2	62	0.78±0.02	20±2
>100 Gy	66	0.77±0.02	20±3	39	0.90±0.02	10±2	44	0.81±0.03	18±3
>125 Gy	34	0.80±0.03	20±3	23	0.92±0.02	9±2	26	**0.83±0.03**	17±3
>150 Gy	15	**0.87±0.04**	17±4	15	0.93±0.03	9±3	10	0.81±0.04	11±4
>175 Gy	10	0.84±0.04	13±4	9	0.93±0.03	3±5	5	0.79±0.07	15±7
>200 Gy	5	0.86±0.03	0±30	6	**0.94±0.04**	5±5	2	0.72±0.10	0
$>D_{given}$	8	0.80±0.03	9±4	6	**0.94±0.04**	5±5	4	0.76±0.08	16±8
L-EVA-1083 (given dose: 208 Gy)									
D_0 range		88-642 Gy			92- 322 Gy			75- 263 Gy	
all	56	0.94±0.02	9±2	45	0.87±0.02	6±2	57	0.75±0.03	25±3
>100 Gy	54	0.94±0.02	10±2	43	0.88±0.02	6±2	49	0.77±0.03	24±3
>125 Gy	35	0.96±0.02	11±2	30	0.87±0.02	8±2	35	0.79±0.04	26±4
>150 Gy	27	0.95±0.97	12±3	21	0.87±0.02	7±3	26	0.79±0.05	29±5
>175 Gy	14	**0.97±0.04**	9±4	14	**0.89±0.02**	0	14	**0.81±0.06**	25±6
>200 Gy	9	0.93±0.02	0	9	0.88±0.02	0	7	0.72±0.09	30±10
$>D_{given}$	8	0.92±0.03	0	7	0.84±0.02	12±5	5	0.70±0.11	34±12
L-EVA-1218 (given dose: 180 Gy)									
D_0 range		67-360 Gy			70-218 Gy			41-284 Gy	
all	52	0.89±0.03	19±3	44	0.85±0.02	7±3	51	0.75±0.03	27±3
>50 Gy	-	-	-	-	-	-	48	0.77±0.03	25±3
>75 Gy	50	0.91±0.03	16±3	43	0.85±0.02	7±3	38	0.84±0.02	14±3
>100 Gy	39	0.95±0.03	16±3	33	0.86±0.03	10±3	29	0.85±0.03	14±3
>125 Gy	21	**0.98±0.05**	20±5	22	**0.88±0.04**	15±5	18	0.85±0.04	15±4
>150 Gy	13	0.97±0.08	25±7	15	0.83±0.05	16±5	10	0.83±0.05	16±6
>175 Gy	6	1.08±0.07	8±8	8	0.85±0.04	8±6	5	**0.93±0.09**	14±10
>200 Gy	5	1.07±0.07	9±8	2	0.69±0.20	35±24	4	0.89±0.08	12±10
$>D_{given}$	5	1.07±0.07	9±8	6	0.86±0.05	9±6	5	**0.93±0.09**	14±10
L-EVA-1221 (given dose: 205 Gy)									
D_0 range		77-241 Gy			63-407 Gy			62-628 Gy	
all	42	0.81±0.02	15±3	85	0.78±0.02	15±2	87	0.76±0.02	19±2
>75 Gy	-	-	-	83	0.79±0.02	14±2	85	0.77±0.02	19±2
>100 Gy	34	0.82±0.03	16±3	64	0.80±0.02	15±2	67	0.79±0.02	20±2
>125 Gy	23	0.78±0.04	19±4	40	0.81±0.02	14±3	50	0.79±0.03	22±3
>150 Gy	9	0.84±0.04	0	24	0.79±0.03	15±4	33	0.77±0.04	26±4
>175 Gy	5	0.90±0.05	0	13	**0.83±0.03**	7±5	23	0.74±0.04	25±5
>200 Gy	2	**0.93±0.08**	0	9	0.82±0.05	12±6	16	0.74±0.05	26±6
$>D_{given}$	2	**0.93±0.08**	0	9	0.82±0.05	12±6	16	0.74±0.05	26±6

[1]Total number of grains measured per sample.
[2]Determined using the Central Age Model (Galbraith et al., 1999).

Supplementary Figures

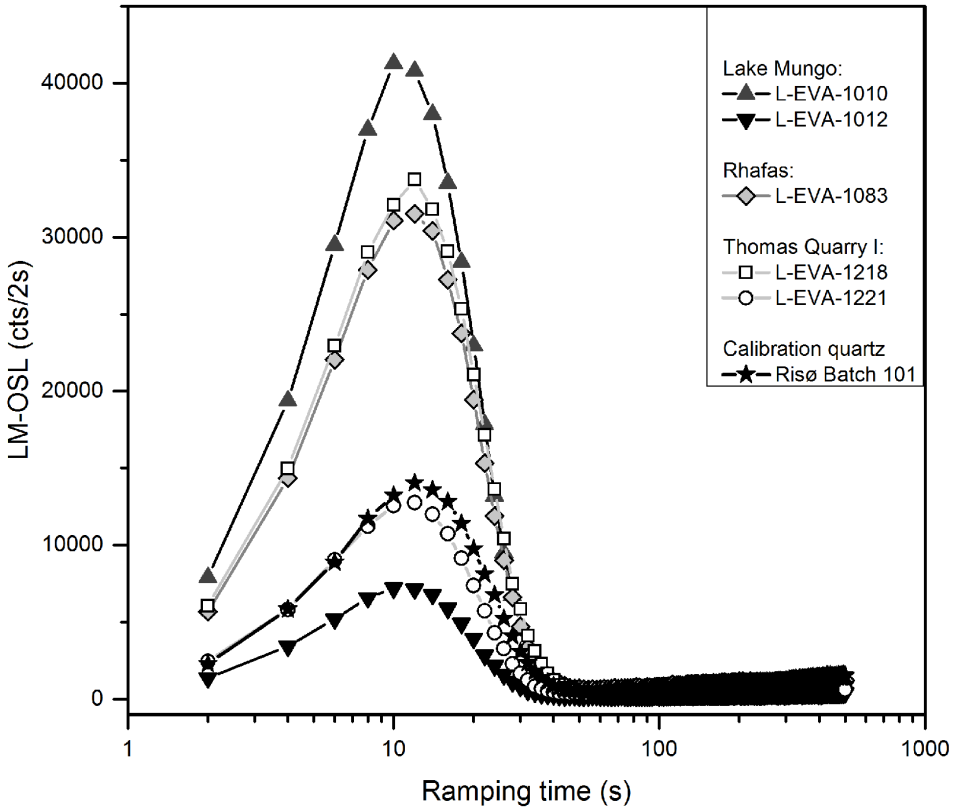

Fig. S1. LM-OSL curves for all samples in this study, showing dominant fast OSL signal components.

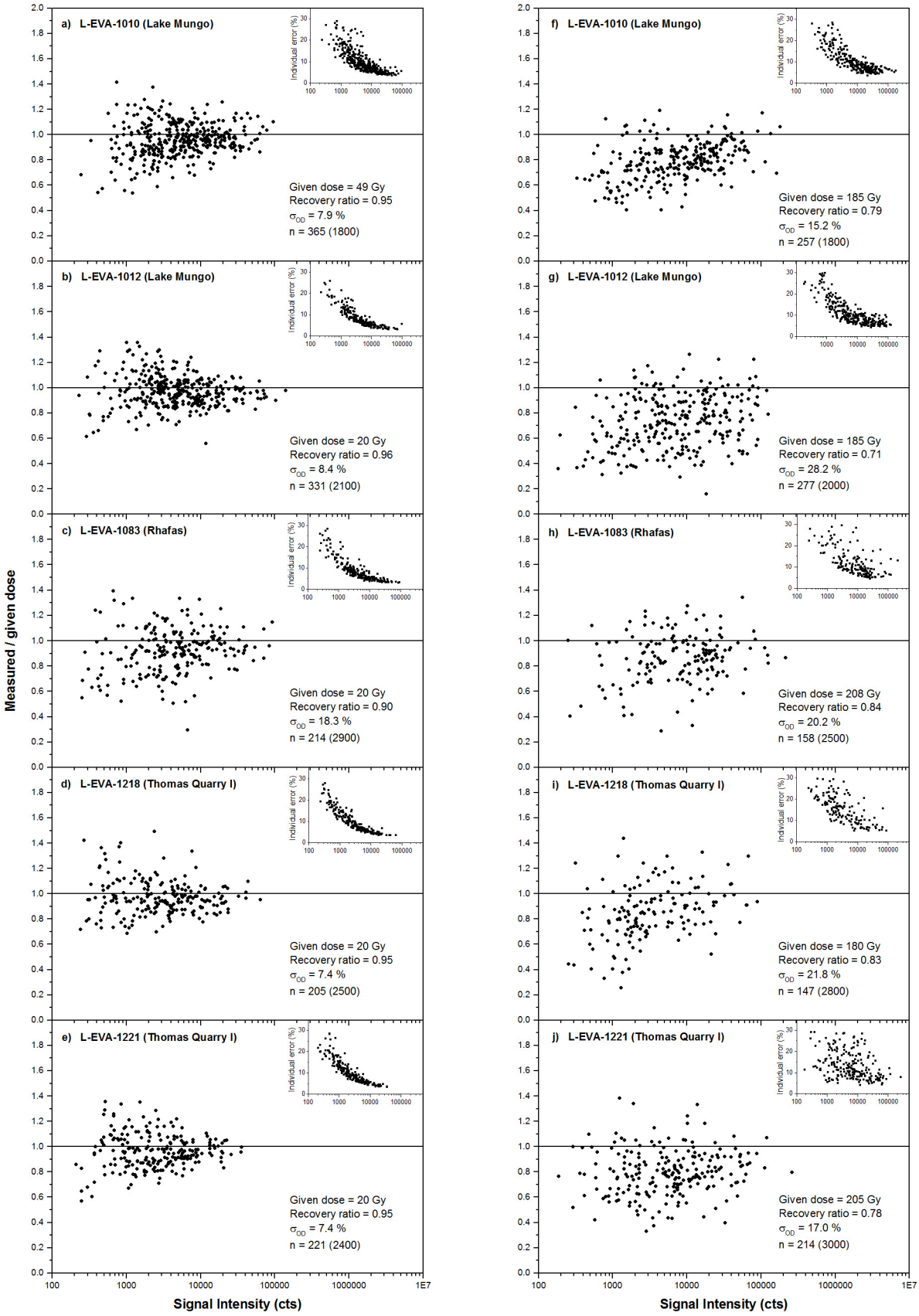

Fig. S2. Single grain dose distributions from dose recovery experiments after administration of low (a-e) and high given doses (f-j) for each sample. Measured/given dose ratios and (as inset) individual errors are plotted against L_N signal intensities (note logarithmic scale).

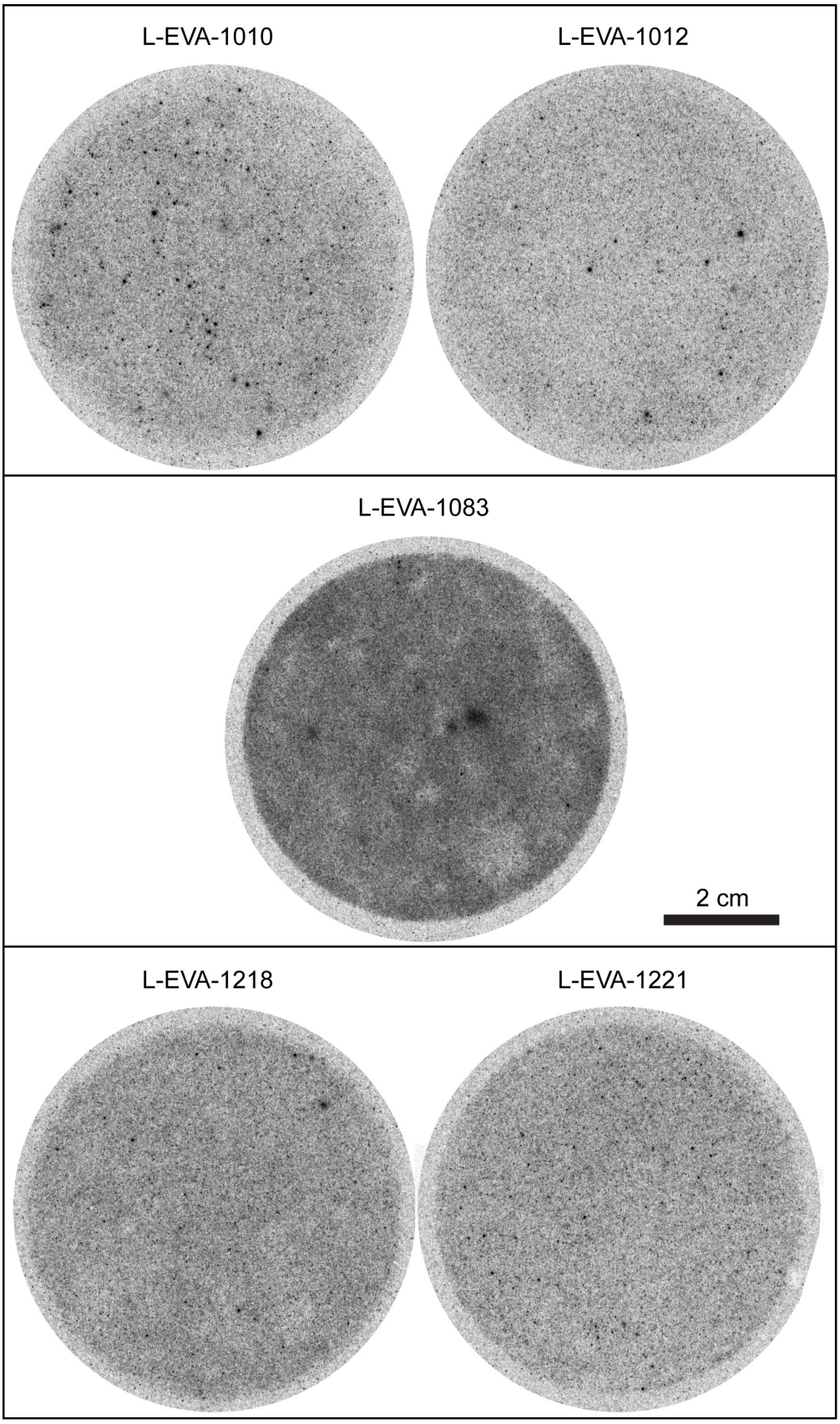

Fig. S3. Autoradiographs of unconsolidated sample material from Lake Mungo (L-EVA-1010 and L-EVA-1012), Rhafas (L-EVA-1083) and Thomas Quarry I (L-EVA-1218 and L-EVA-1221). Variability in the brightness of the autoradiographs results from differences in the thickness of the sample layers. Exposure time was 309-311 h.

References

Galbraith, R.F., Roberts, R.G., Laslett, G.M., Yoshida, H., Olley, J.M., 1999. Optical dating of single and multiple grains of quartz from Jinmium rock shelter, northern Australia: Part I, experimental design and statistical models. Archaeometry 41, 339-364.

Appendix C

Supplementary information of Doerschner et al. (in press), Quaternary International

S1 Table

Previous chronological work at the Vanguard Cave site.

OSL ages (Pettitt and Bailey, 2000; Rhodes, 2013)

Sample	Lab. code	Stratigraphic context		D_e (Gy)	Dose rate (Gy/ka)	Age (ka)	Reference
		1995-1998[1]	recent excavations				
VAN01-U02	X730	A 1-49	Layer 1	52.0±2.8	0.71±0.03	73.7±5.3	(Rhodes, 2013)
VAN1	OxL-1029	B 50	n/a[2]	36.3±1.0	0.78±0.05	46.3±3.3	(Pettitt and Bailey, 2000)
VAN01-U01	X729	B 50	n/a[2]	40.7±1.5	0.30±0.02	134.9±10.2	(Rhodes, 2013)
VAN01-U01 SG[3]	X729	B 50	n/a[2]	30.9±1.5	0.30±0.02	102.4±8.3	(Rhodes, 2013)
VAN01-M02	X724	B 51-150	n/a[2]	46.4±1.8	0.40±0.02	116.8±8.3	(Rhodes, 2013)
VAN01-M06	X728	C 151	n/a[2]	52.2±2.6	0.39±0.02	133.1±10.3	(Rhodes, 2013)
VAN98-OSL8	X369	C 154-155	n/a[2]	70.5±4.8	0.57±0.03	123.5±10.1	(Rhodes, 2013)
VAN7	OxL-1030	middle part of the	n/a[2]	68.7±2.5	0.74±0.05	93.4±7.0	(Pettitt and Bailey, 2000)
VAN2	OxL-1029	sequence, probably C/D	n/a[2]	99.7±5.9	0.89±0.06	111.9±10.0	(Pettitt and Bailey, 2000)
VAN01-L01	X720	E 169	n/a[2]	58.7±2.1	0.50±0.03	116.7±7.8	(Rhodes, 2013)
VAN01-L03	X174	E 174	n/a[2]	54.6±3.8	0.42±0.02	131.1±11.7	(Rhodes, 2013)

AMS radiocarbon dates (Pettitt and Bailey, 2000)

Sample	Lab. code	Stratigraphic context		Material	δ13C (‰)	Radiocarbon age (ka BP)	Calibrated Age (ka cal BP)
		1995-1998[1]	recent excavations				
VAN-S 96377	OxA-7389	A upper part	approx. Layer 6	charcoal	-25.5	45.2±2.4	49.1±3.0
VAN-S 96245	OxA-6998	B 52	approx. Layer 22	charcoal	-25.1	41.8±1.4	45.5±1.5
VAN-S 96230	OxA-7191	B 52	approx. Layer 22	bone	-15.1	10.2±0.1[4]	11.8±0.3
VAN-S 96347	OxA-7127	B 55	n/a[2]	charcoal	-24.4	>49.4	>55.2
VAN-S 96285a	OxA-6891	B hearth	n/a[2]	charcoal	-22.1	54.0±3.3	out of range
VAN-S 96285b	OxA-6892	B hearth	n/a[2]	charcoal	-22.6	46.9±1.5	50.6±2.6
VAN-N 96351	OxA-7078	Hyaena Cave		charcoal	-23.9	>44.1	>47.6

[1](Barton et al., 2013; Stringer et al., 2000)

[2]Recent excavations do not reach this level, yet.

[3]Single-grain measurement.

[4]Considered as underestimate by Pettitt and Bailey (2000).

S2 Table
Single-aliquot regenerative-dose (SAR) protocol for single-grains used in this study.

Run	Treatment
1	Dose (except before first run)
2	Preheat (240°C or 260°C for 10s)
3	Optical stimulation with IR diodes for 100s at 20°C (only for last run)
4	Optical stimulation with green laser for 1s at 125°C
5	Test dose
6	Cutheat (200°C or 220°C for 10s)
7	Optical stimulation with green laser for 1s at 125°C
8	Repeat from beginning

S3 Table
Single-aliquot regenerative-dose (SAR) protocol for multi-grain aliquots used in this study.

Run	Treatment
1	Dose (except before first run)
2	Preheat (240°C or 260°C for 10s)
3	Optical stimulation with IR diodes for 100s at 20°C (only for last run)
4	Optical stimulation with blue LEDs for 40s at 125°C
5	Test dose
6	Cutheat (200°C or 220°C for 10s)
7	Optical stimulation with blue LEDs for 40s at 125°C
8	Repeat from beginning

S4 Table

Single-grain characteristics.

Sample	n[1]	No signal[2]	Dim grains[3]	No L_N/T_N intersection	Recuperation >5%	Poor recycling	Depletion by IR	Grubbs test[4]	accepted grains	
	(100%)	(%)	(%)	(%)	(%)	(%)	(%)	(%)	total	(%)
Vanguard Cave										
L-EVA-1327	1400	81.6	10.1	2.0	0.0	1.5	0.1	0.2	63	4.5
L-EVA-1328	1200	81.2	9.2	2.7	0.0	1.6	0.1	0.1	61	5.1
L-EVA-1329	2000	84.6	8.5	1.6	0.1	1.2	0.2	0.2	71	3.6
L-EVA-1330	2200	83.2	9.2	2.7	0.1	1.5	0.2	0.0	69	3.1
L-EVA-1331	1900	82.4	10.2	1.9	0.0	1.4	0.4	0.0	71	3.7
L-EVA-1332	1200	81.1	9.5	1.1	0.1	1.6	0.3	0.1	74	6.2
L-EVA-1333	1200	73.8	13.8	1.3	0.3	2.0	0.7	0.3	93	7.8
L-EVA-1334	1200	74.8	12.8	2.5	0.3	2.7	0.8	0.3	69	5.8
L-EVA-1335	1200	78.0	11.2	2.7	0.5	1.6	0.4	0.0	67	5.6
L-EVA-1336	1200	80.2	10.2	1.4	0.0	1.5	0.9	0.1	68	5.7
L-EVA-1337	1200	76.1	10.6	2.5	0.0	2.2	0.8	0.3	90	7.5
L-EVA-1338	2200	82.5	9.5	2.1	0.1	2.1	0.2	0.0	78	3.5
L-EVA-1494	1200	72.4	17.6	1.8	0.1	1.0	0.6	0.1	77	6.4
L-EVA-1495	1200	73.3	17.4	1.5	0.2	0.7	0.3	0.5	73	6.1
L-EVA-1496	1200	78.9	13.2	1.0	0.1	0.6	0.6	0.2	65	5.4
Hyaena Cave										
L-EVA-1339	2400	86.8	6.5	1.6	0.0	1.6	0.4	0.1	72	3.0
L-EVA-1340	2200	87.1	5.9	2.4	0.3	0.7	0.5	0.0	69	3.1
L-EVA-1341	2100	87.5	5.8	2.1	0.2	0.9	0.4	0.0	65	3.1

[1]Total numbrt of grains measured per sample.

[2]Percentage of grains not yielding an initial luminescence signal above background.

[3]Percentage of grains rejected due to insufficient test-dose signal: relative uncertainty on T_N exceeds 15% (note that this criterion is stricter than the commonly applied T_N > 3 standard deviations above background).

[4]Percentage of grains identified as statistical outliers (Grubbs, 1950).

S5 Table

D_e determination for single-grains, multi-grain aliquots and synthetic aliquots.

Sample	Unit	PH/CH[1] (°C)	Dose recovery[2]	Single-grains			Multi-grain aliquots			Synthetic aliquots			SyA/SG	SyA/MG
				n[3]	D_e[4]	σ_{OD}[4] (%)	n[3]	D_e[4]	σ_{OD}[4] (%)	n[3]	D_e[4]	σ_{OD}[4] (%)	D_e ratio	D_e ratio
Vanguard Cave														
L-EVA-1327	1	260/220	0.95±0.03	63/1400	34.5±1.5	30±3	31/44	42.0±2.6	31±4	11/14	35.8±2.1	18±4	1.04±0.09	0.85±0.06
L-EVA-1328	1c	240/200	1.01±0.03	61/1200	37.0±1.5	25±3	32/44	37.0±1.5	19±3	9/12	47.2±2.9	16±4	1.28±0.12	1.28±0.11
L-EVA-1329	4	240/200	1.04±0.02	71/2000	38.8±1.4	20±3	28/44	36.4±1.8	23±3	17/20	40.0±2.0	17±3	1.03±0.09	1.10±0.09
L-EVA-1330	5a	260/220	0.95±0.02	69/2200	54.7±2.6	32±3	28/44	46.0±2.4	25±4	15/22	61.1±3.3	19±4	1.12±0.10	1.33±0.12
L-EVA-1331	5c	240/200	1.02±0.02	71/1900	46.7±1.8	23±3	30/44	41.5±1.7	19±3	14/19	47.7±2.7	19±4	1.02±0.08	1.15±0.10
L-EVA-1332	6b	260/220	0.97±0.02	74/1200	34.5±1.6	32±3	37/44	34.7±1.2	19±3	11/12	36.8±2.0	16±4	1.07±0.09	1.06±0.08
L-EVA-1333	10a-c	260/220	1.03±0.02	93/1200	35.3±1.2	22±2	41/44	39.0±1.5	20±2	11/12	39.2±1.4	8±3	1.11±0.10	1.01±0.08
L-EVA-1334	10a-c	260/220	1.02±0.02	69/1200	35.7±1.3	18±3	37/44	36.0±1.3	18±2	6/12	35.1±1.5	8±3	0.98±0.08	0.98±0.07
L-EVA-1335	10d-e	260/220	1.01±0.04	67/1200	35.8±1.6	29±3	33/44	36.5±1.3	17±2	9/12	34.2±1.7	13±3	0.96±0.07	0.94±0.07
L-EVA-1336	12	260/220	1.03±0.02	68/1200	34.1±1.4	25±3	28/44	33.8±1.6	20±3	9/12	38.6±2.0	14±4	1.13±0.10	1.14±0.09
L-EVA-1337	14	260/220	1.03±0.02	90/1200	33.2±1.2	26±3	40/44	33.7±1.1	15±2	11/12	39.8±3.0	24±5	1.20±0.11	1.18±0.10
L-EVA-1338	15	240/200	0.99±0.02	78/2200	40.5±1.7	28±3	29/44	40.6±1.6	17±3	16/22	42.8±4.9	44±8	1.06±0.09	1.05±0.09
L-EVA-1494	18c	240/200	0.96±0.02	77/1200	34.3±1.4	28±3	26/44	37.3±2.1	28±4	10/12	40.0±2.5	18±4	1.17±0.11	1.07±0.08
L-EVA-1495	20c	240/200	0.97±0.02	73/1200	34.8±1.1	23±3	29/44	39.0±1.7	20±3	11/12	41.3±3.2	25±6	1.19±0.10	1.06±0.09
L-EVA-1496	22b	240/200	0.96±0.02	65/1200	33.5±1.7	35±4	30/44	32.9±2.5	40±5	8/12	35.0±2.0	14±4	1.04±0.09	1.06±0.08
Hyaena Cave														
L-EVA-1339	top	260/220	1.04±0.04	72/2400	46.4±2.0	27±3	31/44	43.3±2.0	22±3	16/24	50.6±3.5	25±5	1.09±0.09	1.17±0.10
L-EVA-1340	middle	260/220	0.97±0.02	69/2200	45.0±2.1	31±3	30/44	39.4±1.6	18±3	13/22	50.3±2.4	16±3	1.12±0.09	1.28±0.11
L-EVA-1341	bottom	260/220	1.01±0.02	65/2100	45.3±2.1	30±3	36/44	38.7±1.4	16±2	10/21	52.9±2.0	10±3	1.17±0.11	1.37±0.12

[1]Chosen preheat/cutheat temperatures.

[2]Dose recovery test ratio, measured on four multi-grain aliquots per sample.

[3]Number of accepted/measured grains or aliquots.

[4]Determined using the Central Age Model (Galbraith et al., 1999).

S6 Table

Results of radionuclide analyses and moisture content.

Sample	Unit	Depth (cm)	Moisture content (%)		Specific activities (Bq kg^{-1})							Contribution to dose rate (%)		
			Saturation	In situ	^{238}U	^{226}Ra	^{210}Pb	^{232}Th	^{228}Ra	^{228}Th	^{40}K	^{238}U	^{232}Th	^{40}K
Vanguard Cave														
L-EVA-1327	1	27	18.1	4.4	12.7±2.3	11.6±0.8	10.3±2.0	8.8±0.6	8.8±0.9	8.8±0.6	105±12	34.3	21.0	44.7
L-EVA-1328	1c	43	20.8	5.1	14.1±2.8	16.4±1.1	12.4±2.2	12.7±0.9	12.7±1.2	12.8±0.9	161±14	27.8	22.1	50.1
L-EVA-1329	4	76	18.9	1.0	6.0±1.4	6.6±0.5	7.5±1.4	7.3±0.5	7.3±0.6	7.3±0.5	90±9	22.4	24.1	53.4
L-EVA-1330	5a	90	19.3	4.1	14.1±2.4	14.1±2.4	9.8±2.2	13.1±0.9	12.6±1.3	13.3±1.0	157±17	28.0	22.9	49.2
L-EVA-1331	5c	145	19.4	3.1	12.9±2.5	12.3±0.9	14.3±2.6	11.8±0.8	11.9±1.2	11.7±0.9	153±14	27.3	21.8	50.9
L-EVA-1332	6b	175	17.7	1.2	5.7±1.3	5.5±0.4	8.0±1.5	5.6±0.4	6.1±0.5	5.5±0.4	56±6	29.0	25.4	45.6
L-EVA-1333	10a-c	218	20.2	2.9	11.5±2.3	15.0±1.0	14.6±2.5	11.5±0.8	10.8±1.0	11.7±0.8	128±14	27.5	24.2	48.3
L-EVA-1334	10a-c	230	17.4	1.1	10.9±2.0	7.3±0.5	9.2±1.7	7.3±0.5	7.0±0.7	7.4±0.5	74±7	37.4	22.2	40.4
L-EVA-1335	10d-e	251	18.9	1.9	7.8±1.5	8.8±0.6	8.4±1.4	7.7±0.5	7.4±0.6	7.8±0.5	80±8	28.5	24.9	46.6
L-EVA-1336	12	273	16.6	1.2	6.8±1.9	6.6±0.5	5.1±2.0	6.3±0.5	6.4±0.8	6.3±0.5	56±7	32.2	26.3	41.5
L-EVA-1337	14	296	18.1	1.2	7.2±1.6	6.5±0.5	8.1±1.7	6.4±0.5	6.0±0.7	6.6±0.5	63±6	31.5	24.9	43.6
L-EVA-1338	15	310	18.0	3.3	8.8±1.9	7.7±0.5	6.7±1.9	7.3±0.5	7.6±0.7	7.2±0.5	75±8	32.4	23.6	43.9
L-EVA-1494	18c	345	17.1	0.1	7.0±1.7	6.2±0.5	7.1±2.4	6.9±0.5	6.8±0.6	6.9±0.5	70±6	28.6	25.0	46.4
L-EVA-1495	20c	390	17.9	0.3	5.4±1.2	6.1±0.4	4.8±1.0	6.8±0.4	7.1±0.5	6.7±0.5	68±5	23.9	27.2	48.9
L-EVA-1496	22b	408	17.0	0.3	6.3±1.4	6.1±0.5	6.3±1.4	6.3±0.5	6.2±0.6	6.4±0.5	57±7	29.6	26.7	43.7
Hyaena Cave														
L-EVA-1339	top	82	16.8	2.0	7.2±2.1	6.7±0.5	8.2±1.5	8.7±0.6	7.8±0.7	8.9±0.6	89±9	25.4	26.9	47.7
L-EVA-1340	middle	128	18.1	1.7	8.1±2.0	7.1±0.5	7.9±2.0	8.5±0.6	8.8±0.8	8.4±0.6	98±9	26.1	24.1	49.8
L-EVA-1341	bottom	164	18.7	2.4	9.6±1.9	7.1±0.5	8.1±1.7	7.8±0.5	7.8±0.7	7.8±0.5	91±9	31.3	22.2	46.5

B: Supplementary Figures

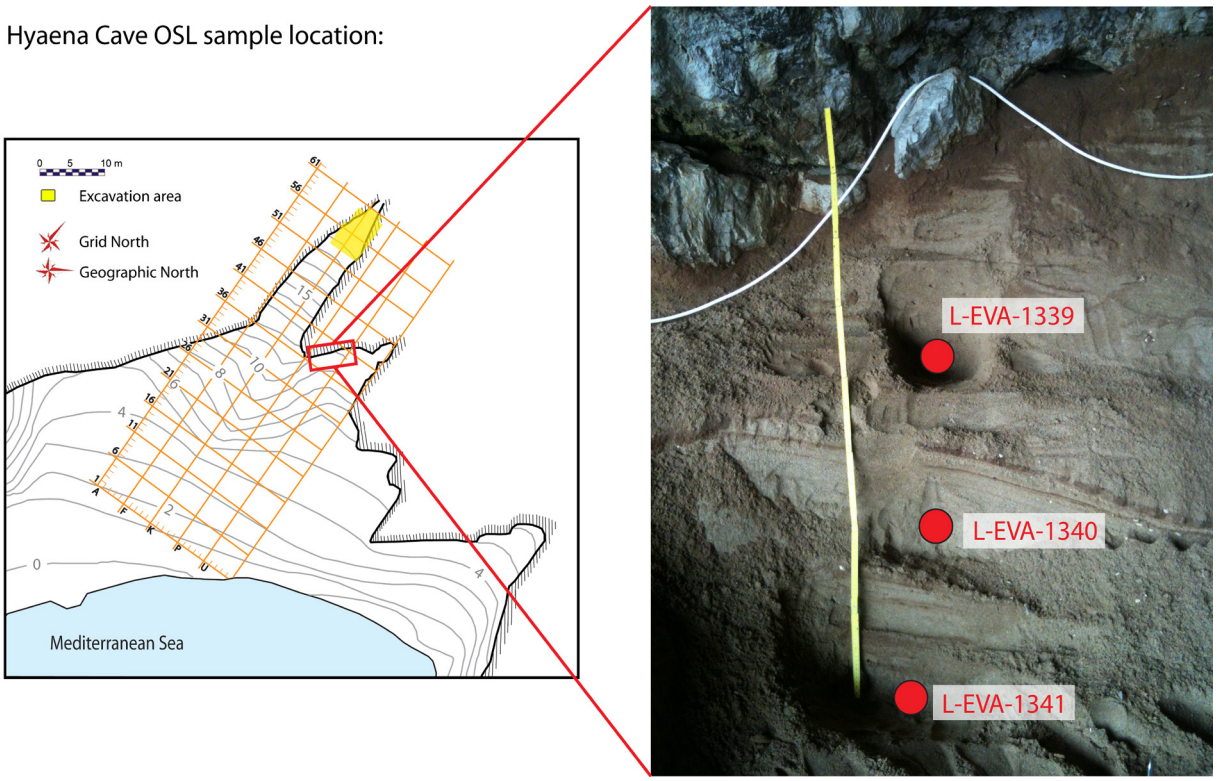

Fig. S1. Location and context of the OSL samples from the Hyaena Cave.

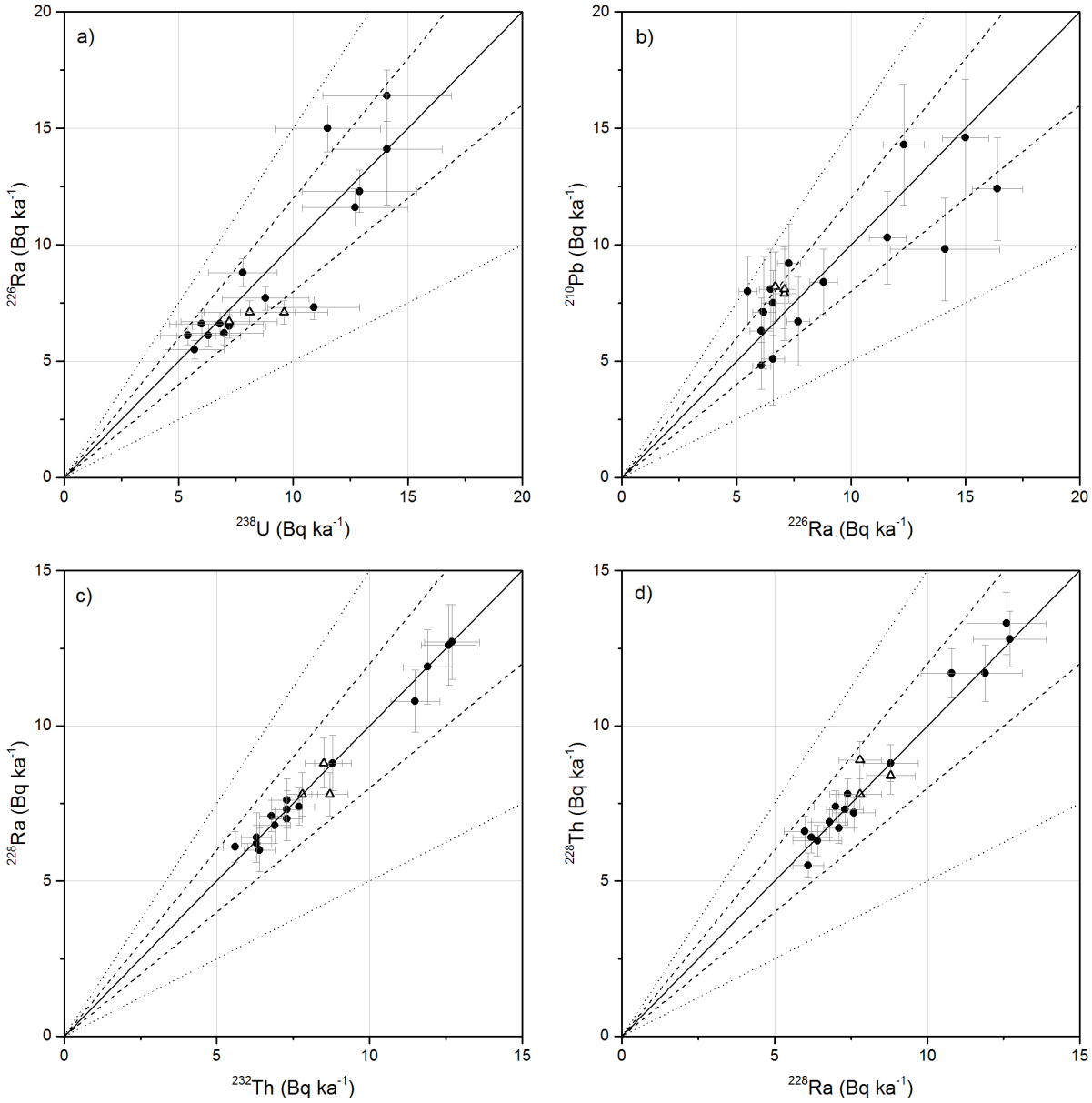

Fig. S2. Parent-daughter equilibrium plots of the ^{238}Uranium and ^{232}Thorium decay chains for the Vanguard Cave (black dots) and Hyaena Cave (open triangles) samples: (a) ^{238}U/^{226}Ra (b) ^{226}Ra/^{210}Pb (c) ^{232}Th/^{228}Ra (d) ^{228}Ra/^{228}Th. Dashed lines represent 20% and dotted lines 50% of equilibrium.

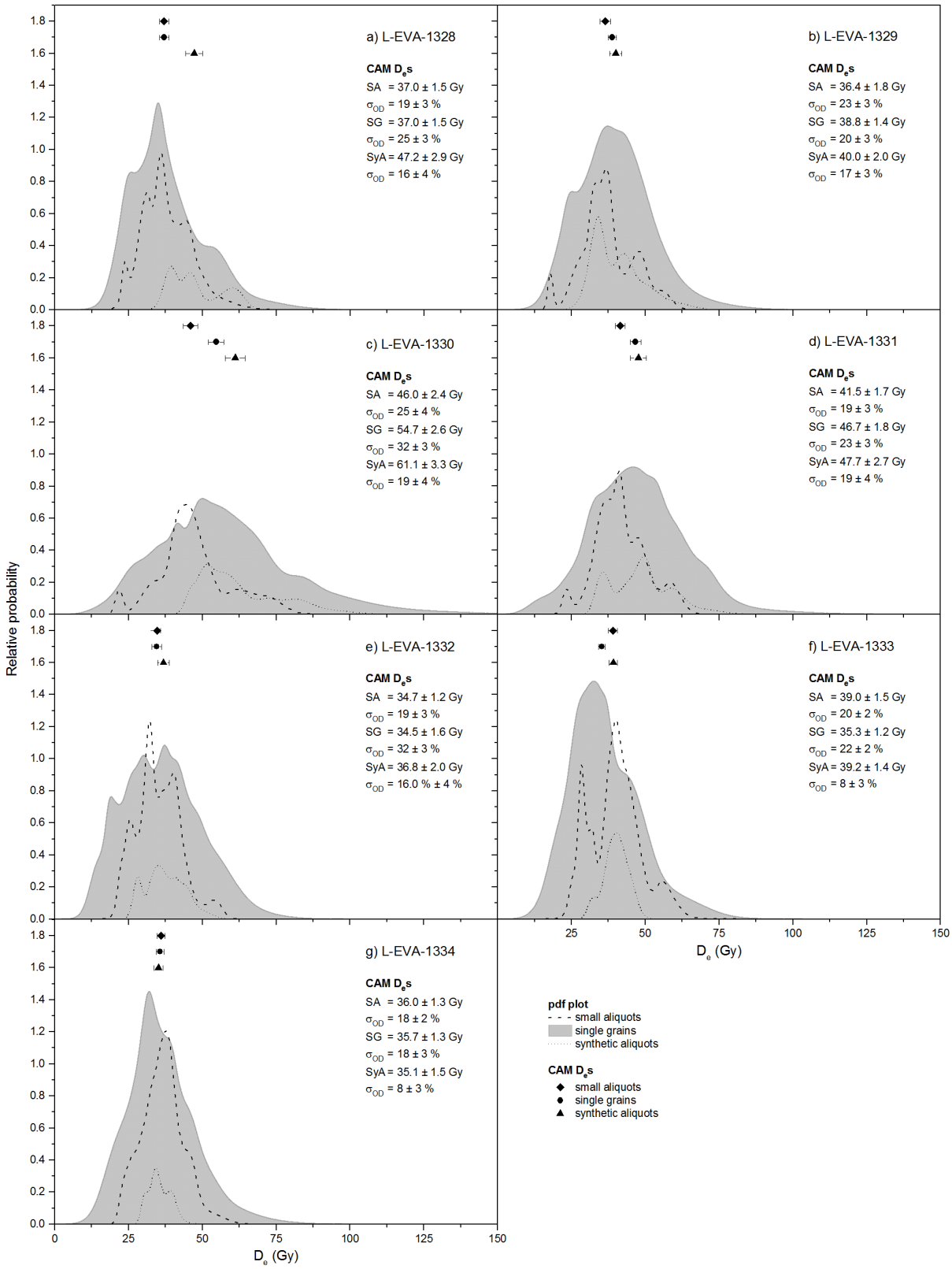

Fig. S3. Probability density function plots of single-grain, multi-grain aliquot and synthetic aliquot D_es for samples (a) L-EVA-1328 (b) L-EVA-1329 (c) L-EVA-1330 (d) L-EVA-1331 (e) L-EVA-1332 (f) L-EVA-1333 and (g) L-EVA-1334 from Vanguard Cave.

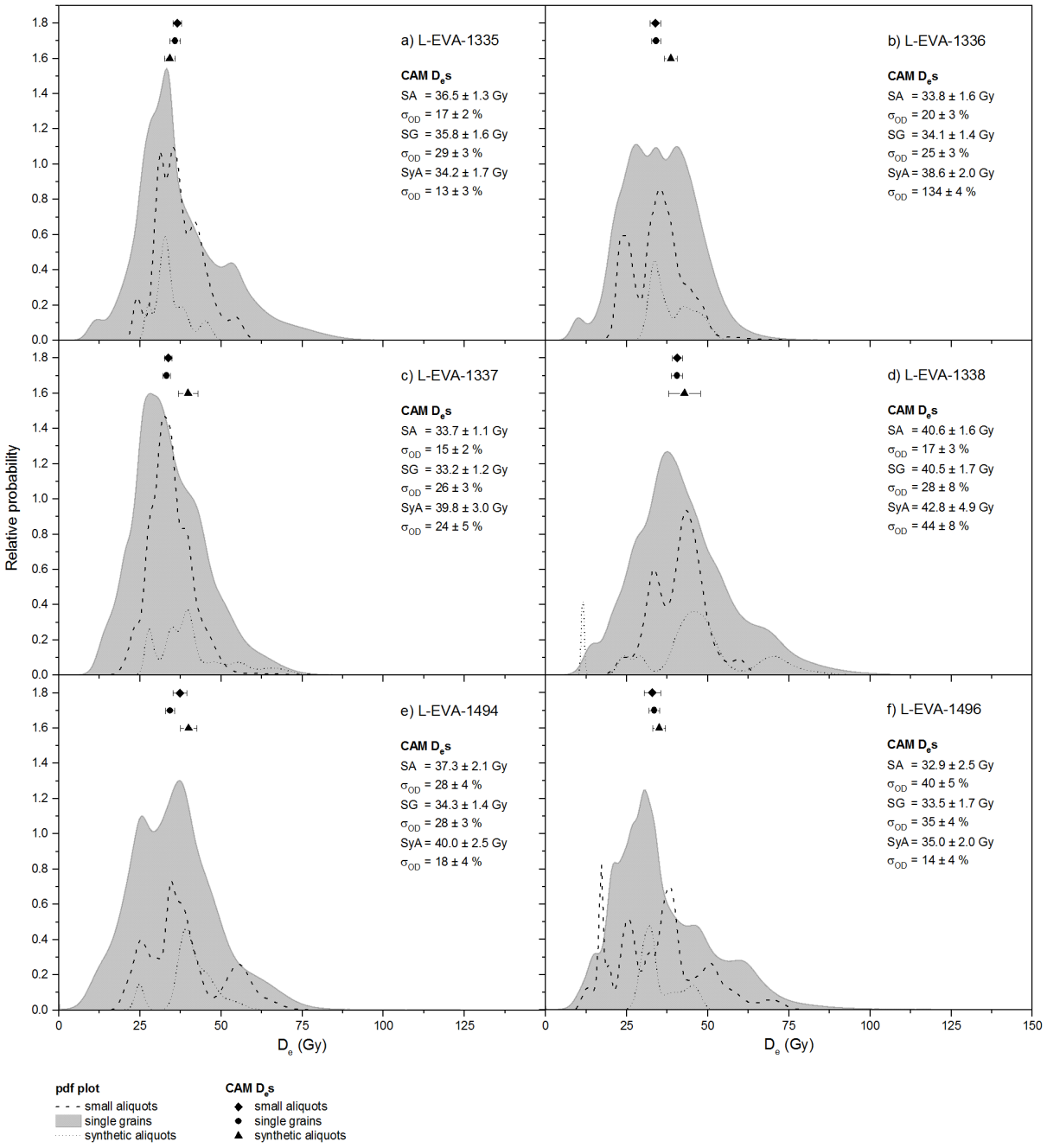

Fig. S4. Probability density function plots of single-grain, multi-grain aliquot and synthetic aliquot D_es for samples (a) L-EVA-1335 (b) L-EVA-1336 (c) L-EVA-1337 (d) L-EVA-1338 (e) L-EVA-1494 and (f) L-EVA-1496 from Vanguard Cave.

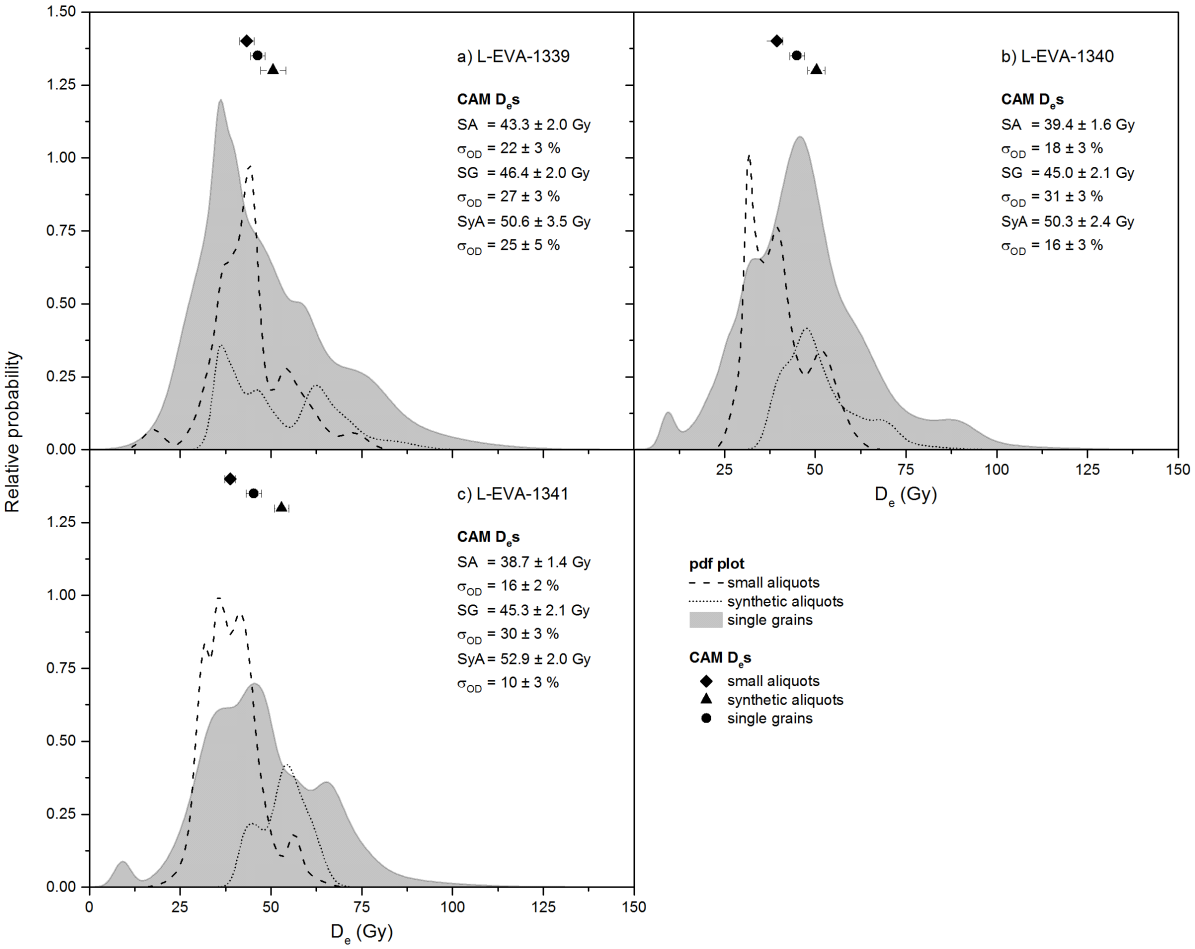

Fig. S5. Probability density function plots of single-grain, multi-grain aliquot and synthetic aliquot D_es for samples (a) L-EVA-1339 (b) L-EVA-1340 and (c) L-EVA-1341 from Hyaena Cave.

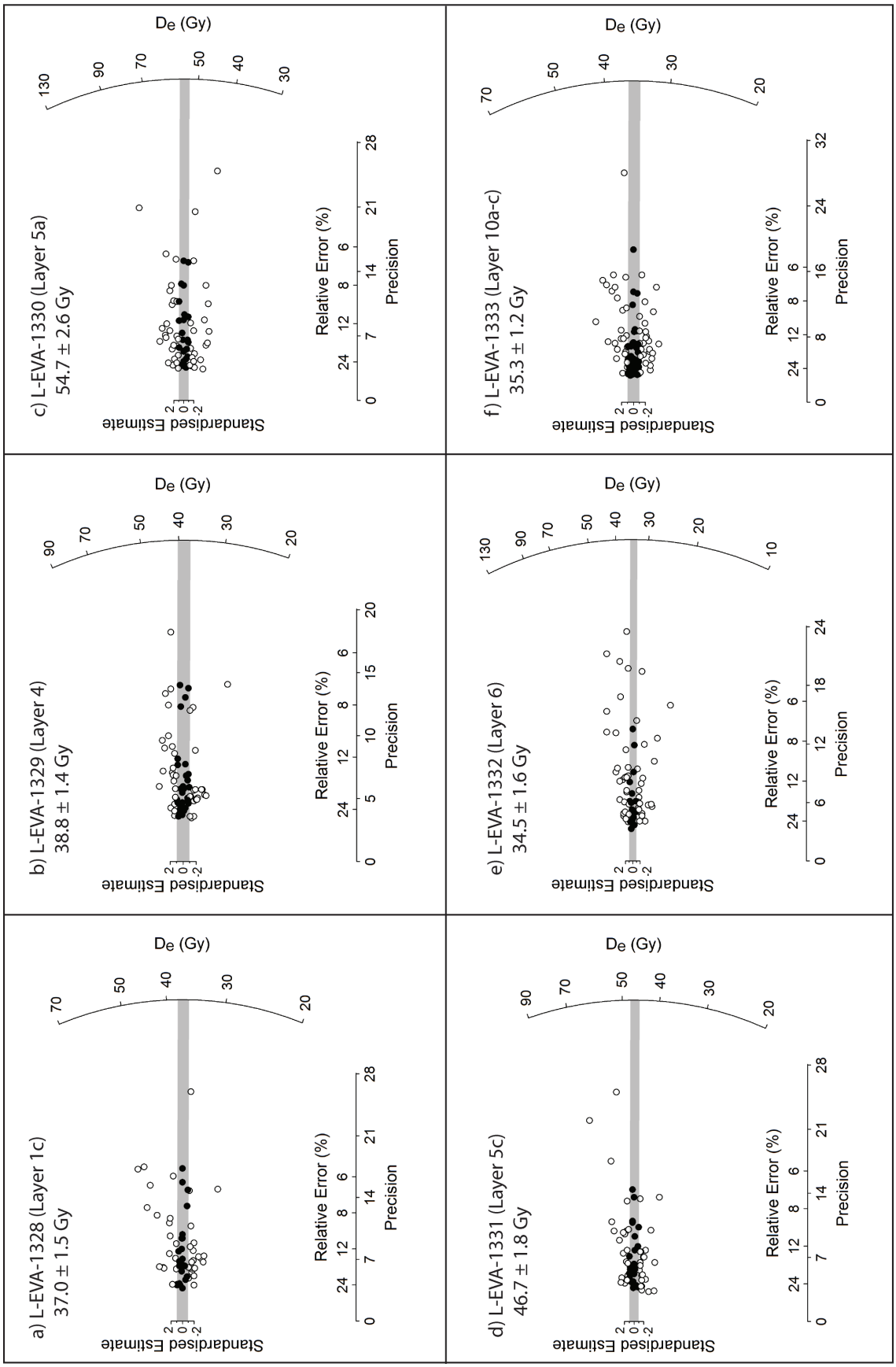

Fig. S6. Radial plots showing single-grain D_e distributions from Vanguard Cave: (a) L-EVA-1328 (b) L-EVA-1329 (c) L-EVA-1330 (d) L-EVA-1331 (e) L-EVA-1332 (f) L-EVA-1333. The shaded bands in the radial plots correspond to the standard error deviation from the calculated D_e.

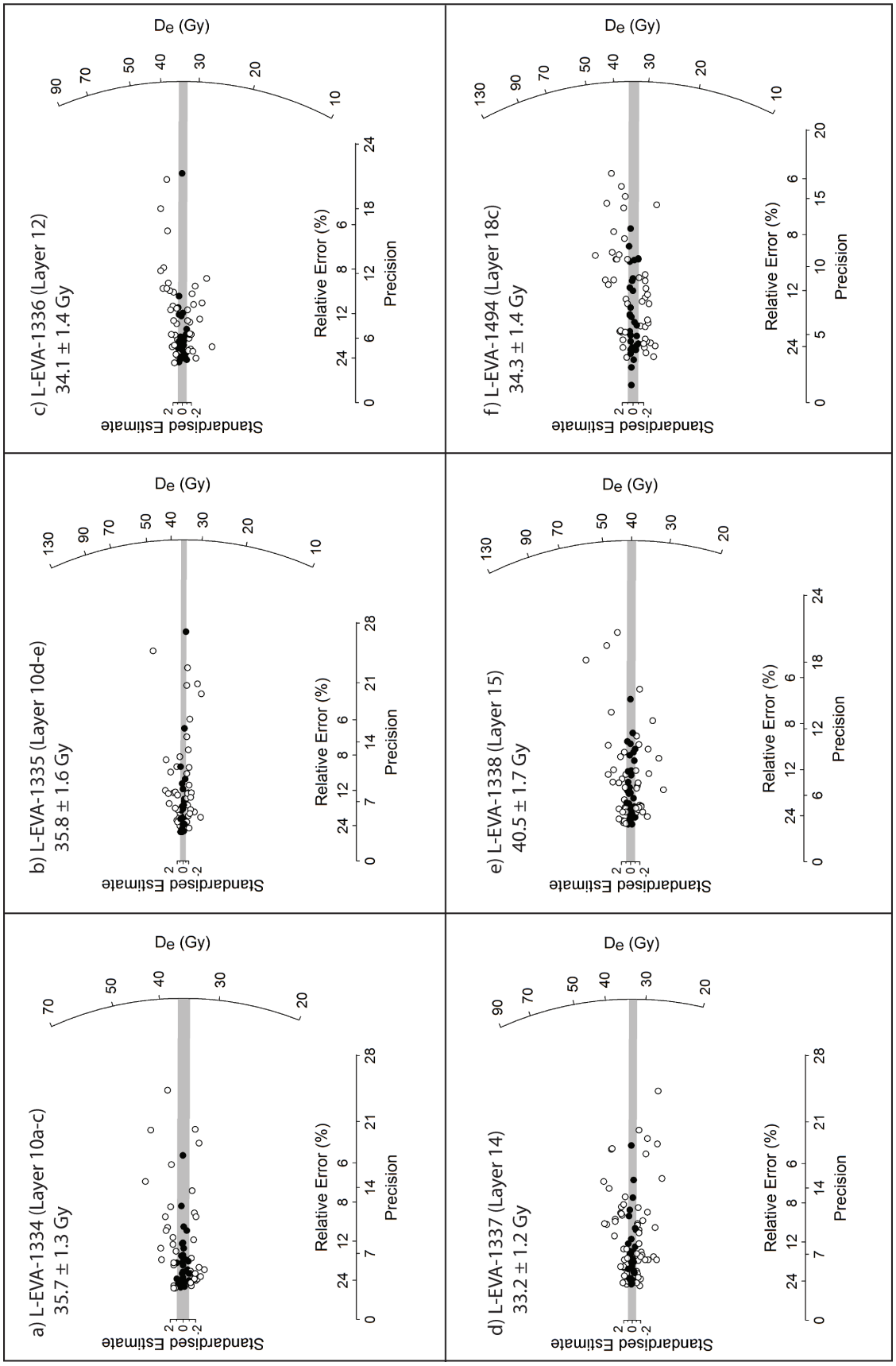

Fig. S7. Radial plots showing single-grain D_e distributions from Vanguard Cave: (a) L-EVA-1334 (b) L-EVA-1335 (c) L-EVA-1336 (d) L-EVA-1337 (e) L-EVA-1338 (f) L-EVA-1494. The shaded bands in the radial plots correspond to the standard error deviation from the calculated D_e.

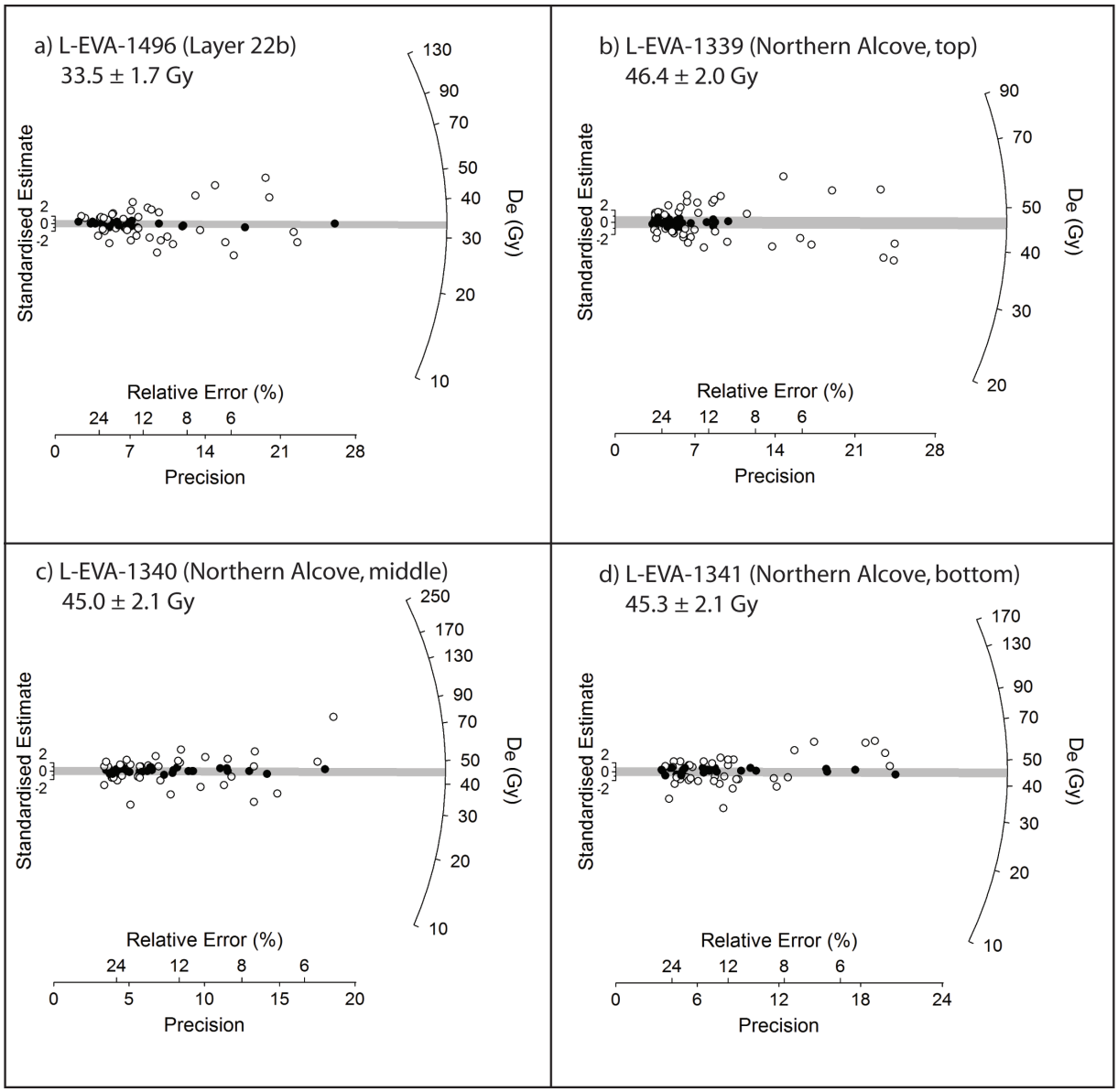

Fig. S8. Radial plots showing single-grain D_e distributions from Vanguard Cave and Hyaena Cave: (a) L-EVA-1496 (b) L-EVA-1339 (c) L-EVA-1340 and (d) L-EVA-1341. The shaded bands in the radial plots correspond to the standard error deviation from the calculated D_e.

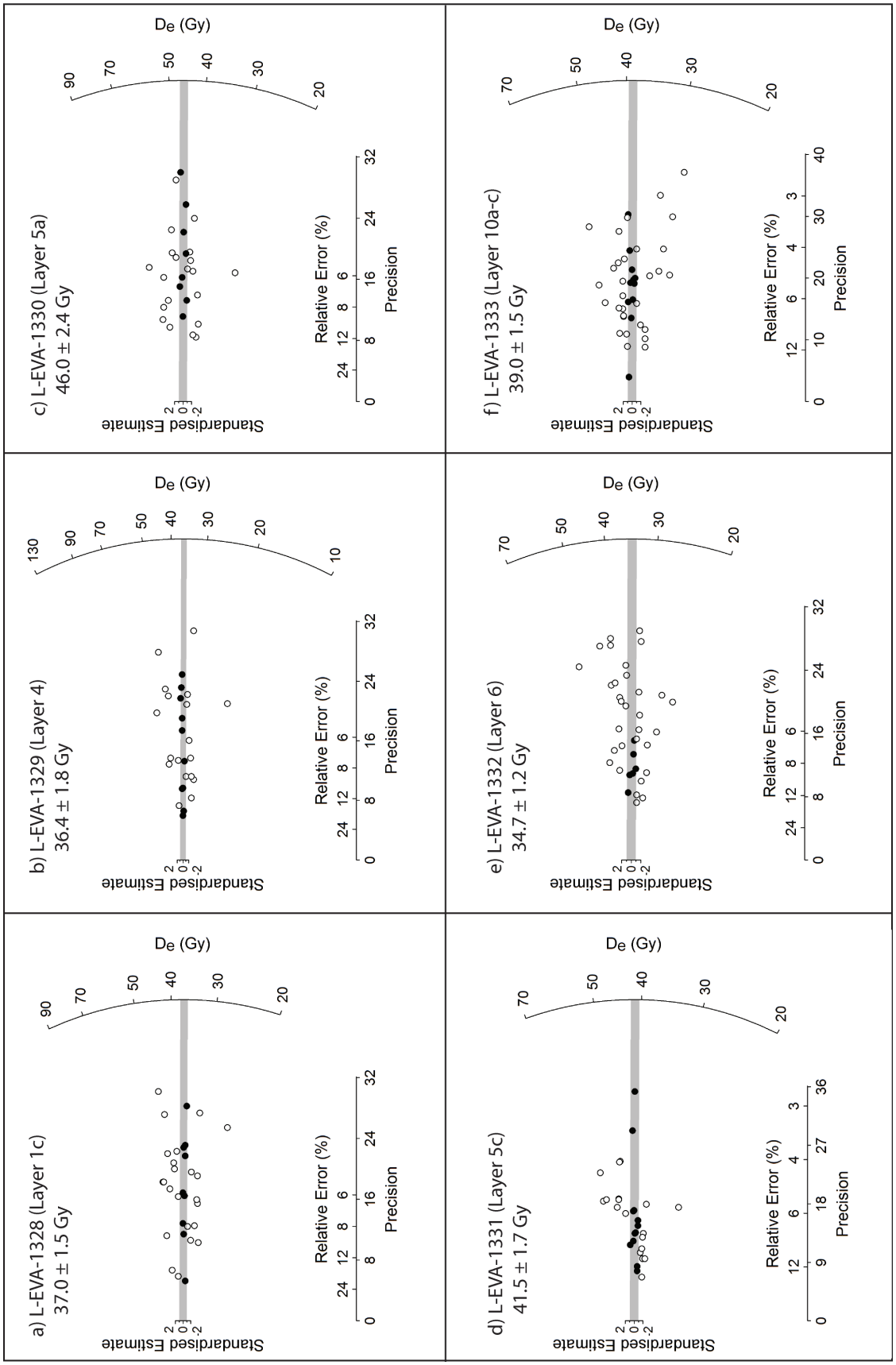

Fig. S9. Radial plots showing multi-grain aliquot D_e distributions from Vanguard Cave: (a) L-EVA-1328 (b) L-EVA-1329 (c) L-EVA-1330 (d) L-EVA-1331 (e) L-EVA-1332 (f) L-EVA-1333. The shaded bands in the radial plots correspond to the standard error deviation from the calculated D_e.

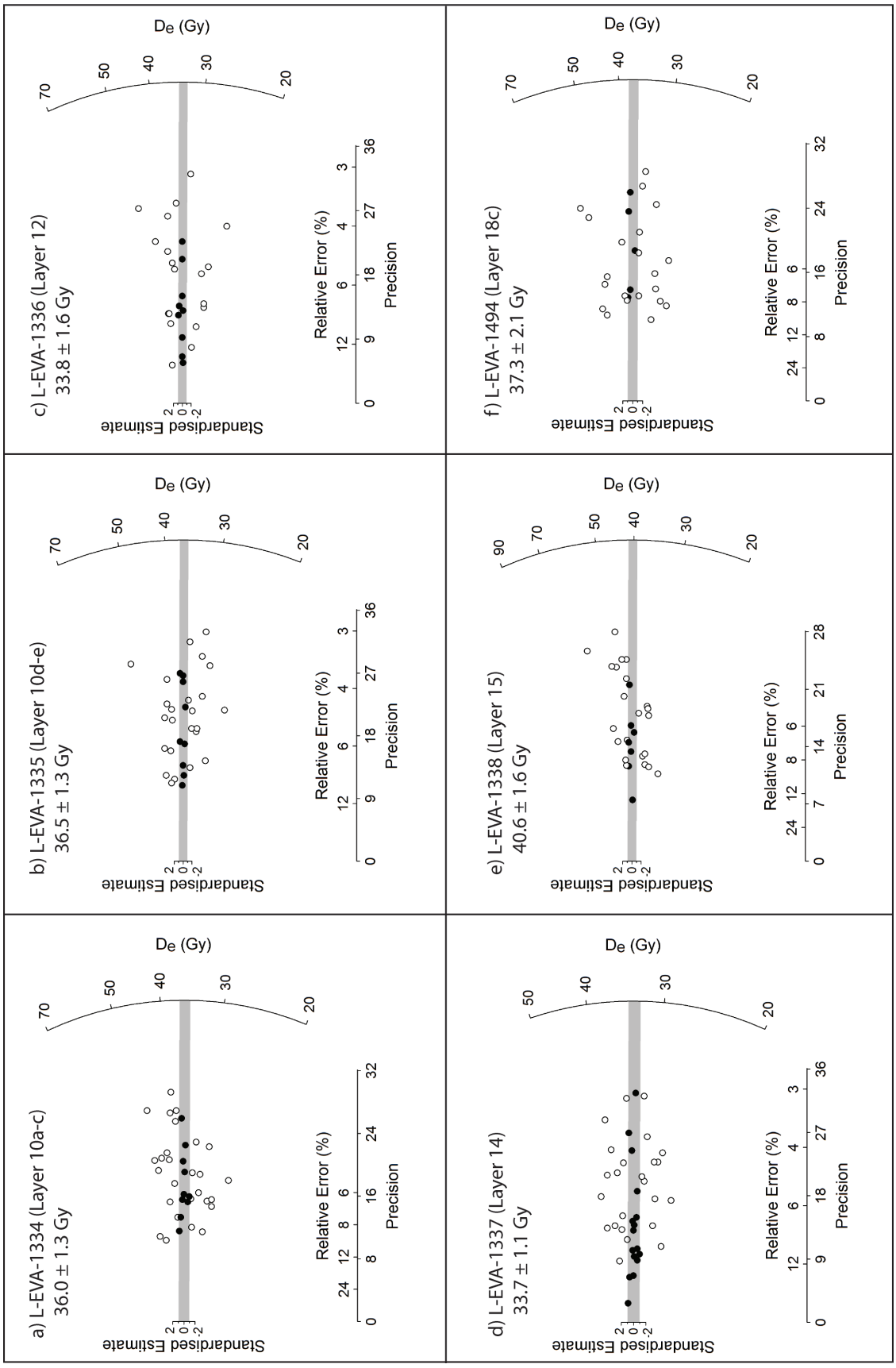

Fig. S10. Radial plots showing multi-grain aliquot D_e distributions from Vanguard Cave: (a) L-EVA-1334 (b) L-EVA-1335 (c) L-EVA-1336 (d) L-EVA-1337 (e) L-EVA-1338 (f) L-EVA-1494. The shaded bands in the radial plots correspond to the standard error deviation from the calculated D_e

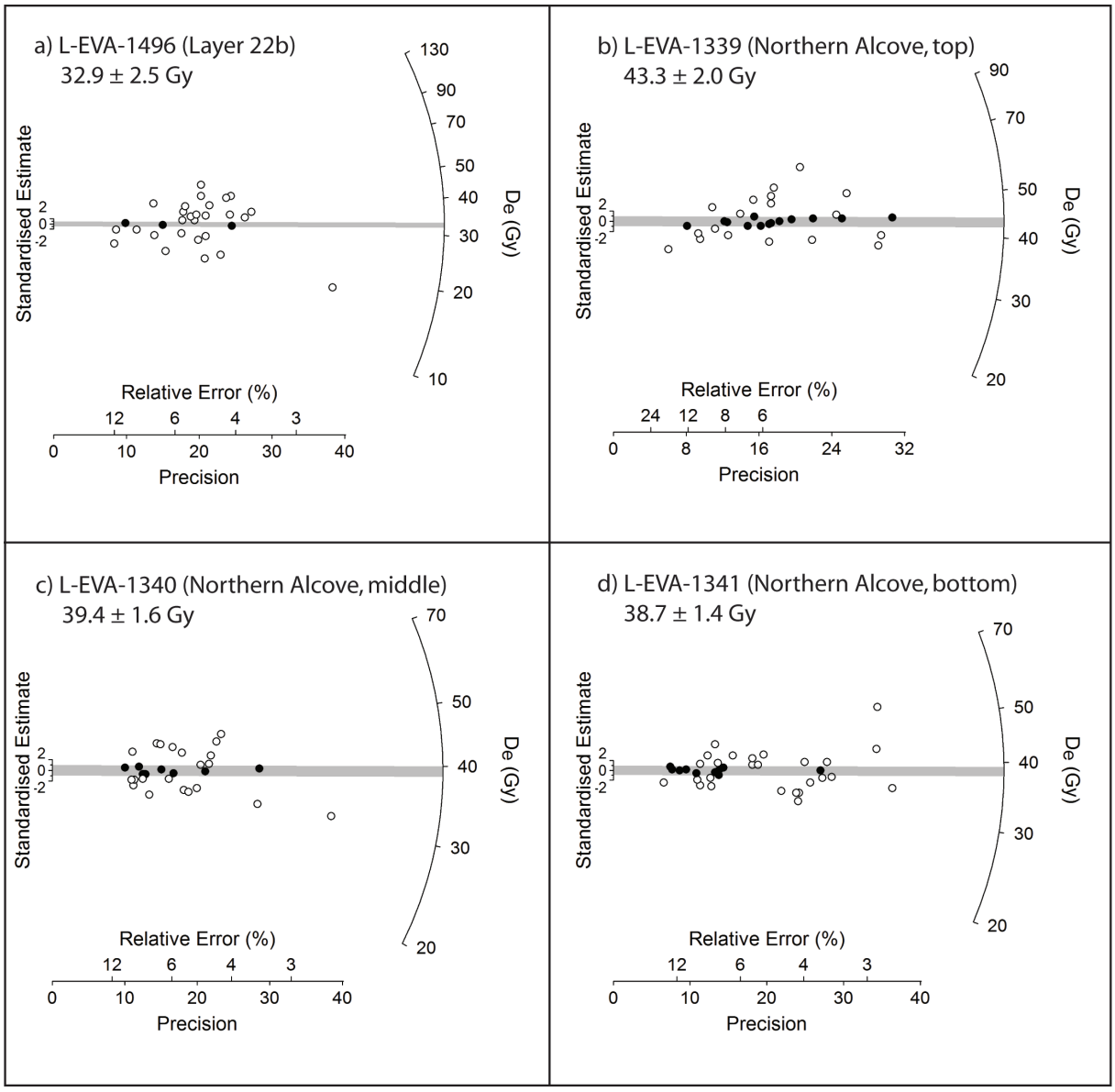

Fig. S11. Radial plots showing multi-grain aliquot D_e distributions from Vanguard Cave and Hyaena Cave: (a) L-EVA-1496 (b) L-EVA-1339 (c) L-EVA-1340 and (d) L-EVA-1341. The shaded bands in the radial plots correspond to the standard error deviation from the calculated D_e.

C: Variability of single-grain luminescence signal intensities and their potential impact on multi-grain and synthetic aliquot D_Es

In this study, synthetic aliquots yielded considerably higher (ratio >1.10, Table S5) D_es than those determined using single-grains (for 9 samples) and multi-grain aliquots (8 samples). For single-grain dating, high proportions of individual grains (93-97%) were excluded from the final D_e calculation of each sample based on a set of selected quality criteria (Table S4). Although acceptance criteria were similarly applied for multi-grain and synthetic aliquots prior to D_e calculation, these quality checks are limited in precision compared to those on individual grains by the fact that the examined aliquots emit averaged luminescence signals of ~30 and 100 individual grains, respectively. Furthermore, accepted aliquots are likely to contain large numbers of individual grains that do not fulfil the complete set of single-grain quality criteria and some of these grains might have falsifying effects on the determined D_es.

Here, we examine the luminescence signal characteristics of different types of individual grains which are separated into the following classes based on single-grain quality criteria:

Accept/reject	Criterion	Clarification
Accept		grains that pass all rejection criteria
Reject	Dim grains	grains rejected due to insufficient test-dose signal: relative uncertainty of T_N exceeds 15%
Reject	Saturated grains	grains showing Ln/Tn ratios above the maximum Lx/Tx of the dose response curves
Reject	Recuperation threshold	grains for which recuperation was >5%
Reject	Recycling threshold	grains with a recycling ratio inconsistent with unity within 2 standard deviations
Reject	IR depletion threshold	grains with a IR depletion ratio inconsistent with unity within 2 standard deviations
Reject	Outliers	grains identified as statistical outliers (Grubbs, 1950)

The aim of this exercise was to investigate the impact that different types of single-grains might have on averaged luminescence signals in multi-grain and synthetic aliquots and to check whether the observed D_e overestimation in synthetic aliquots can be traced back to one (or several) specific grain class(es).

Detailed examinations of individual grains were performed on two single-grain datasets:

1) sample L-EVA-1328, which shows the largest discrepancy between single-grain (37.0 ± 1.5 Gy) and synthetic aliquot (47.2 ± 1.6 Gy) D_es in this study (syA/SG ratio: 1.28), and

2) sample L-EVA-1332, for which single-grain (34.5 ± 1.6 Gy) and synthetic aliquot (36.8 ± 2.0 Gy) D_es are statistically identical (syA/SG ratio: 1.06).

In a first step, Ln signals of synthetic aliquots were compared individually to the summed Ln signal of all accepted grains from the corresponding single-grain disc (Fig. S12a) to determine the size of the offset signal in synthetic aliquots originating from “rejected” individual grains. For sample L-EVA-1332, synthetic aliquot Ln signals are on average ~58% higher than the summed signal of the accepted individual grains. In sample L-EVA-1328, however, the synthetic aliquot Ln signals are on average twice as high as those derived from the summed accepted individual grains or, in other words, the offset signal of the “rejected” grains are of approximately equal intensity as the summed signal of the accepted grains.

In Fig. 12b, synthetic aliquot D_es are plotted as a function of the averaged D_e of all accepted individual grains per single-grain disc for L-EVA-1328 and L-EVA-1332. The latter sample shows a variable pattern

of data points scattering closely around the 1:1 line. Some discs yield higher synthetic aliquot D_es, while for others, averaged single-grain D_es are higher than the corresponding synthetic aliquot value. By comparison, all synthetic aliquots yield higher D_es than those derived from only the accepted individual grains from the same single-grain disc for sample L-EVA-1328.

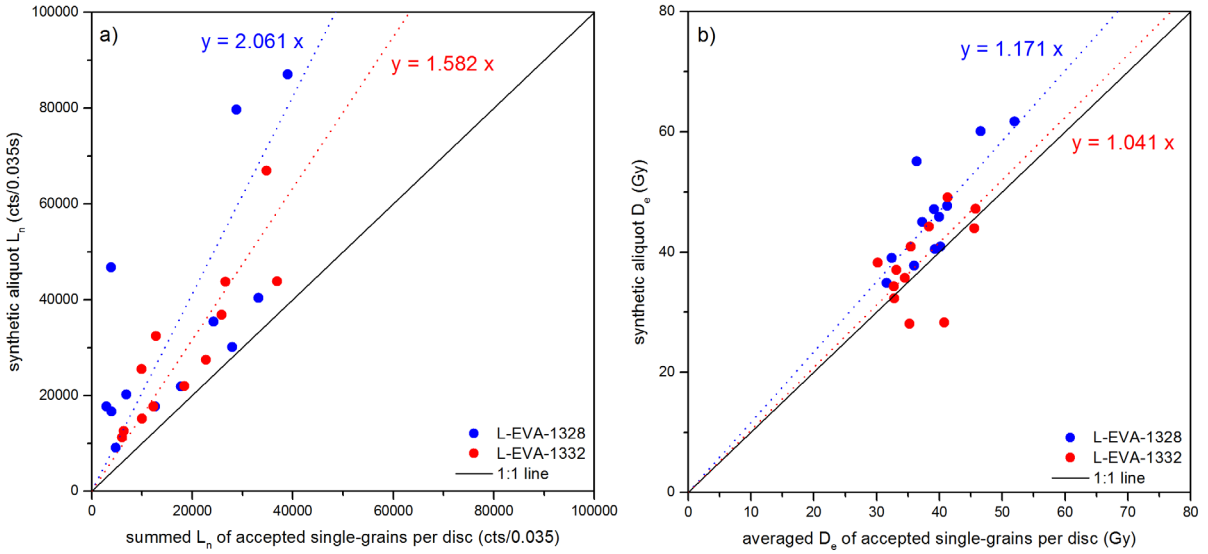

Fig. S12. Comparison between single-grain and synthetic aliquot data sets. (a) Synthetic aliquot Ln signals as a function of the summed Ln signals of accepted individual grains from the same single-grain disc and (b) synthetic aliquot D_es as a function of the averaged D_es of accepted individual grains from the same single-grain disc.

It is not surprising that synthetic aliquot D_es of sample L-EVA-1328 exceed the corresponding values of single-grains, since the syA/SG ratio of this sample is 1.28. However, this plot shows that the apparent D_e overestimation affects – to varying degrees - all synthetic aliquots and not only a few selected outliers, as no single data point lies below the 1:1 line.

To get a better idea of the type of grains that cause the Ln offset signals in both samples, which may explain the D_e overestimation in L-EVA-1328 - as their signal might superimpose the signal of other grains - Ln signals of each grain class were plotted separately in Fig. S13 for comparison. Ln signals of accepted single-grains are quite variable and reach up to ~20,000 counts. The majority of rejected individual grains yield signals below 10,000 counts. While the "dim" grain class yields - as expected - only grains with extremely low signal intensities, other rejection classes ("saturated", "recycling" and "IR depletion") are characterised by the presence of some extremely bright grains (>20,000 counts). The amount of these extremely bright grains is higher in sample L-EVA-1328 (n=3) compared to L-EVA-1332 (n=1). Figure S13 additionally shows that the number of individual grains in each defined class are roughly the same in both samples, except for individual grains rejected due to saturated signals (L-EVA-1328: n=34; L-EVA-1332: n=14).

In the next step, we aim to clarify which grain types yield the highest D_e values and are, therefore, most likely to be the reason for overestimation in synthetic aliquot D_e calculations. Individual grains rejected due to "saturation", however, yield no D_e values since their Ln/Tn ratio exceeds the maximum Lx/Tx of the dose response curve. Consequently, we decided to plot Ln/Tn ratios instead of D_es for each individual grain as a function of their corresponding Ln signal brightness in Fig S14. We are aware of the fact that Ln/Tn ratios are only relative measures and therefore less meaningful than D_e values. Using Ln/Tn ratios, however, enables us to visually compare all rejected and accepted grains from one sample (including "saturated" ones).

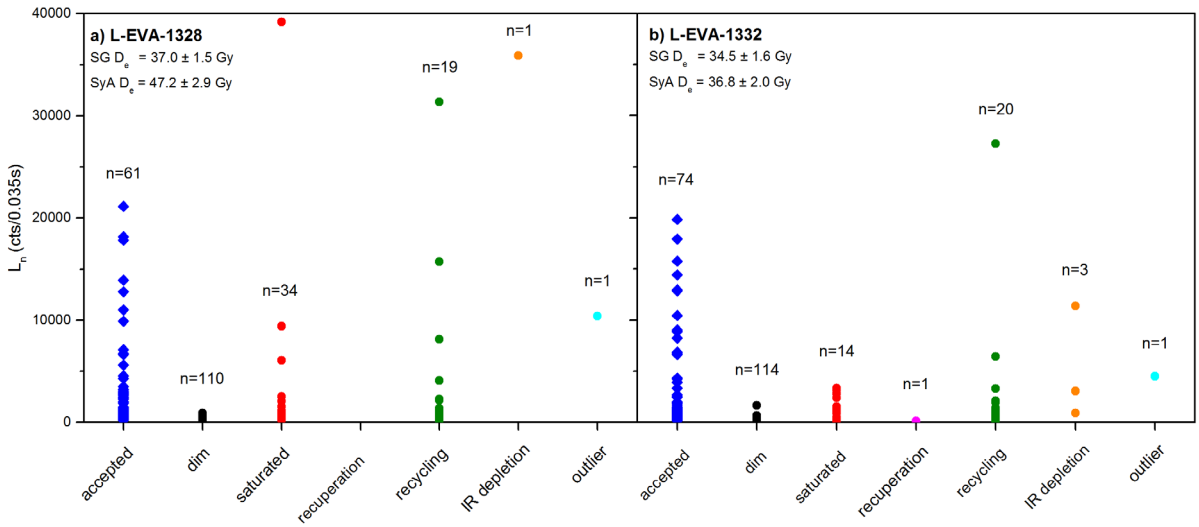

Fig. S13. Ln signal brightness of the different single-grain classes of (a) L-EVA-1328 and (b) L-EVA-1332.

No obvious differences can be observed between the shape of the data distributions of sample L-EVA-1328 and L-EVA-1332, not when plotting the Ln signal intensity on a linear scale (Fig. S14a,b), nor on a $\log_{10}$ scale (Fig. S14c,d). Except for the "dim" grains which yield lower signal intensities, the majority of individual grains from the rejected grain classes plot well within the point cloud of the "accepted" grains. This proves their similarity regarding both Ln signal intensities and Ln/Tn ratios. The individual grains identified as extremely bright in Fig. S13 that were rejected due to "recycling" do not yield Ln/Tn ratios significantly above average in both samples (Fig. S14a,b). Two extremely bright grains from L-EVA-1328 - one classified as "saturated" and the other one as "IR depletion" - however, show increased Ln/Tn ratios and might, therefore, be the reason for D_e overestimation in at least two out of nine synthetic aliquots of sample L-EVA-1328. This appears to be even more likely due to the fact that both grains clearly dominate the Ln signal of the synthetic aliquot they correspond to: the "saturated" grain represent ~45% and the "IR depletion" grain represent ~77% of the total light sums. Moreover, the two synthetic aliquots of these two grains are assigned to yield the highest D_es (>60 Gy) determined for this sample and are clearly recognisable as data points well above the 1:1 and the median ratio line of L-EVA-1328 in Fig. S12b.

Interesting to note is the fact that there is a positive correlation between the Ln/Tn ratios and the Ln signal intensities, albeit weak, when Ln is displayed on a $\log_{10}$ scale with $r^2 = 0.254$ and $r^2 = 0.347$ for L-EVA-1328 and L-EVA-1332, respectively (Fig. S14b). This implies that brighter individual grains are more likely to yield high Ln/Tn ratios in both samples.

In summary, there appear to be three main differences between the luminescence properties of single-grains of sample L-EVA-1328 and L-EVA-1332, which might relate to the observed D_e overestimation in L-EVA-1328:

1) "rejected" grains contribute significantly more to the total Ln signal of synthetic aliquots in L-EVA-1328 (~50%) compared to L-EVA-1332 (~37%).

2) Single-grains with both high Ln signal intensities and high Ln/Tn ratios in L-EVA-1328 significantly alter the D_es of individual synthetic aliquots and consequently also influence calculated synthetic aliquot CAM D_es of this sample. This was not observed in sample L-EVA-1332.

3) The amount of individual grains rejected due to signal saturation is significantly higher in sample L-EVA-1328 (n=34) compared to L-EVA-1332 (n=14).

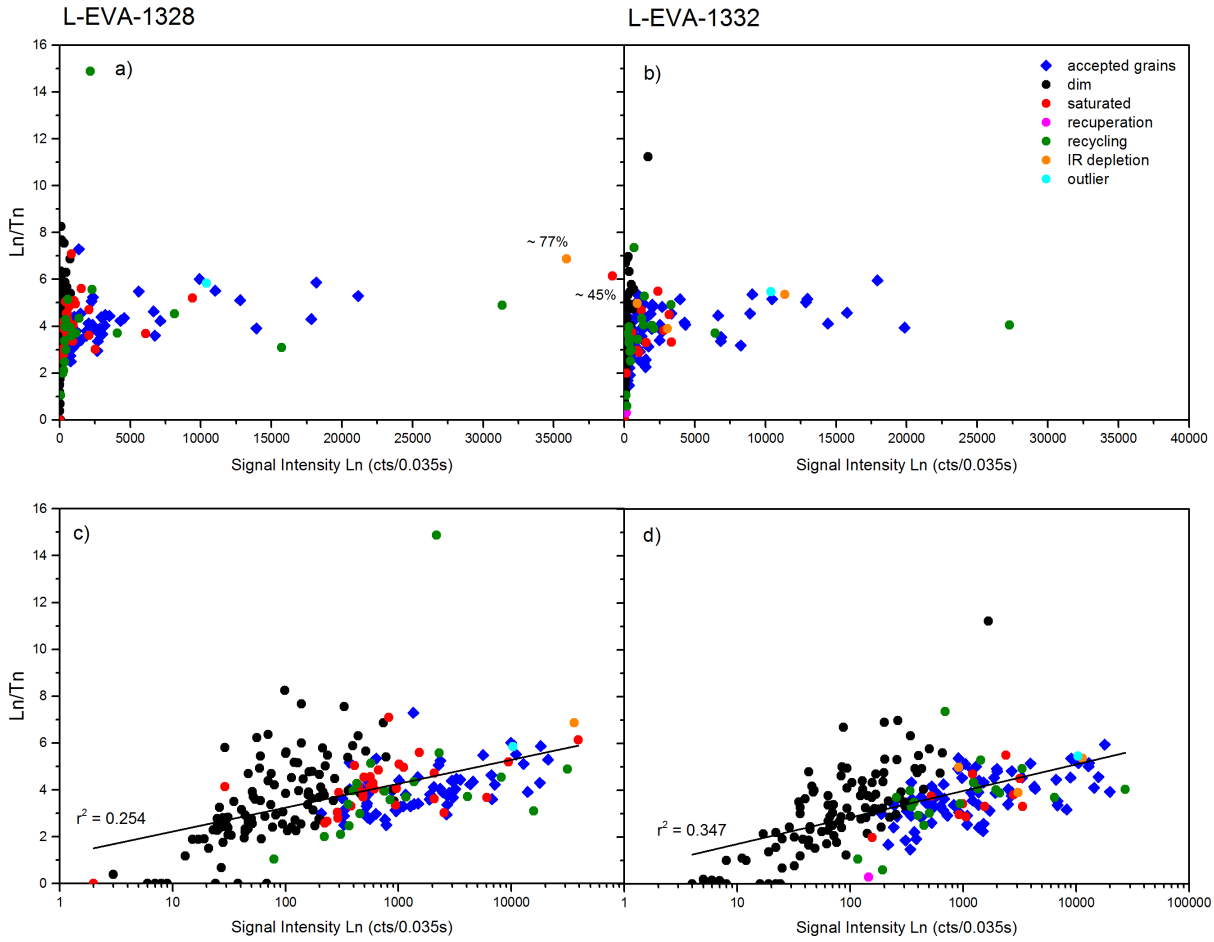

Fig. S14. Ln/Tn ratio as a function of Ln signal intensities for sample L-EVA-1328 and L-EVA-1332 with different scales of the x-axis (a,b) linear and (c,d) log10.

To test whether there is a direct correlation between the amount of "saturated" grains and D_e overestimation in synthetic aliquots compared to single-grains in the samples from VC and HC, syA/SG D_e ratios were plotted as a function of the percentage of "saturated" grains of each sample in this study (Fig. S15). The percentage of "saturated" grains in the VC and HC samples varies between 1.0-2.7% (Table S4), while the syA/SG D_e ratios are between 0.96-1.28 (Table S5).

The data distribution in Fig. S15 clearly shows that there is no correlation between the syA/SG D_e ratio and the percentage of "saturated" grains in our samples. This plot, however, does not yield information as to the brightness of the "saturated" grain signals. As our previous exercise has revealed that very few bright grains can superimpose the Ln signal of synthetic aliquots in our samples, the contribution of "saturated" grain signals to the total light sum of synthetic aliquots was calculated for four samples in this study (blue stars, Fig S15). In samples which yield relatively few "saturated" grains (L-EVA-1332 and L-EVA-1495), these grains contribute on average only 6-7% to the total Ln light sum of their synthetic aliquots, irrespective of the revealed syA/SG ratios. The same pattern was observed for samples yielding significantly higher amounts of "saturated" grains (L-EVA-1328 and L-EVA-1335). The contribution of "saturated" grains to the total Ln light sum increases to 16-17% compared to the samples yielding less amounts of "saturated" grains, the syA/SG D_e ratio of the samples, however, seems to be unaffected by the percentage of "saturated" grains. These results show that samples with above average syA/SG D_e ratios are not necessarily characterised by "saturated" individual grains with extremely bright luminescence signal intensities.

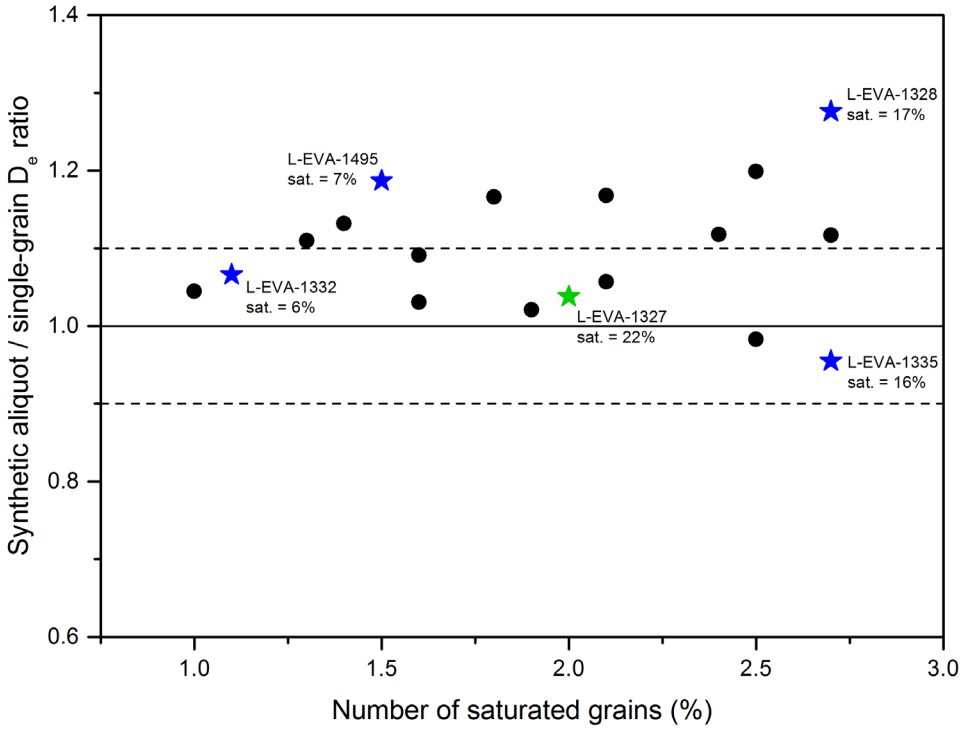

Fig. S15. Synthetic aliquot / single-grain D_e ratio as a function of the percentage of "saturated" grains for each sample at VC and HC. Highlighted as stars are samples for which the percentage of the Ln signal of "saturated" grains to the total light sum of synthetic aliquots was calculated.

This exercise indicates that "saturated" grains in our samples are unlikely to be the only driving force behind D_e overestimation in synthetic aliquots. The most plausible explanation for at least part of the overestimation seem to be related to the presence of extremely bright – not necessarily "saturated" - grains in some of our samples which in addition yield above average Ln/Tn ratios. These grains have the potential to superimpose the Ln signal of all other grains placed on a multiple-grain aliquot, and to increase the determined average D_e for this aliquot by significant means.
The defined single-grain quality criteria in this study have proven to safely reject extremely bright grains with high Ln/Tn ratios from our dataset, but this cannot be unconditionally guaranteed for aliquots yielding averaged luminescence signals of ~30 (multi-grain aliquots) and 100 (synthetic aliquots) individual grains. However, the more grains are placed on a multiple grain disc, the more likely it becomes that this disc is affected by one or more of these extremely bright grains and therefore by D_e overestimation.
It must be noted, that such grains occur infrequently in the VC and HC samples. It remains unresolved whether their presence in only some samples is linked to real differences in luminescence properties or whether they are evenly distributed throughout all sediment layers in the caves. Although it is most likely that the distribution of extremely bright grains is random throughout the sediments from VC and HC, further detailed single-grain analyses would be needed to clarify this with any certainty.

Our comparative exercise between sample L-EVA-1328 and L-EVA-1332 showed that the presence of extremely bright grains with high Ln/Tn ratios can only partly explain the D_e overestimation observed in L-EVA-1328 (Fig S12b). Another difference between the two samples investigated is the size of the offset signal (Fig. S12a) that contributes to the total light sum of the synthetic aliquot data. The offset signal originates from grains rejected according to single-grain quality criteria. In sample L-EVA-1328, higher proportions of rejected grains contribute to the luminescence signal of the synthetic aliquots. Some of these grains might have slightly higher D_e values than the "accepted" ones from the same aliquots and, therefore, increase the D_es of the synthetic aliquots. Additional single-grain analyses would be required to confirm or reject this hypothesis.

Sample L-EVA-1327

We performed a similar exercise on sample L-EVA-1327, in order to identify any presence of individual grains in this sediment layer that may influence multi-grain aliquot results towards D_e overestimation.
Synthetic aliquot D_es of sample L-EVA-1327 are statistically identical to those calculated using single-grains (syA/SG ratio: 1.04, Table S5), but significantly smaller than those derived from multi-grain aliquots (syA/MG ratio: 0.85, Table S5). Rejection due to signal "saturation" affects 2.0% of the analysed single-grains (Table S4, Fig. S15). The contribution to the synthetic Ln signal of these "saturated" grains is high (~22%) compared to the values for samples L-EVA-1328, L-EVA-1332, L-EVA-1335 and L-EVA-1495 (Fig. S15). When plotting Ln/Tn ratios of individual grains as a function of their Ln signal intensities, it is striking that two "saturated" individual grains lie well above (Ln/Tn ratio >5) the average Ln/Tn ratio observed for the majority of grains in this sample (Fig. S16a). L-EVA-1327 contains considerably fewer grains with signal intensities of >10,000 counts compared to sample L-EVA-1328 and L-EVA-1332 (Fig. S14). However, the majority of grains yield – as for L-EVA-1328 and L-EVA-1332 - signal intensities between 1000-5000 counts. With signal intensities of ~10,000 counts the two "saturated" grains belong to the five brightest grains in this sample.

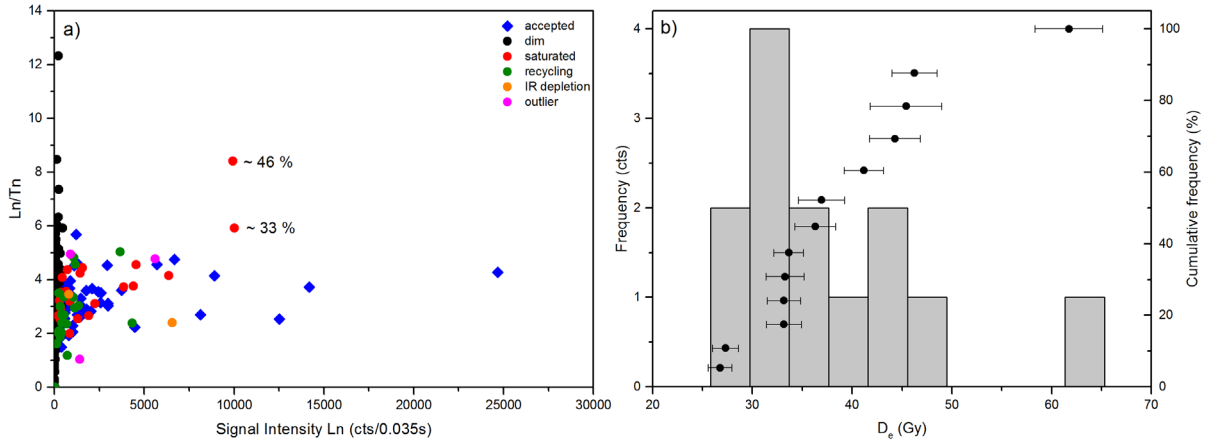

Fig. S16. (a) Ln/Tn ratio as a function of Ln signal intensities for sample L-EVA-1327 and (b) frequency histogram of synthetic aliquot D_e values of sample L-EVA-1327.

The two "saturated" grains are the most likely candidates influencing D_e overestimation in the synthetic aliquots of sample L-EVA-1327. Interestingly, no such overestimation can be inferred from the synthetic aliquot CAM D_e of the sample (syA/SG ratio: 1.04, Table S5). The explanation for this is that both "saturated" grains derive from single-grain discs which do not pass the synthetic/multi-grain aliquot quality criteria: The "saturated" grain with a Ln/Tn ratio of ~8 contributes significantly to the total Ln light sum (~46%) of its corresponding synthetic aliquot and this aliquot was rejected from final D_e calculation due to signal saturation. The contribution of the second "saturated" grain (Ln/Tn ratio ~6) to the total Ln light sum of its corresponding synthetic aliquot is ~33%. This synthetic aliquot with a D_e of ~62 Gy (Fig. S16b) was identified as a statistical outlier (Grubbs, 1950) and was also rejected from the final D_e calculation.
The contribution of "rejected" grains to the total Ln signal of synthetic aliquots of L-EVA-1327 (~34%) is comparable to the value obtained for L-EVA-1332 (~37%) and considerably less than for L-EVA-1328 (~50%). It seems that other than sample L-EVA-1328, L-EVA-1327 yields an overall homogeneous distribution of D_e values irrespective of whether grains were rejected or accepted for final D_e calculation. This was also observed for sample L-EVA-1332. Other than L-EVA-1332, however, L-EVA-1327 contains a few individual grains with bright Ln signal intensities and high Ln/Tn ratios. These have the potential to dominate the Ln signal in aliquots containing multiple grains and cause overestimation of their D_e. This

combination of grains with different luminescence properties might explain the excellent agreement observed between single-grain and synthetic aliquot CAM D_es, after rejection criteria were applied (Table S5). However, it does not explain the cause for the higher CAM D_es of multi-grain aliquots compared to those derived from single-grains and synthetic-aliquots. It may be that the multi-grain aliquots of L-EVA-1327 contain by chance more very bright grains with high Ln/Tn ratios than the synthetic aliquots. Alternatively, our single-grain discs may contain by chance below average amounts of bright grains. Unfortunately we cannot examine the luminescence properties of the individual grains contributing to the luminescence signal of each multi-grain aliquot. We can, nevertheless, safely conclude that there are individual grains present in sample L-EVA-1327 that can significantly alter the D_es of multi-grain aliquots which might result in an overestimation of the burial age of Layer 1 from VC.

References

Barton, R.N.E., Stringer, C.B., Finlayson, J.C., 2013. Neanderthals in Context. A report of the 1995-1998 excavations at Gorham's and Vanguard Caves, Gibraltar, Oxford University School of Archaeology, Oxford, p. 328.

Galbraith, R.F., Roberts, R.G., Laslett, G.M., Yoshida, H., Olley, J.M., 1999. Optical dating of single and multiple grains of quartz from Jinmium rock shelter, northern Australia: Part I, experimental design and statistical models, Archaeometry 41, 339-364.

Grubbs, F.E., 1950. Sample Criteria for Testing Outlying Observations, 27-58.

Pettitt, P.B., Bailey, R.M., 2000. AMS Radiocarbon and Luminescence Dating of Gorham's and Vanguard Caves, Gibraltar, and Implications for the Middle to Upper Palaeolithic Transition in Iberia, In: Stringer, C.B., Barton, R.N.E., Finlayson, J.C. (Eds.), Neanderthals on the Edge, Oxbow BooksOxford, pp. 155-162.

Rhodes, E.J., 2013. OSL age estimates from Vanguard Cave, In: Barton, R.N.E., Stringer, C.B., Finlayson, J.C. (Eds.), Neanderthals in Context. A report of the 1995-1998 excavations at Gorham's and Vanguard Caves, Gibraltar, Oxford University School of ArchaeologyOxford, pp. 211-217.

Stringer, C.B., Barton, R.N.E., Finlayson, J.C., 2000. Neanderthals on the Edge, Oxbow, Oxford, p. 267.